Comparing, matching, detecting, and predicting drought-induced tree mortality in the Sierra Nevada, California

Liz van Wagtendonk

A dissertation submitted in partial fulfillment of the requirements for the degree of

Doctor of Philosophy

University of Washington

2023

Reading Committee:

Van R. Kane, Chair

Brian J. Harvey

L. Monika Moskal

Program Authorized to Offer Degree:

School of Environmental and Forest Sciences

Abstract

Comparing, matching, detecting, and predicting drought-induced tree mortality in the Sierra Nevada, California

Liz van Wagtendonk

Van R. Kane
School of Environmental and Forest Sciences

In the last decade, technology and computing capabilities have evolved to allow the detection of individual trees with remote sensing. This innovation is invaluable to researchers and managers who seek precision methods to measure forest condition in a rapidly changing world. To apply remotely sensed methods to evaluate population trends, a framework is required to enable the application of these methods to detect and predict the trends of tree populations. Such a framework requires assessing the uncertainty and bias associated with applying remotely sensed methods to reflect the population trends of individual trees. The goal of my dissertation was to establish a framework for defining the population trends of remotely sensed trees in the context of an extensive tree mortality event. Further, I endeavored to measure the uncertainty and bias associated with applying remotely sensed trees to represent drought-induced mortality trends.

Between 2012 and 2016, California experienced its first warm drought that resulted in an extensive tree mortality event. During the drought, several novel remote sensing approaches documented tree mortality and the potential ecological drivers of the mortality. However, how the remotely sensed trees reflected population trends were not well defined.

To examine how remotely sensed trees (i.e., tree models segmented from lidar and combined with high-resolution imagery) reflected drought-induced tree mortality trends, I compared and matched remotely sensed and field data collected pre- and post-drought. I examined these trends by measuring the uncertainty associated with the remotely sensed trees and the bias affiliated with the remotely sensed methods. The study was conducted in a fire excluded, late seral mixed conifer forest in the southern Sierra Nevada. In Chapter Two, I compared the mortality trends of pre- and post-drought field trees and remotely sensed trees. This study revealed that on average, each remotely sensed tree contained a dominant visible tree and two subordinate trees, which were undetectable to the airborne sensors. In Chapter Three, I matched field to remotely sensed trees to define the subset of the population detected by high resolution lidar and orthoimagery. Of the 9,761 conifer trees in the study, 2,814 or 29% of the population matched to the remotely sensed trees. Chapter 4 involved applying machine learning models for the detection of drought induced mortality and decay of matched, remotely sensed trees. By using matched trees in the analysis, I found that remotely sensed trees captured the survivorship and decay of overstory trees, and pine species were better represented than fir species in the study area.

I discovered that remotely sensed trees were an effective means of evaluating the mortality and decay patterns of overstory trees. Importantly, I identified the uncertainty of the population trends and the bias related to the remotely sensed methods. This knowledge can aid the development of future artificial intelligence models to evaluate overstory tree population trends. The framework provided in this dissertation study can be adapted to conduct paired field assessments in other locations to promote the application of remotely sensed trees for population studies.

TABLE OF CONTENTS

LIST OF FIGURES

LIST OF TABLES

ACKNOWLEDGMENTS

This dissertation study was possible due to many important research collaborators as well as mentors, family members, and friends.

First, I could not have achieved this work without the partnership of my husband, Kent van Wagtendonk, and our daughter, Ava Jeanne van Wagtendonk. I am so fortunate and grateful for your incredible support and patience. Thank you to my sister, April Osmanof, who has always supported and humored me even if it involved dragging her into the night to catch salamanders. Thank you to my amazing extended family whose support to Kent, Ava Jeanne, and myself was so encouraging.

I dedicate my dissertation to all my parents, living and dead, who encouraged me to see this process through: Sandra and Carl Cathey, Kent and Madeline Chattin, Sadik Osmanof, and Jan and Margene van Wagtendonk. It is not easy to lose parents when doing a dissertation, but anyone who was so fortunate to have fantastic parents is grateful just to have them along for part of the journey.

Van Kane, thank you so much for every effort you made in these last years that enabled me to reach this point. You went above and beyond to support my doctorate program as a patient mentor and kind and empathetic friend. I look forward to our future collaborations, even to writing a few more grant proposals.

Monika Moskal, your leadership, mentorship, and friendship has been a true gift in every way. Your positive and thoughtful leadership of the Precision Forestry Collaborative is marked by the many outstanding and diverse students that are in the PFC. I am eager to work together and plan future camping trips.

Jessica Lundquist, thank you for your thoughtful mentorship and our friendship. I am excited for future collaborations to study snow and forest interactions. I look forward to many future coffee breaks and camping trips, so we can solve the mystery that is SPS.

Malcolm North, thank you very much for your mentorship and friendship over the years. You made this research possible by helping to provide the data for this study. More importantly, you shared your time and the Teakettle Experimental Forest in person, which allowed me to re-focus my perspective on remote sensing in the context of population studies.

Brian Harvey, thank you for being an incredible teacher, mentor, and friend. I am grateful for your patient guidance in approaching forest ecology and what resilience means in the broader context. I look forward to collaborating with you in future efforts.

Ernesto Alvarado, obrigada, I feel very fortunate to have many discussions with you regarding fire ecology and the importance of indigenous experience and expertise in this arena. I will never forget the visit to the Yakima Nation, the experience has shaped the way I listen and approach forest collaborators.

Pratima KC, you have been my wonderful research partner and friend through this doctoral journey. I'm looking forward to many research collaborations with you in the future.

Sean Jeronimo, thank you for your terrific mentorship and friendship. You made this dissertation possible by going before me and establishing your methods. I look forward to future collaborations with you.

Nic Enstice, thank you for your friendship and collaboration in this journey.

Susan Prichard, Eric Rowell, and Tom Painter, thank you for the wonderful discussions and collaborations now and into the future.

Jonathan Kane, Bryce Bartl-Geller, and Bob McGaughey thank you all for your support in helping me to understand the important nuances of applying remote sensing data in an ecological context. Your guidance has been invaluable.

Caden Chamberlain, Gina Cova, Astrid Sana, and Hannah Redford, thank you all for your terrific feedback and help as I completed this dissertation. I'm so fortunate to work with you all. Thank you to all the past and present students and friends in the Forest Resilience Lab and the Remote Sensing Lab whose support, collaboration, and fun make me so grateful every day for being able to work in our field.

Chapter 1. INTRODUCTION

Forests around the globe are rapidly changing as droughts, heat waves, wildfires, resource extraction, insect and disease outbreaks interact synoptically with climate change (Millar and Stephenson, 2015; Mueller et al., 2020; Trumbore, S.; Brando, P.; Hartmann, 2015). California has experienced unprecedented warm droughts for which there are no historical analogs (Swain, 2015) and multiple mass fires in the last decade. Eighteen fires in California accounted for most acres burned (Cova et al., 2023) in the last 10 years, and the 2012 to 2016 drought resulted in the death of an estimated 80 to 120 million trees (United States Forest Service, Region 5, 2019).

In the fire-frequent forests of California's Sierra Nevada and the intermountain West, warm and dry conditions persisted following the 2012-2016 drought. The drought perpetuated tree mortality (Fettig et al., 2019; Pile et al., 2019; Restaino et al., 2019; Stephens et al., 2018; Young et al., 2017) and influenced regeneration rates (North et al., 2019; Wright et al., 2021; Young et al., 2020). Hundreds of millions of trees reportedly perished during California's 2012-2016 drought (United States Forest Service, Region 5, 2019), and regeneration rates are significantly dampened when dry years follow fires (Shive et al., 2018). Warm and dry conditions support recurrent and mass wildfires in the fire suppressed forests of the Sierra Nevada and the intermountain West (Coop et al., 2020; Lutz et al., 2009; Mueller et al., 2020; North et al., 2019; Williams et al., 2019). The challenge for managers is to greatly increase the pace and scale of fire and forest management. Millions of acres of forests are at risk of conversion to non-forest cover (Coop et al., 2020). Conversion to non-forest ecosystems has the potential for concomitant losses to invaluable ecosystem services such as carbon and nutrient cycling, habitat, wildlife species, and diminished snowpack for water supply (Mueller et al., 2020).

The potential for conversion to non-forest cover is influenced by climate (Stewart et al., 2021), community composition and structure, disturbance regimes, and biophysical setting

(Jeronimo, 2018; Kane et al., 2019). As the amplitude of climatic cycles increase in California, extended years of hot and dry weather are punctuated with extremely wet conditions (Winitsky et al., 2023). California just experienced the wettest year on record in 2023, which followed on the heels of the three driest years (Ince, 2023).

The vast extent of forests, complex structure, and large number of individual trees limits the assessment of population trends in a rapidly changing climate. Population ecology is fundamentally rooted in the assessment of trends of individuals, populations, and species, across time and niche, in response to biophysical and climatic setting and processes (Begon, 2021; Freiderichs, 1958; Odum, 1971). In forest ecology, a complete census of all individuals over large areas is commonly infeasible because of the cost and effort of field studies. Instead, ecologists use in-situ or field-based sampling to represent population trends.

Long-term field studies are the gold standard for collecting the data necessary to assess the population trends of species. Long-term in-situ study plots (Lutz et al., 2018; North, 2002) and monitoring programs including the US Forest Service's Forest Inventory and Analysis (Burkman, 2005) sample population trends through time and across generations. However, long-term field studies of trees are more uncommon due to the long-lived nature of trees. Most field studies are constrained by the temporal frequency and extent of the sampling events. In addition, field studies collect individual tree metrics specific to the research questions of interest, which complicates comparisons (Cansler et al., 2020) and interpolations across vegetation community types and biophysical settings. Depending upon the frequency and representative sampling across species, bias also influences interpolating these datasets to broader extents (Breidenbach et al., 2010; Ene et al., 2018; Kennedy et al., 2017).

Since 2010, researchers developed the ability to capture or model individual trees from remotely sensed data (Lines et al., 2022), and this capability has rapidly evolved. For example, individual tree crowns are being delineated from imagery (Das et al., 2022; Fricker et al., 2019) or segmented from lidar (Hamraz et al., 2017; Jeronimo et al., 2018; Polewski et al., 2015; Zhou

et al., 2018). Remotely sensed tree detection has evolved to the point where understory trees are segmented from airborne lidar (Yun et al., 2022). In addition, a variety of platforms from small commercial satellites, fixed wing, backpack, and other or mobile lidar systems (Donager et al., 2021) are available to support individual tree mapping and monitoring at field sites.

Researchers are fusing high resolution remotely sensed data to identify individual trees across broad extents (Chen et al., 2018; Donager et al., 2021; Gutierrez et al., 2023; Zhou et al., 2018). Fused remotely sensed trees are created with two or more datasets collected from a variety of sensor platforms including airborne, mobile, and terrestrial platforms. For example, a manually delineated tree crown (Das et al., 2022; Fricker et al., 2019) or a tree canopy segmented from lidar can be combined with reflectance bands to examine taxonomic, structural characteristics, and mortality status. Although remotely sensed methods can identify and map individual trees, preliminary analytical steps are required to apply them as proxies for trees in ecological analysis (Stephenson and Das, 2020; Stovall et al., 2019).

Remotely sensed trees are not always one-to-one proxies of individual trees representative of all species present. For example, remotely sensed trees may fully represent individual trees in a less structurally complex oak woodland or savannah, where all trees are equally detectable (Sousa and Davis, 2020). However, a census level analysis of mortality is not possible in a complex, multi-strata forest using fixed-wing or satellite platforms (Stephenson and Das, 2020; Stovall et al., 2019). In these forests, the species and mortality status of the trees in the understory are hidden from view of passive sensors on fixed wing and satellite platforms. Therefore, it is necessary to define the population trends of species of interest represented by remotely sensed trees prior to analysis.

The focus of this dissertation study was to develop and test a framework for conducting the analytical steps necessary to use remotely sensed trees to assess population trends. The first step of the framework was to identify whether the methods being applied census a population or a subset of a species population. This first step was the focus of chapter two

where I directly compared the mortality and decay status of remotely sensed trees to in-situ (i.e., field trees). The second step of the framework was to identify the error or bias in the sampling method at the species level, which was necessary as multiple tree species were studied. The aim of my third chapter was to individually match field to remotely sensed trees to identify sources of error that affected the detection of population trends, by species. Further, I measured how matched trees represented the mortality and decay trends of the field trees and which trees were missed. Third, the remotely sensed trees were validated with in-situ data to enable the prediction of population trends. My final chapter applied the matched remotely sensed trees from Chapter 2 for the prediction of tree mortality and decay, which enabled me to assess predication efficacy by species.

To test this analytical framework, I studied the tree mortality and decay trends of trees in the control plots of a long-term fire and fire surrogates study within the Teakettle Experimental Forest in the southern Sierra Nevada, California. The control plots contained complex, multi-strata mixed Sierran conifer forests (Goodwin et al., 2020; North, 2002; Odland et al., 2021) fire excluded since the late 1800s. These trees experienced drought-induced tree mortality following California's drought-induced 2012-2016 tree mortality event.

I applied and tested the analytical framework using the watershed segmentation algorithm (Jeronimo et al., 2018) to model trees from airborne lidar "lidar trees", pre-drought, Figure 1.

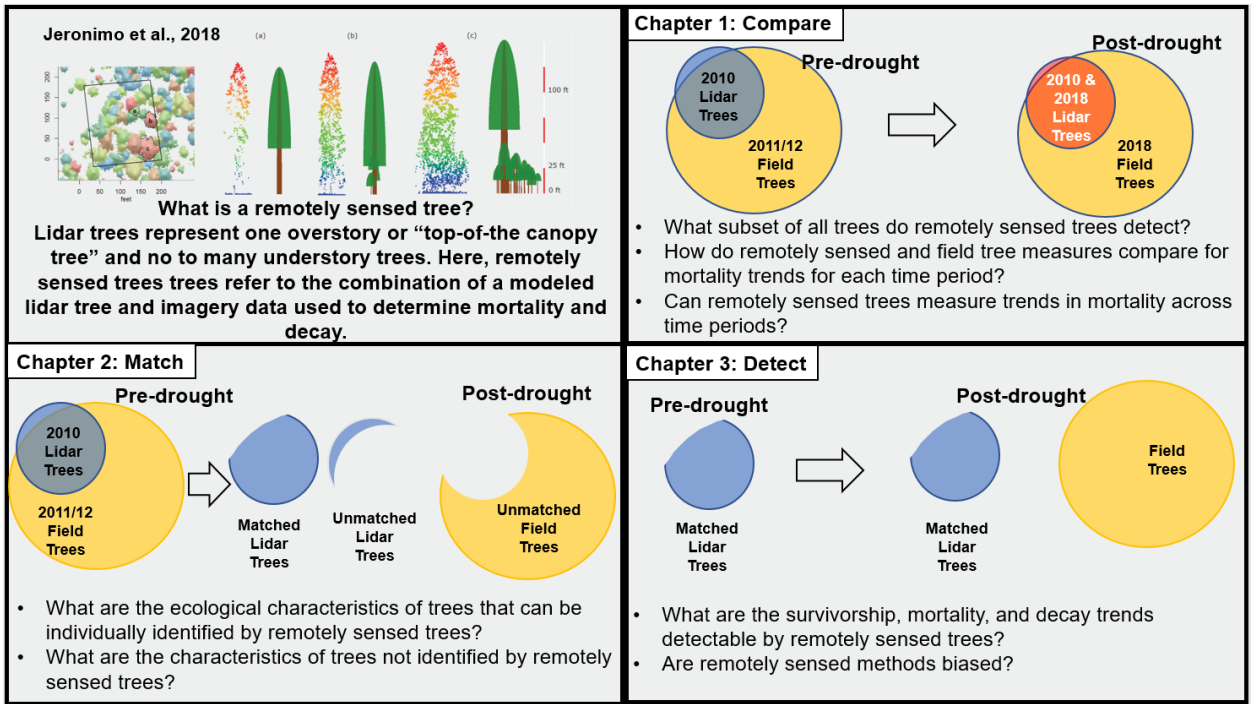

Figure 1. The methodological framework for assessing the population trends and error associated with the application of remotely sensed trees in the Sierra Nevada, California.

Further, I fused the modeled lidar trees with high-resolution imagery to identify tree mortality and decay tree trends following the drought. I selected the watershed segmentation method because it is applied to analyze forest structure conditions across large extents. In the dry, fire adapted forests of the Sierra Nevada and Intermountain West, fire repeatedly sculpts patterns of individual trees, tree clumps, and openings (i.e., ICO patterns) that confer resistance to future fires (Larson and Churchill, 2012; Churchill et al., 2017). Jeronimo et al., 2019 and Kane et al. 2019 developed methods to analyze the three-dimensional spatial patterns of these modeled trees for conformity to reference conditions (i.e., lidar-based ICO or LICO analysis). To test for conformity, they compared forests of interest to reference conditions with matching climate, fire return intervals, vegetation, and topographic setting considered resilient to future fire and climate change.

At the time of writing, these LICO analytical methods are in operational use to support and implement forest management in the Sierra Nevada[1]. As part of my dissertation research, I applied the analytical framework to investigate whether the watershed segmentation method can be extended to also capture mortality and decay trends of individual trees across large extents. By conducting this examination, individual tree mortality and decay status of remotely sensed trees can be incorporated into future assessments applying LICO-based analyses. Further, the analytical framework provided includes methods to evaluate the population trends of remotely sensed trees with field validation.

I endeavored to investigate how the mortality and decay trends of remotely sensed trees compared, matched, and predicted in-situ trends. Ultimately, the results of this dissertation are intended to inform and enable future analysis of population trends involving drought and mortality using LICO-based analyses.

I initiated this examination in chapter two. This chapter involved comparing remotely sensed trees to in-situ trees pre- and post-drought. The research and management goals of chapter three were to describe which trees are best sampled by remotely sensed trees; how remotely sensed trees may capture a tree mortality event over time; and propose a classification for tree mortality and decay. In this study, I investigated datasets collected pre- and post-drought that varied in temporal and spatial resolution. Finally, I compared remotely sensed tree mortality information with field-based data to improve the application of remotely sensed surveys of tree mortality events.

For chapter four, I fused remotely sensed “lidar trees” with high resolution imagery. After the lidar trees were fused, they were matched to field trees on a one-to-one basis. I applied the matched tree to test the efficacy of applying the mortality and decay trends of fused trees to

[1] The Tahoe Central Sierra Initiative, Social and Ecological Resilience Across the Landscape in the Stanislaus National Forest, and the Southern Sierra All-lands Restoration and Resilience Program in California have all applied methods developed and in practice by the University of Washington, Forest Resilience Lab and described in (Jeronimo, 2018).

explain in-situ mortality trends resulting from California's 2012-2016 drought. The research and management questions of this final chapter were to develop a validated dataset that can be applied in future studies to assess the biophysical drivers of top-of-the-canopy tree mortality and decay using LICO-based analysis and other approaches.

1.1 REFERENCES

Adams, H.D., Guardiola-claramonte, M., Barron-gafford, G.A., Villegas, C., Breshears, D.D., Zou, C.B., Troch, P.A., Huxman, T.E., Mooney, H.A., Adamsab, H.D., Guardiola-claramonte, M., Barron-gaffordab, G.A., Villegasade, J.C., Breshearsa, D.D., Trochac, P.A., Huxmanabf, T.E., 2018. Temperature sensitivity of drought-induced tree mortality portends increased regional die-off under global-change-type drought. Proc. Natl. Acad. Sci. U. S. A. 106, 7063–7066.

Allen, B.H., 2005. Sierran Mixed Conifer, California Wildlife Habitat Relationships System. Sacramento.

Asner, G.P., Brodrick, P.G., Anderson, C.B., Vaughn, N., Knapp, D.E., Martin, R.E., 2016. Progressive forest canopy water loss during the 2012–2015 California drought. Proc. Natl. Acad. Sci. 113, E249–E255. https://doi.org/10.1073/pnas.1523397113

Axelson, J., Battles, J., Bulaon, B., Cluck, D., Cousins, S., Cox, L., Estes, B., Fettig, C., Hefty, A., Hishinuma, S., Hood, S., Kocher, S., McMahon, D., Mortenson, L., Koltunov, A., Kuskulis, E., Poloni, A., Ramirez, C., Restaino, C., Safford, H., Slaton, M., Smith, S., Tubbesing, C., Wayman, R., Young, D., 2019. The California Tree Mortality Data Collection Network — Enhanced communication and collaboration among scientists and stakeholders, California Agriculture. https://doi.org/10.3733/ca.2019a0001

Begon, M. and C.R.T., 2021. Ecology: From Individuals to Ecosystems, 5th Edition, 5th Editio. ed. Wiley.

Berner, L.T., Law, B.E., Meddens, A.J.H., Hicke, J.A., 2017. Tree mortality from fires , bark beetles , and timber harvest during a hot and dry decade in the western United States (2003 – 2012). Environ. Res. Lett. 12, 065005. doi:10.1088/1748–9326/aa6f94.

Breidenbach, J., Næsset, E., Lien, V., Gobakken, T., Solberg, S., 2010. Prediction of species specific forest inventory attributes using a nonparametric semi-individual tree crown approach based on fused airborne laser scanning and multispectral data. Remote Sens. Environ. 114, 911–924. https://doi.org/10.1016/j.rse.2009.12.004

Breiman, L.E.O., 2001. Random forests. Mach. Learn. 45, 5–32. https://doi.org/10.1023/A:1010933404324

Burkman, B., 2005. Forest inventory and analysis sampling and plot design, FIA fact sheet series [WWW Document]. U.S. Dep. Agric. For. Serv. URL https://www.fia.fs.fed.us/library/fact-sheets/data-collections/Sampling and Plot Design.pdf

Campbell, James B., Wynne, R.H., 2011. Introduction to Remote Sensing, Fifth. ed. The Guilford Press, New York.

Cansler, C.A., Hood, S.M., Varner, J.M., van Mantgem, P.J., Agne, M.C., Andrus, R.A., Ayres, M.P., Ayres, B.D., Bakker, J.D., Battaglia, M.A., Bentz, B.J., Breece, C.R., Brown, J.K., Cluck, D.R., Coleman, T.W., Corace, R.G., Covington, W.W., Cram, D.S., Cronan, J.B., Crouse, J.E., Das, A.J., Davis, R.S., Dickinson, D.M., Fitzgerald, S.A., Fulé, P.Z., Ganio, L.M., Grayson, L.M., Halpern, C.B., Hanula, J.L., Harvey, B.J., Kevin Hiers, J., Huffman, D.W., Keifer, M.B., Keyser, T.L., Kobziar, L.N., Kolb, T.E., Kolden, C.A., Kopper, K.E., Kreitler, J.R., Kreye, J.K., Latimer, A.M., Lerch, A.P., Lombardero, M.J., McDaniel, V.L., McHugh, C.W., McMillin, J.D., Moghaddas, J.J., O'Brien, J.J., Perrakis, D.D.B., Peterson, D.W., Prichard, S.J., Progar, R.A., Raffa, K.F., Reinhardt, E.D., Restaino, J.C., Roccaforte, J.P., Rogers, B.M., Ryan, K.C., Safford, H.D., Santoro, A.E., Shearman, T.M., Shumate, A.M., Sieg, C.H., Smith, S.L., Smith, R.J., Stephenson, N.L., Stuever, M., Stevens, J.T., Stoddard, M.T., Thies, W.G., Vaillant, N.M., Weiss, S.A., Westlind, D.J., Woolley, T.J., Wright, M.C., 2020. The Fire and Tree Mortality Database, for empirical modeling of individual tree mortality after fire. Sci. Data 7, 1–14. https://doi.org/10.1038/s41597-020-0522-7

Chen, T., Guestrin, C., 2015. XGBoost: Reliable Large-scale Tree Boosting System, in: Proceedings of the 22nd SIGKDD Conference on Knowledge Discovery and Data Mining, San Francisco, CA, USA. pp. 1–6.

Chen, Wei, Hu, X., Chen, Wen, Hong, Y., Yang, M., 2018. Airborne LiDAR remote sensing for individual tree forest inventory using trunk detection-aided mean shift clustering techniques. Remote Sens. 10, 1–25. https://doi.org/10.3390/rs10071078

Churchill, D.J., Carnwath, G.C., Larson, A.J., Jeronimo, S.A., 2017. Historical forest structure, composition, and spatial pattern in dry conifer forests of the western Blue Mountains, Oregon. USDA For. Serv. Pacific Northwest Res. Stn. PNW-GTR-95.

Coop, J.D., Parks, S.A., Stevens-Rumann, C.S., Crausbay, S.D., Higuera, P.E., Hurteau, M.D., Tepley, A., Whitman, E., Assal, T., Collins, B.M., Davis, K.T., Dobrowski, S., Falk, D.A., Fornwalt, P.J., Fulé, P.Z., Harvey, B.J., Kane, V.R., Littlefield, C.E., Margolis, E.Q., North, M., Parisien, M.A., Prichard, S., Rodman, K.C., 2020. Wildfire-Driven Forest Conversion in Western North American Landscapes. Bioscience 70, 659–673. https://doi.org/10.1093/biosci/biaa061

Cova, G., Kane, V.R., Prichard, S., North, M., Cansler, C.A., 2023. The outsized role of California's largest wildfires in changing forest burn patterns and coarsening ecosystem scale. For. Ecol. Manage. 528, 120620. https://doi.org/10.1016/j.foreco.2022.120620

Das, A.J., Slaton, M.R., Mallory, J., Asner, G.P., Martin, R.E., Hardwick, P., 2022. Empirically validated drought vulnerability mapping in the mixed conifer forests of the Sierra Nevada. Ecol. Appl. 32, 1–19. https://doi.org/10.1002/eap.2514

Diffenbaugh, N.S., Swain, D.L., Touma, D., Lubchenco, J., 2015. Anthropogenic warming has increased drought risk in California. Proc. Natl. Acad. Sci. U. S. A. 112, 3931–3936. https://doi.org/10.1073/pnas.1422385112

Donager, J.J., Sánchez Meador, A.J., Blackburn, R.C., 2021. Adjudicating perspectives on forest structure: How do airborne, terrestrial, and mobile lidar-derived estimates compare? Remote Sens. 13, 1–18. https://doi.org/10.3390/rs13122297

Duncanson, L., Dubayah, R., 2018. Monitoring individual tree-based change with airborne lidar. Ecol. Evol. 8, 5079–5089. https://doi.org/10.1002/ece3.4075

Ene, L.T., Gobakken, T., Andersen, H.E., Næsset, E., Cook, B.D., Morton, D.C., Babcock, C., Nelson, R., 2018. Large-area hybrid estimation of aboveground biomass in interior Alaska using airborne laser scanning data. Remote Sens. Environ. 204, 741–755. https://doi.org/10.1016/j.rse.2017.09.027

ESRI ArcGIS Pro Version 2.8, 2021.

Fagan, M.E., 2020. A lesson unlearned? Underestimating tree cover in drylands biases global restoration maps. Glob. Chang. Biol. 26, 4679–4690. https://doi.org/10.1111/gcb.15187

Falk, D.A., Watts, A.C., Thode, A.E., 2019. Scaling Ecological Resilience. Front. Ecol. Evol. 7, 1–16. https://doi.org/10.3389/fevo.2019.00275

Fettig, C.J., Mortenson, L.A., Bulaon, B.M., Foulk, P.B., 2019. Tree mortality following drought in the central and southern Sierra Nevada, California, U.S. For. Ecol. Manage. 432, 164–178. https://doi.org/10.1016/j.foreco.2018.09.006

Franklin, J.F., Spies, T.A., Pelt, R. Van, Carey, A.B., Thornburgh, D.A., Berg, D.R., Lindenmayer, D.B., Harmon, M.E., Keeton, W.S., Shaw, D.C., Bible, K., Chen, J., 2002. Disturbances and structural development of natural forest ecosystems with silvicultural implications, using Douglas-fir forests as an example. For. Ecol. Manage. 155, 399–423. https://doi.org/10.1016/S0378-1127(01)00575-8

Freiderichs, K., 1958. A Definition of Ecology and Some Thoughts About Basic Concepts. Ecology 39, 154–159.

Fricker, G.A., Ventura, J.D., Wolf, J., North, M.P., Frank, W., 2019. A Convolutional Neural Network classifier identifies tree species in mixed-conifer forest from hyperspectral imagery 1–24.

Fry, D.L., Stephens, S.L., Collins, B.M., North, M.P., Franco-Vizcaíno, E., Gill, S.J., 2014. Contrasting spatial patterns in active-fire and fire-suppressed mediterranean climate old-growth mixed conifer forests. PLoS One 9. https://doi.org/10.1371/journal.pone.0088985

Gallery, W., 2022. Neon Algorithm Theorectical Basis Document (Atbd) Aop Digital Camera Image Orthorectification Prepared By.

Gibson, P.B., Waliser, D.E., Guan, B., Deflorio, M.J., Ralph, F.M., Swain, D.L., 2020. Ridging associated with Drought across the Western and Southwestern United States: Characteristics, trends, and predictability sources. J. Clim. 33, 2485–2508. https://doi.org/10.1175/JCLI-D-19-0439.1

Goodwin, M.J., North, M.P., Zald, H.S.J., Hurteau, M.D., 2020. Changing climate reallocates the carbon debt of frequent-fire forests. Glob. Chang. Biol. 26, 6180–6189. https://doi.org/10.1111/gcb.15318

Gutierrez, A.A., Allison, S.D., Randerson, J.T., 2023. Estimating Individual Tree Mortality in the Sierra Nevada Using Lidar and Multispectral Reflectance Data Journal of Geophysical Research : Biogeosciences 1–18. https://doi.org/10.1029/2022JG007234

Hamraz, H., Contreras, M.A., Zhang, J., 2017. Forest understory trees can be segmented accurately within sufficiently dense airborne laser scanning point clouds. Sci. Rep. 7, 1–9. https://doi.org/10.1038/s41598-017-07200-0

Holling, C.S., 1973. Resilience and Stability of Ecological Systems. Annu. Rev. Ecol. Syst. 4, 1–23.

Hood, S.M., Varner, J.M., Van Mantgem, P., Cansler, C.A., 2018. Fire and tree death: Understanding and improving modeling of fire-induced tree mortality. Environ. Res. Lett. 13. https://doi.org/10.1088/1748-9326/aae934

Huang, C. ying, Anderegg, W.R.L., Asner, G.P., 2019. Remote sensing of forest die-off in the Anthropocene: From plant ecophysiology to canopy structure. Remote Sens. Environ. 231, 111233. https://doi.org/10.1016/j.rse.2019.111233

Ince, J., 2023. California ' s Snowpack is Now One of the Largest Ever , Bringing Drought Relief , Flooding Concerns [WWW Document]. Calif. Dep. Water Resour. URL https://water.ca.gov/News/News-Releases/2023/April-23/Snow-Survey-April-2023 (accessed 4.5.23).

Jeronimo, S.A.M., 2018. Restoring forest resilience in the Sierra Nevada mixed-conifer zone, with a focus on measuring spatial patterns of trees using airborne lidar. University of Washington.

Jeronimo, S.M.A., Kane, V.R., Churchill, D.J., McGaughey, R.J., Franklin, J.F., 2018. Applying LiDAR individual tree detection to management of structurally diverse forest landscapes. J. For. 116, 336–346. https://doi.org/10.1093/jofore/fvy023

Jiao, W., Wang, L., McCabe, M.F., 2021. Multi-sensor remote sensing for drought characterization: current status, opportunities and a roadmap for the future. Remote Sens. Environ. 256, 112313. https://doi.org/10.1016/j.rse.2021.112313

Kane, V.R., Bartl-Geller, B.N., North, M.P., Kane, J.T., Lydersen, J.M., Jeronimo, S.M.A., Collins, B.M., Monika Moskal, L., 2019. First-entry wildfires can create opening and tree clump patterns characteristic of resilient forests. For. Ecol. Manage. 454, 117659. https://doi.org/10.1016/j.foreco.2019.117659

Kangas, A., Räty, M., Korhonen, K.T., Vauhkonen, J., Packalen, T., 2019. Catering information needs from global to local scales-potential and challenges with national forest inventories. Forests 10, 1–17. https://doi.org/10.3390/f10090800

Kennedy, R.E., Ohmann, J., Gregory, M., Roberts, H., Yang, Z., Bell, D.M., Kane, V., Hughes, M.J., Cohen, W.B., Powell, S., Neeti, N., Larrue, T., Hooper, S., Kane, J., Miller, D.L., Perkins, J., Braaten, J., Seidl, R., Braaten, J., Hooper, S., Neeti, N., Gregory, M., Kane, J., Ohmann, J., Bell, D.M., Cohen, W.B., Powell, S., Roberts, H., Larrue, T., Kennedy, R.E., Yang, Z., Perkins, J., Hughes, M.J., 2017. An empirical, integrated forest biomass monitoring system. Environ. Res. Lett. 13, 025004. https://doi.org/10.1088/1748-9326/aa9d9e

Koontz, M.J., Latimer, A.M., Mortenson, L.A., Fettig, C.J., North, M.P., 2021. Cross-scale interaction of host tree size and climatic water deficit governs bark beetle-induced tree mortality. Nat. Commun. 12, 1–13. https://doi.org/10.1038/s41467-020-20455-y

Krause, K., Goulden, T., 2015. NEON L0-TO-L1 DISCRETE RETURN LiDAR ALGORITHM THEORETICAL BASIS DOCUMENT (ATBD) PREPARED BY.

Krofcheck, D.J., Hurteau, M.D., Scheller, R.M., Loudermilk, E.L., 2017. Restoring surface fire stabilizes forest carbon under extreme fire weather in the Sierra Nevada. Ecosphere 8. https://doi.org/10.1002/ecs2.1663

Kuhn, M., Wickham, H., 2020. Tidymodels: a collection for modeling and machine learning using tidyverse principles.

Lines, E.R., Fischer, F.J., Owen, H.J.F., Jucker, T., 2022. The shape of trees: Reimagining forest ecology in three dimensions with remote sensing. J. Ecol. 110, 1730–1745. https://doi.org/10.1111/1365-2745.13944

Lutz, J.A., Larson, A.J., Swanson, M.E., 2018. Advancing fire science with large forest plots and a long-term multidisciplinary approach. Fire 1, 1–7. https://doi.org/10.3390/fire1010005

Lutz, J.A., Wagtendonk, J.W. Van, Thode, A.E., Miller, J.D., 2009. Snowpack , Lightning Ignitions , and Fire Severity in Yosemite National Park Research Scope and Rationale. Int. J. Wildl. Fire 18, 765–774.

McDowell, N.G., Michaletz, S.T., Bennett, K.E., Solander, K.C., Xu, C., Maxwell, R.M., Middleton, R.S., 2018. Predicting Chronic Climate-Driven Disturbances and Their Mitigation. Trends Ecol. Evol. 33, 15–27. https://doi.org/10.1016/j.tree.2017.10.002

Millar, C.I., Stephenson, N.L., 2015. Temperate forest health in an era of emerging megadisturbance. Science (80-.). 349, 823–826. https://doi.org/10.1126/science.aaa9933

Mueller, S.E., Thode, A.E., Margolis, E.Q., Yocom, L.L., Young, J.D., Iniguez, J.M., 2020. Climate relationships with increasing wildfire in the southwestern US from 1984 to 2015. For. Ecol. Manage. 460, 117861. https://doi.org/10.1016/j.foreco.2019.117861

Näsi, R., Honkavaara, E., Lyytikäinen-Saarenmaa, P., Blomqvist, M., Litkey, P., Hakala, T., Viljanen, N., Kantola, T., Tanhuanpää, T., Holopainen, M., 2015. Using UAV-based photogrammetry and hyperspectral imaging for mapping bark beetle damage at tree-level. Remote Sens. 7, 15467–15493. https://doi.org/10.3390/rs71115467

North, M., Oakley, B., Chen, J., Erickson, H., Gray, A., Izzo, A., Schowalter, T., 2002. Vegetation and ecological characteristics of mixed conifer and red fir forests at the teakettle experimental forest.

North, M.P., 2002. Vegetation and ecological characteristics of mixed-conifer and red fir forests at the Teakettle Experimental Forest.

North, M.P., Stevens, J.T., Greene, D.F., Coppoletta, M., Knapp, E.E., Latimer, A.M., Restaino, C.M., Tompkins, R.E., Welch, K.R., York, R.A., Young, D.J.N., Axelson, J.N., Buckley, T.N., Estes, B.L., Hager, R.N., Long, J.W., Meyer, M.D., Ostoja, S.M., Sa, H.D., Shive, K.L., Tubbesing, C.L., Vice, H., Walsh, D., Werner, C.M., Wyrsch, P., 2019. Tamm Review : Reforestation for resilience in dry western U . S . forests 432, 209–224. https://doi.org/10.1016/j.foreco.2018.09.007

Odland, M.C., Goodwin, M.J., Smithers, B. V., Hurteau, M.D., North, M.P., 2021. Plant community response to thinning and repeated fire in Sierra Nevada mixed-conifer forest understories. For. Ecol. Manage. 495, 119361. https://doi.org/10.1016/j.foreco.2021.119361

Odum, E. and G.W.B., 1971. Fundamentals of ecology. W B Saunders Co; 3rd edition (January 1, 1971).

Paul, T.S.H., Kimberley, M.O., Beets, P.N., 2019. Thinking outside the square: Evidence that plot shape and layout in forest inventories can bias estimates of stand metrics. Methods Ecol. Evol. 10, 381–388. https://doi.org/10.1111/2041-210X.13113

Paz-Kagan, T., Brodrick, P.G., Vaughn, N.R., Das, A.J., Stephenson, N.L., Nydick, K.R., Asner, G.P., 2017. What mediates tree mortality during drought in the southern Sierra Nevada? Ecol. Appl. 27, 2443–2457. https://doi.org/10.1002/eap.1620

Pile, L., Meyer, M., Rojas, R., Roe, O., Smith, M., 2019. Drought Impacts and Compounding Mortality on Forest Trees in the Southern Sierra Nevada. Forests 10, 237. https://doi.org/10.3390/f10030237

Polewski, P., Yao, W., Heurich, M., Krzystek, P., Stilla, U., 2015. Detection of single standing dead trees from aerial color infrared imagery by segmentation with shape and intensity priors. ISPRS Ann. Photogramm. Remote Sens. Spat. Inf. Sci. 2, 181–188. https://doi.org/10.5194/isprsannals-II-3-W4-181-2015

Restaino, C., Young, D.J.N., Estes, B., Gross, S., Wuenschel, A., Meyer, M., Safford, H., 2019. Forest structure and climate mediate drought-induced tree mortality in forests of the Sierra Nevada, USA. Ecol. Appl. 29, 1–14. https://doi.org/10.1002/eap.1902

Sousa, D., Davis, F.W., 2020. Scalable mapping and monitoring of Mediterranean-climate oak landscapes with temporal mixture models. Remote Sens. Environ. 247, 111937. https://doi.org/10.1016/j.rse.2020.111937

Stephens, S.L., Collins, B.M., Fettig, C.J., Finney, M.A., Hoffman, C.M., Knapp, E.E., North, M.P., Safford, H., Wayman, R.B., 2018. Drought, Tree Mortality, and Wildfire in Forests Adapted to Frequent Fire. Bioscience XX, 1–12. https://doi.org/10.1093/biosci/bix146

Stephenson, N.L., Das, A.J., 2020. Height-related changes in forest composition explain increasing tree mortality with height during an extreme drought. Nat. Commun. 11, 1–14. https://doi.org/10.1038/s41467-020-17213-5

Stephenson, N.L., Das, A.J., Ampersee, N.J., Cahill, K.G., Caprio, A.C., Sanders, J.E., Williams, A.P., 2017. Patterns and correlates of giant sequoia foliage dieback during California's 2012-2016 hotter drought. For. Ecol. Manage. 0–1. https://doi.org/10.1016/j.foreco.2017.10.053

Stevens-Rumann, C.S., Morgan, P., 2019. Tree regeneration following wildfires in the western US: a review. Fire Ecol. 15, 1–17. https://doi.org/10.1186/s42408-019-0032-1

Stewart, J.A.E., van Mantgem, P.J., Young, D.J.N., Shive, K.L., Preisler, H.K., Das, A.J., Stephenson, N.L., Keeley, J.E., Safford, H.D., Wright, M.C., Welch, K.R., Thorne, J.H., 2021. Effects of postfire climate and seed availability on postfire conifer regeneration. Ecol. Appl. 31, 1–14. https://doi.org/10.1002/eap.2280

Stovall, A.E.L., Shugart, H., Yang, X., 2019. Tree height explains mortality risk during an intense drought. Nat. Commun. 10, 1–6. https://doi.org/10.1038/s41467-019-12380-6

Swain, D.L., 2015. A tale of two California droughts: Lessons amidst record warmth and dryness in a region of complex physical and human geography. Geophys. Res. Lett. 42, 9999–10003. https://doi.org/10.1002/2015GL066628

Thorne, J.H., Choe, H., Stine, P.A., Chambers, J.C., Holguin, A., Kerr, A.C., Schwartz, M.W., 2017. Climate change vulnerability assessment of forests in the Southwest USA. Clim. Change 1–16. https://doi.org/10.1007/s10584-017-2010-4

Trumbore, S.; Brando, P.; Hartmann, H., 2015. Forest health and global change. Science (80-.). 349, 814–818.

United States Forest Service, Region 5, P.S.R., 2019. California 2018 Aerial Detection Survey.

Williams, A.P., Abatzoglou, J.T., Gershunov, A., Guzman-Morales, J., Bishop, D.A., Balch, J.K., Lettenmaier, D.P., 2019. Observed Impacts of Anthropogenic Climate Change on Wildfire

in California. Earth's Futur. 7, 892–910. https://doi.org/10.1029/2019EF001210

Wing, B.M., Ritchie, M.W., Boston, K., Cohen, W.B., Olsen, M.J., 2015. Individual snag detection using neighborhood attribute filtered airborne lidar data. Remote Sens. Environ. 163, 165–179. https://doi.org/10.1016/j.rse.2015.03.013

Winitsky, A.G., Meko, D.M., Taylor, A.H., Biondi, F., 2023. Species Sensitivity to Hydrologic Whiplash in The Tree-Ring Record of the High Sierra Nevada. Environ. - MDPI 10. https://doi.org/10.3390/environments10010012

Wright, M.C., van Mantgem, P., Stephenson, N.L., Das, A.J., Keeley, J.E., 2021. Seed production patterns of surviving Sierra Nevada conifers show minimal change following drought. For. Ecol. Manage. 480, 118598. https://doi.org/10.1016/j.foreco.2020.118598

Young, D.J.N., Meyer, M., Estes, B., Gross, S., Wuenschel, A., Restaino, C., Safford, H.D., 2020. Forest recovery following extreme drought in California, USA: natural patterns and effects of pre-drought management. Ecol. Appl. 30, 1–18. https://doi.org/10.1002/eap.2002

Young, D.J.N., Stevens, J.T., Earles, J.M., Moore, J., Ellis, A., Jirka, A.L., Latimer, A.M., 2017. Long-term climate and competition explain forest mortality patterns under extreme drought. Ecol. Lett. 20, 78–86. https://doi.org/10.1111/ele.12711

Yuan, Q., Shen, H., Li, T., Li, Z., Li, S., Jiang, Y., Xu, H., Tan, W., Yang, Q., Wang, J., Gao, J., Zhang, L., 2020. Deep learning in environmental remote sensing: Achievements and challenges. Remote Sens. Environ. 241, 111716. https://doi.org/10.1016/j.rse.2020.111716

Yun, Z., Zheng, G., Geng, Q., Monika Moskal, L., Wu, B., Gong, P., 2022. Dynamic stratification for vertical forest structure using aerial laser scanning over multiple spatial scales. Int. J. Appl. Earth Obs. Geoinf. 114, 103040. https://doi.org/10.1016/j.jag.2022.103040

Zhou, T., Popescu, S., Malambo, L., Zhao, K., Krause, K., 2018. From LiDARWaveforms to hyper point clouds: A novel data product to characterize vegetation structure. Remote Sens. 10, 1–23. https://doi.org/10.3390/rs10121949

Chapter Two: A TALE OF TWO FORESTS: DROUGHT WITNESSED BY FIELD AND LIDAR TREES

2.1 ABSTRACT

Drought-induced tree mortality has been examined with remotely sensed methods, yet, comparisons with field data are necessary to address uncertainty and bias. In this study, we asked what subset of the population of trees are remotely sensed trees detecting pre- and post-drought. In addition, we also examined if multi-band imagery and lidar can detect mortality trends consistent to in-situ data. Finally, we investigated the role of error and data age in biasing post-drought mortality and decay detection. We did so by comparing pre and post drought-induced tree mortality with bi-temporal lidar and field datasets in a fire excluded forest in the Sierra Nevada. Prior to and following the drought, we found that remotely sensed trees represented top-of-the-canopy trees, which are observable to the sensor and best segmented using our methods. On average, each of the pre- and post-drought remotely sensed tree canopies represented ~3 field trees. We also examined the lidar datasets for the presence and influence of error on mortality detection. In our study area, lidar segmentation errors such as commission and shadows from imagery can both over inflate and diminish mortality detection, respectively. Overall, pre- and post-drought remotely sensed trees accounted for 1/3 of all trees and ~2/3 of live and dead basal area. The pre-drought remotely sensed tree footprints of decayed trees proved useful for the detection of tree decay stages. We found significant differences in the detection of coarse woody debris and regeneration in the pre-drought lidar canopies than the post-drought data.

2.2 INTRODUCTION

Individual scale tree mortality information that better captures the structural nature of forest canopies such as height and canopy area is important for ecological and wildfire risk

analyses. From an ecological perspective, persistent drought, extensive tree mortality, and wildfires can interact and reshape forest canopy architecture and dampen ecological functions (Canelles et al., 2021; Earles et al., 2014; Millar and Stephenson, 2015; Wayman and Safford, 2021). Extensive mortality of large trees can reduce live, aboveground carbon storage (Earles et al., 2014; Voelker et al., 2019) and smaller tree mortality and regeneration failure may suppress new conspecific cohorts (Donato et al., 2016; Harvey et al., 2016; North et al., 2019). The 2012-2016 drought-induced mortality event in the Sierra yielded significant reductions in large and small trees throughout the range; however, scientists and mangers did not have a comprehensive understanding of the scale of individual tree mortality and the concomitant changes in live to dead basal area.

Past studies demonstrated the application of using combinations of high resolution airborne lidar and hyperspectral imagery to model drivers of individual, overstory tree mortality in the Sierra Nevada during the drought (Das et al., 2022; Fricker et al., 2019; Paz-Kagan et al., 2017). Importantly, there was concurrence that the normalized difference vegetation index (NDVI) was an important predictor of overstory tree mortality (Brodrick and Asner, 2017; Das et al., 2022), which can be derived from commonly available 4-band orthoimagery. These investigations also supported their model conclusions with field validated mortality information. However, these studies relied upon manual tree crown delineation to detect overstory tree mortality and did not account for individual tree size and basal area. Since manual tree crown delineation is infeasible to apply across broad extents, these methods have limited operational capacity for conducting ecoregional analyses. Further, Paz-Kagan et al., 2017 and Das et al., 2022 used proprietary datasets that are not publicly available. Finally, the convolutional neural network model of species and mortalty detection developed by Fricker et al., 2019 was tested on one flight line of remotely sensed lidar, hyperspectral and orthoimagery data; therefore, it is unknown whether such an approach could be operationally applicable.

The availability of multi-temporal, open source, high resolution remote sensing data products has rapidly increased in terms of spatial extent and resolution in California and the rest of the United States, which offer promise for creating datasets using automated methods (Jeronimo et al., 2018). For example, the US Geological Survey's 3D Elevation Program (Arundel et al., 2018) has expanded their high resolution airborne lidar collections in the United States, and the National Agricultural Inventory Program (USDA, 2023) collects 60 cm and less 4-band orthoimagery in each state on a biennial basis. In addition, The National Ecological Observatory Network (NEON) collects long-term field and airborne campaigns at several sites throughout the United States that leverage high resolution lidar, orthoimagery, and hyperspectral data (Leisso, 2016). The State of California recently acquired 4-band NAIP imagery at 15 cm resolution statewide. These data provide an important opportunity to capture overstory tree mortality and other forest canopy processes across broad ecoregional extents at the scale of overstory trees.

Forest managers and collaborative entities in the Sierra Nevada[2] are already assessing forest structure patterns and planning forest treatments at the scale of individual remotely sensed trees using operational, airborne lidar data and toolsets. Broadly, these operational tools rely on the approaches of (Jeronimo, 2018; Jeronimo et al., 2019; McGaughey, 2018a) and use computationally efficient methods to segment remotely sensed trees across entire acquisitions. Our goal is to provide managers and ecologists with detailed information regarding how these operational tools represent the mortality trends of field populations in the Sierra Nevada. In addition, we want to impart how error biases capturing mortality trends with these operational approaches.

[2] The Tahoe Central Sierra Initiative, Social and Ecological Resilience Across the Landscape in the Stanislaus National Forest, and the Southern Sierra All-lands Restoration and Resilience Program in California have all applied methods developed and in practice by the University of Washington, Forest Resilience Lab and described in (Jeronimo, 2018).

As remotely sensed methods become more frequently applied in research and management related to the study of individual trees (Duncanson and Dubayah, 2018; Hamraz et al., 2017; Hemming-Schroeder et al., 2023; Li et al., 2012; Stovall et al., 2019; Yang et al., 2019; Yun et al., 2022; Zhen et al., 2016), it is imperative to compare these data to ground based measurements for context (Das et al., 2022). Further, this type of assessment is important across the variety of vegetation community types, structural complexity, and climatic setting of tree ecosystems to ensure remotely sensed data are consistent in their representation of these ecosystems. In the absence of such information, assumptions may be present that remotely sensed trees directly represent individual trees on a one-to-one basis, which may only be true in limited settings such as single strata tree ecosystems (Huesca et al., 2021).

In this study, we aimed to improve the ability to predict, measure, and respond to extensive tree mortality in the conifer forests of California's Sierra Nevada. While identifying how remotely sensed trees represent field trees has been the subject of forest inventory assessments (Babcock et al., 2018), it is less common to directly compare remotely sensed to field trees for ecological studies (Das et al., 2022; Stephenson and Das, 2020; Zhen et al., 2016) responding to events such as droughts and fire. We developed remotely sensed trees by segmenting tree canopies from airborne lidar and combing the canopy segments with high resolution orthoimagery for mortality detection. We used the pre- and post-drought and tree mortality remotely sensed tree and field datasets to investigate these research questions:

1) What subset of the population of trees are remotely sensed trees detecting pre- and post-drought?

2) Can multi-band imagery and lidar intensity at 1m resolution be applied to detect pre-drought mortality trends consistent with field assessed mortality?

3) How does error and data age bias post-drought mortality and decay detection? How do remotely sensed tree datasets represent the post-drought mortality and decay trends of field trees?

In the first question, we hypothesized that remotely sensed trees represented the trees that remotely sensed data can detect during a drought event, the overstory trees. To research this

question, we modeled remotely sensed trees and then compared them to the tree population (i.e., “field” trees) on a one-to-one basis. We compared the in-situ and remotely sensed trees by comparing mean tree measurements with a focus of neighborhood relationships. We surmised that when forest structure is dense and multi-strata as our study area, subordinate in-situ trees will be poorly represented in terms of tree counts and mortality by remotely sensed trees.

In addition, we also hypothesized that errors of commission, which are produced during lidar segmentation to generate the remotely sensed trees, influenced the representation of the tree population. Therefore, we compared the remotely sensed and field trees with and without the errors of commission. Last, we also examined how drought mortality influenced the trends of the field and remotely sensed trees. To do so, only trees that were alive in 2018 were selected from the pre- and post-drought remotely sensed tree datasets. In addition, the pre-drought remotely sensed tree height and basal area values were excluded as these values reflected pre-drought conditions.

The hypothesis for the second question was multi-band imagery (>= 1m) and mean lidar intensity (0.75m) are sufficient to detect mortality trends of the tallest trees, but not trees <30m. We surmised that the orthorectification of the imagery to the ground and the 1m resolution of the imagery was inadequate to detect mortality in shorter height strata. If the remote sensing data was applied to detect mortality pre-drought, it would be the largest and tallest trees that were detected. We tested this hypothesis by comparing the manually classified, pre-drought remotely sensed trees to the field tree mortality trends.

The third research question addressed multiple hypotheses focused on post-drought mortality detection. First, we hypothesized that error from multiple sources reduced the mortality detection of remotely sensed trees, post-drought, compared to the field trends. We expected one of the main sources of error to be errors of commission associated with oversegementation of the tree canopy. Oversegmentation produced a main tree segment along with one or more

additional canopy segments. These errors were expected to be most significant in the post-drought collected lidar as the data have less pulse density per meter square than the pre-drought data. We also examined other sources of error related to the application of imagery for mortality detection including the presence of shadows and whether the crown view was on or off nadir.

Second, we hypothesized that remotely sensed trees collected pre-drought were more effective for mortality and decay detection of the entire tree mortality event compared to remotely sensed tree data collected two years post-drought. Since the pre-drought lidar segments included trees that were alive pre-drought but died during the tree mortality event, they were expected to be more effective for mortality and decay detection. For example, we expected the pre-drought segments combined with post-drought imagery to display more decay evidence such as logs, coarse woody debris, and emergent vegetation with coarse woody debris. The post-drought lidar segments were anticipated to capture fewer decayed trees. Decaying trees were frequently shorter stature, <=2m thus rendering them less likely to be segmented. If the data supported this hypothesis, older remotely sensed tree “footprints” may be useful for comparing how tree patterns change over time.

Finally, we compared the post-drought remotely sensed tree datasets to the field collected datasets to examine the representation of drought induced tree mortality. We hypothesized that both remotely sensed datasets well represented the mortality trends of the tallest trees, >30m.

In summary, our research goals were to describe which trees were best sampled by remotely sensed trees; how remotely sensed trees captured a tree mortality event over time; and propose a classification framework for tree mortality and decay. In this study, we examined datasets collected pre- and post-drought that varied in temporal and spatial resolution. We compared remotely sensed tree mortality information with field-based data to improve the application of remotely sensed surveys of tree mortality events.

2.3 METHODS

2.3.1 Study Area

The study area was composed of nine, four-hectare plots (Figure 2.1) of mature, multi-strata Sierran mixed-conifer forest in the Teakettle Experimental Forest (Allen, 2005; Goodwin et al., 2020) in the southern Sierra Nevada, California. The study area was selected because it was fire excluded and had minimal to no management onsite. These conditions allowed the examination of drought-induced tree mortality. The other criteria for site selection was the availability of concurrently collected, pre- and post-drought, field and remotely sensed tree mortality data. The field and lidar data were collected prior to and following California's 2012-2016 drought and tree mortality event (Fettig et al., 2019; Swain, 2015).

The nine unburned plots of the study area were the control plots for a long-term fire and fire surrogates study within the 1,300 hectare Teakettle Experimental Forest and met the study criteria (Goodwin et al., 2020; North et al., 2002). The Teakettle Experimental Forest is nested within the north fork of the Kings River watershed in the southern portion of the Ecoregion and

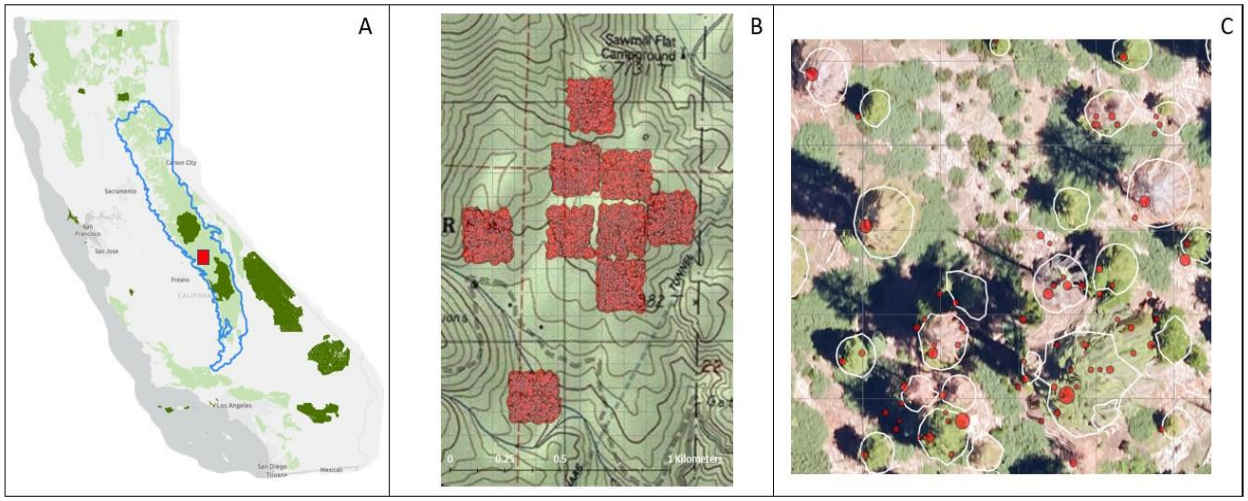

Figure 2.1. Study Area Figures. The Sierra Nevada Ecoregion (A) is a montane, conifer dominated region of California with a Mediterranean climate. The study area (B) is in the Teakettle Experimental Forest in the southern Sierra Nevada, which experienced significant tree mortality during California's first warm drought from 2012-2016. The study area includes nine field plots, each four hectares in area, that were stem mapped with tree measurements collected in 2011 and 2018. Airborne lidar was collected in 2010, which was used to segment trees (Jeronimo et al. 2018) using a watershed segmentation algorithm. Panel (C) shows remotely sensed tree segments as white with red circles representing the field trees from a zoomed in, aerial view of a portion of one of the nine field plots overtop 2018 NEON orthoimagery (Gallery, 2022).

was vegetated with late-seral, mixed Sierran conifer forests (Fry et al., 2014; Goodwin et al., 2020; North, 2002). The study area had a Mediterranean climate with warming and drought events characteristic of the Ecoregion (Asner et al., 2016; Diffenbaugh et al., 2015; Gibson et al., 2020; Swain, 2015). The elevation of the study area ranged from approximately 1,900 to 2,600 m, and annual temperature and precipitation vary from -3° to 25°C and 50 to 125cm, respectively (Goodwin et al., 2020; Krofcheck et al., 2017).

2.3.2 Remote Sensing and Field Data and Datasets for Analysis

2.3.2.1 Remote Sensing Data

Pre-drought, 2010 Airborne Lidar

Watershed Sciences Inc. (Sciences, 2011) collected airborne lidar (i.e., light detection and ranging) over the study area, in the summer of 2010, pre-drought, which was used to segment remotely sensed trees. Details regarding the acquisition are provided in Table 2.1.

Pre-drought, 2010 Airborne Orthoimagery

The 2010 National Agricultural Imagery Program (NAIP) (US Department of Agriculture, 2010), 4-band: 1.0m resolution orthoimagery was used to identify the mortality status of the pre-drought remotely sensed trees. The acquisition parameters are described in Table 2.1.

Post-drought, 2018 Airborne Lidar and Orthoimagery Collection

The National Ecological Observatory Network (NEON) acquired airborne lidar and high resolution RGB imagery, post drought, in the summer of 2018 across the study area (Gallery, 2022; Krause and Goulden, 2015). The lidar data were used to model the remotely sensed trees, and the imagery was examined to identify the mortality status and presence of errors of both the pre-drought and post-drought remotely sensed tree datasets. Acquisition details are provided in Table 2.1.

Table 2.1
Remote Sensing Acquisition Parameters including data type and vendor at the time of collection, time of acquisition, active or remote sensing sensor used to acquire data, acquisition parameters detailing how data was collected, and the geographic coordinate information of the acquisition.

Data Type & Vendor	Data acquisition	Sensor	Acquisition Parameters	Coordinate Information
Airborne lidar, Watershed Sciences Inc.	Pre-drought Summer 2010	Leica ALS50 Phase II sensors	8 pulses/m2, 83kHz 1100 to 1500m altitude Scan angle ±14° from nadir	NAD 83, NAVD88 geoid, Universal Transverse Mercator (UTM)
4-band orthoimagery, National Agricultural Imagery Program	Pre-drought Summer 2010	DMC (Intergraph) and ADS (Leica)	1m resolution 30% lateral overlap Orthorectified to digital elevation model	NAD83, UTM
RGB imagery, National Ecological Observatory Network (NEON)	Post-drought Summer 2018	Phase One D8900 and IXU-RS-1000	0.1m resolution 30 to 50% lateral overlap, 60% image overlap	ITRF00, UTM
Airborne lidar, NEON	Post-drought Summer 2018	Optech, Inc Gemini lidar sensor 12SEN311	≥4-6 pulses/m2 100khz	ITRF00, NAVD88, UTM

2.3.2.2 Field-based tree measurements, "field trees"

Field tree measurements used in this analysis were collected as part of the Teakettle Fire and Fire Surrogates Study and are further described in (Goodwin et al., 2020). Prior to the inception of the drought in the summers of 2011 and 2012, all field trees ≥5 cm in the nine plots (Figure 1) were stem mapped with a total station. Each tree was measured for longitude and

latitude (x, y) and elevation (z). The measurements were collected based on the location of a central, cardinal tree to ensure the relative position of trees to each other was consistent (North et al., 2007, 2004).

In 2018, the stem mapping tree measurements were repeated with a LTI Laser Technology Criterion 400 Survey Laser Meter/Rangefinder. The location of the trees was collected in the WGS84 datum and projected to the Universal Transverse Mercator (UTM), Zone 11N. The location measurements collected in 2011 were updated using linear regression, and the formula is described in Appendix A.

In addition to stem mapping, field trees were measured pre (2011-2012) and post-drought (2018) for: 1) diameter at breast height in cm (DBH), 2) identification to species, 3) mortality status (i.e., Alive/Dead) and decay status (Maser et al., 1979), and 4) agents of mortality (i.e., bark was examined for the presence or evidence of bark beetles such as *Dendroctonus* spp. or *Scolytus* spp).

Of the trees measured, five conifer species were present: *Abies concolor*, white fir; *Abies magnifica*, red fir; *Calocedrus decurrens*, California incense cedar; *Pinus jeffreyi*, Jeffrey pine; and *Pinus lambertiana*, sugar pine. Seventy-one oak trees (*Quercus* spp.) and 43 unidentified species were stem mapped; however, these trees were not measured for DBH and were not included in this study as height and canopy spread comparisons could not be ascertained.

Allometric equations

Total tree height and crown spread in meters were estimated for all conifer trees using the species specific allometric equations from (Jeronimo, 2015). For all unknown species that were measured for DBH, a general formula was applied to estimate height and crown spread, respectively. The allometric equations for height and crown spread are provided in Appendix A.

2.3.3 Data Processing & Classification

2.3.3.1 Remotely Sensed Tree Modeling/Segmentation

Jeronimo et al., 2018 described trees segmented from lidar as tree approximate objects. Generally, tree approximate objects represent one canopy tree plus zero to many subordinate canopy trees. We applied that definition of tree approximate objects here to mean a remotely sensed tree, and we also used the same methods to segment the pre-drought (2010 lidar) and post-drought (2018 lidar) trees (Jeronimo et al., 2018; McGaughey, 2018b).

We selected the watershed segmentation algorithm (Jeronimo et al., 2018; McGaughey, 2018b) from the FUSION package to model overstory trees for the pre- and post-drought lidar data. Although alternate lidar-derived tree modeling approaches can segment subordinate trees (Li et al., 2012; Yun et al., 2022), we selected the watershed segmentation algorithm as it was well tested for our forest type and area by co-author Jeronimo et al. 2018.

To create the remotely sensed trees, the US Forest Service's FUSION software package (McGaughey, 2018) was used to produce a canopy surface model (CSM) at 0.75 m resolution. Next, the FUSION's TreeSeg utility was applied to model individual trees from the CSM using a watershed transform algorithm to produce lidar derived trees within the 9 plots in the study area (Figure 2.2). The TreeSeg utility also produced a vector file format of lidar-based trees identified as individual polygons or segments delineating the fullest extent of the canopy. In addition, the TreeSeg utility provided an accompanying attribute table with location information (i.e., X and Y), tree height (i.e., as Z), and cross-sectional area.

The TreeSeg utility also produced a 0.75m resolution raster of the first returns of lidar intensity. We collected the lidar intensity information to support the identification of the mortality status of the pre-drought remotely sensed trees consistent to (Grulke et al., 2020; Huang et al., 2015; Roche et al., 2018).

2.3.3.2 Classifying Lidar-derived Tree Mortality & Lidar Errors

Pre-drought Mortality Status

The mortality status of the pre-drought remotely sensed trees was ascertained by the primary author by visually inspecting each remotely sensed tree with the 2010 lidar intensity, 2010 Normalized Differenced Vegetation Index (NDVI) values derived from the 2010 NAIP imagery, and the true color NAIP imagery. Table A.1 in Appendix A provides the rubric with visual examples used to label each of the pre-drought remotely sensed trees as live, dead, mixed, or other via photointerpretation. The class "Other" which essentially included the capture of boulders was added to the labeling using the 2018 NEON imagery. The mortality status of each of the pre-drought remotely sensed trees was conducted in ArcMap Pro, Version 2.8 ("ESRI ArcGIS Pro Version 2.8," 2021).

Post-drought Mortality Status, Error, and Imagery Alignment Classification

The mortality status of the combined and post-drought remotely sensed trees was also ascertained by the primary author using the 2018 NEON RGB imagery. Each of the remotely sensed trees was individually examined for mortality and decay status; the presence of lidar segmentation errors; and whether the imagery and remotely sensed tree were on nadir or displayed shadows according to the rubric in Table A.2, Appendix A. This process was also conducted using manual classification in ArcMap Pro, Version 2.8 ("ESRI ArcGIS Pro Version 2.8," 2021) in a similar approach to the pre-drought assessment.

2.3.3.3 Pre- and Post-Drought Remotely Sensed and Field Tree Datasets

In this study, a remotely sensed tree is defined as a tree canopy outline produced from segmenting airborne lidar and the orthoimagery used to examine the tree of interest through photogrammetry. Figure 2.2 illustrates an example of a remotely sensed tree where the lidar-derived canopy segment overtops the orthoimagery used to identify the mortality status. This study involved the comparison of multiple pre- and post-drought, field and remote sensing tree datasets to carry out the research questions (Figure 2.3).

Figure 2.2. Example of a remotely sensed tree with canopy segment derived from lidar and orthoimagery.

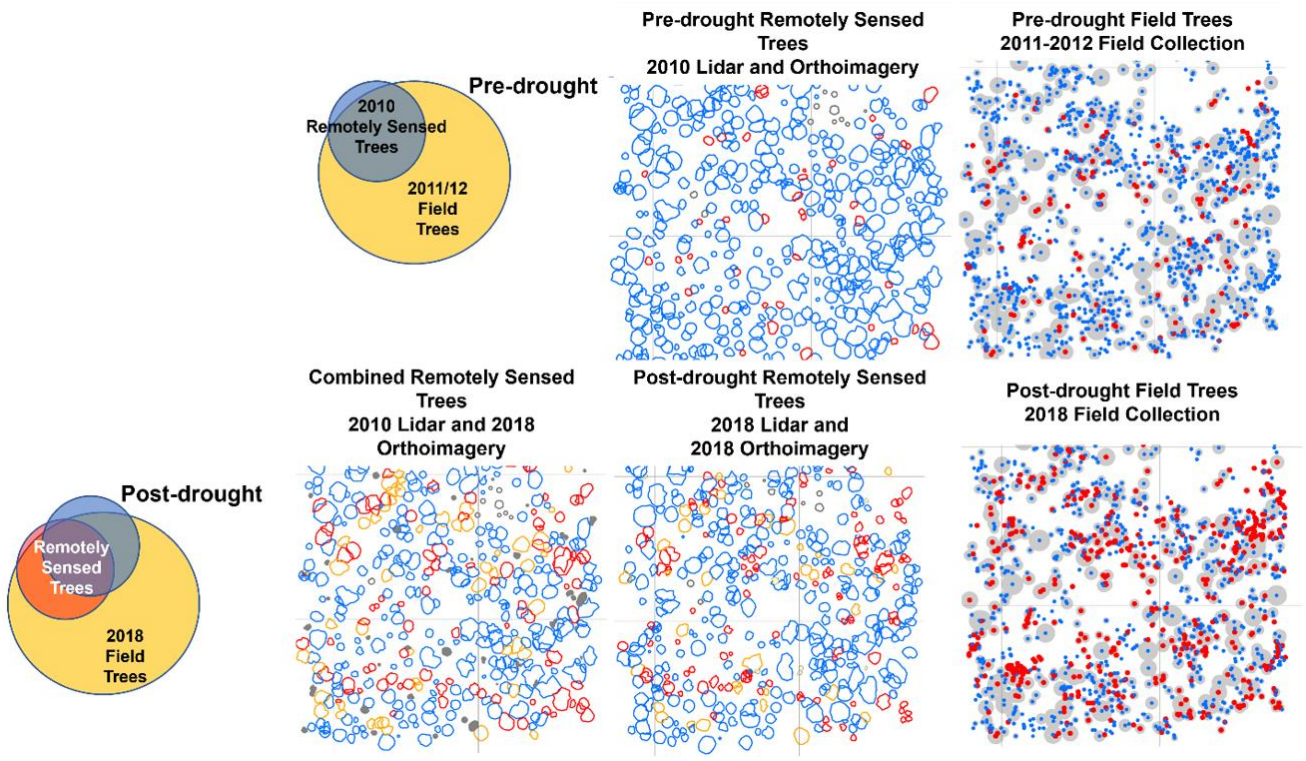

Figure 2.3. Pre- and Post-drought remotely sensed tree and field (in-siu) tree datasets.

While the field data were collected pre and post drought to create two distinct field datasets, three different datasets of remotely sensed trees were produced from fusing the lidar and orthoimagery. First, the pre-drought remotely sensed tree dataset was developed, which included the 2010 lidar trees combined with the 2010 NAIP data. The "combined" remotely sensed tree dataset was produced by fusing the 2010 lidar trees with the 2018 imagery. Finally, the post-drought remotely sensed tree dataset was created using airborne lidar and orthoimagery collected in 2018. These datasets are used to address different research questions throughout this study, and the dataset names will be specifically called out as pre-drought, combined, or post-drought remotely sensed data, as necessary.

2.3.4 Analysis

2.3.4.1 Question 1: What subset of the population of trees are remotely sensed trees detecting pre- and post-drought?

We compared the pre- and post-drought trends of remotely sensed and field trees by examining tree counts, height, basal area, number of neighbors, and distance to neighbors. Our

goal was to describe whether remotely sensed trees represented field trees on a one-to-one basis or one larger tree and one or more subordinate trees, pre and post drought. In addition, we evaluated these comparisons using the datasets with and without the presence of errors of commission.

Pre-drought

The pre-drought remotely sensed tree dataset were prepared for analysis by removing errors of commission (i.e., errors of commission are described in Table A.2, Appendix A). Lidar segmentation yielded errors of commission and omission. However, it is the errors of commission that were involved in oversegmented canopies or segmentation of a boulder that could be quantified and compared. The additional canopy segments and boulders were removed from the dataset. Further, any remotely sensed tree identified as a boulder that did not show the presence of a tree in the imagery was also removed.

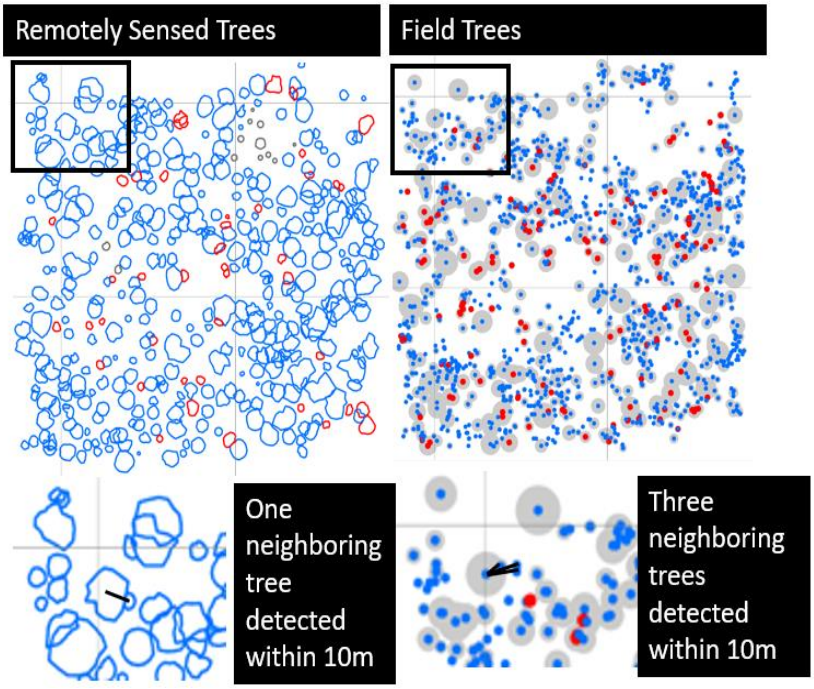

Figure 1.4. Remotely Sensed and Field-based Tree Neighborhoods. We will measure the number of tree neighbors, heights, and calculate mean distance to neighbors of both the remotely sensed and field trees. Above, the remotely sensed tree on the left shows one neighbor within 10m while the field tree on the right shows three neighbors within 10m. We expect the large number of tree clumps to obscure tree mortality capture

After the errors of commission were removed, the mean and standard deviation values for height (m), number of neighbors within 10m for <=30 individuals, and distance to neighbors (m) were calculated. To identify all neighbors and distance to neighbors of the remotely sensed and field trees, the Generate Near Tool in ArcGIS Pro ("ESRI ArcGIS Pro Version 2.8," 2021) was applied and measurements were captured in meters.

All neighbors within a 10m radius for ≤ 30 neighbors were identified and associated with each remotely sensed and field tree. The mean number of field trees that were “hiding” beneath the canopy of a remotely sensed tree were also assessed. To do so, a one-to-many Spatial Join in ArcGIS Pro was applied to identify the field trees associated with each remotely sensed tree canopy. For the Spatial Join, all live and dead field trees were selected.

Basal area was treated separately from the other metrics in terms of errors of commission involving oversegmented canopies. The basal area of all live and dead trees was calculated with and without the errors of commission.

Post-drought

For the post-drought analysis, the field tree dataset as well as the combined remotely sensed tree and post-drought remotely sensed tree datasets (Figure 2.2) was compared. To do so, only trees that survived the drought were selected from the remote sensed and field tree datasets. Afterwards, all the steps and metrics generated for the pre-drought assessment were repeated. However, the 2010 remotely sensed tree height and basal area values were excluded as these values reflected pre-drought conditions.

Statistical Analysis

To compare the frequencies between the pre- and post-drought datasets for all metrics, two-sided t-tests will be performed and differences in means will be examined with ANOVA.

2.3.4.2 Question 2: Can multi-band imagery and lidar intensity at 1m resolution be applied to detect pre-drought mortality trends consistent with field assessed mortality?

We hypothesized that 4-band imagery, 1m resolution, and lidar intensity, 0.75m resolution, applied to classify the mortality status of pre-drought trees produced consistent trends to the tallest field trees (>30m). To investigate this question, we compared the pre-drought mortality trends of the remotely sensed and field trees in terms of frequencies and basal area by three height classes (0 to 10m, 10m to 30m, and +30m).

Statistical Analysis

The Chi-square goodness of fit test was performed to examine the differences between counts of dead remotely sensed and field trees.

2.3.4.3 Question 3: How does error and data age bias post-drought mortality and decay detection? How do remotely sensed tree datasets represent the post-drought mortality and decay trends of field trees?

How does error and data age bias post-drought mortality and decay detection?

We hypothesized that the errors associated with capturing remotely sensed tree information influenced the representation of post-drought mortality trends compared to the field trees. Specifically, the influence of errors of commission and omission associated with lidar segmentation, shadows in imagery, and imagery alignment on post-drought induced tree mortality and decay were evaluated and compared between the combined and post-drought remotely sensed tree datasets. To test this hypothesis, the frequencies and basal area of the errors by mortality and decay classes were examined by height strata (0 to 10m, 10 to 30m, and +30m).

Can pre-drought remotely sensed trees detect tree decay?

We also hypothesized that data age (i.e., when the data were collected) influenced the mortality and decay patterns captured by remotely sensed trees. The combined dataset included airborne lidar that was collected pre-drought in 2010, and the post-drought dataset that included lidar collected post-drought in 2018. This hypothesis was examined by evaluating differences in frequencies of the mortality and decay classes between these two datasets by height strata (0 to 10m, 10 to 30m, and +30m).

Statistical Analysis

The proportions and Chi-square tests was conducted to ascertain if differences between the combined and post-drought remotely sensed tree datasets were statistically significant.

How do remotely sensed tree datasets represent the post-drought mortality and decay trends of field trees?

The combined and post-drought remotely sensed tree mortality datasets were hypothesized to represent the field tree mortality trends of the tallest trees. This hypothesis was tested by comparing the frequencies and basal area of mortality between the remotely sensed and field datasets by height strata (0 to 10m, 10 to 30m, and +30m). These data were compared with and without the presence of errors of commission involving additional lidar canopy segments.

Statistical Analysis

T-tests were applied to test for differences in the post-drought basal area metrics, and the proportions tests was used to examine differences in frequencies between the remotely sensed and field tree datasets.

2.3.5 Computing Environment

All comparisons of remotely sensed to field trees were conducted in the R computing environment (version 4.2.2) with RStudio (version2022.07.2+576) accept where noted. Base r and tidymodels (1.0.0) infer package (1.0.4) were applied to conduct descriptive and basic statistical tests to compare frequencies and proportions tests (Chi-square), group means (T-test and analysis of variance (ANOVA), respectively.

2.4 RESULTS

2.4.1 Question 1: What subset of the population of trees are remotely sensed trees detecting pre- and post-drought?

We analyzed how remotely sensed trees represented field trees and their associated mortality trends prior to and following a tree mortality event (Table 2.2).

Table 2.2

How remotely sensed trees compare to field trees. Remotely sensed or field tree type, number of lidar or field trees (n), mean height (MH), standard deviation of height (StH), total cumulative basal area, mean field trees intercepted pre-drought (MTPr), mean field trees intercepted, post-drought (MTPo), mean number of neighbors (MNN), standard deviation of neighbors (StN), mean distance to neighbors (MDN), standard deviation of neighbor distance (StDN). All additional segments produced from oversegementation were removed prior to analysis.

1) Mean height for field trees is based on the estimated heights acquired from the allometric equations applied based on the taxonomic status. 2) Remotely sensed trees-RSE

*p-value <0.05 **p-value <0.005 ***p-value<0.0005

Summary of Field and Remotely sensed tree Values

Type	n	MH[1] (m)	StH (m)	Total Basal Area (m^2)	MTPr	MTPo	MNN	StN	MDN	StDN
Pre-drought Live and Dead Trees*										
RSE[2]	3,066	23.9	16.7	1,899.7	2.1	NA	7.1	3.0	5.1	1.2
Field Trees	9,780	15.5	13.0	1,850	NA	NA	13.9	8.2	5.9	1.3
t-test statistic		27.5 ***			-2.39 *		-66 ***		-28.4 ***	
Post-drought, Trees Alive in 2018*										
Combined RSE[2]	2,053	NA	NA	NA	NA	2.0	5.0	2.5	5.0	1.6
Field Trees	6,047	15.6	11.8	1,527	NA	NA	8.6	5.8	5.8	1.8
Post-drought RSE[2]	2,165	24.6	15.8	1,343	NA	2.0	5.2	2.6	5.0	1.6
ANOVA statistic		30.2 ***					763 ***		464 ***	

Specifically, Table 2.2 includes the comparison of the pre-drought live and dead field and remotely sensed trees. In contrast, the post-drought values represent the surviving field and remotely sensed trees datasets.

All metrics were reported without the additional segments produced as errors of commission except for basal area. The basal area values were estimated with and without the additional canopy segments for all the remotely sensed datasets. The pre-drought basal area with the additional canopy segments was 2,223 m^2, which was larger than the pre-drought field tree basal area by 373 $m.^2$ The post-drought remotely sensed tree dataset overestimated the surviving tree basal area with the additional segments by 352 m^2 at 1,879 m^2 compared to underestimating live basal area by -184 m^2 without the additional segments when compared to the field trees (Table 2.2).

2.4.2 Question 2: How do the pre-drought mortality trends of remotely sensed trees differ from field trees?

Pre-drought mortality was compared between the lidar and the field trees. Overall, the pre-drought mortality of the remotely sensed trees poorly represented the field tree mortality (Figure 2.5). The number of dead remotely sensed trees identified with the lidar intensity and NAIP NDVI data was one-third of the proportion of field trees in each of the height class (0 to 10m, 10 to 30 m, and +30m), respectively. In addition, the pre-drought remotely sensed trees also poorly represented the basal area across all height classes (Appendix A, Figure A.1).

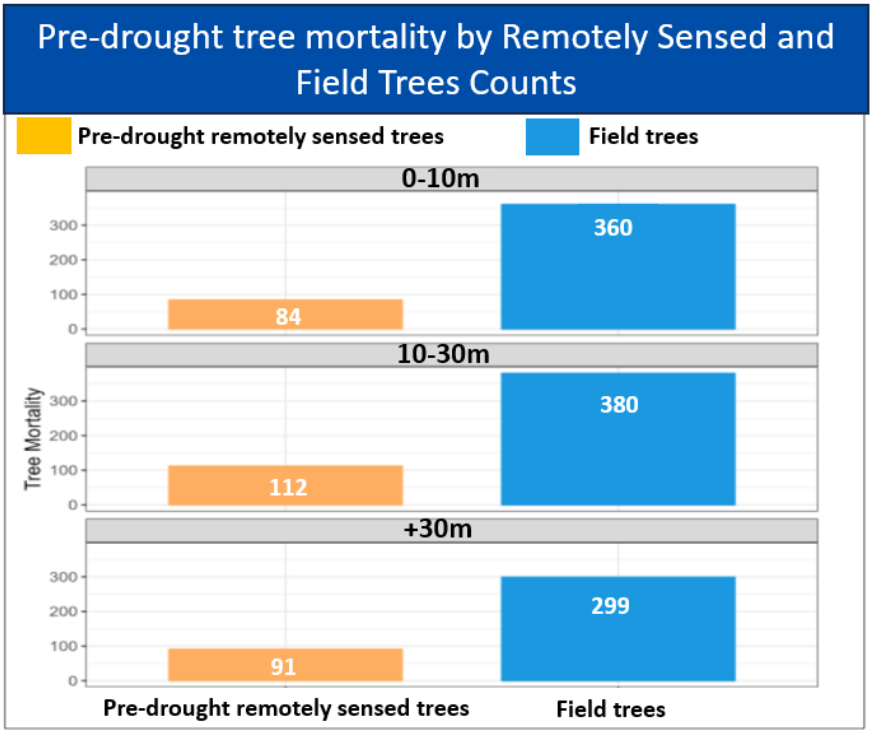

Figure 2.5. Number of pre-drought remotely sensed trees and field trees identified as dead per height strata, chi-square statistic of 7.6, one degree of freedom, and p-value=0.006.

2.4.3 Question 3: How does error and data age bias post-drought mortality and decay detection? How does error bias mortality detection?

The influence of error associated with lidar tree segmentation and imagery were evaluated in both remotely sensed tree datasets (i.e., the combined (2010 lidar tree) and post-drought remotely sensed tree datasets (2018 lidar tree)) by examining the post-drought imagery. Multiple sources of error were considered including lidar segmentation, shadows, and imagery alignment (Appendix A, Figure A.2). First, the errors of commission and omission associated with lidar segmentation were evaluated. The Chi-square goodness of fit test confirmed that the errors of

commission involving oversegementation and omission of trees were different between the remotely sensed trees groups, X-squared = 327.52, df = 2, p-value < 2.2e-16. Despite these differences, both remotely sensed trees groups had 66% of segments with no visible evidence of lidar segmentation errors.

The post-drought remotely sensed trees were expected to have more errors of commission due to the lower lidar pulse density of the data collection, which can yield commission errors involving the tree canopy during lidar segmentation (Figure 2.6 and Appendix A, Figure A.3). The distribution of errors of commission between the remotely sensed trees by live and dead status is depicted in (Appendix A, Figure A.3). Figure A.3 in Appendix A shows that the post-drought (i.e., 2018 lidar trees) remotely sensed trees had the greatest number of oversegementation errors, and these errors were most common in live trees. Additionally, the proportions test supported these differences, test statistic of 246, df=2, and p-value= 4.35e-54.

The frequency of errors of commission that involved the detection of boulders was also compared. The overall rate of detection of the boulders was low (Figure 2.6); however, the combined remotely sensed trees contained 66 boulders and the post-drought remotely sensed trees had seven, which represents <1%.

Of the trees that died during the drought, the combined remotely sensed trees showed a 4-fold increase in errors of omission compared to the post-drought remotely sensed trees (Figure 2.6 and Appendix A, Figure A.4). The proportions test also supported this difference; the test statistic was 178, df=1, and a p-value=1.38e-40. Although the combined remotely sensed trees were identified as having greater errors of omission, this status was applied using post-drought imagery. Many of the errors of omission may not be true errors. Instead, they may be a product of the remotely sensed trees revealing subordinate vegetation in place of a dominant tree that died. However, this theory cannot be tested as the pre-drought imagery did not provide the spatial resolution to examine errors of omission.

Both remotely sensed tree datasets were also assessed for whether the imagery alignment was on nadir, Table A.2, Appendix A. Of all remotely sensed trees, imagery alignment or “on nadir” was 71% for combined remotely sensed trees and 76% for post-drought remotely sensed trees. The proportions test was conducted to evaluate whether the combined and post-drought remotely sensed trees had consistent proportions of imagery in alignment. The test statistic was 839 with df=2 and a p-value of 5.36e-183, which demonstrates these proportions were not consistent between these two groups. These differences may be attributed to the lidar and imagery data being collected in different geographic datums.

Finally, the role of shadows was evaluated for reducing tree mortality detection, and the influence was most pronounced in the shortest of trees (Figure 2.6). Shadows obscured the view of four percent of the combined remotely sensed trees in the 0 to 10m height class and three percent of the post-drought remotely sensed trees, respectively. This number is not insignificant as detecting mortality of trees <10m is the most represented of all the height classes. The proportions test did indicate that the combined and post-drought remotely sensed trees were

different in terms of shadowing. The test statistic was 4.48, with df=1 and a p-value of 0.03 for the two-sided test.

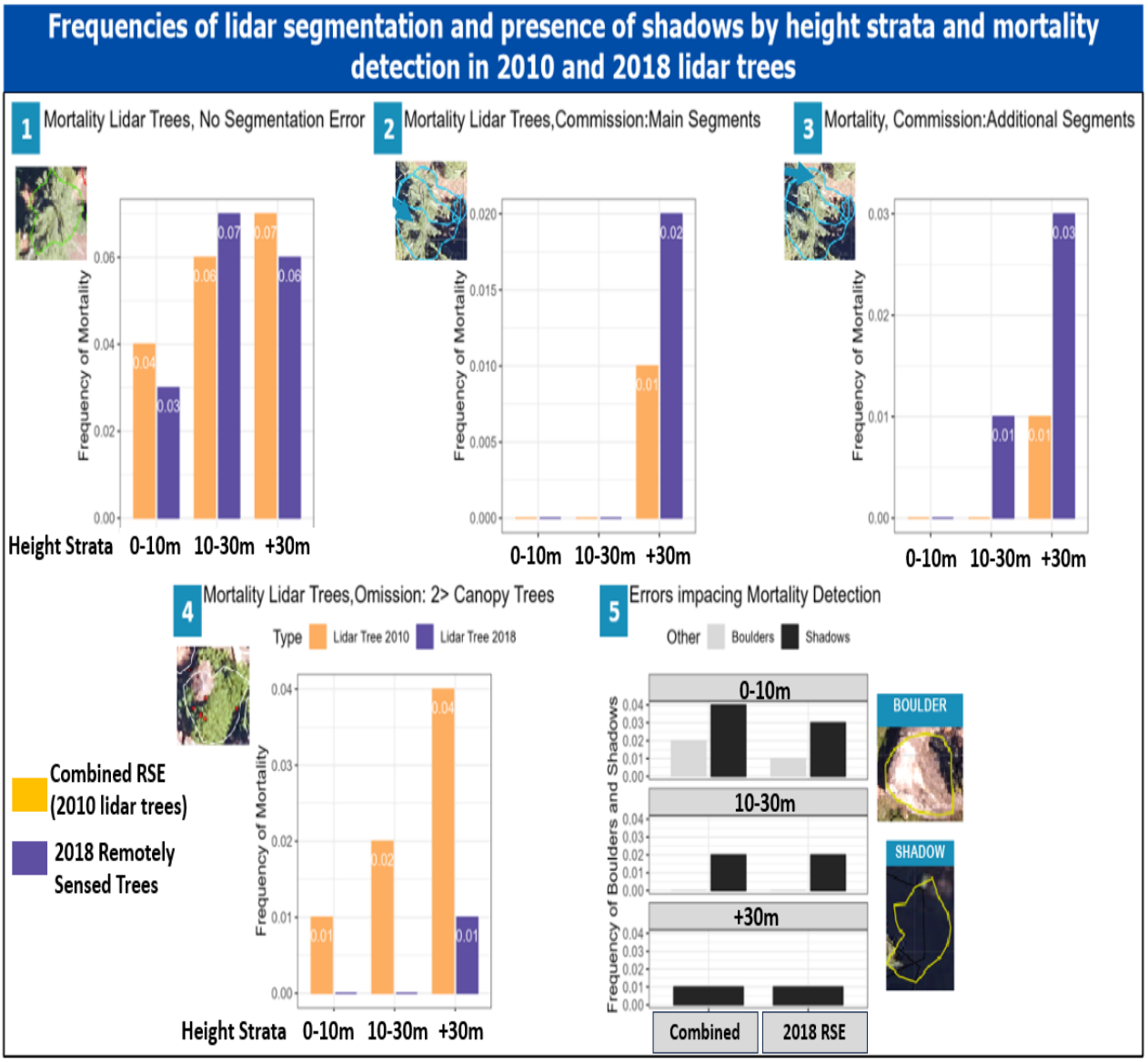

Figure 2.6. Frequencies of lidar segmentation errors and other error sources. This graph displays the frequency of post-drought mortality by height strata (0 to 10m, 10 to 30m, and +30m) of combined and post-drought remotely sensed trees by remotely sensed tree segments that appeared free of segmentation errors;2) displays the frequency of post-drought mortality by height strata of combined and post-drought remotely sensed trees of the main segments (errors of commission); 3) displays the frequency of post-drought mortality by height strata of combined and post-drought remotely sensed trees of the additional segments;4) displays the frequency of post-drought mortality by height strata of combined and post-drought remotely sensed trees based on errors of omission of trees; and 5) displays the frequency boulders and shadows of the combined and post-drought remotely sensed trees as these errors can impact mortality detection.

Can pre-drought remotely sensed trees (data age) aid in detecting tree mortality and decay?

Figure 2.7 depicts the comparison that illustrates only the combined remotely sensed tree dataset captured tree decay following the snag stage across all height classes. The proportions test revealed significant differences between the pre- and post-drought remotely sensed tree mortality classes with a test statistic of 173, df=6, and p-value of 9.57e-35.

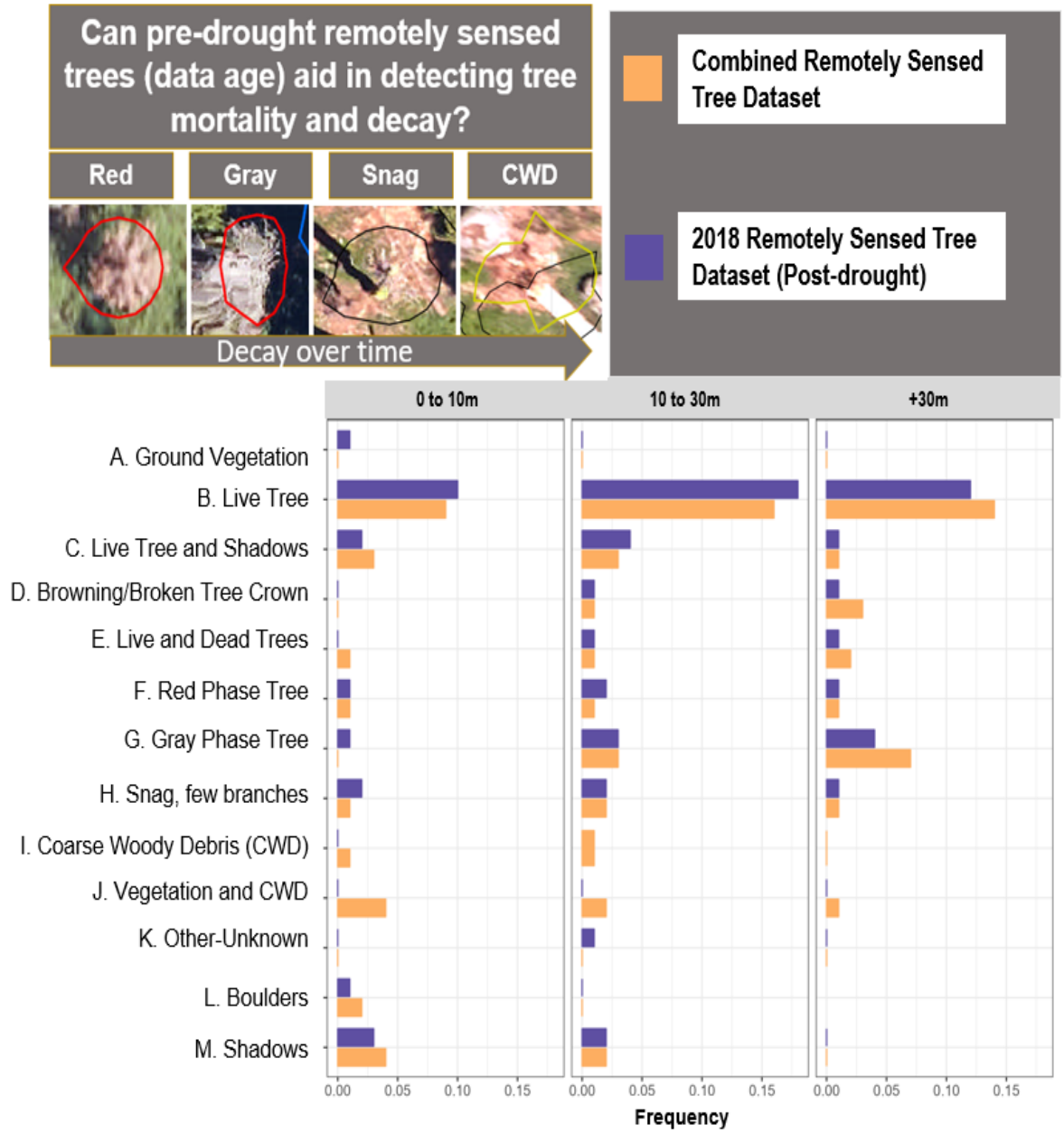

Figure 2.7. Comparing the ability of remotely sensed trees to capture tree mortality and decay. Dead and decay proportions of combined and post-drought remotely sensed trees as identified in the 2018 NEON, post-drought imagery. The class descriptions and rubric are described in Table A.2, Appendix A.

How do remotely sensed trees collected pre- and post-drought detect tree mortality compared to field tree trends?

The post-drought frequencies of dead tree counts and basal area of both remotely sensed tree datasets were compared to the field trees (Figure 2.8). The comparisons were made with and without errors of commission (i.e., additional canopy segments). The presence of additional segments most influenced the post-drought remotely sensed tree dataset, and this dataset was captured with poorer resolution lidar data. Without the lidar segmentation errors, the combined remotely sensed data better represented the numbers of trees present than the post-drought data. Overall, the representation of dead tree counts precipitously increases with tree height

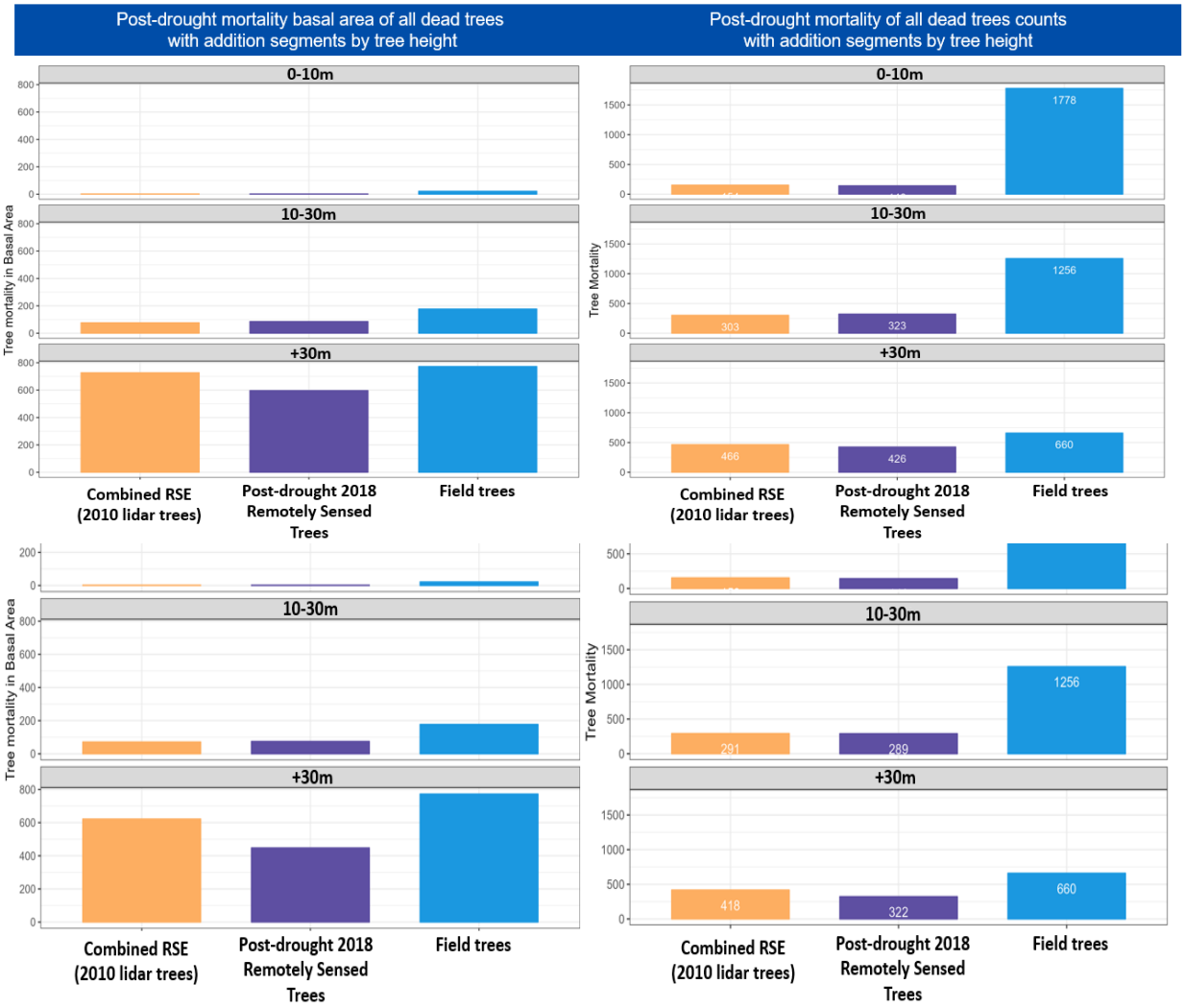

Figure 2.8. Post-drought basal area and tree counts with and without addition segments by height strata for the combined, post-drought remotely sensed trees and field trees. The top two graphs represent tree mortality by basal area and tree frequencies for the combined and post-drought remotely sensed trees and the field trees. The bottom two graphs capture the same measurements; however, the additional

(Figure 2.8) In terms of basal area, the additional segments produced from lidar segmentation error did support capturing >70% of the dead basal area. The tallest dead trees represented most of the dead basal area, which the remotely sensed trees represented.

2.5 DISCUSSION

In this study, we examined how pre- and post-drought remotely sensed tree datasets that were produced using high resolution lidar and imagery represented in-situ or field trees. In addition, we addressed the role of spatial resolution, error, and data age to represent tree mortality trends. Our findings support the importance of testing and field validation (Babcock et al., 2015; Fassnacht et al., 2016; Murray et al., 2019) in the application of remotely sensed tree assessment approaches (Lines et al., 2022). Testing is especially important in novel forest types under a variety of forest structure conditions and in response to perturbations. As remotely sensed tree datasets increase in availability, it is necessary to evaluate the effectiveness of representing forest ecosystem diversity in response to ecological and environmental changes.

Question 1: What subset of the population of trees are remotely sensed trees detecting pre- and post-drought?

In this study area, the local forest structure was influential in determining whether a field tree was detected and represented as a remotely sensed tree (Table 2.2). Smaller stature trees were overwhelmingly more numerous, but they were not evenly dispersed. Instead, they were close in proximity to tall, dominant trees and were hidden in the canopy of the larger trees .This outcome suggests that single strata forests surveyed with high resolution remote sensing may better reflect population trends assuming a minimum tree size threshold and relevant imaging for the respective phenomenon (Huesca et al., 2021). Dense, multi-strata forests such as Teakettle can belie population trends such as mortality when the smallest and most numerous trees die and remain hidden from view. Two mechanisms explain why these smaller dead trees may remain hidden. First, nearby shorter stature and dominant trees may be subject to errors of omission during tree segmentation, and second, shadows cast by larger trees can occlude mortality detection in imagery (Arkin et al., 2023; Huemmrich, 1996; Polewski et al., 2015).

In contrast, we expect that tree mortality will be overrepresented in multi-strata forests when mortality favors dominant or tall trees, which were well captured by remote sensing. For example, the ponderosa pine forests of the lower elevations of the Sierra were reported to have higher incidence of tall *Pinus* mortality at the drought's inception, which were well captured by remotely sensed data (Fettig et al., 2019; Stephenson and Das, 2020; Stovall et al., 2019). Since tree mortality is highly dependent upon species and host tree selection during a drought or wildfire, field assessments are important for validating any trends exclusively captured by remotely sensed data with similar automated individual tree detection methods to our study (Casas et al., 2016; Hemming-Schroeder et al., 2023; Ma, 2018; Murray et al., 2019; Stovall et al., 2019). New methods for detecting smaller trees in the understory are available (Yun et al., 2022). However, it is important to test and empirically validate any approaches in different vegetation types and against events that can elicit significant changes in mortality and forest canopy architecture (Murray et al., 2019).

In summary, the numbers of pre- and post-drought field trees outnumbered all remotely sensed tree datasets by an average of 3:1. Pre- and post-drought remotely sensed trees reflected the trends of the top-of-the-canopy field trees. In other words, the remotely sensed trees represented the dominant field trees that were visible to the lidar and camera sensors regardless of being tall or short. However, most top-of-the-canopy trees were very tall in the study area, >30m, which biased the representation of remotely sensed trees to the tallest or dominant field trees. This trend was also supported by the basal area measurements. Despite remotely sensed trees representing a third of the field trees, the basal area measurements were in the range of the field tree basal area with or without errors of commission from lidar segmentation (i.e., the additional lidar segments).

Question *2: How do the pre-drought mortality trends of remotely sensed trees differ from field trees?*

Although pre-drought airborne imagery and lidar intensity were available for evaluation of mortality detection in the remotely sensed trees, the frequency of mortality detection in this study was poor in comparison to the field data prior to the drought. We expected detection to be greater in the tallest height strata as these trees often have large, visible canopies, which were observable by the sensors. Since the same methods for mortality detection were successfully applied to the detection of post-drought remotely sensed tree mortality, we surmised that the lack of detection in the pre-drought remotely sensed trees was due to properties of the pre-drought imagery.

The pre-drought, 2010 NAIP orthoimagery used in this study was 4 band, which provided the ability to use both natural color and NDVI for crown mortality detection. However, several aspects of this imagery likely contributed to very limited mortality detection. The combination of the spatial resolution, relief displacement, and radial distortion (Campbell, James B., Wynne, 2011) of the imagery most likely contributed to poor mortality discrimination. Overall, we found using NAIP imagery that was orthorectified to the ground produced oblique views of the tree canopies, which made attempting to determine the presence of a tree canopy or it's mortality status very difficult. Further, differentiating between the ground and dead tree canopies was limited whether using true color, NDVI, or lidar intensity values for mortality detection. Another factor that likely reduced detection was the imagery and lidar data were collected in different coordinate systems, which yielded a shift in alignment between the canopy segments and imagery. Although the imagery was re-projected to the coordinate system of the lidar data, the mortality detection continued to yield poor detection.

We found more effective tree mortality detection with the higher resolution (0.1m), post-drought, NEON RGB imagery, which was orthorectified to reduce relief displacement, compared to the 1m, 4-band NAIP. In other words, the orthorectification of the higher resolution, post-drought imagery produced more nadir canopy views. These direct views of the top of the canopy condition allowed for accurate mortality detection. At first pass, our results using higher

resolution imagery to detect mortality seemed to contrast with the results of the Lodgepole pine (*P. contorta*) tree mortality classification study of Meddens et al., 2011. They aggregated 0.3 m imagery to 2.4 m resolution and experienced improved tree mortality crown classification (Meddens et al., 2011). Several explanations may explain the differences in mortality detection between this study and Meddens et al., 2011. First, more powerful machine and deep learning approaches are now available that aid in discriminating high-resolution imagery. Second, the differences in forest structure between the two study areas may have also influenced mortality detection with more coarse imagery. Although we do not know the exact forest structure present in the Meddens et al., 2021 study, generally lodgepole pine forests tend to be more densely packed due to their longer fire intervals than our study area. In our study area, tree clumps and gaps were present, and the needle cast covered gaps were challenging to discriminate from the trees.

Question 3: How does error and data age bias post-drought mortality and decay detection? How do remotely sensed tree datasets represent the post-drought mortality and decay trends of field trees?

How does error and data age bias post-drought mortality and decay detection?

We found the presence of error to be very important in influencing the detection of mortality by remotely sensed trees. Based on our methods and results, errors of commission and omission as well as shadows in imagery limited the number of in-situ tree capture and representation by a combined average of 10-15%. This influence is not trivial when on average we were only accounting for capturing a third of the tree mortality overall. Errors of commission such as oversegmentation of the large tree canopies exaggerated the numbers of remotely sensed trees. In addition, although these additional segments were tall, they can underrepresent the canopy size of dominant trees and minimize average tree biomass. However, even with the presence of errors of commission, the frequency of these errors did not produce overestimates of tree numbers.

In contrast, errors of omission can result in many trees being undetected, reducing tree counts and the ability to track survivorship. We found that the age of a lidar tree segment potentially inflated the appearance of errors of commission following a tree mortality event. The most likely explanation for this occurrence is that the dominant tree died after segmentation and exposed multiple subordinate trees below. Shadows also played an important role in reducing tree mortality detection, and shadows most influenced the capture of survivorship in the shortest stature trees. Our results suggest that the occurrence of shadows in imagery (Arkin et al., 2023; Huemmrich, 1996; Polewski et al., 2015), the method of individual tree detection, and data age can individually and cumulatively reduce detection, which can diminish population representation.

Can the pre-drought remotely sensed trees detect tree decay?

Older lidar tree canopies proved worthwhile for tracking overstory tree mortality and decay. This outcome is very important for the future application of remotely sensed trees to track tree survivorship and decay through time. The combined lidar tree canopies acted as “footprints” of former trees. These footprints represented live and dead trees when collected pre-drought. Since eight years passed between their segmentation, the drought, and then the 2018 imagery, trees that died may also have decayed beyond the snag stage. Therefore, the pre-drought canopy tree footprints were effective for capturing coarse woody debris with and without vegetation as well as emergent live and dead trees.

These footprints provided novel ways to track forest canopy structure changes at the scale of overstory trees. As such, this information can aid in tracking the fate of trees following complex events such as drought and fire relationships in the Sierra (Stephens et al., 2022; Wayman and Safford, 2021), forest stage transformation (Stephens et al., 2018), regeneration (Young et al., 2019), and reforestation (North et al., 2019)

How do remotely sensed tree datasets represent the post-drought mortality and decay trends of field trees?

The underrepresentation of mortality in smaller stature trees was to be expected since on average each dominant remotely sensed tree concealed an average of two subordinate trees pre-drought. The finding that many, shorter stature trees died and were undercounted is ecologically important as similar studies consistently reported greater mortality in the tallest trees (Stovall et al., 2019; Young et al., 2017; Fettig et al., 2019; Koontz et al., 2021). There were many potential factors responsible for this study's findings of greater tree mortality in the shortest stature trees.

First, we assessed mortality trends two years post-drought in 2018. Most of the tree mortality study findings of the 2012-2016 drought were based on data collected during the drought event (Asner et al., 2016; Das et al., 2022; Fettig et al., 2019; Paz-Kagan et al., 2017; Stephens et al., 2018; Stephenson and Das, 2020). At the inception of the drought mortality event, tree mortality was reported to be most profound in the tallest trees (Stovall et al., 2019; Young et al., 2017; Fettig et al., 2019; Koontz et al., 2021) and more concentrated in *P. ponderosa* forests, which were in lower elevations that our study area. Large numbers of taller *Pinus* trees dying was attributed to the preference of *D. brevicomis* (Axelson et al., 2019; Fettig et al., 2019; Stephens et al., 2018). Therefore, it was possible that our study captured delayed mortality of smaller trees that may have perished at the end or after the drought.

It is also possible that our study area in the Teakettle Experimental Forest, which includes some higher elevation Red fir forests, experienced mortality differences related to environmental and species differences. For example, our study area was dominated by *A. concolor*, which is more uncommon in the lower elevations of the Sierra. *A. concolor* is more likely to experience significantly shorter tree mortality related to competition (Barbour et al., 2002; Smith et al., 2005) and due to the host preferences of *Scolytus* spp (Ferrell et al., 1994). Although ecological and environmental factors may have contributed to the greater mortality of shorter trees or their delayed mortality, it is also possible the mortality patterns of these hidden, shorter trees were

missed by previous remotely sensed studies (Hemming-Schroeder et al., 2023; Stephenson and Das, 2020; Stovall et al., 2019) due to the absence of ground validation.

Our study illustrates the importance of investigating error by conducting field validation in the inventory and population based assessments of forest trends with air and space-borne based remote sensing of trees. These platforms are particularly susceptible to missing trends in the understory (Jakubowski et al., 2013; Jeronimo et al., 2018; Vauhkonen et al., 2012); therefore, population-based studies of forests may consider modifying sampling or experimental designs to ensure representation. Several important lessons from this study can be applied to future study designs that use high fidelity remote sensing and field data to examine ecological phenomena at the scale of individual trees or other phenomena (Das et al., 2022).

Future research

We recommend that future research efforts ensure the evaluation of error or uncertainty as well as the bias of their remotely sensed tree measurements. This study relied on a computationally efficient method to model remotely sensed trees. This method, watershed segmentation, was selected principally because it was field tested on Sierran mixed-conifer forests nearby to the study area by co-author Jeronimo. Further, it is an efficient approach and in use by scientists in the Sierra Nevada Ecoregion[1]. Therefore, it is possible to extend this approach to other regions of the Sierra Nevada where high fidelity lidar and imagery are available. However, error assessments and field validation will be necessary to address uncertainty (Antonarakis et al., 2017; Babcock et al., 2018; Friedlingstein et al., 2022; Song, 2018) and bias related to remotely sensed methods such as shadows (Arkin et al., 2023; Campbell, James B., Wynne, 2011; Huemmrich, 1996; Polewski et al., 2015) or imagery alignment (Campbell, James B., Wynne, 2011).

As a range of new, high resolution remote sensing data become more ubiquitous, novel remotely sensed tree datasets could be created by coupling a variety of datasets such as lidar and small satellite data that is <1m resolution. In 2022, the State of California collected high

resolution lidar across large regions and NAIP imagery statewide (Pers. Communication with N. Roth and L. Moreno, State of California, December 2022). These data afford many opportunities to extend this approach and develop other capabilities (Hemming-Schroeder et al., 2023; Jiao et al., 2021; Swatantran et al., 2011) to examine forest condition in high fidelity.

While our methods involved a lidar segmentation approach, other methods (Casas et al., 2016; Donager et al., 2021; Zhou et al., 2018) could use this methodology or other techniques for tree mortality detection and likely improve upon it. Algorithms such as (Yun et al., 2022) are available that may afford better detection of smaller stature trees and other vegetation from lidar. Such approaches may better detect understory trees, and these methods may be more effective for limited areas where tree density is significant and multi-strata forests exist. However, all methods will likely be unable to identify the mortality status of smaller stature trees and shrubs in the understory of canopy trees because these individuals are obscured from the view of fixed wing and satellite-based remotely sensed platforms. In other words, it may be possible to segment a tree from a point cloud, but field assessment whether by site visit or with a unmanned aerial vehicles (UAV) will be required to determine its fate. While dead understory trees may not be substantial in terms of biomass, they represent an important aspect of forest ecology and regeneration.

The rapid increase in the application of terrestrial and mobile lidar and unmanned aerial vehicles (Donager et al., 2021; Hastings et al., 2020; Marchi et al., 2018; Mohammadpour, Pegah, and Viegas, 2022; Paczkowski et al., 2021) as well as traditional field sampling afford new opportunities to identify, monitor, and understand the status of all trees, particularly the understory of forests. We recommend that stem mapping and remote sensing collection efforts be aligned as best as possible in terms of consistent geographic coordinates and temporal periods. The assessment of error and field validation to address uncertainly were critical components to ensuring the accurate representation of population trends in remote sensing of the environment.

Conclusion

Field validation to address uncertainty is critical to the interpretation of high resolution remotely sensed phenomena (Fadili et al., 2019; Hu et al., 2019; Hudak et al., 2012). Climate change is yielding rapid and extensive changes in ecosystems, which makes the case for addressing uncertainty in remotely sensed tree measures crucial to effective mitigation efforts. Field validation campaigns can be very costly; however, improved field and UAV mounted with lidar and imaging cameras could reduce costs and improve the resolution of the understory (Donager et al., 2021; Marchi et al., 2018; Nitoslawski et al., 2021).

Evaluating remotely sensed errors is also becoming increasingly important as the field evolves and new methods are applied to ecological studies. Variability and error exist in all ecological studies and assessments (McCune et al., 2002); therefore, it is imperative that error be evaluated in remotely sensed studies. This necessity is especially true as these methods are more commonly applied as proxies to the assessment and trends of populations. It will be necessary to address whether bias leads to over representing taller trees, live versus dead, certain species, or if the temporal collection of data improves some population estimations in-lieu of others. Future studies applying new individual tree detection methods can benefit from capturing error rates (Babcock et al., 2018; Murray et al., 2019; Olofsson et al., 2014) and field validation to address the limitations of these approaches in representing in-situ trends.

APPENDIX A, Chapter 2

A.1: Remote Sensing Acquisitions

2018 NEON Orthoimagery-Mortality Status

The NEON program collected 3-band, 0.1 m imagery over the Lower Teakettle Area of Interest, which subsumes the study area (Figure 1) and provided a detailed overstory view of tree status in high spatial resolution. Unlike traditional orthorectification to the digital terrain model that often results in distorted side-views of tall trees, the NEON program used an orthorectification process to balance distortion related to taller objects such as trees. Instead, the images were spatially resampled to reduce the discrepancy in resolution from lidar to camera, which provided a more nadir (i.e., top of the crown) view of trees.

Field-based tree measurements, "field trees"

To update the locations of each tree the original value was multiplied times the slope and the original intercept value was applied to each x, y, and z coordinate, respectively. For this analysis, the updated tree measurements acquired from the linear regression were reprojected to the coordinate system of the airborne lidar data.

A.2: Allometric equations

These formulas were derived from lidar based measurements of trees in the southern Sierra Nevada in the Sierra Mixed Conifer forest type, which occupies the study area and are described in (Jeronimo, 2015).

$$\log(Height) \cong -0.34 + 0.84 * \log(DBH) + c\ (spc1)$$

$$CrownSpread \cong 0.98 + 0.04 * DBH + c(spc3)$$

The species-specific constant for Height ($_{spc1}$) for *A. concolor* is 0.19, *A. magnifica* is 0.17*, C. decurrens* is 0, *P. jeffreyi* is -0.06, and *P. lambertiana* is 0.18. For crown spread, the species-specific constants ($_{spc3}$) are *A. concolor* is 0.12, *A. magnifica* is -0.19*, C. decurrens* is 0, *P. jeffreyi* is -0.58, and *P. lambertiana* is 1.30.

The estimated measures of height and crown spread are necessary to compare field trees to remotely sensed trees, which include maximum height, canopy area, and circumference. The

basal area of all trees included in the analysis were calculated from the DBH using the following formula.

$$Basal\ area\ \cong pi * (\frac{DBH}{200})\text{^}2$$

A.3: Pre-drought (2010) Remotely Sensed Tree Mortality Classification

Table A.1. Rubric of Pre-drought (2010) Remotely sensed tree Mortality Classification

Pre-drought (2010) Remotely sensed tree Mortality Class	Lidar Intensity Visual Examples	Definition
Live	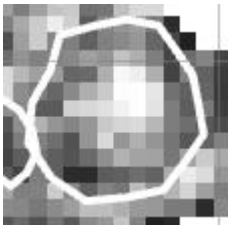	Remotely sensed tree segments were labeled as live if ~≥2/3 of the canopy area was dominated by the upper third of the intensity values (>170) with the crown center usually displaying the highest intensity values. In addition, the true color NAIP 2010 & NDVI values derived from the NAIP 2010 data were visualized to support labeling a tree as live. A tree was labeled as live if the upper 1/3 of NDVI values intersected the lidar segment, or if the tree canopy appeared green in the true color imagery. The lidar intensity values received the priority for labeling as they were on nadir and finer in resolution.
Mixed		Remotely sensed tree segments were labeled as mixed if ~≥2/3 of the canopy area was dominated by the middle third of the intensity values in the range of (85>x<170). Or, if remotely sensed tree segments were labeled as mixed if half of the segment appeared as a live tree and the other half as a dead tree. In addition, the true color NAIP 2010 & NDVI values were examined to support labeling as Mixed, but the lidar intensity values received the priority for labeling as they were on nadir and finer in resolution.
Dead	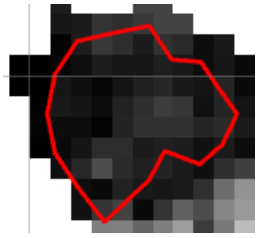	Remotely sensed tree segments were labeled as dead if ~≥2/3 of the canopy area was dominated by the lower third of the intensity values (<85) with the crown center usually displaying the lowest values. In addition, the true color NAIP 2010 & NDVI values derived from the NAIP 2010 data were visualized to support labeling a tree as dead. A tree was labeled as dead if the lower 1/3 of NDVI values intersected the lidar segment, or if the tree canopy appeared beige or brown in the true color imagery. The lidar intensity values received priority for labeling as they were on nadir and finer in resolution.
Other (Boulders)		All combined (2010) remotely sensed trees that were identified as boulders using the 2018 NEON imagery were also labeled as "Other" in the remotely sensed tree mortality labeling.

The other class applied to error of commission that produced remotely sensed trees that were boulders and not vegetation trees, which could be identified in the 2018 imagery. Remotely sensed trees were labeled as live if 2/3 of more of the canopy area appeared to contain lidar intensity values in the upper 1/3 of the range of intensity values (1-255) (e.g., >170 in intensity reflectance). In addition, the 2010 NAIP NDVI and 2010 true color imagery appeared to corroborate that a tree was alive. A remotely sensed tree was defined as mixed if ~2/3 of the canopy area had lidar intensity reflectance values in the middle range (e.g., 85>x<170), or if the canopy area had grouped higher and lower intensity values suggesting the presence of a live and dead tree. The mixed status was also supported by visually examining the values of the NAIP true color and NAIP NDVI values. Finally, a remotely sensed tree was labeled as dead if ~2/3 or more of the canopy area was dominated by the lower third of lidar intensity values (e.g., <85), and the NAIP true color and NAIP NDVI values also appeared to suggest the presence of a dead tree due to the remotely sensed tree appearing beige/brown or having lower NDVI values.

A.4. Post-drought Remotely Sensed Tree Classification

Table A.2. Rubric of 2018 Mortality and Decay, Lidar Segmentation Errors, and Nadir Status for Classification of the combined and post-drought remotely sensed trees by the Post-mortality status

General Remotely sensed tree Mortality Class for Comparison with Field Tree Mortality	Detailed Mortality and Decay Class Labels	Example	Detailed Mortality and Decay Class Definitions applied to 2018 NEON 0.10 m resolution imagery
Live	Live	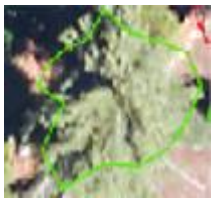	A probable live tree occupies ~≥2/3 of a remotely sensed tree segment, and the remainder is other material (e.g., ground, coarse woody debris, ground vegetation, rock, dead tree, or unknown). A live tree appears as a shade of green in RGB data.

Live	Live Shadow	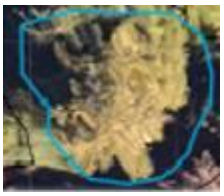	A probable live tree occupies ~≥2/3 of a remotely sensed tree segment and the remainder of segment is composed of shadow. A live tree appears as a shade of green in RGB data, with the lower part of the crown shrouded in shadow. This class was created to examine the rate of potential misclassification as dead.
Live (likely Regeneration)	Live with CWD		An emergent live tree or shrub occupies ~1/3 of the remotely sensed tree segment while another ~1/3 is occupied by coarse woody debris that likely represents the dead dominant tree that represented the remotely sensed tree segment. The remaining 1/3 of the lidar segment may be occupied by other material.
Live	Live Ground Vegetation		Imagery within the remotely sensed tree segment displays probable live, green ground vegetation with a minimum of ~≥2/3 of the segment, and the remotely sensed tree has a maximum height <3m with no apparent shadow in the imagery. It is unknown if this lidar segment represents an error of commission, vegetation cover (i.e., a shrub), or is a tree.
Live	Mixed Top		A browning crown or decadent top occupies 25% or less of the remotely sensed tree in the imagery, the remainder of the remotely sensed tree segment appears to be composed of live, green tree cover. Together the browning crown/decadent top and the live canopy occupy ~2/3 of the segment. The remainder of the pixels in the imagery may include other material.

Live	Mixed Stress		A yellowing or browning tree canopy cover occupies ~≥2/3 of the remotely sensed tree segment, and the remainder is not the tree canopy (e.g., ground, coarse woody debris, ground vegetation, rock, dead tree, or unknown). The yellowing or browning tree may have evidence of branches without needles.
Mixed	Mixed Live and Dead		A combination of live and red or gray phase dead trees where at least a third of the imagery is occupied by a live tree, a third by a dead tree, and the remainder may include a view of the ground cover and/or ground vegetation.
Dead	Dead Red Phase		A presumed dead, red phase tree cover occupies ~≥2/3 of remotely sensed tree segment and remainder of segment is composed of material other than the tree canopy. The red phase of a tree is typically associated with post tree mortality where the needles have not fallen off the branches.
Dead	Dead Gray Phase		A dead, gray phase tree cover occupies ~≥2/3 of the remotely sensed tree segment and the remainder of segment is composed of material other than the tree canopy. In the gray phase, a portion of the top may have broken off; however, the tree branches remain mostly in-tact and the snag appears almost white gray.
Dead	Dead Stump		A dead standing tree snag without evidence of significant branching occupies the remotely sensed tree segment and may occupy <25% of the remotely sensed tree segment area. The rest of the segment area may be occupied with other material (e.g., ground, coarse woody debris, ground vegetation,

			rock, live vegetation, dead tree, or unknown).
Dead	Other Course Woody Debris		Coarse woody debris occupies ~≥2/3, of remotely sensed tree segment and the remainder is other material (e.g., ground, coarse woody debris, ground vegetation, rock, dead tree, or unknown).
Other	Other/Unknown		A combination of live and dead vegetation, mixed ground cover, CWD, ground vegetation, or rocks each of minority proportions for which the viewer could not identify the remotely sensed tree segment or mortality status.
Other	Other Ground		The remotely sensed tree segment provides a view of the ground and may be composed of pine needles or dirt filling ~≥2/3 of the remotely sensed tree segment. The remainder of the remotely sensed tree segment may include live or dead vegetation or other material.
Other	Other Boulder		A boulder occupies ~≥2/3 of remotely sensed tree segment, and the remainder is not the boulder (e.g., ground, coarse woody debris, ground vegetation, dead or live tree, or unknown).
Other	Other Shadow		A shadow occupies ~≥2/3 of remotely sensed tree segment, and the remainder is not the shadow (e.g., ground, coarse woody debris, ground vegetation, dead or live tree, or unknown).
Nadir Status		**Example**	**Description**

On nadir		A bird's eye view of the tree canopy within the remotely sensed tree segment.
Tilt		A side view of the tree within the remotely sensed tree segment.
Off nadir		Most of the crown or portion of the canopy is outside of the remotely sensed tree segment, and the view may also be obscured or appear in a swirl like pattern.
Lidar Segmentation Errors: Omission and Commission	**Example**	**Description**
No lidar segmentation error observed "No error"	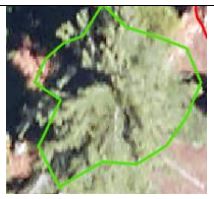	Remotely sensed trees without segmentation errors appear to capture the full extent of the dominant tree canopy.
Commission-over-segmentation of the lidar canopy	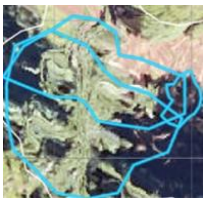	Remotely sensed tree segments that were associated with the same dominant tree canopy and of the same relative height (i.e., within 3m in height) were labeled as over-segmented. The largest of the canopy segments was labeled as main and was considered as a single tree, and the remaining segments were labeled as additional. Unless noted, the additional segments were not included in the comparisons with field trees except to report total frequencies, where noted.

Omission-2 or canopy trees observed in the lidar segment		Remotely sensed trees were labeled as errors of omission when two or more canopy trees were clearly visible within the remotely sensed tree segment.
Commission-boulders		Boulders are common natural features in the Sierra Nevada, and they can be the same relative height and canopy spread as a smaller tree. They were labeled as specific errors of commission.

A.4: Post-drought Mortality Status-2018

The NEON 2018 RGB orthoimagery provided high-resolution imagery to detect mortality and decay status. In addition, the lidar height and canopy area measurements along with the NEON imagery allowed each combined and post-drought remotely sensed tree to be examined for errors of lidar segmentation commission and omission (Figure 4). Despite the NEON 2018 imagery being collected in narrow flight lines with overlap, the combination of the image overlap, tall trees, and orthorectification still produced view of trees that were not a nadir (i.e., birds eye view) of the trees. For each of the combined and post-drought remotely sensed trees, the mortality and decay status, presence or absence and type of lidar segmentation error, and nadir status was observed and recorded. Table A.2, Appendix A provides detailed information regarding the acquisition and orthorectification process that are relevant to identifying the mortality status of the remotely sensed trees in 2018.

A.5: Results

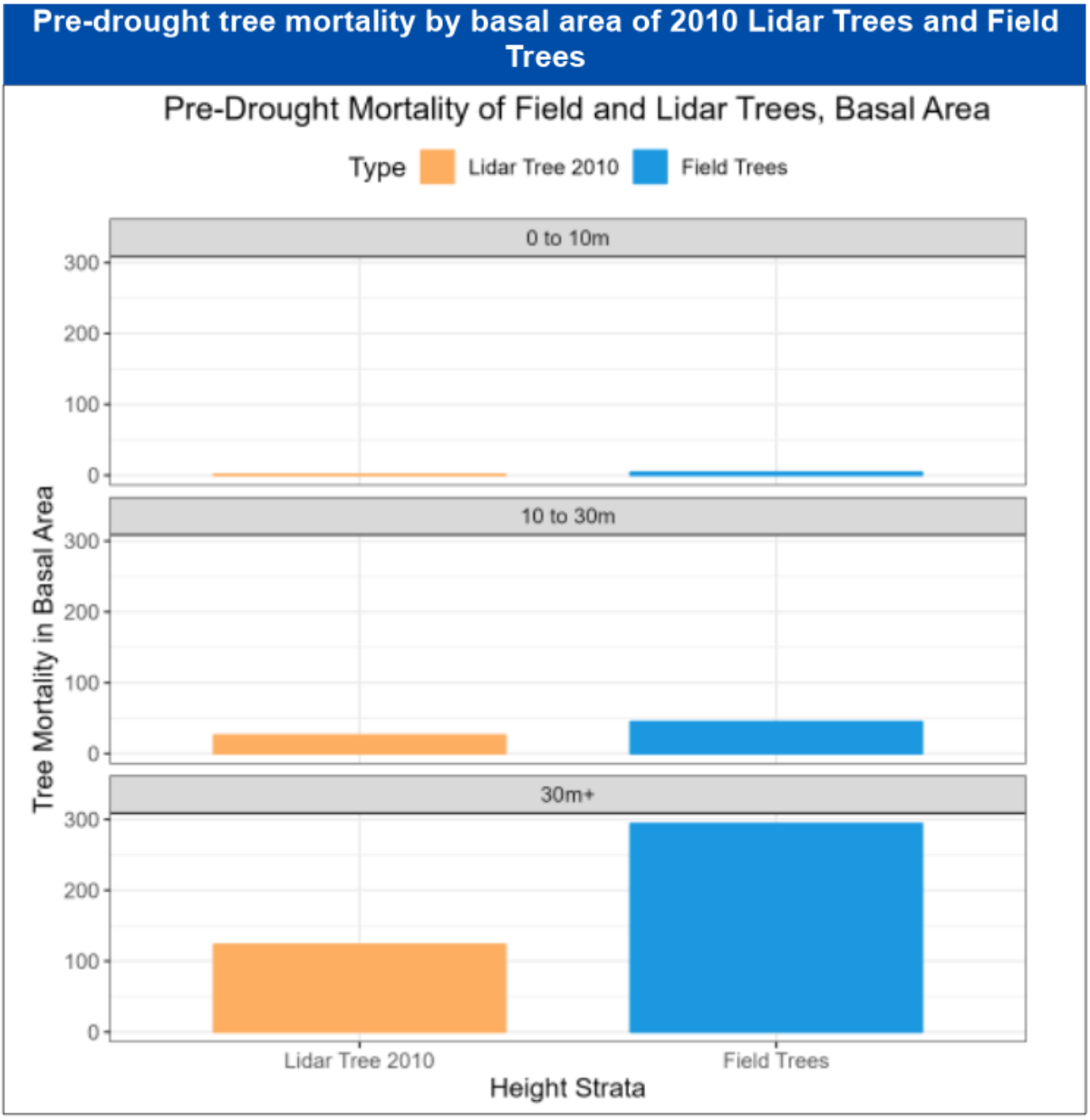

Figure A.1. Basal are per lidar (remotely sensed trees) and the field trees pre-drought are shown by height strata within the study area.

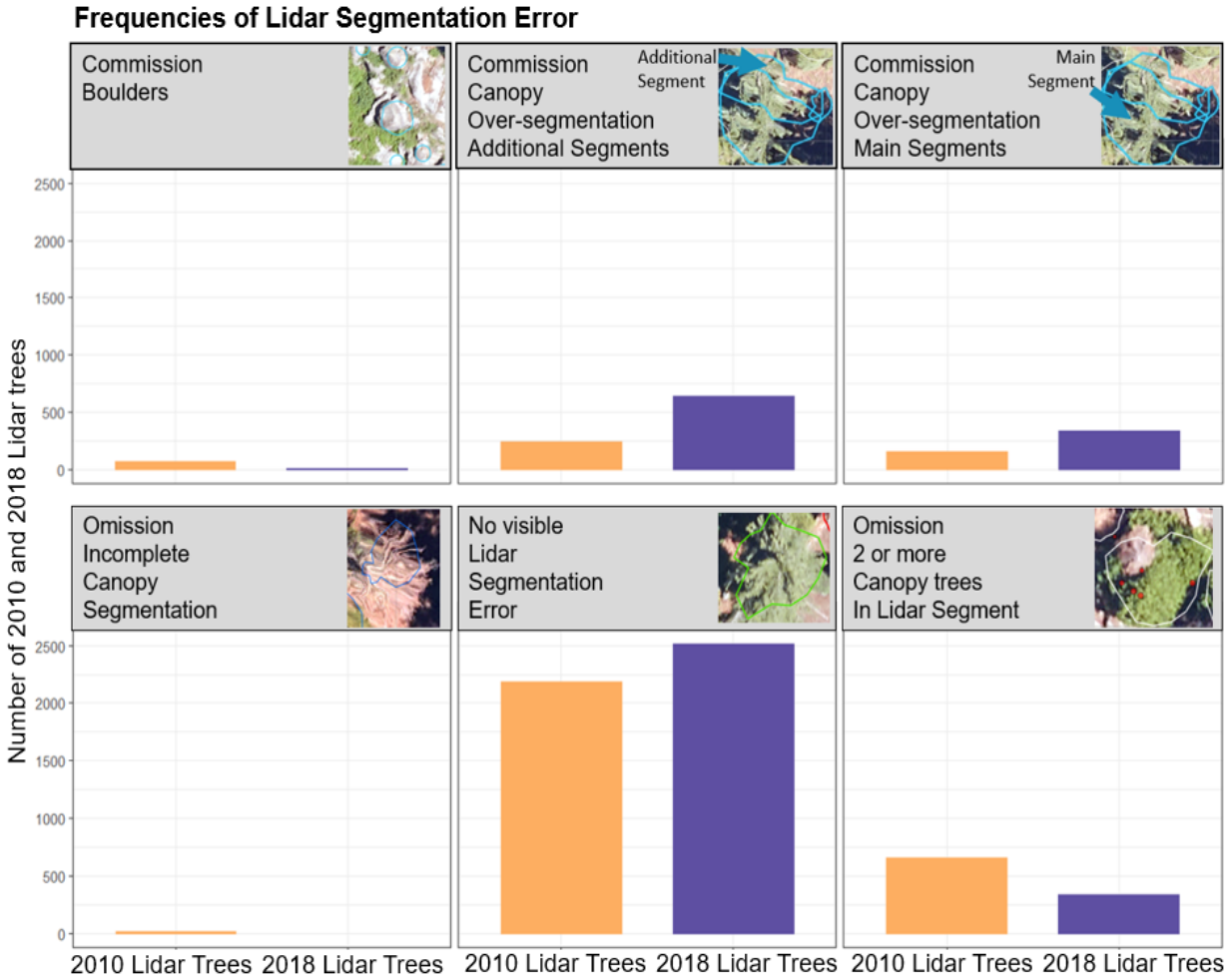

Figure A.2. Counts of lidar segmentation errors are displayed by the pre-drought (2010) and post-drought (2018) remotely sensed trees based on the different types of lidar segmentation errors encountered, per remotely sensed tree when examined with the NEON 2018 0.1m resolution imagery.

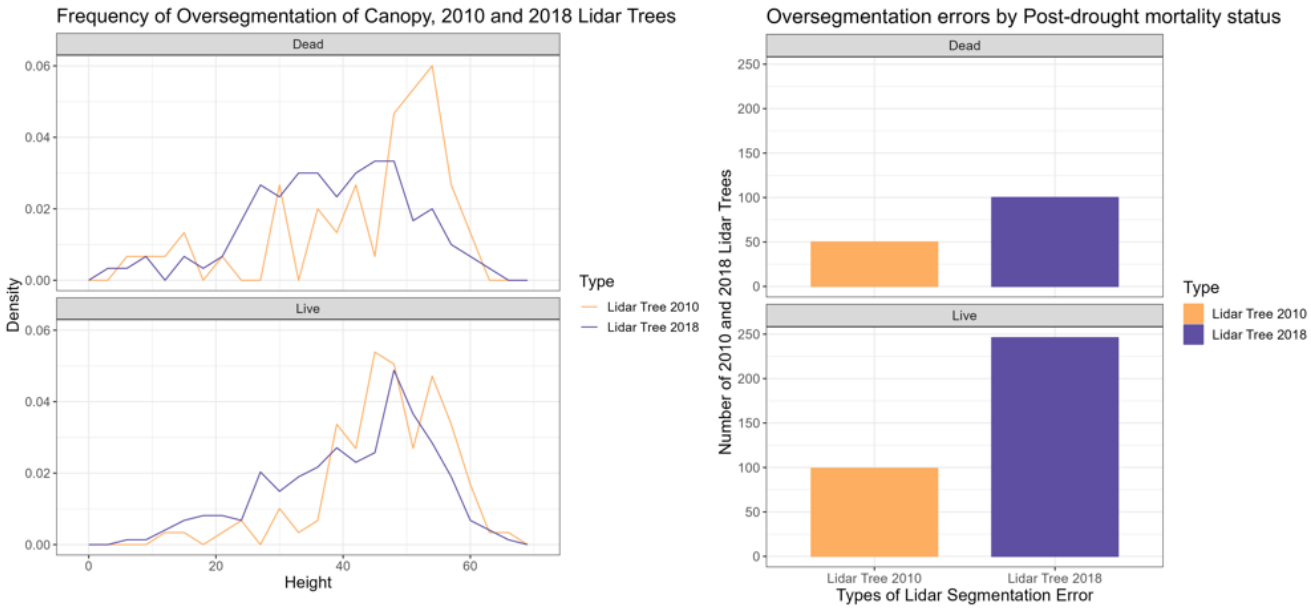

Figure A.3. Frequency of commission (oversegmentation) errors by remotely sensed tree type, mortality, and height. The top left graph displays the frequency of errors of commission involving oversegmentation of the canopy for lidar (remotely sensed trees) identified as dead for the 2010-orange and 2018-purple lidar trees by tree height. The bottom left graph also shows the frequency of errors of commission involving oversegmentation of the canopy by height for live trees. The top and bottom right graphs display the counts of 2010 and 2018 lidar trees with errors of commission involving oversegmentation of the canopy for dead and live, respectively.

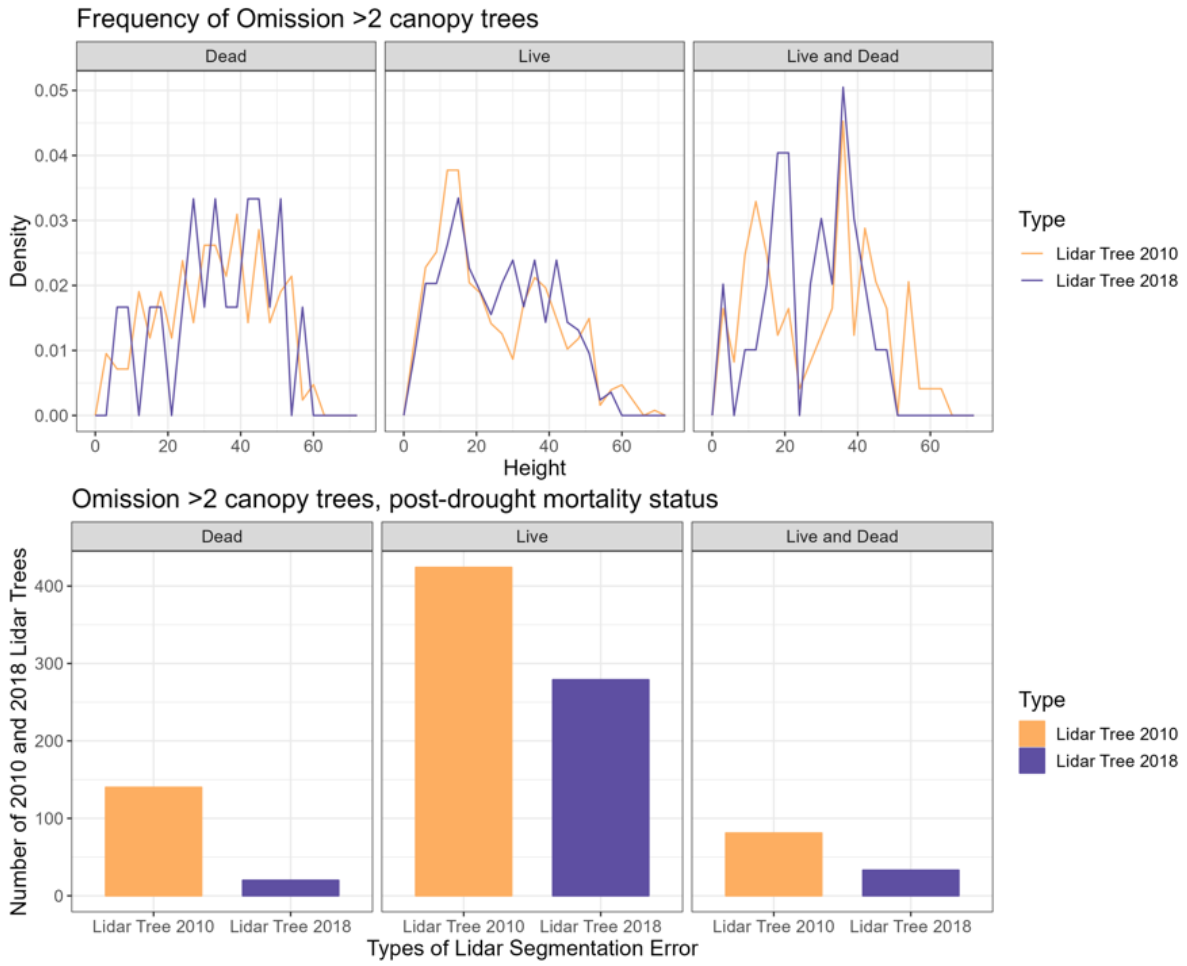

Figure A.4. Frequency of omission errors by remotely sensed tree type, mortality, and height. The top panel of graphs displays the frequency of errors of omission by mortality status per height for the 2010-orange and 2018-purple lidar trees (remotely sensed trees). The bottom panel of graphs displays the counts of errors of omission by mortality status for the 2010-orange and 2018-purple lidar trees (remotely sensed trees).

Table A.3. Frequency of Remotely sensed trees in complete shadow by height class

Type	Height Strata 0 to 10m	Frequency of all remotely sensed trees by year	Height Strata 10 to 30m	Frequency of all remotely sensed trees by year	Height Strata +30m	Frequency of all remotely sensed trees by year
Pre-drought remotely sensed trees (2010)	118	4%	78	2%	34	1%
Post-drought remotely sensed trees (2018)	101	3%	82	2%	38	1%

2.6 CITATIONS

Allen, B.H., 2005. Sierran Mixed Conifer, California Wildlife Habitat Relationships System. Sacramento.

Allen, C.D., Breshears, D.D., McDowell, N.G., 2015. On underestimation of global vulnerability to tree mortality and forest die-off from hotter drought in the Anthropocene. Ecosphere 6, 1–55. https://doi.org/10.1890/ES15-00203.1

Anderegg, W.R.L., Anderegg, L.D.L., Kerr, K.L., Trugman, A.T., 2019. Widespread drought-induced tree mortality at dry range edges indicates that climate stress exceeds species' compensating mechanisms. Glob. Chang. Biol. 25, 3793–3802. https://doi.org/10.1111/gcb.14771

Antonarakis, A.S., Siqueira, P., Munger, J.W., 2017. Using multi-source data from lidar, radar, imaging spectroscopy, and national forest inventories to simulate forest carbon fluxes. Int. J. Remote Sens. 38, 5464–5486. https://doi.org/10.1080/01431161.2017.1341666

Arkin, J., Coops, N.C., Daniels, L.D., Plowright, A., 2023. A novel post-fire method to estimate individual tree crown scorch height and volume using simple RPAS-derived data. Fire Ecol. 19. https://doi.org/10.1186/s42408-023-00174-7

Asner, G.P., Brodrick, P.G., Anderson, C.B., Vaughn, N., Knapp, D.E., Martin, R.E., 2016. Progressive forest canopy water loss during the 2012–2015 California drought. Proc. Natl. Acad. Sci. 113, E249–E255. https://doi.org/10.1073/pnas.1523397113

Babcock, C., Finley, A.O., Andersen, H.E., Pattison, R., Cook, B.D., Morton, D.C., Alonzo, M., Nelson, R., Gregoire, T., Ene, L., Gobakken, T., Næsset, E., 2018. Geostatistical estimation of forest biomass in interior Alaska combining Landsat-derived tree cover, sampled airborne lidar and field observations. Remote Sens. Environ. 212, 212–230. https://doi.org/10.1016/j.rse.2018.04.044

Brodrick, P.G., Asner, G.P., 2017. Remotely sensed predictors of conifer tree mortality during severe drought. Environ. Res. Lett. 12, 115013. https://doi.org/10.1088/1748-9326/aa8f55

Brown, E.G., 2015. Proclamation of a State of Emergency, Sacramento.

California Department of Transportation, 2017. Clearing Out the Deadwood: Caltrans Responds to Massive Tree Die-Off Along State Highway System. Sacramento.

Campbell, James B., Wynne, R.H., 2011. Introduction to Remote Sensing, Fifth. ed. The Guilford Press, New York.

Canelles, Q., Aquilué, N., James, P.M.A., Lawler, J., Brotons, L., 2021. Global review on interactions between insect pests and other forest disturbances. Landsc. Ecol. 36, 945–972. https://doi.org/10.1007/s10980-021-01209-7

Casas, Á., García, M., Siegel, R.B., Koltunov, A., Ramírez, C., Ustin, S., 2016. Burned forest characterization at single-tree level with airborne laser scanning for assessing wildlife habitat. Remote Sens. Environ. 175, 231–241. https://doi.org/10.1016/j.rse.2015.12.044

Coleman, T.W., Graves, A.D., Heath, Z., Flowers, R.W., Hanavan, R.P., Cluck, D.R., Ryerson, D., 2018. Accuracy of aerial detection surveys for mapping insect and disease disturbances in the United States. For. Ecol. Manage. 430, 321–336. https://doi.org/10.1016/j.foreco.2018.08.020

Collins, B.M., Fry, D.L., Lydersen, J.M., Everett, R., Stephens, S.L., 2017. Impacts of different land management histories on forest change. Ecol. Appl. 27, 2475–2486. https://doi.org/10.1002/eap.1622

Cova, G., Kane, V.R., Prichard, S., North, M., Cansler, C.A., 2023. The outsized role of California's largest wildfires in changing forest burn patterns and coarsening ecosystem scale. For. Ecol. Manage. 528, 120620. https://doi.org/10.1016/j.foreco.2022.120620

Das, A.J., Slaton, M.R., Mallory, J., Asner, G.P., Martin, R.E., Hardwick, P., 2022. Empirically validated drought vulnerability mapping in the mixed conifer forests of the Sierra Nevada. Ecol. Appl. 32, 1–19. https://doi.org/10.1002/eap.2514

Diffenbaugh, N.S., Swain, D.L., Touma, D., Lubchenco, J., 2015. Anthropogenic warming has increased drought risk in California. Proc. Natl. Acad. Sci. U. S. A. 112, 3931–3936. https://doi.org/10.1073/pnas.1422385112

Donager, J.J., Sánchez Meador, A.J., Blackburn, R.C., 2021. Adjudicating perspectives on forest structure: How do airborne, terrestrial, and mobile lidar-derived estimates compare? Remote Sens. 13, 1–18. https://doi.org/10.3390/rs13122297

Donato, D.C., Harvey, B.J., Turner, M.G., 2016. Regeneration of montane forests 24 years afer the 1988 Yellowstone fires: A fire-catalyzed shif in lower treelines? Ecosphere 7, 1–16. https://doi.org/10.1002/ecs2.1410/supinfo

Earles, J.M., North, M.P., Hurteau, M.D., 2014. Wildfire and drought dynamics destabilize carbon stores of fire-suppressed forests. Ecol. Appl. 24, 732–740. https://doi.org/10.1890/13-1860.1

ESRI ArcGIS Pro Version 2.8, 2021.

Fadili, M., Renaud, J.P., Bock, J., Vega, C., 2019. RegisTree: a registration algorithm to enhance forest inventory plot georeferencing. Ann. For. Sci. 76. https://doi.org/10.1007/s13595-019-0814-2

Fettig, C.J., Mortenson, L.A., Bulaon, B.M., Foulk, P.B., 2019. Tree mortality following drought in the central and southern Sierra Nevada, California, U.S. For. Ecol. Manage. 432, 164–178. https://doi.org/10.1016/j.foreco.2018.09.006

Forzieri, G., Girardello, M., Ceccherini, G., Spinoni, J., Feyen, L., Hartmann, H., Beck, P.S.A., Camps-Valls, G., Chirici, G., Mauri, A., Cescatti, A., 2021. Emergent vulnerability to climate-driven disturbances in European forests. Nat. Commun. 12, 1–12. https://doi.org/10.1038/s41467-021-21399-7

Fricker, G.A., Ventura, J.D., Wolf, J., North, M.P., Frank, W., 2019. A Convolutional Neural Network classifier identifies tree species in mixed-conifer forest from hyperspectral imagery 1–24.

Friedlingstein, P., Jones, M.W., O'Sullivan, M., Andrew, R.M., Bakker, D.C.E., 2022. Global Carbon Budget 2021, report Earth System Science Data. Earth Syst. Sci. Data 14, 1917–2005.

Fry, D.L., Stephens, S.L., Collins, B.M., North, M.P., Franco-Vizcaíno, E., Gill, S.J., 2014. Contrasting spatial patterns in active-fire and fire-suppressed mediterranean climate old-growth mixed conifer forests. PLoS One 9. https://doi.org/10.1371/journal.pone.0088985

Gallery, W., 2022. Neon Algorithm Theoretical Basis Document (Atbd) AOP Digital Camera Image Orthorectification.

Gibson, P.B., Waliser, D.E., Guan, B., Deflorio, M.J., Ralph, F.M., Swain, D.L., 2020. Ridging associated with Drought across the Western and Southwestern United States: Characteristics, trends, and predictability sources. J. Clim. 33, 2485–2508. https://doi.org/10.1175/JCLI-D-19-0439.1

Goodwin, M.J., North, M.P., Zald, H.S.J., Hurteau, M.D., 2020. Changing climate reallocates the carbon debt of frequent-fire forests. Glob. Chang. Biol. 26, 6180–6189. https://doi.org/10.1111/gcb.15318

Grulke, N., Maxfield, J., Riggan, P., Schrader-Patton, C., 2020. Pre-emptive detection of mature pine drought stress using multispectral aerial imagery. Remote Sens. 12, 1–23. https://doi.org/10.3390/rs12142338

Gutierrez, A.A., Allison, S.D., Randerson, J.T., 2023. Estimating Individual Tree Mortality in the Sierra Nevada Using Lidar and Multispectral Reflectance Data Journal of Geophysical Research : Biogeosciences. J. Geophys. Res. Biogeosciences, 128, 128, 1–18. https://doi.org/10.1029/2022JG007234

Hajek, P., Link, R.M., Nock, C.A., Bauhus, J., Gebauer, T., Gessler, A., Kovach, K., Messier, C., Paquette, A., Saurer, M., Scherer-Lorenzen, M., Rose, L., Schuldt, B., 2022. Mutually inclusive mechanisms of drought-induced tree mortality. Glob. Chang. Biol. 28, 3365–3378. https://doi.org/10.1111/gcb.16146

Hartmann, H., Bastos, A., Das, A.J., Esquivel-Muelbert, A., Hammond, W.M., Martínez-Vilalta, J., Mcdowell, N.G., Powers, J.S., Pugh, T.A.M., Ruthrof, K.X., Allen, C.D., 2022. Climate Change Risks to Global Forest Health: Emergence of Unexpected Events of Elevated Tree Mortality Worldwide. Annu. Rev. Plant Biol. 73, 673–702. https://doi.org/10.1146/annurev-arplant-102820-012804

Hartmann, H., Schuldt, B., Sanders, T.G.M., Macinnis-Ng, C., Boehmer, H.J., Allen, C.D., Bolte, A., Crowther, T.W., Hansen, M.C., Medlyn, B.E., Ruehr, N.K., Anderegg, W.R.L., 2018. Monitoring global tree mortality patterns and trends. Report from the VW symposium 'Crossing scales and disciplines to identify global trends of tree mortality as indicators of forest health.' New Phytol. 217, 984–987. https://doi.org/10.1111/nph.14988

Harvey, B.J., Donato, D.C., Turner, M.G., 2016. High and dry: Post-fire tree seedling establishment in subalpine forests decreases with post-fire drought and large stand-replacing burn patches. Glob. Ecol. Biogeogr. 25, 655–669. https://doi.org/10.1111/geb.12443

Hastings, J.H., Ollinger, S. V., Ouimette, A.P., Sanders-DeMott, R., Palace, M.W., Ducey, M.J., Sullivan, F.B., Basler, D., Orwig, D.A., 2020. Tree species traits determine the success of LiDAR-based crown mapping in a mixed temperate forest. Remote Sens. 12. https://doi.org/10.3390/rs12020309

Hessburg, P.F., Miller, C.L., Parks, S.A., Povak, N.A., Taylor, A.H., Higuera, P.E., Prichard, S.J., North, M.P., Collins, B.M., Hurteau, M.D., Larson, A.J., Allen, C.D., Stephens, S.L., Rivera-Huerta, H., Stevens-Rumann, C.S., Daniels, L.D., Gedalof, Z., Gray, R.W., Kane, V.R., Churchill, D.J., Hagmann, R.K., Spies, T.A., Cansler, C.A., Belote, R.T., Veblen, T.T., Battaglia, M.A., Hoffman, C., Skinner, C.N., Safford, H.D., Salter, R.B., 2019. Climate, Environment, and Disturbance History Govern Resilience of Western North American Forests. Front. Ecol. Evol. 7, 1–27. https://doi.org/10.3389/fevo.2019.00239

Hu, T., Ma, Q., Su, Y., Battles, J.J., Collins, B.M., Stephens, S.L., Kelly, M., Guo, Q., 2019. A simple and integrated approach for fire severity assessment using bi-temporal airborne LiDAR data. Int. J. Appl. Earth Obs. Geoinf. 78, 25–38. https://doi.org/10.1016/J.JAG.2019.01.007

Huang, K., Yi, C., Wu, D., Zhou, T., Zhao, X., Blanford, W.J., Wei, S., Wu, H., Ling, D., Li, Z., 2015. Tipping point of a conifer forest ecosystem under severe drought. Environ. Res. Lett. 10. https://doi.org/10.1088/1748-9326/10/2/024011

Hudak, A.T., Strand, E.K., Vierling, L.A., Byrne, J.C., Eitel, J.U.H., Martinuzzi, S., Falkowski, M.J., 2012. Quantifying aboveground forest carbon pools and fluxes from repeat LiDAR surveys. Remote Sens. Environ. 123, 25–40. https://doi.org/10.1016/j.rse.2012.02.023

Huemmrich, K.F., 1996. Effects of shadows on vegetation indices. Int. Geosci. Remote Sens. Symp. 4, 2372–2374. https://doi.org/10.1109/igarss.1996.516990

Jeronimo, S.A.M., 2018. Restoring forest resilience in the Sierra Nevada mixed-conifer zone, with a focus on measuring spatial patterns of trees using airborne lidar. University of Washington.

Jeronimo, S.M., 2015. LiDAR individual tree detection for assessing structurally diverse forest landscapes. Univ. Washingt. University of Washington, Seattle, WA.

Jeronimo, S.M.A., Bartl-Geller, B.N., Griffey, V., van Wagtendonk, L., Shaw, M., Kane, V.R., 2019. Using lidar data to develop silvicultural restoration options and identify potential American marten habitat. Final report to the USDA Forest Service: Malheur National Forest and Wallowa-Whitman National Forest. Agreement 18-CO-11060400-16.

Jeronimo, S.M.A., Kane, V.R., Churchill, D.J., McGaughey, R.J., Franklin, J.F., 2018. Applying LiDAR individual tree detection to management of structurally diverse forest landscapes. J. For. 116, 336–346. https://doi.org/10.1093/jofore/fvy023

Jiao, W., Wang, L., McCabe, M.F., 2021. Multi-sensor remote sensing for drought characterization: current status, opportunities and a roadmap for the future. Remote Sens. Environ. 256, 112313. https://doi.org/10.1016/j.rse.2021.112313

Krause, K., Goulden, T., 2015. NEON L0-TO-L1 DISCRETE RETURN LiDAR ALGORITHM THEORETICAL BASIS DOCUMENT (ATBD).

Krofcheck, D.J., Hurteau, M.D., Scheller, R.M., Loudermilk, E.L., 2017. Restoring surface fire stabilizes forest carbon under extreme fire weather in the Sierra Nevada. Ecosphere 8. https://doi.org/10.1002/ecs2.1663

Leisso, N., 2016. Neon Normaliszed Difference Vegetation Index (Ndvi), Enhanced Vegetation Index (Evi), Atomospherically Resistant Vegetation Index (Arvi), Canopy Xanthophyll Cycle (Pri), and Canopy Lignin (Ndli) Algorithm Theoretical Basis Document.

Lakubowski, M.K., Kelly, M., 2012. A new method for segmenting individual trees from the lidar point cloud. Photogramm. Eng. Remote Sensing 78, 75–84. https://doi.org/10.14358/PERS.78.1.75

Lloret, F., Escudero, A., Iriondo, J.M., Martínez-Vilalta, J., Valladares, F., 2012. Extreme climatic events and vegetation: The role of stabilizing processes. Glob. Chang. Biol. 18, 797–805. https://doi.org/10.1111/j.1365-2486.2011.02624.x

Ma, Q., 2018. Quantifying Forest Structure Parameters and Their Changes from LiDAR Data and Satellite Imagery in the Sierra Nevada. University of California, Merced. https://doi.org/10.21425/F59335464

Marchi, N., Pirotti, F., Lingua, E., 2018. Airborne and Terrestrial Laser Scanning Data for the Assessment of Standing and Lying Deadwood: Current Situation and New Perspectives. Remote Sens. 10, 1356. https://doi.org/10.3390/rs10091356

McGaughey, R.J., 2018a. FUSION/LDV: Software for LIDAR Data Analysis and Visualization: Version 3.70. USDA Forest Service Pacific Northwest Research Station, Seattle, WA.

McGaughey, R.J., 2018b. FUSION / LDV : Software for LIDAR Data Analysis and Visualization. U.S. Department of Agriculture, Forest Service, Pacific Northwest Research Station, University of Washington, Seattle, WA, USA.

Millar, C.I., Stephenson, N.L., 2015. Temperate forest health in an era of emerging megadisturbance. Science (80-.). 349, 823–826. https://doi.org/10.1126/science.aaa9933

Mohammadpour, Pegah, and Viegas, C., 2022. Applications of Multi-Source and Multi-Sensor Data Fusion of Remote Sensing for Forest Species Mapping., in: Advances in Remote Sensing for Forest Monitoring. John Wiley & Sons, Ltd, pp. 255–297. https://doi.org/https://doi.org/10.1002/9781119788157.ch12

NASA, 2020. California's Creek Fire Creates Its Own Pyrocumulonimbus Cloud [WWW Document]. NASA Hazards. URL https://www.nasa.gov/feature/goddard/2020/californias-creek-fire-creates-its-own-pyrocumulonimbus-cloud

Nitoslawski, S.A., Wong-Stevens, K., Steenberg, J.W.N., Witherspoon, K., Nesbitt, L., Konijnendijk van den Bosch, C.C., 2021. The Digital Forest: Mapping a Decade of Knowledge on Technological Applications for Forest Ecosystems. Earth's Futur. 9, 1–28. https://doi.org/10.1029/2021EF002123

North, M., Chen, J., Oakley, B., Song, B., Rudnicki, M., Gray, A., Innes, J., 2004. Forest stand structure and pattern of old-growth western hemlock/Douglas-fir and mixed-conifer forests. For. Sci. 50, 299–311.

North, M., Innes, J., Zald, H., 2007. Comparison of thinning and prescribed fire restoration treatments to Sierran mixed-conifer historic conditions. Can. J. For. Res. 37, 331–342. https://doi.org/10.1139/X06-236

North, M., Oakley, B., Chen, J., Erickson, H., Gray, A., Izzo, A., Schowalter, T., 2002. Vegetation and ecological characteristics of mixed conifer and red fir forests at the teakettle experimental forest.

North, M.P., 2002. Vegetation and ecological characteristics of mixed-conifer and red fir forests at the Teakettle Experimental Forest.

North, M.P., Stevens, J.T., Greene, D.F., Coppoletta, M., Knapp, E.E., Latimer, A.M., Restaino, C.M., Tompkins, R.E., Welch, K.R., York, R.A., Young, D.J.N., Axelson, J.N., Buckley, T.N., Estes, B.L., Hager, R.N., Long, J.W., Meyer, M.D., Ostoja, S.M., Sa, H.D., Shive, K.L., Tubbesing, C.L., Vice, H., Walsh, D., Werner, C.M., Wyrsch, P., 2019. Tamm Review : Reforestation for resilience in dry western U . S . forests 432, 209–224. https://doi.org/10.1016/j.foreco.2018.09.007

Paczkowski, S., Datta, P., Irion, H., Paczkowska, M., Habert, T., Pelz, S., Jaeger, D., 2021. Evaluation of early bark beetle infestation localization by drone-based monoterpene detection. Forests 12, 1–17. https://doi.org/10.3390/f12020228

Pawlikowski, N.C., Coppoletta, M., Knapp, E., Taylor, A.H., 2019. Spatial dynamics of tree group and gap structure in an old-growth ponderosa pine-California black oak forest burned by repeated wildfires. For. Ecol. Manage. 434, 289–302. https://doi.org/10.1016/j.foreco.2018.12.016

Paz-Kagan, T., Brodrick, P.G., Vaughn, N.R., Das, A.J., Stephenson, N.L., Nydick, K.R., Asner, G.P., 2017. What mediates tree mortality during drought in the southern Sierra Nevada? Ecol. Appl. 27, 2443–2457. https://doi.org/10.1002/eap.1620

Polewski, P., Yao, W., Heurich, M., Krzystek, P., Stilla, U., 2015. Detection of single standing dead trees from aerial color infrared imagery by segmentation with shape and intensity priors. ISPRS Ann. Photogramm. Remote Sens. Spat. Inf. Sci. 2, 181–188. https://doi.org/10.5194/isprsannals-II-3-W4-181-2015

Restaino, C., Young, D.J.N., Estes, B., Gross, S., Wuenschel, A., Meyer, M., Safford, H., 2019. Forest structure and climate mediate drought-induced tree mortality in forests of the Sierra Nevada, USA. Ecol. Appl. 29, 1–14. https://doi.org/10.1002/eap.1902

Roche, J.W., Goulden, M.L., Bales, R.C., 2018. Estimating evapotranspiration change due to forest treatment and fire at the basin scale in the Sierra Nevada, California. Ecohydrology 11, 1–10. https://doi.org/10.1002/eco.1978

Sciences, W., 2011. Dinkey Creek / Tea Kettle 2010.

Song, X.-P., 2018. Global Estimates of Ecosystem Service Value and Change: Taking Into Account Uncertainties in Satellite-based Land Cover Data. Ecol. Econ. 143, 227–235. https://doi.org/10.1016/j.ecolecon.2017.07.019

Stephens, S.L., Bernal, A.A., Collins, B.M., Finney, M.A., Lautenberger, C., Saah, D., 2022. Mass fire behavior created by extensive tree mortality and high tree density not predicted by operational fire behavior models in the southern Sierra Nevada. For. Ecol. Manage. 518, 120258. https://doi.org/10.1016/j.foreco.2022.120258

Stephens, S.L., Collins, B.M., Fettig, C.J., Finney, M.A., Hoffman, C.M., Knapp, E.E., North, M.P., Safford, H., Wayman, R.B., 2018. Drought, Tree Mortality, and Wildfire in Forests Adapted to Frequent Fire. Bioscience XX, 1–12. https://doi.org/10.1093/biosci/bix146

Swain, D.L., 2015. A tale of two California droughts: Lessons amidst record warmth and dryness in a region of complex physical and human geography. Geophys. Res. Lett. 42, 9999–10003. https://doi.org/10.1002/2015GL066628

Swatantran, A., Dubayah, R., Roberts, D., Hofton, M., Blair, J.B., 2011. Mapping biomass and stress in the Sierra Nevada using lidar and hyperspectral data fusion. Remote Sens. Environ. 115, 2917–2930. https://doi.org/10.1016/j.rse.2010.08.027

United States Forest Service, Region 5, P.S.R., 2017. 2017 Aerial Detection Survey Report.

US Department of Agriculture, 2010. National Agriculutural Imagery Program County Mosaic.

USDA, 2023. National Agricultural Imagery Program GeoHub [WWW Document]. URL https://naip-usdaonline.hub.arcgis.com/ (accessed 4.6.23).

van Wagtendonk, J., Sugihara, N., Stephens, S., Thode, A., Shaffer, K., Fites-Kaufman, J., Agee, J.K. (Eds.), 2018. Fire in California's Ecosystems, Second. ed. University of California Press, Berkeley.

Voelker, S.L., Merschel, A.G., Meinzer, F.C., Ulrich, D.E.M., Spies, T.A., Still, C.J., 2019. Fire deficits have increased drought sensitivity in dry conifer forests: Fire frequency and tree-ring carbon isotope evidence from Central Oregon. Glob. Chang. Biol. 25, 1247–1262. https://doi.org/10.1111/gcb.14543

Wayman, R.B., Safford, H.D., 2021. Recent bark beetle outbreaks influence wildfire severity in mixed-conifer forests of the Sierra Nevada, California, USA. Ecol. Appl. 31, 1–19. https://doi.org/10.1002/eap.2287

Young, D.J.N., Stevens, J.T., Earles, J.M., Moore, J., Ellis, A., Jirka, A.L., Latimer, A.M., 2017. Long-term climate and competition explain forest mortality patterns under extreme drought. Ecol. Lett. 20, 78–86. https://doi.org/10.1111/ele.12711

Yun, Z., Zheng, G., Geng, Q., Monika Moskal, L., Wu, B., Gong, P., 2022. Dynamic stratification for vertical forest structure using aerial laser scanning over multiple spatial scales. Int. J. Appl. Earth Obs. Geoinf. 114, 103040. https://doi.org/10.1016/j.jag.2022.103040

Zhou, T., Popescu, S., Malambo, L., Zhao, K., Krause, K., 2018. From LiDARWaveforms to hyper point clouds: A novel data product to characterize vegetation structure. Remote Sens. 10, 1–23. https://doi.org/10.3390/rs10121949

Chapter 3. THE SEEN AND UNSEEN TREES, ADDRESSING UNCERTAINTY AND BIAS IN HIGH RESOLUTION, REMOTELY SENSED FORESTED ECOSYSTEMS

3.1 ABSTRACT

Remotely sensed forest assessments are effective for evaluating forest canopy conditions across broad extents. However, they can belie population trends hidden in the understory during a drought-induced tree mortality event. In this study, we investigated drought-induced tree mortality trends of remotely sensed trees by matching field trees to tree objects modeled from lidar. First, we asked how error and species status influenced matching field trees to remotely sensed trees. Second, we investigated what population trends were captured by matched trees and which trends in the population remote sensing misses. Finally, we explored what new approaches could improve or extend the range of population trends remotely sensed trees for ecological and management assessments. To do so, we coregistered or matched individual trees on a one-to-one basis to remotely sensed trees. The remotely sensed trees were segmented from lidar captured in 2010 prior to the inception of California's first warm drought. High-resolution imagery, 0.1m resolution, collected post-drought in 2018 and orthorectified by the National Ecological Observatory Network was examined to assess survivorship and matching efficacy. We compared tree height, basal area, and bark beetle presence by species and mortality status between the matched and unmatched remotely sensed and field-based trees. Our measurements revealed that remotely sensed trees are effective for depicting the top-of-canopy forest trends; however, alternate approaches are required to take a census of understory trees.

3.2 INTRODUCTION

In forest ecology, a complete census of all individuals over large areas is commonly infeasible due to the cost and effort of field work. Instead, ecologists use field-based sampling to best represent population trends. With the rapid evolution of remote sensing of the environment, researchers and managers can implement an array of new remotely sensed methods to conduct field-like sampling efforts. These methods can be implemented to identify individual modeled trees (Chen et al., 2018; Edson and Wing, 2011; Jeronimo, 2018; Wing et al., 2015; Yun et al., 2022) across broad extents with high resolution remote sensing. For example, algorithms have been applied to identify or segment individual trees from lidar point clouds (Donager et al., 2021; Edson and Wing, 2011; Wing et al., 2015). In addition, ortho or hyperspectral imagery may be paired with the canopy surface model or with lidar-derived tree measurements to identify species, mortality status, or characterize tree stress (Asner et al., 2017; Fricker et al., 2019; Huesca et al., 2021).

For ecologists and managers who use remote sensing methods and applications, it is important to establish whether remotely sensed methods are biased in representing populations of interest. For example, remotely sensed and field-based studies of a recent drought-induced tree mortality event in California's Sierra Nevada (Lund et al., 2018) produced inconsistent narratives regarding tree morality trends. Studies using remotely sensed airborne and spaceborne data documented significant mortality of tall trees (Hemming-Schroeder et al., 2023; Stovall et al., 2019) in dense stands with high canopy water deficit (Brodrick and Asner, 2017; Huang et al., 2019; Young et al., 2017). However, field-based studies revealed tree mortality was species and size class specific and driven primarily by individual agents of mortality (Fettig et al., 2019; Furniss et al., 2020; Knapp et al., 2021; Wayman and Safford, 2021). Stephenson and Das, 2020 found total tree mortality was skewed towards taller trees because of the overwhelming proportion of tall trees that were pines. However, mortality of non-*Pinus* trees declined slightly with height. This trend is important because the non-*Pinus* trees represented

90% of the total trees present. If the tree mortality event had singularly impacted only the tallest trees, remote sensing and field-based studies would be aligned.

Both the remotely sensed and field-based methods arrived at relevant conclusions based on the sampling data collected. Yet, they produced different narratives about the population trends because the remotely sampled trees represented overstory trees. Overstory trees are a subset of the population captured by field studies (Campbell et al., 2018; Hamraz et al., 2017; Yun et al., 2022). Remote sampling of individual trees can be biased by variable stand structure as well as the methods applied to model the trees (Yun et al., 2022). To determine how well remotely sensed methods represent population trends (Fadili et al., 2019; Holmgren and Lindberg, 2019; Lindberg et al., 2013), it is necessary to measure uncertainty and bias with field validation.

Matching (i.e., coregistering) individual trees to modeled trees segmented from lidar (Fadili et al., 2019; Hauglin et al., 2014; Pascual et al., 2013) can improve field validation and address bias in the population trends captured by remote sensing. Since tree matching became available, the fidelity and availability of open source, high-resolution lidar and imagery has also increased in availability and extent in California. Together, tree matching and high-resolution imagery present an important opportunity to create fused, 3D individual tree objects. These fused trees may be applied to capture, validate, and track overstory tree fate.

We proposed to test matching remotely sensed and field trees on a one-to-one basis. Our research goal was to measure the range of population trends matched trees can capture in response to drought-induced tree mortality. We did so using data combined from airborne acquired lidar and RGB imagery as well as field data, pre- and post-drought. We tested the efficacy of matched trees to explain field-based tree mortality trends resulting from California's first warm drought in 2012-2016 (Diffenbaugh et al., 2015; Gibson et al., 2020; Swain, 2015). Our research questions were:

1. How does error and species status influence tree matching?

2. What population trends are captured by matched trees, and what mortality trends are being missed in the field population?
3. Given these findings, what new approaches could improve or extend the range of population trends of remotely sensed trees for ecological and management assessments?

We studied these questions in a fire suppressed, Mixed Sierran Conifer forest in the Sierra Nevada that was impacted by the drought and tree mortality event.

3.3 METHODS

3.3.1 Study Area

The study area is composed of forests located in the southern portion of California's Sierra Nevada range. Nine, four-hectare plots (Figure 1) of mature, multi-strata Sierran Mixed Conifer forest in the Teakettle Experimental Forest (Allen, 2005; Goodwin et al., 2020) were included in the study. These nine plots were the controls for a long-term fire and fire surrogates study within the 1,300 hectare Teakettle Experimental Forest (Goodwin et al., 2020; North et al., 2002). The control plots were selected due to their century plus legacy of fire exclusion followed by drought-induced tree mortality (Goodwin et al., 2020). In addition, remotely sensed datasets were available in the study area to individually match the field trees to remotely sensed trees. Hereafter, individual tree measurements acquired from stem mapped trees, are referred to as "field trees." Trees modeled from high resolution lidar and assessed for mortality status with orthoimagery are hereafter referred to as "remotely sensed trees." Both the field and remotely sensed tree mortality data were collected prior to and following California's 2012-2016 drought and tree mortality event (Fettig et al., 2019; Swain, 2015).

The Teakettle Experimental Forest is located along the north fork of the Kings River watershed in the southern portion of the Ecoregion and is vegetated with late-seral, mixed Sierran conifer forests (Fry et al., 2014; Goodwin et al., 2020; North, 2002). The study area has

a Mediterranean climate, which has experienced warming and drought events characteristic of the southern portion of the Ecoregion (Asner et al., 2016; Diffenbaugh et al., 2015; Gibson et al., 2020; Swain, 2015). The elevation of the study area ranged from approximately 1,900 to 2,600 m, and annual temperature and precipitation vary from -3° to 25°C and 50 to 125cm, respectively (Goodwin et al., 2020; Krofcheck et al., 2017).

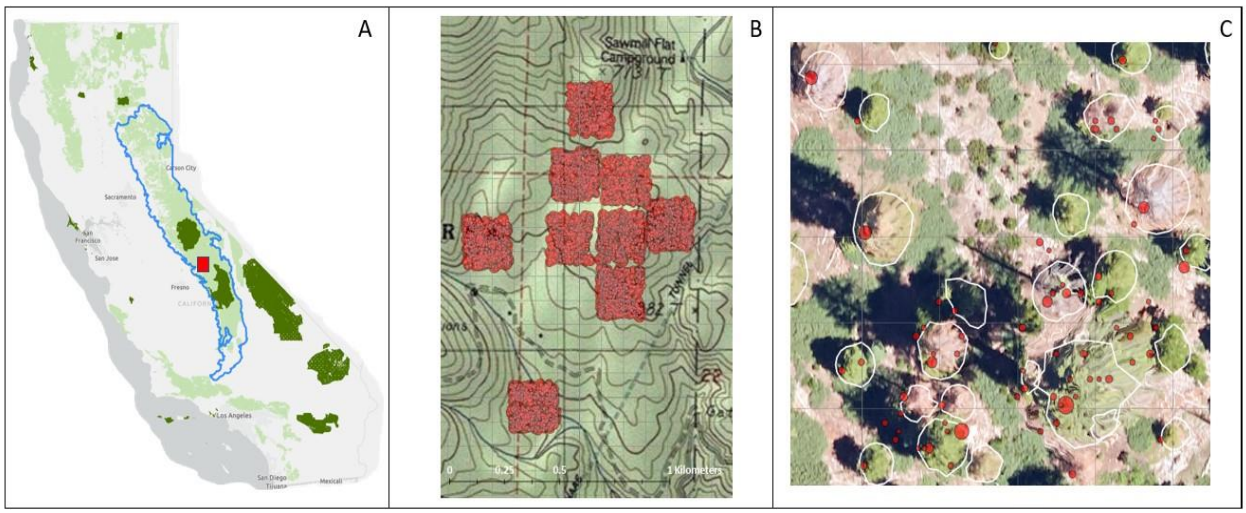

Figure 3.1. Study Area. The Sierra Nevada Ecoregion (A) is a montane, conifer dominated region of California with a Mediterranean climate. The study area (B) is in the Teakettle Experimental Forest in the southern Sierra Nevada, which experienced significant tree mortality during California's first warm drought from 2012-2016. The study area includes nine field plots, each four hectares in area, that were stem mapped with tree measurements collected in 2011 and 2018. Airborne lidar was collected in 2010, which was used to segment trees (Jeronimo et al. 2018) using a watershed segmentation algorithm. Panel (C) shows remotely sensed tree segments as white with red circles representing the field trees from a zoomed in, aerial view of a portion of one of the nine field plots overtop 2018 NEON orthoimagery (Gallery, 2022).

3.3.2. Datasets

3.3.2.1 Pre-drought, 2010 Airborne Lidar

In October of 2010 prior to the inception of California's first warm drought, Watershed Sciences Inc. (Sciences, 2011) collected airborne lidar (i.e., light detection and ranging) over the study area (Figure 3.1). The lidar data were analyzed to segment the remotely sensed trees. Details regarding the acquisition are provided in Table 3.1.

Post-drought, 2018 Airborne Lidar and Orthoimagery Collection

Two years following the cessation of the drought in June 2018, the National Ecological Observatory Network (NEON) acquired high resolution RGB imagery across the study area

(Gallery, 2022; Krause and Goulden, 2015). The imagery was examined to identify the mortality and decay status as well as the presence of lidar segmentation errors of the remotely sensed trees. Acquisition details are provided in Table 3.1.

3.3.2.2 Pre- and Post-drought Field Tree Measurements

The field tree measurements were collected as part of the Teakettle Fire and Fire Surrogates Study and were further described in (Goodwin et al., 2020). In the summers of both 2011 and 2012, prior to the inception of the drought, all field trees ≥5 cm in the nine plots (Figure 3.1) were stem mapped with a total station. All trees were measured for longitude, latitude (x, y), and elevation (z). The measurements for each tree were collected relative to the location of a central, cardinal tree to ensure each tree's position within the plot was consistent (North et al., 2007, 2004). The tree locations were collected in the WGS84 datum and projected to Universal Transverse Mercator (UTM), Zone 11N. In 2018, all tree coordinates were updated using linear regression using the formula described in Appendix B.

Table 3.1.
Remote Sensing Acquisition Parameters including data type and vendor at the time of collection/acquisition, active or remote sensing sensor used to acquire data, acquisition parameters detailing how data was collected, and the geographic coordinate information of the acquisition.

Data Type & Vendor	Data acquisition	Sensor	Acquisition Parameters	Coordinate Information
Airborne lidar, Watershed Sciences Inc.	Pre-drought Summer 2010	Leica ALS50 Phase II sensors	8 pulses/m2, 83kHz 1100 to 1500m altitude Scan angle ±14° from nadir	NAD 83, NAVD88 geoid, Universal Transverse Mercator (UTM)
RGB imagery, National Ecological Observatory Network (NEON)	Post-drought Summer 2018	Phase One D8900 and IXU-RS-1000	0.1m resolution 30 to 50% lateral overlap, 60% image overlap	ITRF00, UTM

In addition to stem mapping, field trees were measured pre (2011-2012) and post-drought (2018) for: 1) diameter at breast height in cm (DBH), 2) identification to species, 3) mortality status (i.e., Alive/Dead), 4) decay status (i.e., methods of Maser et al., 1979), and 5) agents of

mortality (i.e., bark was examined for the presence or evidence of bark beetles such as *Dendroctonus* spp. or *Scolytus* spp).

Of the trees measured, five conifer species were present: *Abies concolor*, white fir; *Abies magnifica*, red fir; *Calocedrus decurrens*, California incense cedar; *Pinus jeffreyi*, Jeffrey pine; and *Pinus lambertiana*, sugar pine. Seventy-one oak trees (*Quercus* spp.) and 43 trees unidentified to species were stem mapped. However, the oaks and unidentified trees were excluded from this study because they were not measured for height and basal area, which were required for matching.

3.3.3 Data processing

3.3.3.1 Allometric equations

Total tree height and crown spread in meters were calculated for all conifer trees using the species specific formulas from (Jeronimo, 2015). The allometric equations for height and crown spread were provided in Appendix B.

3.3.3.2 Remotely sensed tree Modeling/Segmentation

Co-author Jeronimo et al., 2018 described trees segmented from lidar as tree approximate objects. Generally, tree approximate objects represent a single canopy tree or a canopy tree plus one to several subordinate canopy trees. Here, a remotely sensed tree was also defined by the imagery used to identify the mortality and decay status of the tree of interest located within the lidar segment. We selected the watershed segmentation algorithm (Jeronimo et al., 2018; McGaughey, 2018b) from the US Forest Service's FUSION package to model overstory trees from the 2010 lidar data. Although alternate lidar-derived tree modeling approaches can segment subordinate trees (Campbell et al., 2018; Hamraz et al., 2017; Li et al., 2012; Yun et al., 2022), the watershed segmentation algorithm is computationally efficient. We chose this approach due to the computation ease to produce these segments and because

it was commonly applied for forest management analysis in the Sierra Nevada. In addition, the accuracy of this method has been evaluated against a range of trees and stand structures in nearby forests in the southern Sierra Nevada (Jeronimo et al. 2018).

The FUSION software package (McGaughey, 2018) was applied to the airborne lidar to model the remotely sensed trees. First, the canopy surface model (CSM) was produced at 0.75 m resolution, which was necessary to create the remotely sensed trees. Next, the FUSION's TreeSeg utility was applied to model individual trees from the CSM using a watershed transform algorithm, Figure 1. The TreeSeg utility also produced a vector file of the remotely sensed trees, which represents individual tree segments as polygons delineating the fullest extent of a modeled canopy. In addition, the TreeSeg utility provided an accompanying attribute table with location information (i.e., X and Y), tree height (i.e., as Z), and cross-sectional area, per tree.

3.3.3.3 Post-drought Mortality Status, Error, and Imagery Alignment Classification

The mortality status of the trees post-drought was ascertained by the primary author. Each of the remotely sensed trees was individually examined for mortality and decay status; the presence of lidar segmentation errors; whether the top of each tree crown was visible (i.e., nadir), or displayed shadows according to the rubric in Table B.1, Appendix B. This process was conducted by using manual classification in ArcMap Pro, Version 2.8 ("ESRI ArcGIS Pro Version 2.8," 2021) by viewing the 2018 NEON RGB imagery.

3.3.3.4 Matching Field to Remotely sensed trees

We matched or coregistered the field to remotely sensed trees using a multi-step process (Figure 3.2). First, an algorithm developed by co-author Jeronimo was implemented to coregister or one-to-one match field trees to remotely sensed trees, which are presumed to be the same tree. Hereafter, we refer to these matches as "matched trees." This algorithm produced parsimonious matches based on calculating minimum distance measures of location (i.e., X and Y), tree height (i.e., Z), and selecting tree associates within an area of interest (e.g.,

one of the nine plots). To implement the matching algorithm, we used R Studio ("R Studio: Integrated Development for R.," 2022) with R version 4.0 ("R: A language and environment for statistical computing.," 2022). The algorithm steps are further described in Appendix B.

The second step involved a visual, manual evaluation of matching success and probable matches that the algorithm missed. Each of the 3,310 remotely sensed trees were manually examined using the NEON 2018 RGB data. The visual examination was performed after the remotely sensed trees were classified for mortality and decay status, lidar segmentation errors, and the presence of shadows. To do so, each matched pair, unmatched remotely sensed tree, and nearby neighboring field trees were visually inspected for matching accuracy. Trees were inspected for similar mortality status, height, and species to validate matching success or identify and label a new, visual match. The visual examination, was conducted in ArcMap Pro, Version 2.8 ("ESRI ArcGIS Pro Version 2.8," 2021). The rubric for the algorithm, error checking, and visual matching steps was described in Table B.2 on Appendix B. Figure 2 provides a visual example of matched trees in the study area.

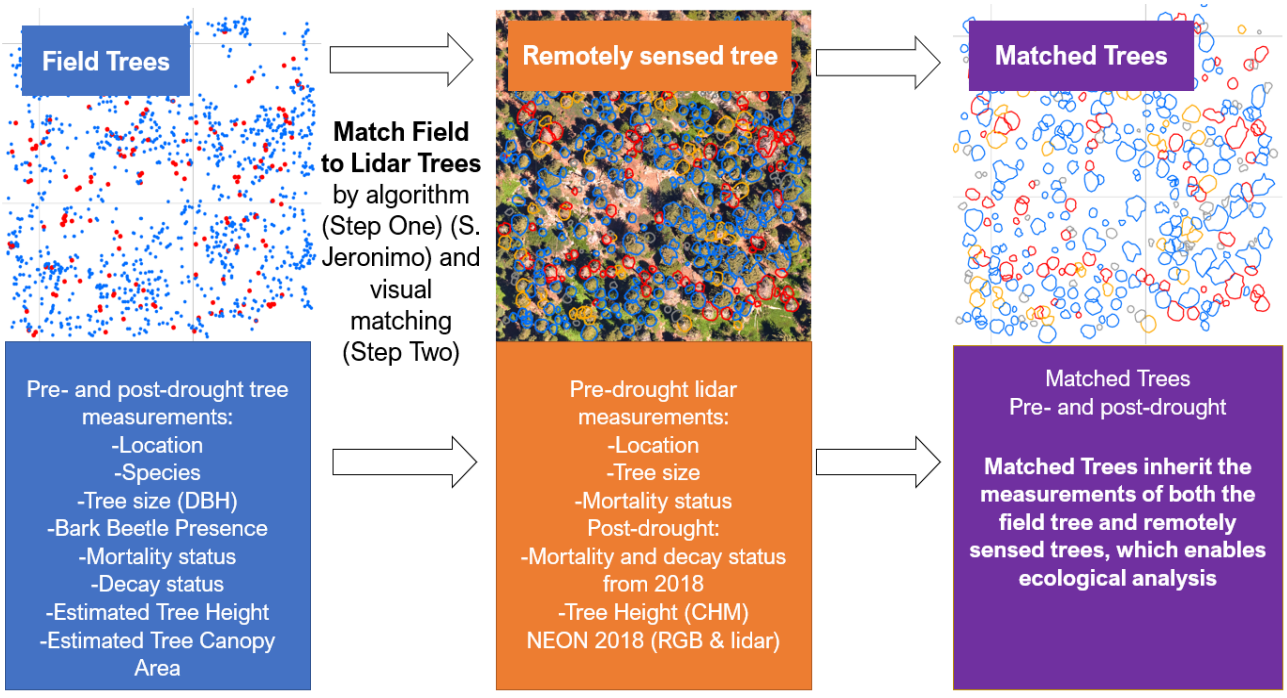

Figure 3.2. Field trees on the left are one-to-one coregistered or pairwise matched to remotely sensed trees on the right to produce matched trees as depicted in the center panel.

3.3.4 Analysis

This examination focused on assessing the tree population trends that matched trees capture in comparison to the trends of the larger field population. Remotely sensed trees that can be successfully matched inherit the measurements of field trees. Matched trees provide the means to assess the proportion of a population sampled with remotely sensed trees. In addition, the field data can be enriched with canopy status information obtained from the examination of high-resolution imagery. For example, a decadent top associated with mature trees or browning crowns from bark beetle (e.g., *Dendroctonus* spp.) presence in *Pinus* spp. can be observed and recorded, which may not be observable during field assessments.

We investigated the population trends of the matched, remotely trees compared to the unmatched remotely sensed and field trees. Hereafter, unmatched trees are defined as all field trees that were not matched to the remotely sensed trees via algorithm or visual matching. In addition, unmatched remotely sensed trees describe any remotely sensed trees not matched via algorithm or visual matching.

All comparisons of remotely sensed to field trees were conducted in the R computing environment (version 4.2.2) with RStudio (version2022.07.2+576) accept where noted. Base r, tidyverse (2.0.0), tidymodels (1.0.0), and the infer package (1.0.4) were applied to conduct statistical tests, respectively.

3.3.4.1 Question 1: How does error and species status influence tree matching?

We quantified the frequencies of lidar segmentation errors including errors of commission and omission in relation to the performance of the matching type (i.e., algorithm or visual matching). Next, the frequency of lidar segmentation error and matching type was compared by taxonomic status. Since lidar segmentation with our methods best models overstory trees (Jeronimo et al., 2018), which are generally the tallest trees, the rate of matching by species and height were compared. The analysis of variance (ANOVA) test was applied to

examine significant differences between tree species, height, and matching status. The ANOVA test was also performed to evaluate if significant differences existed between height, species, and lidar segmentation errors.

3.3.4.2 Question 2: What population trends are captured by matched trees, and what mortality trends are in the field population?

Comparing lidar to field trees: post drought tree mortality

The first question was to establish whether the patterns of tree mortality captured by remotely sensed and field trees were consistent across the nine plots. The frequency of remotely sensed tree mortality detection compared to the field-based tree mortality detection was evaluated using linear regression. The analysis was split into three regressions by height strata classes representing smaller, intermediate, and the tallest trees, respectively, (0 to 10m, +10 to 30m, and +30m) for the nine study plots. This assessment provided insight into two aspects of mortality detection. One, how do remotely sensed trees represent mortality across the field plots by height and between plots? Two, how does remotely sensed tree mortality, as identified with high resolution, RGB orthoimagery, compare to the mortality status of field trees across the height strata classes and plots? To conduct this analysis, only trees alive pre-drought (i.e., prior to 2012) were selected as well as all trees that were identified as dead, post-drought in 2018.

Matching by tree counts and basal area

We evaluated the mortality trends of the remotely sensed and field trees in terms of tree counts and basal area as these are common metrics used in forest management. We conducted the examination by three height strata classes (0 to 10m, +10 to 30m, and +30m). Basal area represents the total cross-section area of all tree stems within a defined area as measured at DBH, and this assessment provided insight into the distribution of tree mortality by

basal area and by height. We performed a two-sided t-test to compare the mean heights of the unmatched remotely sensed and field trees >=30 m.

Matching by conifer species and height

As each matched and visually matched tree inherits the taxonomic information from the field tree, we were able to examine mortality trends by species and by their height. First, we removed additional tree crown segments that were produced as errors of commission (i.e., "oversegmentation") during the lidar segmentation process. We hypothesized that smaller stature trees are poorly represented by remotely sensed trees regardless of taxonomic status.

Matching by survivorship, mortality, and decay

We explored whether remotely sensed trees represented the post-drought mortality (and survivorship) and decay stages of the field trees. To do so, the mortality and decay classes applied to the remotely sensed trees were cross walked to the classes used for the field trees (Maser et al., 1979). Next, the cross-walked classes of all the trees were evaluated by height strata (0 to 10m, +10 to 30m, and +30m).

We also evaluated the accuracy of the post-drought, matched and visually matched tree mortality to the field mortality classes by producing a confusion matrix. For each mortality class, the user accuracy was identified and potential reasons for classification error was discussed. Finally, potential improvements for future examinations of post-drought mortality using remotely sensed tree classification was considered.

Matching by bark beetle presence and tree species

All measured field trees were assessed for the presence of beetles pre- and post-drought, which includes an analysis of evidence of bark beetle activity. Where possible, the field assessment included the identification of bark beetle species. In this analysis, the matched,

visually matched, and unmatched field trees were compared to determine how the frequencies of beetle presence and absence varied by tree species and height.

3.4 RESULTS

3.4.1 Question 1: How does error influence field to remotely sensed tree matching and by species?

Of the 9,785 field trees that were stem mapped, 9,761 conifer trees were available for matching. After the matching algorithm was performed, a total of 2,359 (71%) matches

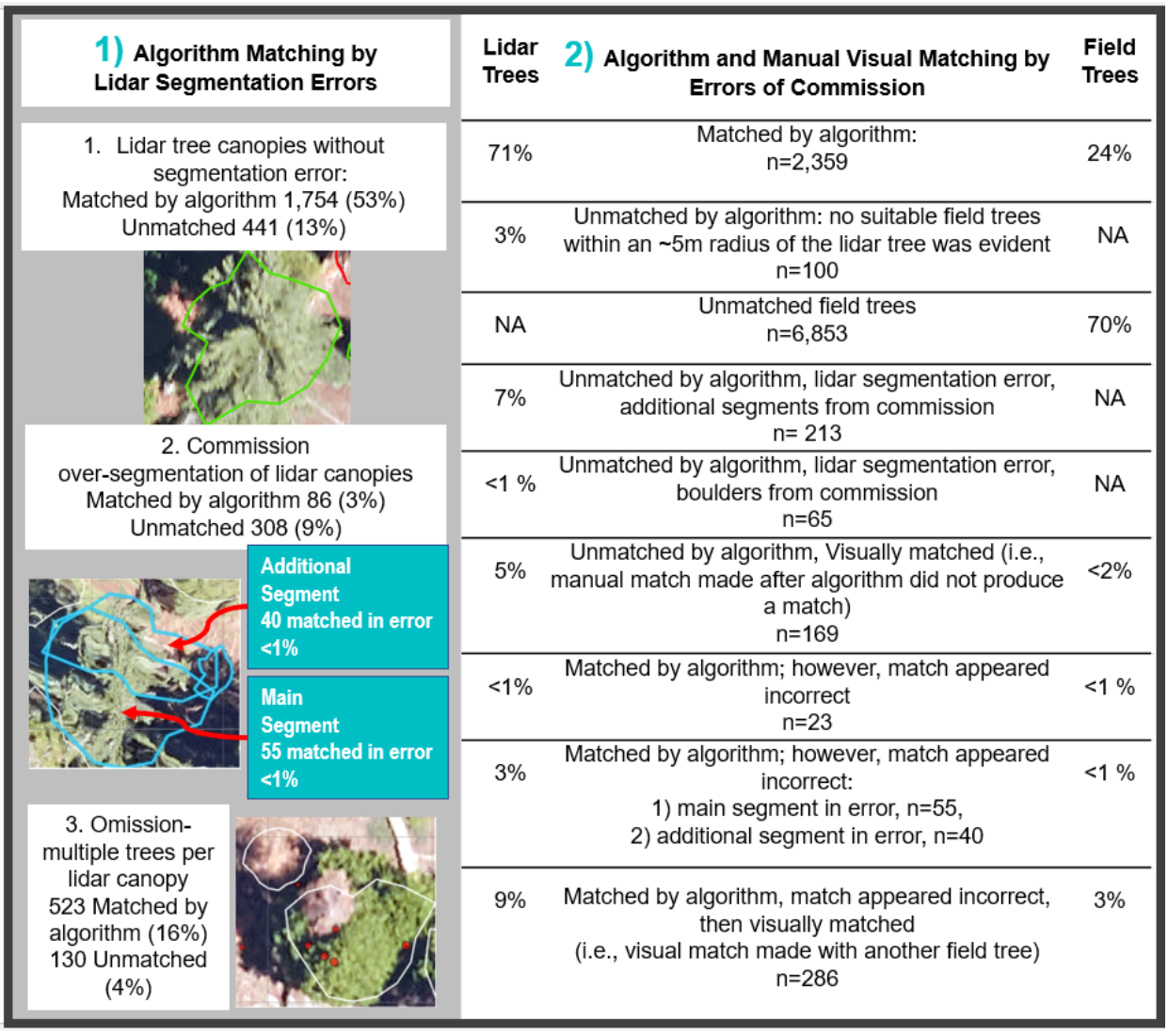

Lidar Trees	2) Algorithm and Manual Visual Matching by Errors of Commission	Field Trees
71%	Matched by algorithm: n=2,359	24%
3%	Unmatched by algorithm: no suitable field trees within an ~5m radius of the lidar tree was evident n=100	NA
NA	Unmatched field trees n=6,853	70%
7%	Unmatched by algorithm, lidar segmentation error, additional segments from commission n= 213	NA
<1 %	Unmatched by algorithm, lidar segmentation error, boulders from commission n=65	NA
5%	Unmatched by algorithm, Visually matched (i.e., manual match made after algorithm did not produce a match) n=169	<2%
<1%	Matched by algorithm; however, match appeared incorrect n=23	<1 %
3%	Matched by algorithm; however, match appeared incorrect: 1) main segment in error, n=55, 2) additional segment in error, n=40	<1 %
9%	Matched by algorithm, match appeared incorrect, then visually matched (i.e., visual match made with another field tree) n=286	3%

Figure 3.3. Lidar Segmentation errors by manual and algorithm matching. Panel 1) Displays the matching frequency of the algorithm by lidar segmentation error; and Panel 2) the algorithm and manual visual matches made by errors of commission involving oversegmented canopies by lidar and field trees.

appeared to be correct (Figure 3.3). The manual, visual matching produced an additional 455 (14% of all remotely sensed trees) matches (Figure 3.3 and Appendix B, Figure B.1).

After evaluating the influence of errors of commission and omission of the remotely sensed trees, the frequency of matching by error type and conifer species was evaluated (Figure 3.4). This analysis revealed that in terms of species trends, pine trees (*Pinus* sp.) had the greatest frequency of algorithm and visual matches. In addition, pines also had the most errors of commission compared to firs (*Abies* sp.), Figure 3.4. The frequency of visual matches was also slightly elevated in *Pinus* spp. compared to the first (Figure 3.4). Finally, the influence of lidar segmentation error on matching was evaluated by species and height with ANOVA. The results of the ANOVA indicated significant differences were present between species by lidar segmentation errors by height (statistic=4.19, df=8, and p-value-5.25e-5).

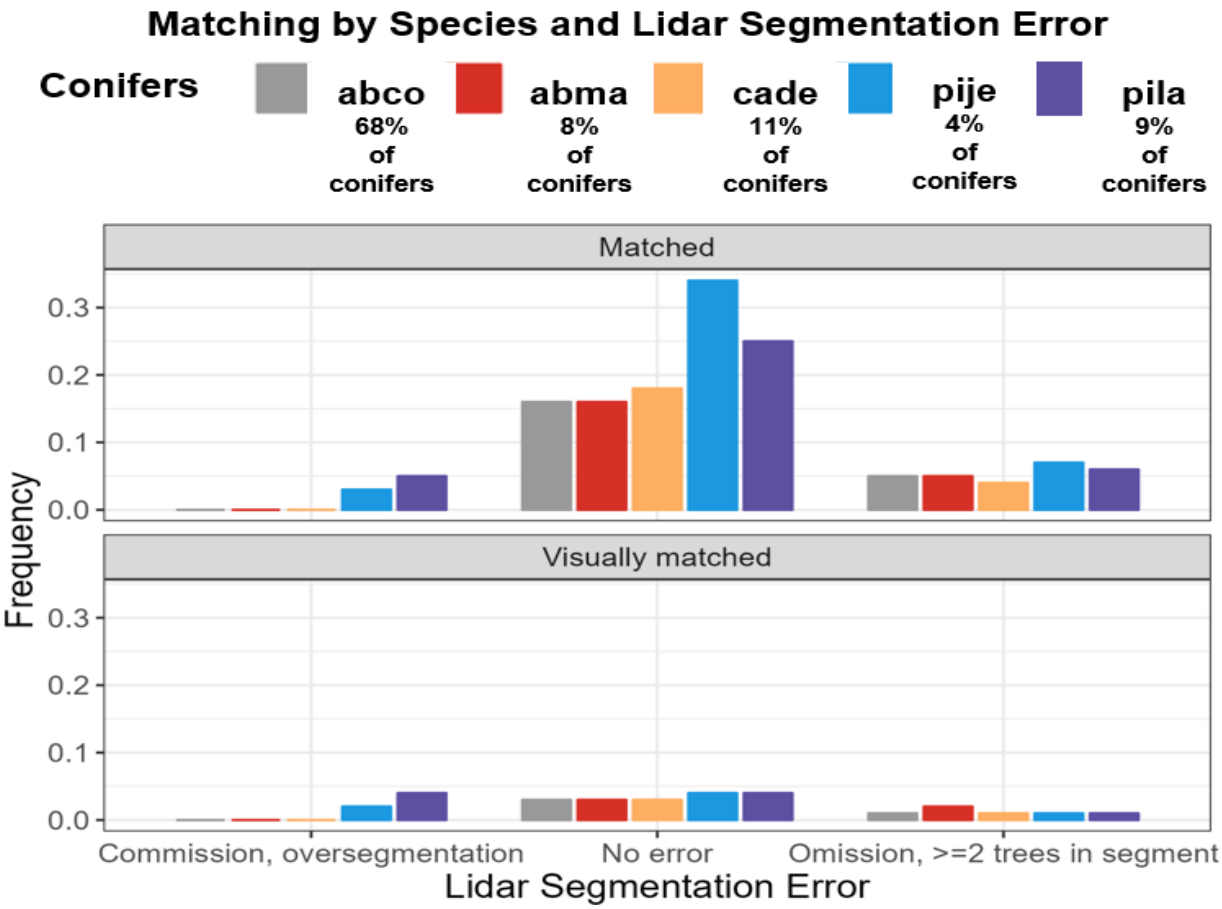

Figure 3.4. Matching by species and lidar segmentation error. The top graph displays the frequency of lidar segmentation error and successful matches by species from the matching algorithm. The bottom graph displays the frequency of lidar segmentation error and visual matched by species. The species codes are abco (A. concolor), abma (A. magnifica), cade (C. decurrens), pije (P. jeffreyi), and pila (P. lambertiana).

3.4.2 Question 2: What population trends are captured by matched trees, and what trends of the field population are being missed in terms of tree mortality?

3.4.2.1 Comparing lidar to field trees: post drought tree mortality

In terms of our comparison of mortality between the 2018 image classified remotely sensed trees and the field-based mortality, the image classified mortality detected 77% to 88% of the field-based mortality, depending upon tree stature (Figure 3.5). When the mortality status of matched and visually matched trees was compared to that of the field assessment, the dead tree detection accuracy was 89%, n=592 and the live classification was 95%, n=1,577.

In addition, 104 remotely sensed trees were classed as mixed live and dead. The post-drought mortality of the remotely sensed trees was ascertained eight years post lidar collection.

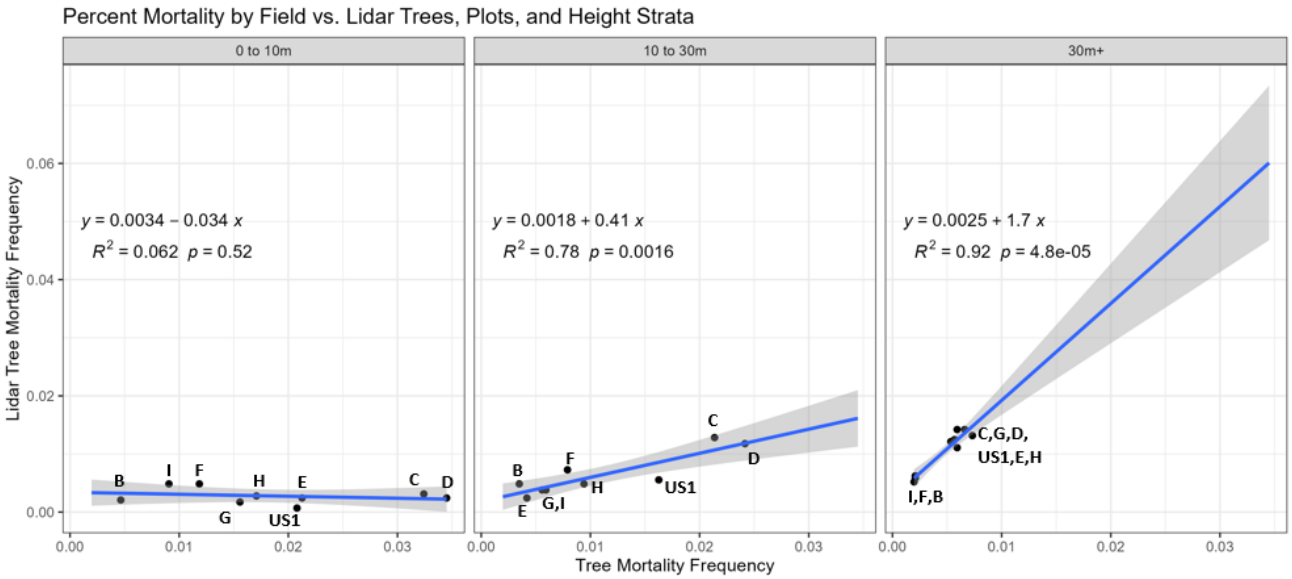

Figure 3.5. Field tree mortality compared to remotely sensed tree mortality by height strata across the nine field plots.

3.4.2.2 Matching by tree counts and basal area

The matched trees captured 69% of the live basal area in the 30m+ height strata, but they represented 53% of the total dead basal area of the trees >=30m. If the visually matched trees were paired by the algorithm, the basal area of dead trees would have increased to 83%. We hypothesized that many of the large remotely sensed trees that died were unmatched due to potential discrepancies in the allometric equation-based heights of the field trees and the remotely sensed tree heights. A two-sided t-test of the unmatched lidar and field trees produced a test statistic of 6.6 (df=126, and p-value=0.1e-9). Thus, the null hypothesis was rejected as the mean heights were significantly different at 37.9 and 43.7, respectively, for the remotely sensed and field trees.

In terms of tree counts, the matched trees poorly represented tree frequencies in the two shortest height classes, and they captured 46% of the dead tree counts in the tallest height

class. Matched trees and remotely sensed trees in general will produce a skewed representation of mortality to the tallest trees. The mortality in the study area was dominated by smaller stature, unmatched trees likely hidden from view, Figure 3.6.

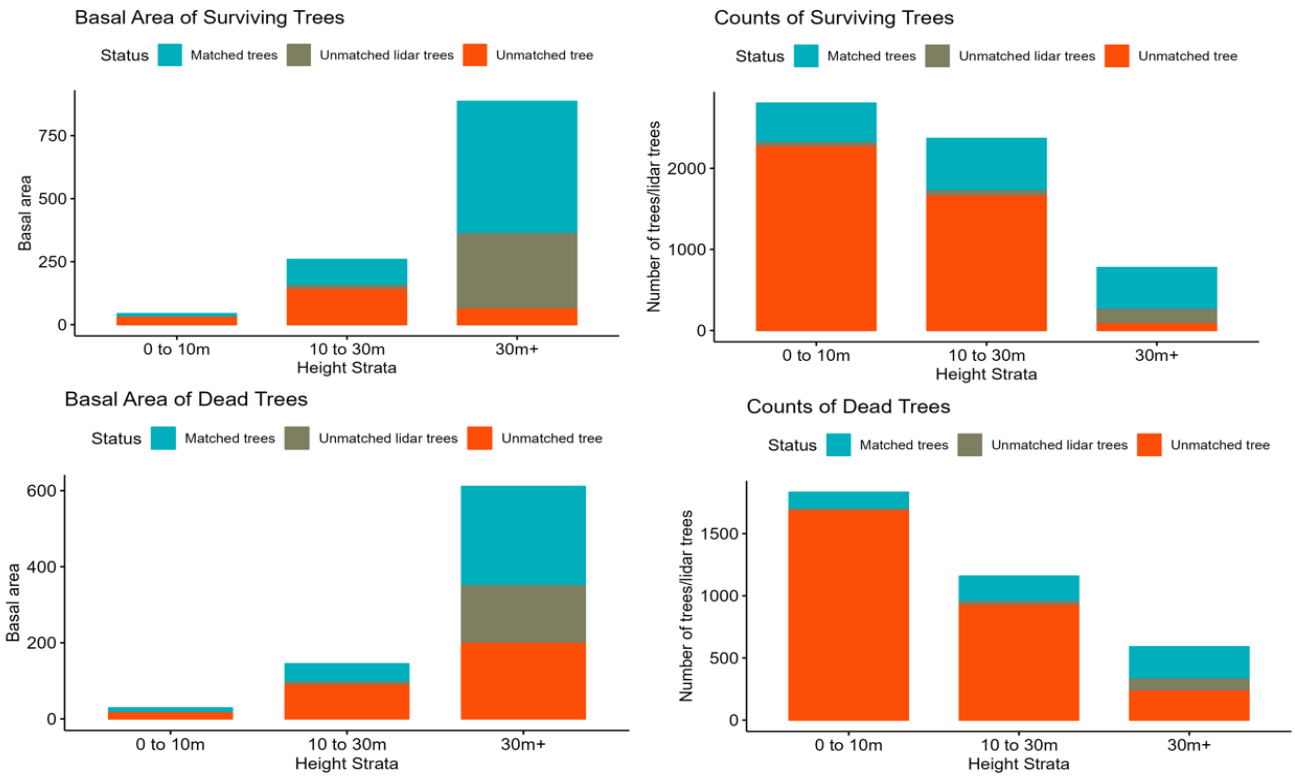

Figure 3.6. Basal area and tree counts by matched, unmatched remotely sensed trees, and unmatched field trees by height classes and surviving trees in the top graphs. The bottom graphs display the trees that died since 2012.

3.4.2.3 Matching by conifer species and height

Of the 8,387 conifer field trees that were alive pre-drought, 581 of these trees were matched and visually matched and perished since 2012. These trees represented 7% of all conifers present. In contrast to the findings of (Hemming-Schroeder et al., 2023), tree mortality

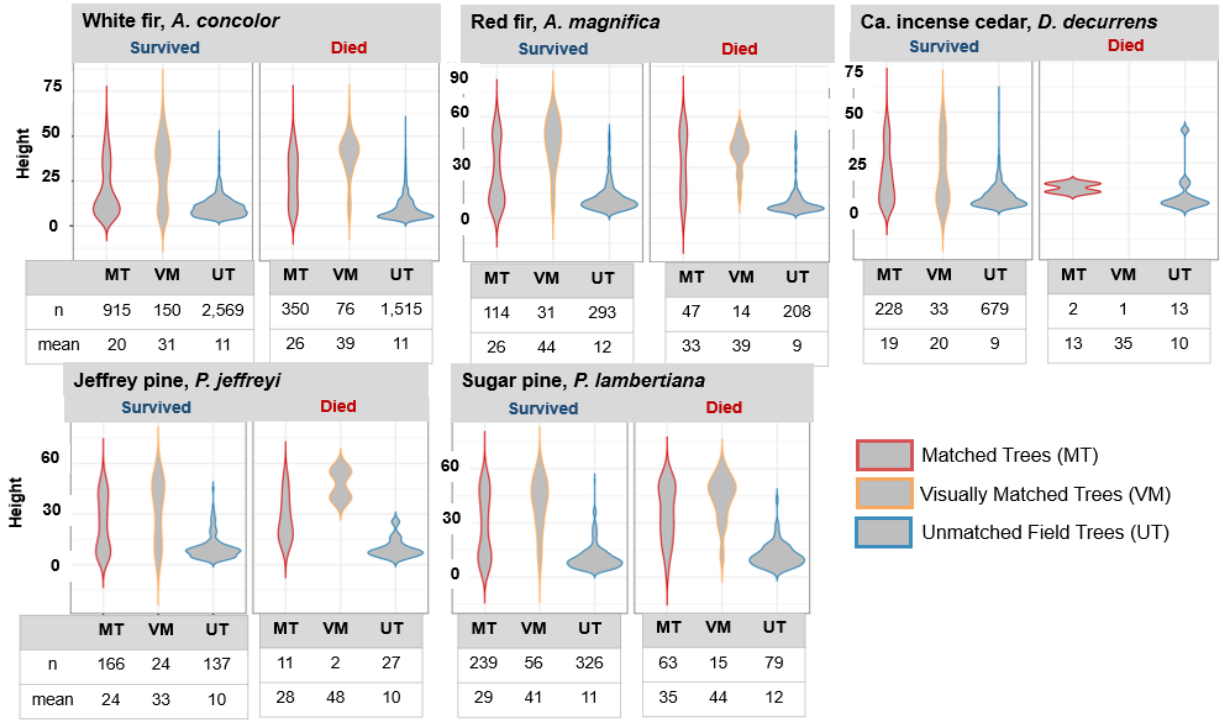

White fir, *A. concolor*	Survived			Died		
	MT	VM	UT	MT	VM	UT
n	915	150	2,569	350	76	1,515
mean	20	31	11	26	39	11

Red fir, *A. magnifica*	Survived			Died		
	MT	VM	UT	MT	VM	UT
n	114	31	293	47	14	208
mean	26	44	12	33	39	9

Ca. incense cedar, *D. decurrens*	Survived			Died		
	MT	VM	UT	MT	VM	UT
n	228	33	679	2	1	13
mean	19	20	9	13	35	10

Jeffrey pine, *P. jeffreyi*	Survived			Died		
	MT	VM	UT	MT	VM	UT
n	166	24	137	11	2	27
mean	24	33	10	28	48	10

Sugar pine, *P. lambertiana*	Survived			Died		
	MT	VM	UT	MT	VM	UT
n	239	56	326	63	15	79
mean	29	41	11	35	44	12

Figure3.7. Violin plots of distributions of matched and unmatched trees by taxonomic and mortality status by height. The distributions of each conifer species that were alive prior to the inception of the drought displayed in terms of height, by matching status and survivorship to 2018. Each species plot includes the total number of trees per category, n, and the mean height in meters, mean.

in this study area was skewed to the shortest trees (Figure 3.7). However, the post-drought mortality for this study was measured in 2018, one year after the mortality measurements collected by Guiterrez et al., 2023. The unmatched field trees that died had a mean height of <=12m and represented 22% of the conifer population.

Sixteen percent of fir trees (*Abies* spp.) that survived the drought were matched. In comparison, 94% of the unmatched trees that died were firs and the mean height was 10.5m. In contrast to the pine trees (*Pinus* spp.) and *D. decurrens,* fir trees were most numerous but least represented in terms of matching and mortality. For example, in terms of mortality 78% of the *A. concolor* that died were unmatched and 77% of *A. magnifica* hat perished were also unmatched. Thus, matched trees poorly reflect the mortality trends of *Abies* spp., which could lead to biased assumptions about fir mortality from a purely remotely sensed perspective.

Last, the matching and visual matching status was evaluated per species by height using ANOVA (Figure B.1, Appendix B). The interaction between species and matching status by height produced a test statistic of 17.4 (df=8, and p-value=4.95-e26). This test statistic was unsurprising considering the stark contrasts in matched and unmatched tree numbers, Figure 3.7.

The post-drought (2018) mortality by taxonomic status was not aligned with the 2000-2002 time period in the Teakettle plots (Smith et al., 2005). Smith et al., 2005 found no taxonomic differences in mortality with an overall mortality rate of 8.7%. In the same plots in 2018, the overall mortality rate was 29% with *Abies* spp. experiencing the greatest mortality.

3.4.2.4 Matching by survivorship, mortality, and decay

The matched trees effectively captured the +30m height class of trees, Figure 3.8. However, the matched and visually matched trees missed most of the dead trees in the 0 to 10m and 10 to 30m height classes in all stages of decay.

Overall, the accuracy of trees identified as dead was >=79%, Table 3.2. However, the remotely sensed tree mortality classification included mixed classes and decay status. Mixed classes include the detection of live and dead vegetation within a remotely sensed tree segment (i.e., the lidar segment). In addition to mixed classes, shadows were responsible for obscuring the mortality status of trees. Seven percent of the matched and visually matched trees were classified as shadows.

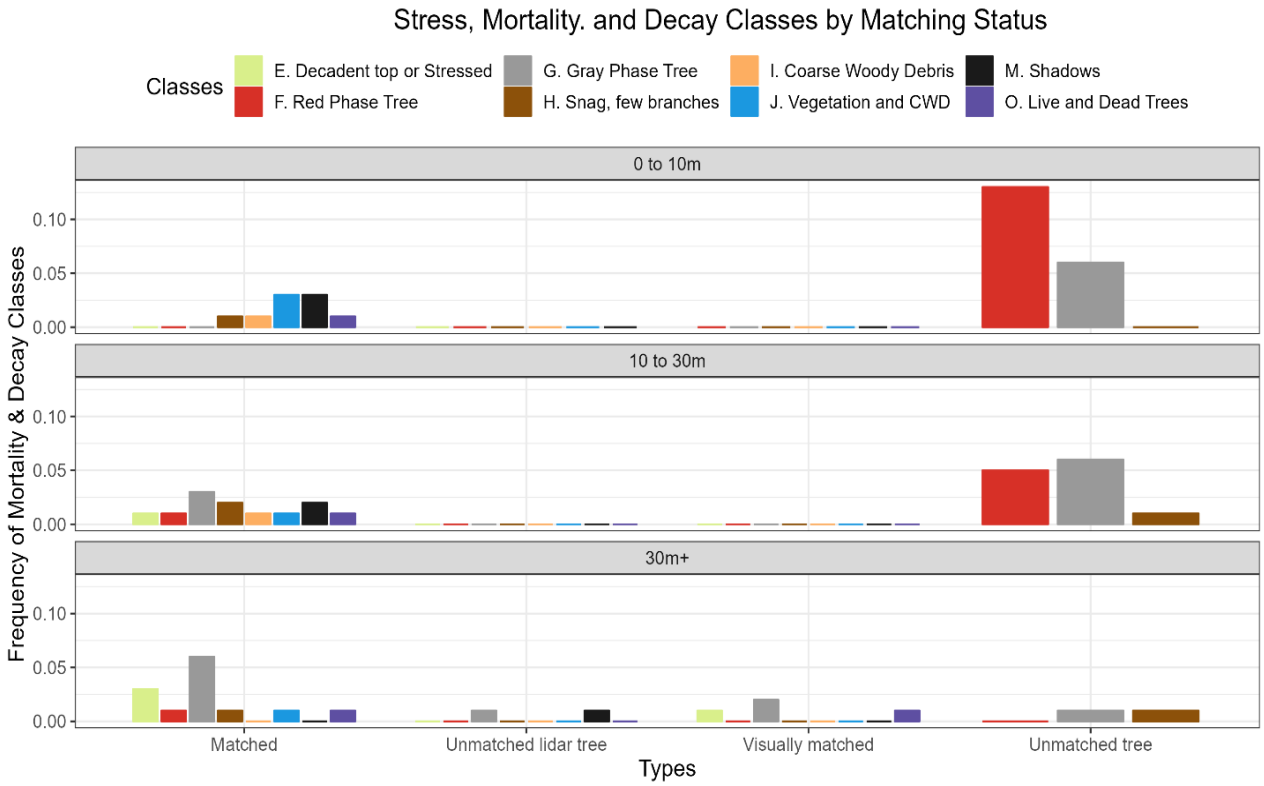

Figure 3.8. Stress, Mortality, and Decay Classes by Matching Status. The mortality and decay classes from the remotely sensed trees were cross walked to the mortality and decay classes of the field trees to produce a comparison of mortality and decay frequencies by tree height.

Table 3.2.
Matched and Visually Matched Mortality Classification Confusion Matrix

Remotely sensed tree Mortality Class	Counts & Accuracy	Error and Potential Classification Improvements
Live	n=1198 97%	Likely producer's error.
Live Ground vegetation	n=12 50%	Live ground vegetation, <3m, may obscure a smaller dead matched neighbor, which can be missed. This class should likely be split based on height of the lidar data. For example, large and tall remotely sensed trees likely represent the footprint of a dead tree where ground vegetation or regeneration is now present.
Live and Coarse Woody Debris (CWD)	n=171 NA	This is a mixed class that is detecting both dead tree material as well as live tree(s). The remotely sensed tree height and age of the lidar could be applied to delineate regeneration and mortality.
Live Shadow	n=202 95%	Shadow may mask the matched tree mortality status.
Live and Dead	n=96 NA	This class is likely produced due to lidar segmentation error or lidar age.
Mixed Stress	n=19 3 dead, 16 live	Monitoring would be required to determine if canopies labeled as stressed eventually die. In other words, is this class predicting mortality or variability in canopy condition?
Mixed Top	n=156 14 dead, 112 live	This class should likely be split into decadent top and browning top to distinguish an older tree from a tree potentially infected with bark beetles that is dying or dead.
Dead Red Phase	n=71 79%	The post drought imagery may be signaling crown stress that is not observable from the field. Five of the 15 trees identified as alive in the field were infected with bark beetles. If these five trees perish, the mortality accuracy increases to 86%. Future imagery collections should be examined for mortality status to determine if classification error or early mortality detection was present.
Dead Gray Phase	n=339 94%	This error may be due to producer's error. Ten of the 32 misclassified live trees did include the presence of bark beetles. This class should be examined for the presence of a decadent top instead of a gray phase dead tree.
Dead, snag	n=123 92%	This class can include other vegetation besides the snag, which could be the matched tree. This class should be examined for splitting into snag and live and snag, or for producer's error.
Other, Coarse Woody Debris	n=51 96%	Error likely due to misclassification
Shadows	n=56 dead trees, n=118 live trees	Shadows occluded the mortality status of 6.6% of the matched and visually matched trees.

3.4.2.5 Matching by bark beetle presence and tree species

Seventy-five percent of the matched and visually matched trees had no bark beetle present, matched n=1,923 and visually matched n=204, Figure 3.9. In the unmatched field trees, 81% or n=5,677 were free of bark beetles. Overall, these trends are consistent. However, the frequencies of bark beetles were not consistent between the unmatched trees and the matched & visually matched by height classes per species.

The 30m+ height class well represented bark beetle presence across the taxonomic groups. In addition, the middle height class (10 to 30m) of the matched and visually matched trees combined reflected the trends of the unmatched trees by taxonomic status. In contrast, the shortest height class of the matched and visually matched trees did not adequately reflect the frequency or bark beetle presence and missed *A. magnifica*.

By proportion per species, the mortality of *A. magnifica* was greatest of all trees in the 0-10m height class. Yet, the matched and visually matches trees combined represented 50% of the infected Jeffrey pines. In summary, the largest frequency of bark beetle presence in *Abies* spp. was hidden from the view of the remotely sensed platform consistent to the tree mortality.

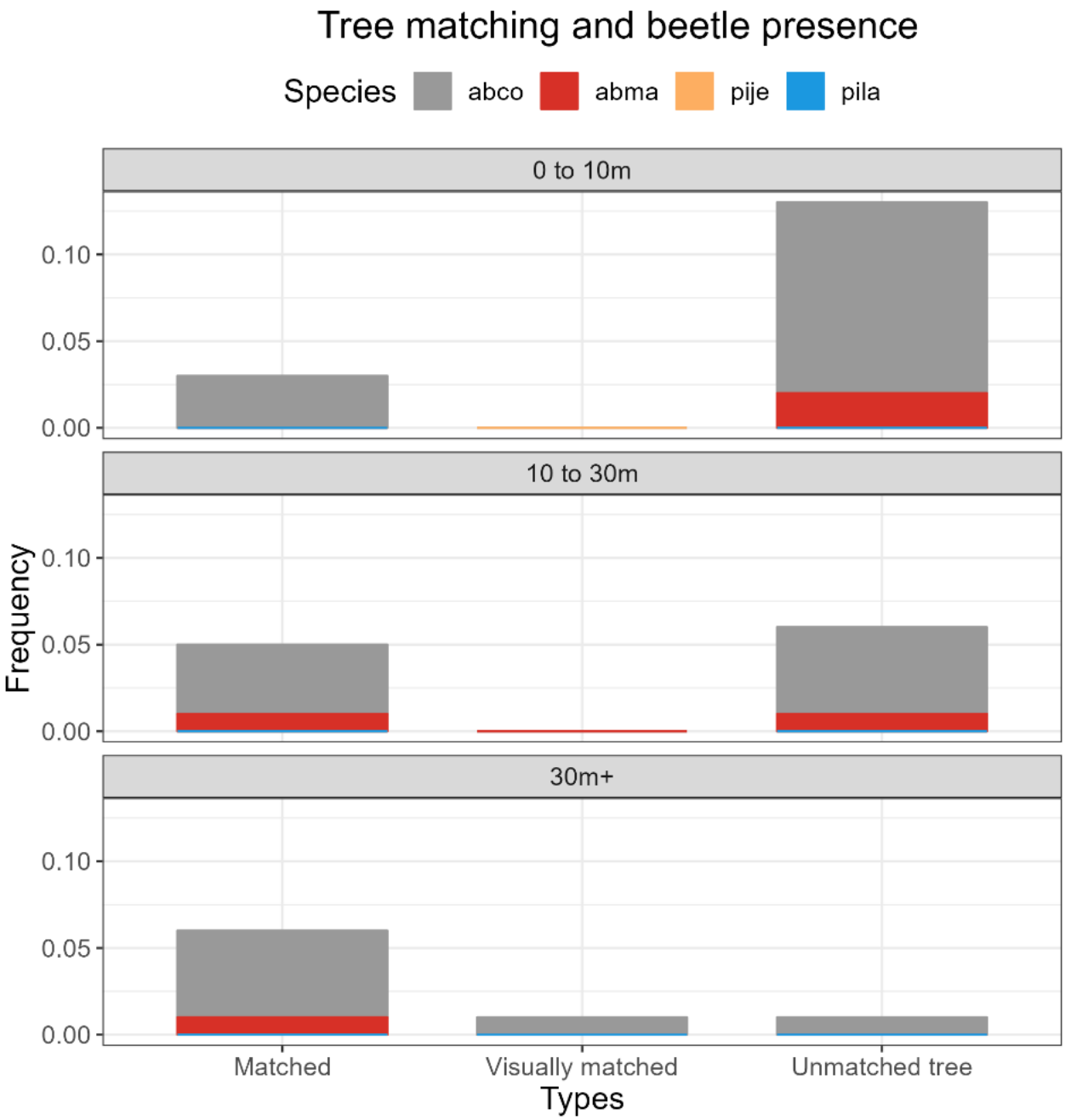

Figure 3.9. Tree Matching and Beetle Presence. The frequency of beetle presence by taxonomic status in matched, visually matched, and unmatched field trees by height strata.

3.5 DISCUSSION

Extensive tree mortality events are increasing globally (Allen et al., 2015; Cansler et al., 2020; Hajek et al., 2022; Hartmann et al., 2022; Huang et al., 2019; Sousa and Davis, 2020; Swann et al., 2018); however, documenting the influence of these events on populations is a pervasive challenge. Remotely sensed trees have been applied as proxies for the assessment of population trends including drought-induced mortality trends. Yet, differences have arisen in reported mortality trends between remotely sensed (Gutierrez et al., 2023; Stovall et al., 2019) and field-based (Axelson et al., 2019; Fettig et al., 2019; Stephenson et al., 2019) studies. These differences highlight the need to assess how remotely sensed trees represent tree populations and trends as well as how bias influences representation. The application of remotely sensed trees is becoming more ubiquitous in ecological and inventory studies of forests (Lisiewicz et al., 2022; Ma et al., 2022; Mokroš et al., 2021; Persson et al., 2022; Piermattei et al., 2019; Qin et al., 2022; Su et al., 2020). However, studies of remotely sensed trees that involve validation through tree matching are emergent (Das et al., 2022; Murray et al., 2019; Zhen et al., 2016), and additional research is required to identify how to integrate novel remotely sensed tree methods into population ecology. Therefore, we sought a greater understanding of the uses and limitations of remotely sensed trees for capturing drought-induced tree mortality trends.

We examined how uncertainty and bias influenced capturing conifer populations and their affiliated mortality trends with remotely sensed trees following the 2012-2016 drought-induced tree mortality event in California's Sierra Nevada. Here, uncertainty is defined as the unmeasured portion of the tree population by field and remotely sensed methods that reduces the representation of the population and associated trends (Bird et al., 2021; Clark, 2003; Rocchini et al., 2016, 2013). Bias is the error present in the application of the methods that further reduces population representation and trends. By matching field trees to remotely sensed trees, large uncertainly was discovered in how remotely sensed trees reflected the tree

population. Less than a third of the tree population and even less of the mortality was represented. The distribution of remotely sensed trees were skewed to the overstory trees, the trees remotely sensed platforms can observe whether tall or short. Consequently, the understory trees that were most numerous, shortest in stature (Figure 3.6), affected by bark beetle (Figure 3.9), and died in larger proportions than their taller conspecifics (Figure 3.7) were obscured from view of the remotely sensing platforms. Live overstory trees were better detected compared to snags (i.e., standing dead trees). Sources of bias most frequently observed included errors of commission, crown oversegmentation, as well as taxonomic bias towards overrepresentation of the most infrequent species. If the remotely sensed trees were independently used to predict tree mortality patterns, large trees would represent the greatest frequency of tree mortality in contrast to the population trends. Our research provides a cautionary tale for the application of remotely sensed trees for population ecology, which requires uncertainty and bias to be addressed as well as repeat, representative sampling in response to environmental changes such as warm drought.

Question 1: The role of error and species status in tree matching

Uncertainty, bias (Babcock et al., 2015; Olofsson et al., 2014; Song, 2018), and taxonomic status influenced how remotely sensed trees represented the conifer populations and mortality trends in the study area. Tree matching and visually inspecting remotely sensed trees with high resolution, post-drought imagery revealed that much of the conifer populations was hidden from view; tree segmentation errors reduced representation; and taxonomic bias was present. For example, our individual tree detection method, watershed segmentation, resulted in an overrepresentation of *Pinus* spp compared to the more ubiquitous *Abies* spp. In terms of mortality patterns, live overstory trees were better detected than snags as measured by remotely sensed trees compared to the field-based methods.

Uncertainty was the greatest source of error in the remotely sensed trees. In the study area, field data showed that small stature trees in the understory were both most numerous and

likely to die. Unfortunately, current airborne and spaceborne based methods will continue to miss the survivorship status of understory trees as they remain out of sight of the sensors. Collectively, we observed several types of errors of commission and omission (Figure 3.3) that elevated uncertainty. These errors were attributed to bias resulting from our tree detection method.

Two forms of errors of omission were observed. The first type of omission errors were overstory trees visible in the imagery that were not segmented, and the second was multiple trees observed within a tree segment. The unsegmented overstory trees that were visible in the post-drought imagery were not assessed. Although we determined which trees in the field population were matched or not, we were unable to identify which overstory trees were unsegmented and thus, unmatched. The NAIP imagery conterminous with the lidar collection in 2010 was too poor in resolution to identify unsegmented trees. Further, it was not possible to assess whether the mortality status at the time of lidar collection in 2010 influenced segmentation. The second type of error of omission was recorded when multiple field trees were observed within a tree segment in the post-drought imagery. However, the presence of these errors did not influence tree matching to the extent of errors of commission. In addition, it is probable that these were not errors of omission in the traditional context. Instead, we surmise that these segments are showing tree mortality changes in a limited area over time. Sometime after segmentation, the overstory tree within a segment of interest likely died, decayed, and exposed multiple subordinate trees creating the appearance of an error of omission.

Based on the data available for analysis, two types of commission errors were present. First, segmentation of boulders were observed as false trees but represented a small fraction of bias and the remotely sensed trees. The second commission error type was oversegmented tree canopies, which most influenced tree matching and mortality detection. Canopy oversegmentation was most frequently associated with large and asymmetrically shaped canopies such as *P. lambertiana* regardless of being live or snag (Figure 3.4). Despite these

biases that influenced uncertainty, the watershed segmentation method applied in this study was demonstrated to perform well for tree segmentation in nearby forests of the same vegetation composition by co-author Jeronimo (Jeronimo et al., 2018; McGaughey, 2018b; Vincent et al., 1991). All individual tree detection methods will have associated bias related to their approaches, which are important to document.

When post-drought, live and snag tree matching was compared by height strata, more live trees were matched in the tallest height strata, >=30m. Importantly, we only evaluated tree matching and tree counts for trees alive at the inception of the study. It seems most probable that the taller unmatched trees that died during the drought were subordinate trees (Figure 3.6). In addition, these trees were likely in the understory and were outcompeted for resources by taller neighbors (Hajek et al., 2022). Future population studies could consider the spatial patterns of bark beetle mortality. Since bark beetle induced mortality is species specific and related to proximity of conspecifics (Fettig et al., 2019; Stephens et al., 2018; Stephenson et al., 2019), it is possible tree density and larger tree clumps may limit mortality detection. Testing multiple individual tree detection methods and by different species composition may benefit future assessments.

Other sources of bias in the field and remotely sensed measurements likely influenced the population uncertainty and mortality trends. Since the field sampling approach was not designed for tree matching, several measurements were lacking for effectively capturing bias. For example, tree height was not measured in the field. It was estimated using lidar-based allometric equations, which may not reliably predict the height of the largest trees effectively (i.e., trees > 50m in height). In addition, while all trees >=5 cm in DBH in were stem mapped and identified to species, tree size measurements of *Quercus* spp. were not collected. Consequently, tree matching did not include the rarest of tree species represented in the study population nor any deciduous trees. Second, tree locations were mapped using older stations in different coordinate systems from the airborne lidar, which was analyzed to segment into the

remotely sensed trees. Third, the airborne lidar from 2010 and the 2018 high resolution imagery were captured in different coordinate systems too, which produced tree alignment error. Data collection in consistent coordinate systems and using more accurate global positioning systems such as Lamping et al., 2021 can improve tree mapping, matching, error assessment, and population trend evaluation.

To improve future comparisons, it would be productive to have consistent classification schemes applied to lidar and field trees to promote direct comparison. In addition, examination of future imagery collections can establish if mixed top, stressed, or red phase classes are correlated with mortality. Table 3.2 also includes explanations for potential misclassification error and highlights several potential classification improvements.

Future studies addressing uncertainty and bias in population studies and trend evaluation would benefit from attempting several strategies to improve outcomes. Multiple tree detection approaches (Edson and Wing, 2011; Hamraz et al., 2017; Jakubowski et al., 2013; Li et al., 2012; Yun et al., 2022; Zhou et al., 2018); testing for taxonomic and survivorship status (Casas et al., 2016; Duncanson and Dubayah, 2018; Wing et al., 2015); and deploying a variety of remotely sensed platforms (Donager et al., 2021; Guan et al., 2020; Yan et al., 2020) could improve results whether these strategies are individually or cumulatively deployed. As Murray et al., 2019 and Zhen et al., 2016 discussed, validating remotely sensed trees is not commonly documented in studies, but it is necessary to evaluate population trends.

Question 2: What population trends are captured by matched trees, and what mortality trends are being missed in the field population?

If the tree mortality story was written exclusively from the perspective of the remotely sensed trees, the mortality trends would indicate that the tallest trees disproportionally died. In addition, the remotely sensed tree data indicated that *Pinus* spp. died in the greatest proportion despite their lower frequency in the overall tree population. The application of tree matching revised the mortality story. Tree matching elucidated that overstory trees and their mortality

trends are observable while the mortality status of understory trees remain out of view (Figure 3.6). While matched trees captured over half of the tallest dead trees (>=30m), twice the number of intermediate trees died (10 to 30m), and more than three times the number of the shortest trees died (0 to 10m). Tree mortality representation by matched trees is inversely related to height. Further, the tree mortality was largely comprised of *Abies* spp. Overall, these trees, were less than 10m in height, positive for the presence of bark beetles, and died. Remotely sensed trees were not effective for capturing mortality trends of the conifer populations across tree species and heights.

In terms of bark beetle presence, species, and mortality trends, mortality detection did not exceed half of the population rate for any species. However, the mortality detection of remotely sensed trees neared half the population for *P. lambertiana* despite this species representing less than a tenth of the conifers. This outcome is expected as *D. ponderosae*, the most common predator of *P. lambertiana*, prefers the tallest trees, which are observable by remotely sensed trees (Axelson et al., 2019; Fettig et al., 2019; Stephens et al., 2018; Stephenson et al., 2019). The proportion of field trees with confirmed bark beetle that were observable by the remotely sensed trees was consistent to the mortality and taxonomic trends. However, the field detection of bark beetle in *Pinus* spp. was lower than the overall mortality rates. This outcome may be due to the pines dying and decaying before the post-drought field study could determine the cause of death by examining beetle galleries. In lower elevations areas, *P. ponderosa* died earlier in the drought with the tallest trees falling prey to bark beetle before shorter conspecifics were attacked (Axelson et al., 2019; Fettig et al., 2019; Stephens et al., 2018; Stephenson et al., 2019).

While tree matching demonstrated the fidelity at which remotely sensed trees could track overstory tree mortality, improved field and remotely sensed tree methods coupled with rigorous repeat measures may aid population and trend detection. For example, studies using remotely sensed trees can incorporate the collection of field sampling in a statistically robust way to

support validation. Repeated measures data are repeatedly collected measurements of representative individuals of a population or a specific portion of the population over time (Taylor, 2004). Repeated measures facilitate tracking population trends in response to events such as droughts, bark beetle outbreaks, root rot, or fire using field or remotely sensed methods. However, repeated measures are only effective in detecting population trends if uncertainty of the field population is low.

Question 3: New approaches to extend remotely sensed tree measurements to population ecology

Our investigation focused on one facet of validation in remote sensing, investigating how remotely sensed trees and their associated error influenced the representation of tree mortality trends. Validation of any remotely sensed information is critical to understanding how the natural and physical worlds are represented (Finley et al., 2017; Kennedy et al., 2017; Song, 2018; Taylor-Rodriguez et al., 2018). Yet, the nature, intensity, and frequency of the verification required in remote sensing is specific to the research or management quesiton. For example, active remote sensors such as lidar can directly measure forest structure, which is important for assessing patterns and the drivers of such patterns. Such studies will require less frequent or rigorous field validation and error assessments (Babcock et al., 2015; Congalton, 2001; Duncanson et al., 2020; Kane et al., 2010a, 2010b) depending upon the question of interest. Since remotely sensed trees are effective for sampling overstory tree mortality (Das et al., 2022; Hemming-Schroeder et al., 2023; Stovall et al., 2019) or quantifying the majority of dead biomass, validation may not be as comprehensive as population studies such as monitoring mortality trends. In contrast, newer remotely sensed technologies and passive sensors used in new applications require more intensive validation and bias assessment (Murray et al., 2019; Zhen et al., 2016).

Population studies and validation

Population studies are unique in the degree of validation necessary to represent and repeatedly assess a population and measure trends. In terms of assessing tree population trends, these studies require representative sampling of individuals through time in response to stimuli (Falk et al., 2019; McCune et al., 2002; Rocchini et al., 2016; Stephenson and Van Mantgem, 2005), which is a difficult threshold for remotely sensed trees that are biased to the overstory trees. Population studies require uncertainty, bias, representative sampling, and repeated measures to effectively detect trends. Studies that analyze remotely sensed trees that do not meet these requirements are not rendered obsolete; they contribute to important research and management questions that describe conditions or correlations with biophysical settings (Jeronimo et al., 2018; S. M. A. Jeronimo et al., 2019; Kane et al., 2019). However, assumptions drawn from unvalidated data regarding population trends have a much greater probability of being incorrect (Babcock et al., 2015; Bird et al., 2021; Friedlingstein et al., 2022; Holling, 1973; Song, 2018).

Ideally, the research or management question should drive the experimental design, remotely sensed data collection, and relevant field validation approach in population studies for trees. However, many studies such as this one are opportunistic in nature, and the research questions are sometimes developed post-hoc. In post-hoc studies with an absence of validation datasets, it is advisable to restrict the interpretation of the remotely sensed data within the bounds of the measurable unit (Stephenson and Das, 2020) such as overstory trees. Otherwise, insufficient information can yield uncertainty and bias that can skew observed trends away from the population mean (Bird et al., 2021; Friedlingstein et al., 2022; Holling, 1973; Song, 2018). While the focus of attention in this study is remotely sensed tree methods for population studies, field-based studies cover constrained areas and have uncertainty and bias as well. However, in this study the field-based measurements are the metric for comparing the fidelity of the remotely sensed trees to assess the measured population In attempting to

determine the range of the tree population represented by our post-hoc data, we found several limitations of our data that can also influence population studies of trees.

We encountered challenges in verifying how remotely sensed trees represented the tree populations in terms of recording drought-induced mortality. The post-hoc nature of our study was one of several limitations that restricted our success in identifying the population represented by remotely sensed trees and the observed mortality trends. For example, our field and remotely sensed data were independent collections not intended for the express purpose of tree matching or validation. Our datasets were collected in different coordinate systems and spatial resolutions, which were not optimal for validation. In addition, not all tree species were consistently measured and tree height was estimated with allometric equations. For future studies, collecting tree data with high-grade global positioning units or UAV with sufficient ground control (Lamping et al., 2021; Qin et al., 2022; Yan et al., 2020) and in consistent coordinate systems to other data is important. If population studies are the goal, it is vital to collect taxonomic, location, and size measurements, especially height and crown area, as consistently as possible.

The need for defining the population trends of remotely sensed trees in ecology

Significant advancements in remote sensing of individual trees have occurred in the last several years using a variety of platforms (Lisiewicz et al., 2022; Ma et al., 2022; Mokroš et al., 2021; Persson et al., 2022; Piermattei et al., 2019; Qin et al., 2022; Su et al., 2020). New technologies now exist to identify trees from hand-held (Donager et al., 2021; Mokroš et al., 2021), backpack (Su et al., 2020), terrestrial (Rowell et al., 2020), unmanned aerial vehicles (UAV) (Guan et al., 2020; Hastings et al., 2020; Lamping et al., 2021; Mohammadpour, Pegah, and Viegas, 2022; Paczkowski et al., 2021), and airborne collected lidar, orthoimagery and hyperspectral imagery in a variety of vegetation types and complex structured forests (Brodrick and Asner, 2017; Jeronimo, 2015; Kane et al., 2019). New technology is evolving at breakneck speeds to apply artificial intelligence to map forests using individual tree detection with high

resolution remote sensing (Kattenborn et al., 2021; Khatri-chhetri et al., 2023; Shivaprakash et al., 2022; Wagner et al., 2020) These technologies and methods provide significant opportunities for improving the ecological understanding of tree-based ecosystems. Here, we discuss what approaches may support population studies such as the assessment of trends in drought-induced mortality.

Researchers who intend to deploy remotely sensed trees to evaluate population trends should consider a framework for incorporating field validation in their methods. This methodological framework should address uncertainty, bias, repeated measures, and representative sampling to successfully investigate a population study. Representative sampling is a fundamental requirement of population studies (Grafström and Schelin, 2014). It ensures that the breadth of individuals representing various demographic conditions and biophysical setting are evaluated for responses to changes in the environment. In single strata tree ecosystems such as a savannah or oak woodland, representative sampling may be possible with remotely sensed trees and validated with field-based observations (Huesca et al., 2021). However, even in single strata tree ecosystems, field-based assessments for validating remotely sensed observations (Campbell, James B., Wynne, 2011; Congalton, 2001) for population studies are important. For example, remotely sensed data can be applied to capture stress or mortality from root rot in individual overstory trees (Allen et al., 2022; Calamita et al., 2021) with accuracies in the range of >=70%. Yet, these approaches can miss emergent changes in tree status, which may be important for monitoring ecosystems experiencing significant environmental stress such as a novel pathogen. In complex, multi-strata forests such as our study area, additional considerations are important for conducting representative sampling.

In extensive forested areas with complex, multi-strata forests representative sampling can be a daunting challenge. These forests may be composed of diverse forest types, multiple species, large numbers of individuals occupying multi-strata, and topographically rich terrain.

These conditions complicate representative sampling and repeat sampling (Atkinson, P.M. and Foody, 2002; Grafström and Schelin, 2014; Rocchini et al., 2016). Yet, a variety of new technologies in remote sensing may provide the means to improve population studies involving trees and promote increased representative and repeat sampling.

For example, new automated algorithms may afford improved detection of understory trees and other vegetation from airborne lidar (Chen et al., 2018; Yun et al., 2022). While these approaches can aid in tree identification and mapping including characterizing stand structure and tree patterns (Jeronimo et al., 2019; Kane et al., 2019), additional approaches will be needed to validate the remote sensing data; identify species; and classify survivorship. Capturing understory tree mortality trends will likely include more extensive and repeated field surveys via traditional assessment means or hand-held (Donager et al., 2021; Mokroš et al., 2021), backpack (Su et al., 2020), terrestrial (Rowell et al., 2020), and unmanned aerial vehicles (UAV) (Guan et al., 2020; Hastings et al., 2020; Lamping et al., 2021; Mohammadpour, Pegah, and Viegas, 2022; Paczkowski et al., 2021) with lidar and imaging platforms.

Researchers could experiment and compare the efficacy of several new technologies in long term monitoring plots where the field population is well documented. Mobile lidar, traditional cameras, and UAV platforms instrumented with lidar and imaging cameras could be compared for their capabilities to acquire representative samples in established plots. If subordinate trees can be modeled and matched, UAV acquired imagery and field validation could support tracking individual trees through time. In addition, terrestrial and mobile lidar systems and UAV collected imagery (Donager et al., 2021; Hastings et al., 2020; Marchi et al., 2018; Mohammadpour, Pegah, and Viegas, 2022; Paczkowski et al., 2021) could be paired with traditional field sampling.

Collectively, these sampling approaches could be implemented using more efficient and cost-effective study designs. Since many researchers employ various remote sensing and field sampling efforts across disciples, opportunities exist to leverage partnerships and share

resources to collect field data. For example, the Airborne Snow Observatories, Inc. (Ferraz et al., 2018; Painter et al., 2016) has partnered with the State of California and other agencies to capture higher fidelity snow off airborne lidar and hyperspectral data, which is also applied to examine post-fire forest conditions.

Greater access to open-source data along with innovation is improving the ability to track individuals and population trends through time. For example, new software applications such as plantTracker (Stears et al., 2022) allow maps of plant occurrences to be translated into demographic data and tracked through time. In addition, artificial intelligence provides many avenues for improving the capture of individuals and population trends in forest ecosystems (Shivaprakash et al., 2022). As open source, benchmark datasets become available that include information capable of tracking individual trees, the application of artificial intelligence in population studies will likely increase exponentially. Regardless of the technology and innovation applied, addressing uncertainty, bias, repeated measures, and representative sampling will remain important requirements to transitioning remote sensing of trees to population ecology.

Appendix B, Chapter 3

B.1: Remote Sensing Acquisitions
2018 NEON Orthoimagery-Mortality Status

The NEON program collected 3-band, 0.1 m imagery over the Lower Teakettle Area of Interest, which subsumes the study area (Figure 1) and provided a detailed overstory view of tree status in high spatial resolution. Unlike traditional orthorectification to the digital terrain model that often results in distorted side-views of tall trees, the NEON program used an orthorectification process to balance distortion related to taller objects such as trees. Instead, the images were spatially resampled to reduce the discrepancy in resolution from lidar to camera, which provided a more nadir (i.e., top of the crown) view of trees.

B.2: Post-drought Mortality Status-2018

The NEON 2018 RGB orthoimagery provided high-resolution imagery to detect mortality and decay status. In addition, the lidar height and canopy area measurements along with the NEON imagery allowed each remotely sensed tree to be examined for errors of lidar segmentation commission and omission (Figure 4). Despite the NEON 2018 imagery being collected in narrow flight lines with overlap, the combination of the image overlap, tall trees, and orthorectification still produced view of trees that were not a nadir (i.e., birds eye view) of the trees. For each of remotely sensed trees, the mortality and decay status, presence or absence and type of lidar segmentation error, and nadir status was observed and recorded.

Table B.1.

Rubric of 2018 Mortality and Decay, Lidar Segmentation Errors, and Nadir Status for Classification of the pre-drought and post-drought remotely sensed trees by the Post-mortality status

General Remotely sensed tree Mortality Class for Comparison with Field Tree Mortality	Detailed Mortality Label	Crosswalk to Decay Classes applied to Field Trees	Example	Detailed Mortality and Decay Class Definitions applied to 2018 NEON 0.10 m resolution imagery
Live	Live	A Fully intact, Graphed as "A. to D. Live trees"	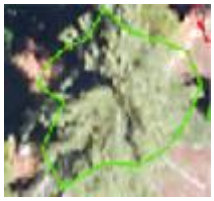	A probable live tree occupies ~≥2/3 of a remotely sensed tree segment, and the remainder is other material (e.g., ground, coarse woody debris, ground vegetation, rock, dead tree, or unknown). A live tree appears as a shade of green in RGB data.
Live	Live Shadow	A Fully intact, Graphed as "A. to D. Live trees"	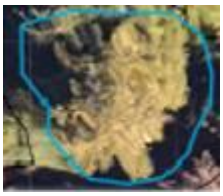	A probable live tree occupies ~≥2/3 of a remotely sensed tree segment and the remainder of segment is composed of shadow. A live tree appears as a shade of green in RGB data, with the lower part of the crown shrouded in shadow. This class was created to examine the rate of potential misclassification as dead.
Live (likely Regeneration)	Live with CWD	Not part of the field decay class as this object no longer represents a snag.		An emergent live tree or shrub occupies ~1/3 of the remotely sensed tree segment while another ~1/3 is occupied by coarse woody debris that likely represents the dead dominant tree that represented the remotely sensed tree segment. The remaining 1/3 of the lidar segment may be occupied by other material.

Live	Live Ground Vegetation	A Fully intact, Graphed as “A. to D. Live trees”		Imagery within the remotely sensed tree segment displays probable live, green ground vegetation with a minimum of ~≥2/3 of the segment, and the remotely sensed tree has a maximum height <3m with no apparent shadow in the imagery. It is unknown if this lidar segment represents an error of commission, vegetation cover (i.e., a shrub), or is a tree.
Live	Mixed Top	A Fully intact, Graphed as “E. Decadent top or Stressed”		A browning crown or decadent top occupies 25% or less of the remotely sensed tree in the imagery, the remainder of the remotely sensed tree segment appears to be composed of live, green tree cover. Together the browning crown/decadent top and the live canopy occupy ~2/3 of the segment. The remainder of the pixels in the imagery may include other material.
Live	Mixed Stress	A Fully intact, Graphed as “E. Decadent top or Stressed”		A yellowing or browning tree canopy cover occupies ~≥2/3 of the remotely sensed tree segment, and the remainder is not the tree canopy (e.g., ground, coarse woody debris, ground vegetation, rock, dead tree, or unknown). The yellowing or browning tree may have evidence of branches without needles.
Mixed	Mixed Live and Dead	Not applicable as this is a lidar segmentation error		A combination of live and red or gray phase dead trees where at least a third of the imagery is occupied by a live tree, a third by a dead tree, and the remainder may include a view of the ground cover and/or ground vegetation.

Dead	Dead Red Phase	A Fully intact, Graphed as “F. Red Phase Tree”		A presumed dead, red phase tree cover occupies ~≥2/3 of remotely sensed tree segment and remainder of segment is composed of material other than the tree canopy. The red phase of a tree is typically associated with post tree mortality where the needles have not fallen off the branches.
Dead	Dead Gray Phase	B Recently dead, intact top, fine branching and bark, Graphed as G Gray Phase Tree		A dead, gray phase tree cover occupies ~≥2/3 of the remotely sensed tree segment and the remainder of segment is composed of material other than the tree canopy. In the gray phase, a portion of the top may have broken off; however, the tree branches remain mostly in-tact and the snag appears almost white gray.
Dead	Dead Stump	F Dead, top repeatedy broken. No coarse branches, bark unknown, <=6m, Graphed as H Snag, few branches		A dead standing tree snag without evidence of significant branching occupies the remotely sensed tree segment and may occupy <25% of the remotely sensed tree segment area. The rest of the segment area may be occupied with other material (e.g., ground, coarse woody debris, ground vegetation, rock, live vegetation, dead tree, or unknown).
Dead	Other Course Woody Debris	Not part of the field decay class as this object no longer represents a snag.		Coarse woody debris occupies ~≥2/3, of remotely sensed tree segment and the remainder is other material (e.g., ground, coarse woody debris, ground vegetation, rock, dead tree, or unknown).

Other	Other/Unknown	Not applicable as this is an imagery alignment issue		A combination of live and dead vegetation, mixed ground cover, CWD, ground vegetation, or rocks each of minority proportions for which the viewer could not identify the remotely sensed tree segment or mortality status.
Other	Other Ground	Not part of the field decay class as this object no longer represents a snag.		The remotely sensed tree segment provides a view of the ground and may be composed of pine needles or dirt filling ~≥2/3 of the remotely sensed tree segment. The remainder of the remotely sensed tree segment may include live or dead vegetation or other material.
Other	Other Boulder	Not applicable as this is a lidar segmentation error		A boulder occupies ~≥2/3 of remotely sensed tree segment, and the remainder is not the boulder (e.g., ground, coarse woody debris, ground vegetation, dead or live tree, or unknown).
Other	Other Shadow	Not applicable as this is related to object position, other objects and sun angle		A shadow occupies ~≥2/3 of remotely sensed tree segment, and the remainder is not the shadow (e.g., ground, coarse woody debris, ground vegetation, dead or live tree, or unknown).
Lidar Segmentation Errors: Omission and Commission		**Example**		**Description**
No lidar segmentation error observed “No error”				Remotely sensed trees without segmentation errors appear to capture the full extent of the dominant tree canopy.

Commission-over-segmentation of the lidar canopy		Remotely sensed tree segments that were associated with the same dominant tree canopy and of the same relative height (i.e., within 3m in height) were labeled as over-segmented. The largest of the canopy segments was labeled as main and was considered as a single tree, and the remaining segments were labeled as additional. Unless noted, the additional segments were not included in the comparisons with field trees except to report total frequencies, where noted.
Omission-2 or canopy trees observed in the lidar segment		Remotely sensed trees were labeled as errors of omission when two or more canopy trees were clearly visible within the remotely sensed tree segment.
Commission-boulders		Boulders are common natural features in the Sierra Nevada, and they can be the same relative height and canopy spread as a smaller tree. They were labeled as specific errors of commission.

B.3: Field-based tree measurements, "field trees"

To update the locations of each tree the original value was multiplied times the slope and the original intercept value was applied to each x, y, and z coordinate, respectively. For this analysis, the updated tree measurements acquired from the linear regression were reprojected to the coordinate system of the airborne lidar data.

B.4: Allometric equations

These formulas were derived from lidar based measurements of trees in the southern Sierra Nevada in the Sierra Mixed Conifer forest type, which occupies the study area and are described in (Jeronimo, 2015).

$$\log(Height) \cong -0.34 + 0.84 * \log(DBH) + c\ (spc1)$$

$$CrownSpread \cong 0.98 + 0.04 * DBH + c(spc3)$$

The species-specific constant for Height ($_{spc1}$) for *A. concolor* is 0.19, *A. magnifica* is 0.17*, C. decurrens* is 0, *P. jeffreyi* is -0.06, and *P. lambertiana* is 0.18. For crown spread, the species-specific constants ($_{spc3}$) are *A. concolor* is 0.12, *A. magnifica* is -0.19*, C. decurrens* is 0, *P. jeffreyi* is -0.58, and *P. lambertiana* is 1.30.

The estimated measures of height and crown spread are necessary to compare field trees to remotely sensed trees, which include maximum height, canopy area, and circumference. The basal area of all trees included in the analysis were calculated from the DBH using the following formula.

$$Basal\ area \cong pi * (\frac{DBH}{200})\text{^}2$$

B.5: Tree matching: examining matched pairs and visually matching pairs
Step One: Matching algorithm

We implemented a two-step process to match field to remotely sensed trees. First, the algorithm for automated matching is described. The first step was to calculate the high and low heights of field trees by applying the 95% confidence interval to the height of each tree. By producing a range of height values, the probability of correct matching increases as allometrically based tree heights are estimates with error and remotely sensed tree heights are directly measured. A new value for crown spread was also calculated to examine potential pairs after matching; the overall crown spread error was added to each field tree's crown spread value. Next, for each field and remotely sensed tree in each plot, a distance matrix was calculated, dist.3d, from the X, Y and Z locations of each field and remotely sensed tree,

respectively. The dist.3d matrix serves as the input into a function where the minimum distance values are applied to identify potential associates. These associates are probable, one-to-one field to remotely sensed tree pairs. The lidar derived height of each candidate pair is then examined to determine if it is within the height ranges of the field trees. Tree pairs that met this height criteria were labeled as coregistered or matched.

Step Two: Evaluating matches, assigning visual matches, and labeling probable error

We manually examined each 2010 remotely sensed tree segment with the NEON 2018 imagery to evaluate matching status, the presence for potential visual tree matches; and error. For example, we labeled matches as likely incorrect when the remotely sensed tree in the 2018 imagery was a tree stump and the field tree was identified as alive in 2018. Another example of potential error occurred when there were no suitable field trees for a visual match. In addition, all unmatched lidar and unmatched field trees were evaluated for potential matches. To conduct the error evaluation and visual matching, a rubric was developed and implemented, which is provided in Table B.2, Appendix B.

Table B.2. Rubric for evaluating remotely sensed trees for coregistration or matching status		
Class	**Statistical Analysis**	**Description**
1. Matched	Matched Tree	The x, y, and z location of the field and remotely sensed tree appeared to produce a parsimonious match. The mortality status of the field and remotely sensed trees appeared to match.
2. Matched to main segment	Matched Tree	See 1, with the exception the algorithm matched the field tree to a main segment
3. Unmatched	Unmatched Lidar or Field Tree	A parsimonious match was not made between a field and remotely sensed tree. In addition, no suitable field trees within an ~5m radius of the remotely sensed tree was evident.
4. Unmatched, additional segment	Analyzed for influence of error on matching	See 4, except the remotely sensed tree of interest was an additional segment
5. Unmatched, boulder	Analyzed for influence of error on matching	The lidar segment displayed a boulder with no tree on top of or to the side of the boulder.
6. Unmatched to visually matched	Visually matched	We visually matched pairs if their mortality status was consistent to the field tree and the heights were within + or – 10m. Trees in the plots exceed 60m in height; therefore, the allometric equations may not have predicted the tallest of trees or large, mature trees with decadent or broken tops.
7. Unmatched main segment to visually matched	Visually matched	See 6, the steps were the same with the exception that visual matched were made to a main stem of an oversegmented canopy.
8. Matched, however, probable incorrect match	Unmatched	The x, y, and z location of the field and remotely sensed tree appeared to be incorrect to produce a relevant match, or the mortality status of the field and remotely sensed trees appeared incorrect (i.e., one live tree and one dead tree in the gray phase or later state of decay).
9. Matched to main segment, however, probable incorrect match	Unmatched	See 8 except the remotely sensed tree was a main segment.
10. Matched to additional segment, probable error	Analyzed for influence of error on matching	See 8 except the remotely sensed tree was an additional segment.
11. Matched, however, probable incorrect match, visually matched	Visually matched	The algorithm matched a field to remotely sensed tree; however, the match appears incorrect. A more parsimonious match is visually identified and made.
12. Matched, main stem, probable error to visually matched	Visually matched	See 12 except the remotely sensed tree is a main segment.

B.6: Results

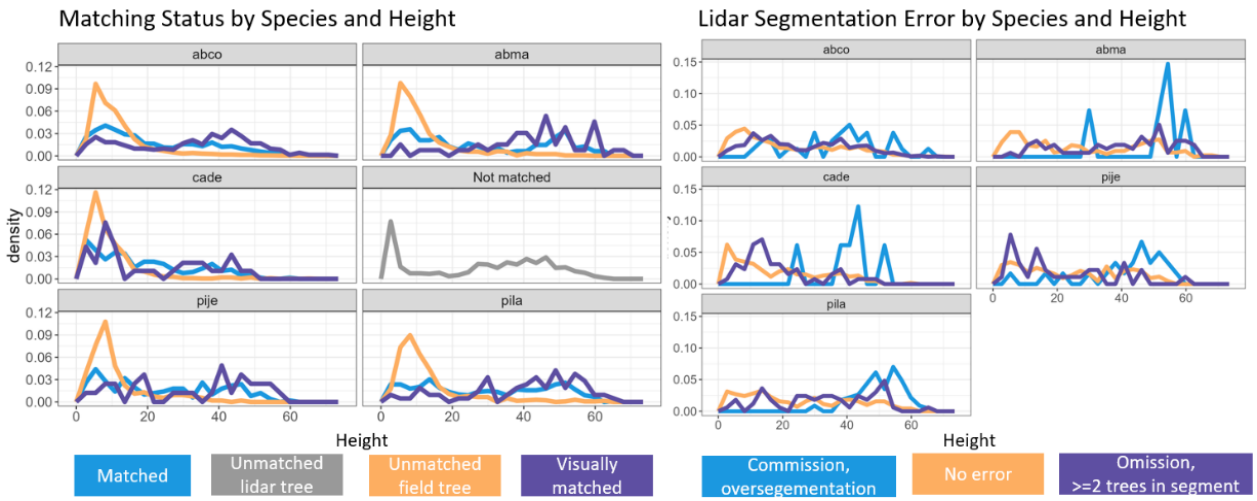

Figure B.1 Matching Status by Species and Height and by lidar segmentation error. Left graph displays the matching status of each species by height: abco (A. concolor), abma (A. magnifica), cade (C. decurrens), Not matched-remotely sensed trees that were not matched via algorithm or manual matching, pije (P. jeffreyi), and pila (P. lambertiana). Right panel shows lidar segmentation errors by species, by height.

3.6 CITATIONS

Allen, B.H., 2005. Sierran Mixed Conifer, California Wildlife Habitat Relationships System. Sacramento.

Asner, G.P., Brodrick, P.G., Anderson, C.B., Vaughn, N., Knapp, D.E., Martin, R.E., 2016. Progressive forest canopy water loss during the 2012–2015 California drought. Proc. Natl. Acad. Sci. 113, E249–E255. https://doi.org/10.1073/pnas.1523397113

Asner, G.P., Martin, R.E., Knapp, D.E., Tupayachi, R., Anderson, C.B., Sinca, F., Vaughn, N.R., Llactayo, W., 2017. Airborne laser-guided imaging spectroscopy to map forest trait diversity and guide conservation. Science 355, 385–389. https://doi.org/10.1126/science.aaj1987

Axelson, J., Battles, J., Bulaon, B., Cluck, D., Cousins, S., Cox, L., Estes, B., Fettig, C., Hefty, A., Hishinuma, S., Hood, S., Kocher, S., McMahon, D., Mortenson, L., Koltunov, A., Kuskulis, E., Poloni, A., Ramirez, C., Restaino, C., Safford, H., Slaton, M., Smith, S., Tubbesing, C., Wayman, R., Young, D., 2019. The California Tree Mortality Data Collection Network — Enhanced communication and collaboration among scientists and stakeholders, California Agriculture. https://doi.org/10.3733/ca.2019a0001

Begon, M. and C.R.T., 2021. Ecology: From Individuals to Ecosystems, 5th Edition, 5th Editio. ed. Wiley.

Brodrick, P.G., Asner, G.P., 2017. Remotely sensed predictors of conifer tree mortality during severe drought. Environ. Res. Lett. 12, 115013. https://doi.org/10.1088/1748-9326/aa8f55

Campbell, M.J., Dennison, P.E., Hudak, A.T., Parham, L.M., Butler, B.W., 2018. Quantifying understory vegetation density using small-footprint airborne lidar. Remote Sens. Environ. 215, 330–342. https://doi.org/10.1016/j.rse.2018.06.023

Chen, Wei, Hu, X., Chen, Wen, Hong, Y., Yang, M., 2018. Airborne LiDAR remote sensing for individual tree forest inventory using trunk detection-aided mean shift clustering techniques. Remote Sens. 10, 1–25. https://doi.org/10.3390/rs10071078

Diffenbaugh, N.S., Swain, D.L., Touma, D., Lubchenco, J., 2015. Anthropogenic warming has increased drought risk in California. Proc. Natl. Acad. Sci. U. S. A. 112, 3931–3936. https://doi.org/10.1073/pnas.1422385112

Donager, J.J., Sánchez Meador, A.J., Blackburn, R.C., 2021. Adjudicating perspectives on forest structure: How do airborne, terrestrial, and mobile lidar-derived estimates compare? Remote Sens. 13, 1–18. https://doi.org/10.3390/rs13122297

Edson, C., Wing, M.G., 2011. Airborne light detection and ranging (LiDAR) for individual tree stem location, height, and biomass measurements, Remote Sensing. https://doi.org/10.3390/rs3112494

ESRI ArcGIS Pro Version 2.8, 2021.

Fadili, M., Renaud, J.P., Bock, J., Vega, C., 2019. RegisTree: a registration algorithm to enhance forest inventory plot georeferencing. Ann. For. Sci. 76. https://doi.org/10.1007/s13595-019-0814-2

Ferraz, A., Saatchi, S., Bormann, K.J., Painter, T., 2018. Fusion of NASA Airborne Snow Observatory (ASO) Lidar Time Series over Mountain Forest Landscapes. Remote Sens. https://doi.org/10.3390/rs10020164

Fettig, C.J., Mortenson, L.A., Bulaon, B.M., Foulk, P.B., 2019. Tree mortality following drought in the central and southern Sierra Nevada, California, U.S. For. Ecol. Manage. 432, 164–178. https://doi.org/10.1016/j.foreco.2018.09.006

Freiderichs, K., 1958. A Definition of Ecology and Some Thoughts About Basic Concepts. Ecology 39, 154–159.

Fricker, G.A., Ventura, J.D., Wolf, J., North, M.P., Frank, W., 2019. A Convolutional Neural Network classifier identifies tree species in mixed-conifer forest from hyperspectral imagery 1–24.

Fry, D.L., Stephens, S.L., Collins, B.M., North, M.P., Franco-Vizcaíno, E., Gill, S.J., 2014. Contrasting spatial patterns in active-fire and fire-suppressed mediterranean climate old-growth mixed conifer forests. PLoS One 9. https://doi.org/10.1371/journal.pone.0088985

Furniss, T.J., Larson, A.J., Kane, V.R., Lutz, J.A., 2020. Wildfire and drought moderate the spatial elements of tree mortality. Ecosphere 11. https://doi.org/10.1002/ecs2.3214

Gallery, W., 2022. Neon Algorithm Theorectical Basis Document (Atbd) Aop Digital Camera Image Orthorectification Prepared By.

Gibson, P.B., Waliser, D.E., Guan, B., Deflorio, M.J., Ralph, F.M., Swain, D.L., 2020. Ridging associated with Drought across the Western and Southwestern United States:

Characteristics, trends, and predictability sources. J. Clim. 33, 2485–2508. https://doi.org/10.1175/JCLI-D-19-0439.1

Goodwin, M.J., North, M.P., Zald, H.S.J., Hurteau, M.D., 2020. Changing climate reallocates the carbon debt of frequent-fire forests. Glob. Chang. Biol. 26, 6180–6189. https://doi.org/10.1111/gcb.15318

Gutierrez, A.A., Allison, S.D., Randerson, J.T., 2023. Estimating Individual Tree Mortality in the Sierra Nevada Using Lidar and Multispectral Reflectance Data Journal of Geophysical Research : Biogeosciences. J. Geophys. Res. Biogeosciences, 128, 128, 1–18. https://doi.org/10.1029/2022JG007234

Hamraz, H., Contreras, M.A., Zhang, J., 2017. Forest understory trees can be segmented accurately within sufficiently dense airborne laser scanning point clouds. Sci. Rep. 7, 1–9. https://doi.org/10.1038/s41598-017-07200-0

Hastings, J.H., Ollinger, S. V., Ouimette, A.P., Sanders-DeMott, R., Palace, M.W., Ducey, M.J., Sullivan, F.B., Basler, D., Orwig, D.A., 2020. Tree species traits determine the success of LiDAR-based crown mapping in a mixed temperate forest. Remote Sens. 12. https://doi.org/10.3390/rs12020309

Hauglin, M., Lien, V., Næsset, E., Gobakken, T., 2014. Geo-referencing forest field plots by co-registration of terrestrial and airborne laser scanning data. Int. J. Remote Sens. 35, 3135–3149. https://doi.org/10.1080/01431161.2014.903440

Holmgren, J., Lindberg, E., 2019. Tree crown segmentation based on a tree crown density model derived from Airborne Laser Scanning. Remote Sens. Lett. 10, 1143–1152. https://doi.org/10.1080/2150704X.2019.1658237

Huang, C. ying, Anderegg, W.R.L., Asner, G.P., 2019. Remote sensing of forest die-off in the Anthropocene: From plant ecophysiology to canopy structure. Remote Sens. Environ. 231, 111233. https://doi.org/10.1016/j.rse.2019.111233

Huesca, M., Ustin, S.L., Shapiro, K.D., Boynton, R., Thorne, J.H., 2021. Detection of drought-induced blue oak mortality in the Sierra Nevada Mountains, California. Ecosphere 12. https://doi.org/10.1002/ecs2.3558

Jeronimo, S.A.M., 2018. Restoring forest resilience in the Sierra Nevada mixed-conifer zone, with a focus on measuring spatial patterns of trees using airborne lidar. University of Washington.

Jeronimo, S.M., 2015. LiDAR individual tree detection for assessing structurally diverse forest landscapes. Univ. Washingt. University of Washington, Seattle, WA.

Jeronimo, S.M.A., Kane, V.R., Churchill, D.J., McGaughey, R.J., Franklin, J.F., 2018. Applying LiDAR individual tree detection to management of structurally diverse forest landscapes. J. For. 116, 336–346. https://doi.org/10.1093/jofore/fvy023

Knapp, E.E., Bernal, A.A., Kane, J.M., Fettig, C.J., North, M.P., 2021. Variable thinning and prescribed fire influence tree mortality and growth during and after a severe drought. For. Ecol. Manage. 479, 118595. https://doi.org/10.1016/j.foreco.2020.118595

Krause, K., Goulden, T., 2015. NEON L0-TO-L1 DISCRETE RETURN LiDAR ALGORITHM THEORETICAL BASIS DOCUMENT (ATBD) PREPARED BY.

Krofcheck, D.J., Hurteau, M.D., Scheller, R.M., Loudermilk, E.L., 2017. Restoring surface fire stabilizes forest carbon under extreme fire weather in the Sierra Nevada. Ecosphere 8. https://doi.org/10.1002/ecs2.1663

Li, W., Guo, Q., Jakubowski, M.K., Kelly, M., 2012. A new method for segmenting individual trees from the lidar point cloud. Photogramm. Eng. Remote Sensing 78, 75–84. https://doi.org/10.14358/PERS.78.1.75

Lindberg, E., Holmgren, J., Olofsson, K., Wallerman, J., Olsson, H., 2013. Estimation of tree lists from airborne laser scanning using tree model clustering and k-MSN imputation. Remote Sens. 5, 1932–1955. https://doi.org/10.3390/rs5041932

Lund, J., Medellin-Azuara, J., Durand, J., Stone, K., 2018. Lessons from California's 2012–2016 Drought. J. Water Resour. Plan. Manag. 144, 04018067. https://doi.org/10.1061/(asce)wr.1943-5452.0000984

Marchi, N., Pirotti, F., Lingua, E., 2018. Airborne and Terrestrial Laser Scanning Data for the Assessment of Standing and Lying Deadwood: Current Situation and New Perspectives. Remote Sens. 10, 1356. https://doi.org/10.3390/rs10091356

McGaughey, R.J., 2018a. FUSION/LDV: Software for LIDAR Data Analysis and Visualization: Version 3.70. USDA Forest Service Pacific Northwest Research Station, Seattle, WA.

McGaughey, R.J., 2018b. FUSION / LDV : Software for LIDAR Data Analysis and Visualization. U.S. Department of Agriculture, Forest Service, Pacific Northwest Research Station, University of Washington, Seattle, WA, USA.

Mohammadpour, Pegah, and Viegas, C., 2022. Applications of Multi-Source and Multi-Sensor Data Fusion of Remote Sensing for Forest Species Mapping., in: Advances in Remote Sensing for Forest Monitoring. John Wiley & Sons, Ltd, pp. 255–297. https://doi.org/https://doi.org/10.1002/9781119788157.ch12

North, M., Chen, J., Oakley, B., Song, B., Rudnicki, M., Gray, A., Innes, J., 2004. Forest stand structure and pattern of old-growth western hemlock/Douglas-fir and mixed-conifer forests. For. Sci. 50, 299–311.

North, M., Innes, J., Zald, H., 2007. Comparison of thinning and prescribed fire restoration treatments to Sierran mixed-conifer historic conditions. Can. J. For. Res. 37, 331–342. https://doi.org/10.1139/X06-236

North, M., Oakley, B., Chen, J., Erickson, H., Gray, A., Izzo, A., Schowalter, T., 2002. Vegetation and ecological characteristics of mixed conifer and red fir forests at the teakettle experimental forest.

North, M.P., 2002. Vegetation and ecological characteristics of mixed-conifer and red fir forests at the Teakettle Experimental Forest.

Odum, E. and G.W.B., 1971. Fundamentals of ecology. W B Saunders Co; 3rd edition (January 1, 1971).

Paczkowski, S., Datta, P., Irion, H., Paczkowska, M., Habert, T., Pelz, S., Jaeger, D., 2021. Evaluation of early bark beetle infestation localization by drone-based monoterpene detection. Forests 12, 1–17. https://doi.org/10.3390/f12020228

Painter, T.H., Berisford, D.F., Boardman, J.W., Bormann, K.J., Deems, J.S., Gehrke, F., Hedrick, A., Joyce, M., Laidlaw, R., Marks, D., Mattmann, C., McGurk, B., Ramirez, P., Richardson, M., Skiles, S.M.K., Seidel, F.C., Winstral, A., 2016. The Airborne Snow Observatory: Fusion of scanning lidar, imaging spectrometer, and physically-based modeling for mapping snow water equivalent and snow albedo. Remote Sens. Environ. 184, 139–152. https://doi.org/10.1016/j.rse.2016.06.018

Pascual, C., Martín-Fernández, S., García-Montero, L.G., García-Abril, A., 2013. Algorithm for improving the co-registration of LiDAR-derived digital canopy height models and field data. Agrofor. Syst. 87, 967–975. https://doi.org/10.1007/s10457-013-9612-2

R: A language and environment for statistical computing., 2022.

R Studio: Integrated Development for R., 2022.

Sciences, W., 2011. Dinkey Creek / Tea Kettle 2010.

Shivaprakash, K.N., Swami, N., Mysorekar, S., Arora, R., Gangadharan, A., Vohra, K., Jadeyegowda, M., Kiesecker, J.M., 2022. Potential for Artificial Intelligence (AI) and Machine Learning (ML) Applications in Biodiversity Conservation, Managing Forests, and Related Services in India. Sustain. 14, 1–20. https://doi.org/10.3390/su14127154

Smith, T.F., Rizzo, D.M., North, M., 2005. Patterns of mortality in an old-growth mixed-conifer forest of the southern Sierra Nevada, California. For. Sci. 51, 266–275. https://doi.org/10.1093/forestscience/51.3.266

Stears, A.E., Adler, P.B., Albeke, S.E., Atkins, D.H., Studyvin, J., Laughlin, D.C., 2022. plantTracker: An R package to translate maps of plant occurrence into demographic data. Methods Ecol. Evol. 13, 2129–2137. https://doi.org/10.1111/2041-210X.13950

Stephenson, N. L., & Das, A. J. 2020. Height-related changes in forest composition explain increasing tree mortality with height during an extreme drought. *Nature Communications*, *11*(1), 3402.

Stovall, A.E.L., 2020. Height Related Drought Mortality Supplement. Nat. Commun.

Swain, D.L., 2015. A tale of two California droughts: Lessons amidst record warmth and dryness in a region of complex physical and human geography. Geophys. Res. Lett. 42, 9999–10003. https://doi.org/10.1002/2015GL066628

Vincent, L., & Soille, P. 1991. Watersheds in digital spaces: an efficient algorithm based on immersion simulations. *IEEE Transactions on Pattern Analysis & Machine Intelligence*, *13*(06), 583-598.

Wayman, R.B., Safford, H.D., 2021. Recent bark beetle outbreaks influence wildfire severity in mixed-conifer forests of the Sierra Nevada, California, USA. Ecol. Appl. 31, 1–19. https://doi.org/10.1002/eap.2287

Wing, B.M., Ritchie, M.W., Boston, K., Cohen, W.B., Olsen, M.J., 2015. Individual snag detection using neighborhood attribute filtered airborne lidar data. Remote Sens. Environ. 163, 165–179. https://doi.org/10.1016/j.rse.2015.03.013

Young, D.J.N., Stevens, J.T., Earles, J.M., Moore, J., Ellis, A., Jirka, A.L., Latimer, A.M., 2017. Long-term climate and competition explain forest mortality patterns under extreme drought. Ecol. Lett. 20, 78–86. https://doi.org/10.1111/ele.12711

Yun, Z., Zheng, G., Geng, Q., Monika Moskal, L., Wu, B., Gong, P., 2022. Dynamic stratification for vertical forest structure using aerial laser scanning over multiple spatial scales. Int. J. Appl. Earth Obs. Geoinf. 114, 103040. https://doi.org/10.1016/j.jag.2022.103040

Chapter 4. DETECTING THE FATE OF OVERSTORY TREES FOLLOWING A DROUGHT-INDUCED TREE MORTALITY EVENT

4.1 ABSTRACT

Artificial intelligence is increasingly applied to assess ecological status and change. However, validation is required to understand the uncertainty and bias inherent in such approaches for ecological studies. We used remotely sensed trees matched to in-situ trees to examine annual survivorship, mortality, and decay detection using machine learning for three years following an extensive tree mortality event. We conducted our assessment in a fire excluded, multi-strata, Sierran mixed conifer forest in California's southern Sierra Nevada, which experienced a warm drought-induced tree mortality event from 2012-2016. We asked how well is post-drought tree mortality status predicted by machine learning validated with field data and if there are differences by species. In addition, we asked if mortality and decay status could be detected over time with repeat measures. Our analysis predictors for the 2017 to 2019 machine learning models, Random Forest (RF) and XGBoost (XGB), included high resolution, airborne collected imagery and lidar-derived canopy height models.

We compared the mortality status detections of the labeled (i.e., remotely sensed trees whose status has been manually identified using orthoimagery) matched tree mortality status, then the modeled detections were validated with in-situ collected survivorship for 2018. In 2018, the RF and XBG detections versus labeled data were both 86% surviving and 78% mortality compared to 78% of field-assessed survivorship and 72% mortality, respectively. Bias related to our remotely sensed tree methods influenced mortality detection and produced taxonomic based differences in detection. On average, a six percent reduction in classification detection was due to matched trees being of an unknown status, and eight percent in full shadows. In terms of mortality detection by species, *A. concolor* mortality was underrepresented; *A.*

magnifica was under predicted by XGB and occluded by shadows in 14% of matched trees; *C. decurrens* was well detected, and *P. jeffreyi* and *P. lambertiana* mortality were over detected. The 2017 and 2018 RF and XGB models well represented decay over time; however, the 2019 model without the canopy surface model had improved detection of coarse woody debris. This finding was surprising and important as it suggests high fidelity imagery may aid decay detection in the absence of lidar data.

4.2 INTRODUCTION

Around the globe, remote sensing of forests has involved well established and validated methods using data such as LANDSAT (Cohen et al., 2016; Huang et al., 2017; Kane et al., 2013; Miller and Thode, 2007) and GEDI (Duncanson et al., 2020; Potapov et al., 2021; Pötzschner et al., 2022; Zhou and Popescu, 2019). These investigations are invaluable for assessing forest condition at the stand-scale across broad extents. Yet, in the last decade, a synergy of innovation in remote sensing of our environment coupled with computational advancements spurred the ability to apply remotely sensed trees detect, model, and predict the occurrence of individual overstory trees (Duncanson and Dubayah, 2018; Jeronimo et al., 2018; Paz-Kagan et al., 2017; Wing et al., 2015; Yun et al., 2022; Zhou et al., 2018).

Increasingly, remotely sensed trees are produced by fusing multiple, high resolution lidar, orthoimagery, or hyperspectral datasets (Hemming-Schroeder et al., 2023; Huang et al., 2019; Jiao et al., 2021; Lines et al., 2022). Remotely sensed trees are then applied as proxies to evaluate individual overstory tree condition. For example, they are applied to map trees as well as to aid species identification (Fricker et al., 2019; Huesca et al., 2021), biomass (Xu et al., 2018) measurements, fuels condition assessments (Rocha et al., 2023), delineating tree patterns (Jeronimo et al., 2018; Kane et al., 2019), canopy conditions (Paz-Kagan et al., 2017), or survivorship status (Hemming-Schroeder et al., 2023; Stovall et al., 2019).

Although remotely sensed trees hold great potential for conducting ecological studies, population ecology research involving remotely sensed trees is nascent (Das et al., 2022; Huesca et al., 2021). Further, examinations involving field validation to address uncertainty and bias are needed (Babcock et al., 2015; Murray et al., 2019; Rocchini et al., 2013) to ensure adequate representation across species and environmental conditions. Conducting this research is fundamental to using remotely sensed trees in future ecological examinations. Unlike assessments of forest condition, population trend analysis requires repeated measures of individuals representative of the entire population (McCune et al., 2002). To repeatedly measure representative individuals, it is necessary to measure the uncertainty of the study population and the bias related to the methods of study.

We endeavored to support building a foundation of research regarding the application of remotely sensed trees in population ecology. We proposed to do so by examining the efficacy of predicting individual overstory tree survivorship, mortality, and decay with machine learning models using field validated (i.e., matched) remotely sensed trees. Here, we defined remotely sensed trees as models created by segmenting overstory tree crowns from airborne lidar and combining the crowns with high resolution imagery (i.e., orthoimagery, 0.1m resolution). We matched or coregistered in-situ trees to remotely sensed trees to ensure our results were accurate at the scale of individual, overstory trees. By matching in-situ to remotely sensed trees, the matched trees inherited the information collected from each field tree, respectively. Further, matched trees greatly reduced uncertainty since each remotely sensed tree being evaluated represented an identified and field-measured individual tree. Since matched trees are the remotely sensed proxies of individual field trees, they provided the necessary information to validate the accuracy of machine learning models and evaluate sources of bias.

We used the control plots of a long-term, fire and fire surrogates study in the Teakettle Experimental Forest in the southern Sierra Nevada California to develop and validate individual overstory tree mortality models using remotely sensed trees. By doing so, we could assess the

accuracy of our models and evaluate bias. We used the matched tree dataset to address the following research questions:

1. How is post-drought mortality of matched trees detected by machine learning and validated with field-based mortality?

2. Are there differences in the detection of mortality by conifer species?

3. Can mortality and decay status be detected over time with machine learning with repeat measures?

4. What are the annual changes in survivorship, mortality, and decay trends of the most common fir and pine species (*A. concolor* and *P. lambertiana*, respectively) up to three years post-drought?

The first research question sought to provide objective data regarding how well machine learning can capture tree mortality about the overstory tree population. Since our field population and remotely sensed trees were both identified, we evaluated sources of bias and their influence on modeling the detection of survivorship and decay. We also examined if tree height and the number of neighbors influenced whether mortality classification was correctly predicted compared to the field-validated, matched trees. The second question was to evaluate whether using machine learning to predict overstory tree mortality was biased in terms of species. Since other tree species were not measured for tree size metrics and represented less than 1% of tree species frequency, this study was limited to the evaluation of conifer species. Third, we examined how well tree mortality and decay could be predicted with machine learning. Such an approach could be cost-effective for evaluating mortality and decay in individual overstory trees, older lidar tree crowns may be useful for examining the fate of tree mortality and forest structure patterns over time. Finally, we examined the survivorship, mortality, and decay patterns of the two most common fir and pine species, *A. concolor* and *P. lambertiana*, respectively, for potential differences. We theorized that the *P. lambertiana* died and decayed earlier post-drought than *A. concolor* due to the presence of the Western pine bark beetle, *D.*

brevicomis. Our research goal was to benefit future efforts involving the detection of individual overstory trees in response to a range of disturbance events and environmental conditions.

4.3 METHODS

4.3.1 Study Area

The study area is occupied by forests located in California's southern Sierra Nevada range. It is composed of nine, four-hectare plots (Figure 1) of mature, multi-strata Sierran Mixed Conifer forest in the Teakettle Experimental Forest (Allen, 2005; Goodwin et al., 2020). The study area was selected because it was fire excluded and experienced drought-induced tree mortality (Goodwin et al., 2020). To examine the influence of drought-induced mortality, we selected the untreated, control plots so we could avoid the potential influence of other mortality sources such as wildfire or wind. In addition, existing pre- and post-drought field and remotely sensed datasets were available to match field trees to the remotely sensed trees. Hereafter, individual tree measurements acquired from in-situ measurements of stem mapped trees, are referred to as field or in-situ trees. Individual tree measurements acquired from high resolution lidar and assessed for mortality status with orthoimagery are hereafter referred to as remotely sensed trees. The field and remotely sensed tree mortality data were collected prior to and following California's 2012-2016 drought and tree mortality event (Fettig et al., 2019; Swain, 2015).

The nine unburned plots of the study area were the control plots for a long-term fire and fire surrogates study within the 1,300 hectare Teakettle Experimental Forest (Goodwin et al., 2020; North et al., 2002). The Teakettle Experimental Forest is located along the north fork of the Kings River watershed in the southern portion of the Ecoregion and is vegetated with late-seral, mixed Sierran conifer forests (Fry et al., 2014; Goodwin et al., 2020; North, 2002). The study area has a Mediterranean climate with warming and drought events characteristic of the Ecoregion (Asner et al., 2016; Diffenbaugh et al., 2015; Gibson et al., 2020; Swain, 2015). The elevation of the study area ranges from approximately 1,900 to 2,600 m, and annual

temperature and precipitation vary from -3° to 25°C and 50 to 125cm, respectively (Goodwin et al., 2020; Krofcheck et al., 2017).

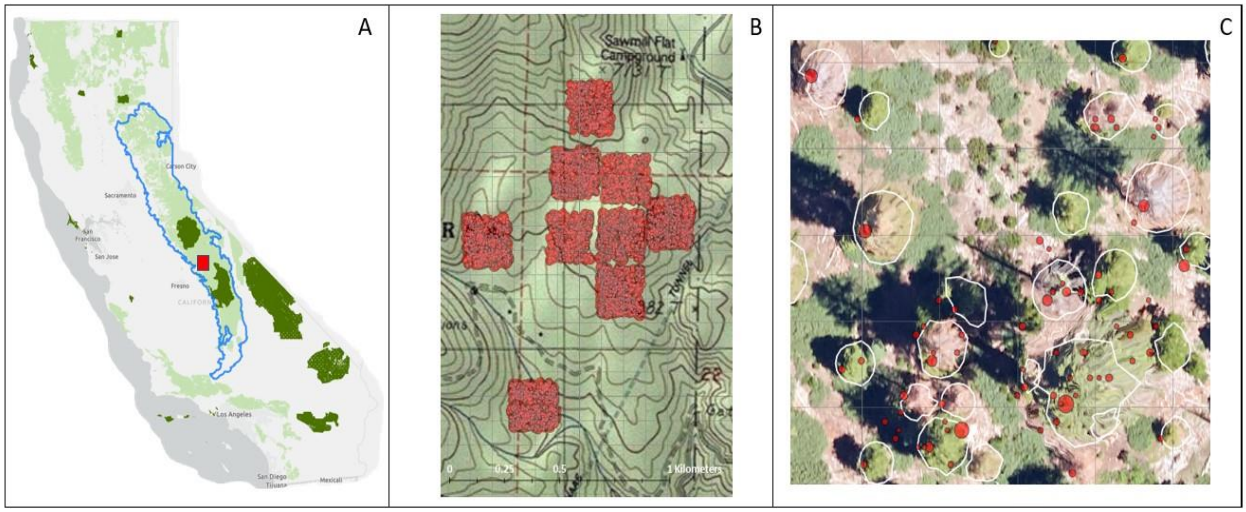

Figure 4.1. The Sierra Nevada Ecoregion (A) is a montane, conifer dominated region of California with a Mediterranean climate. The study area (B) is in the Teakettle Experimental Forest in the southern Sierra Nevada, which experienced significant tree mortality during California's first warm drought from 2012-2016. The study area includes nine field plots, each four hectares in area, that were stem mapped with tree measurements collected in 2011 and 2018. Airborne lidar was collected in 2010, which was used to segment trees (Jeronimo et al. 2018) using a watershed segmentation algorithm. Panel (C) shows lidar tree segments as white with red circles representing the field trees from a zoomed in, aerial view of a portion of one of the nine field plots overtop 2018 NEON orthoimagery (Gallery, 2022).

4.3.2 Matched Trees

Matched trees were the field trees that were pairwise matched on a one-to-one basis with remotely sensed trees (Figure 4.2). The methods applied to coregister or match the field to the remotely sensed trees were described in 3.3.3.4 of Chapter 3. Tree matches were verified by examination of imagery and the comparison of tree measurements. Ecologically, matched trees represented 85% of all the pre-drought remotely sensed trees (i.e., tree models segmented from 2010 airborne lidar whose crown status was visualized with high-resolution imagery). They were the top-of-the-canopy trees or the portion of the overstory visible to remote sensing instruments. In this study area, a remotely sensed tree on average represented the canopy area of a dominant tree and two understory trees, which were identified in the field (Table 2.2). Remotely sensed trees had a mean height of 23.9m pre-drought compared to the field population mean of 15.5m, Table 2.2. Thus, in terms of population ecology, all the analyses

provided hereafter are describing the detection and prediction of trees that were visible to high fidelity fixed wing sensors, the tallest trees at every location, which can vary from a sapling to a large old-growth tree.

Of the 9,761 field trees present in the study area, 2,814 trees, or 85% of the lidar trees, were matched manually or via our algorithm (Chapter 2) creating the matched, remotely sensed trees. The remainder of the lidar or remotely sensed trees represented errors of commission or were not matched to field trees. In this study area, the matched trees represent 29% of the conifers measured, and the conifers account for 99% of the trees present.

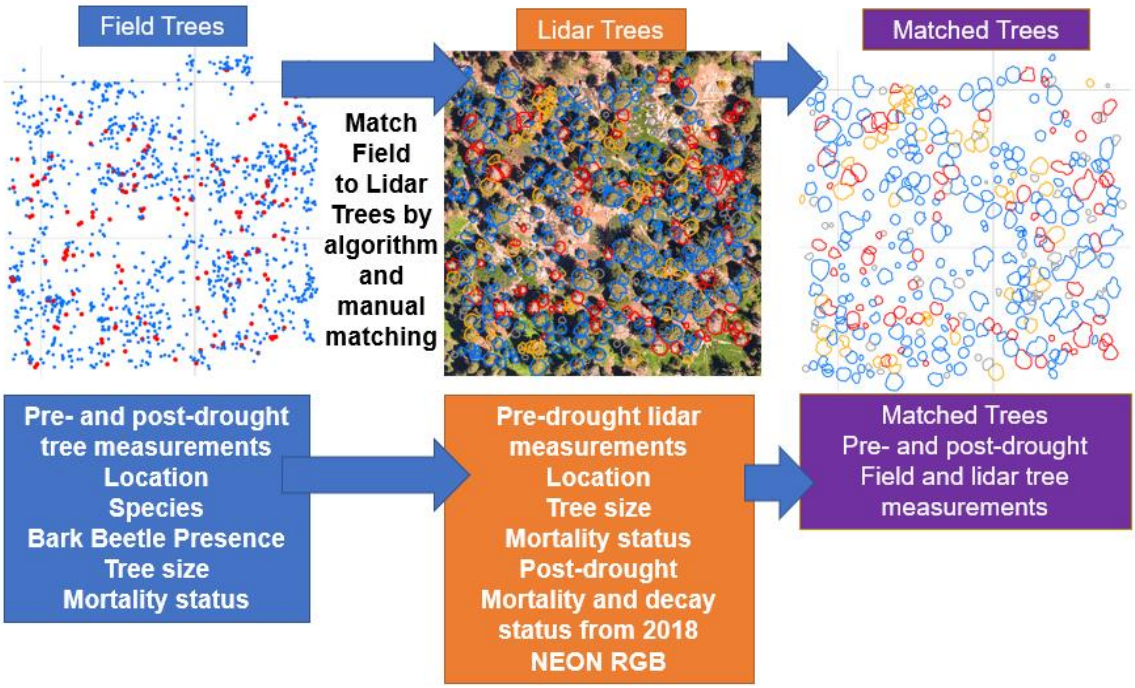

Figure 4.2. Creating matched trees from field and lidar data as well as imagery. Matched trees are the principal unit analyzed for all three questions. In all images, live trees are blue, red are dead, and orange are mixed live and dead trees or stressed.

4.3.3 Question 1: How is post-drought mortality of matched trees detected by machine learning and validated with field-based mortality?

Here, we developed machine learning models to detect post-drought tree mortality exclusively using the matched trees dataset (Figure 4.3). By using the matched tree dataset, the remotely sensed tree mortality detections are field validated; uncertainty regarding the portion of

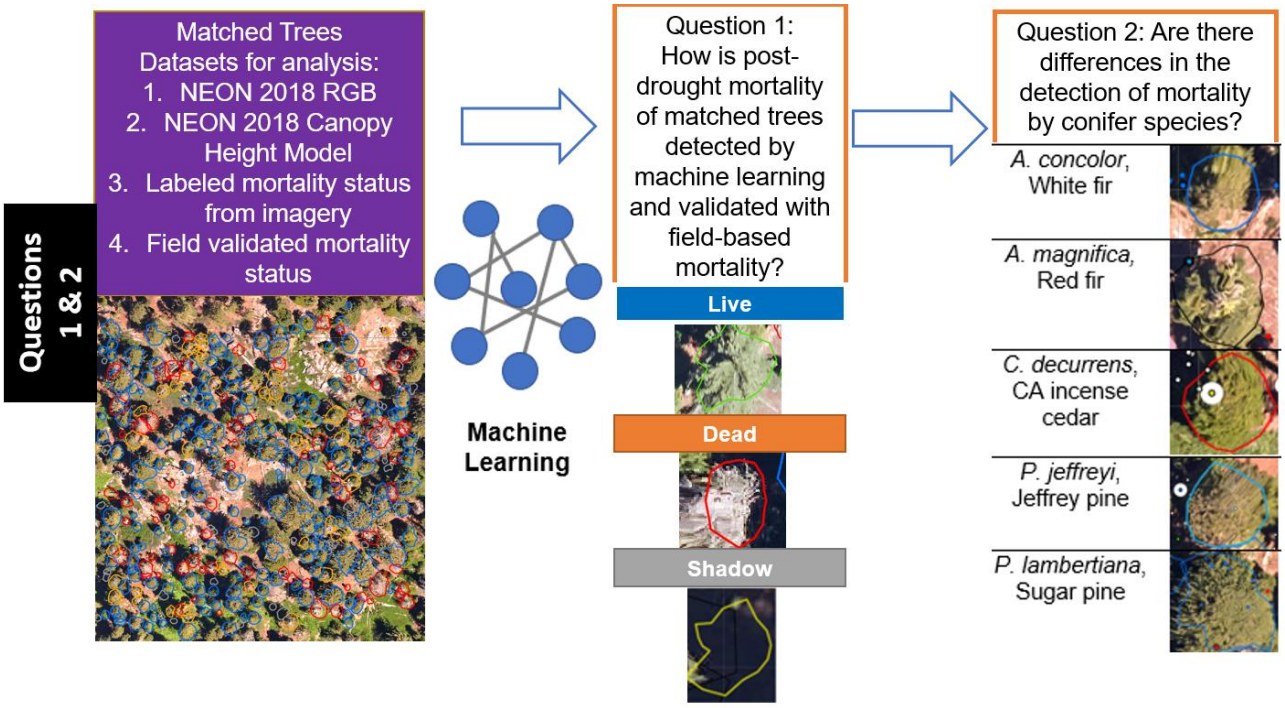

Figure 4.3. Visual diagram of Questions 1 and 2, datasets and workflow.

the population sensed by remotely sensed trees is addressed; and only trees alive pre-drought were included in the analysis.

The mortality detection modeling was performed using image classified matched trees (i.e., the labeled training, validation, and test dataset). The image classification was conducted by visually examining the NEON 2018 orthoimagery (Section 2.5.3). Prior to conducting the machine learning modeling, the mortality classes were collapsed into three basic mortality classes: live (i.e., survived the drought), dead (i.e., died during or up to one-year post-drought (2018)), or shadow (i.e., the matched tree in the 2018 imagery is obscured to the point the mortality status cannot be visually examined). The collapsed classes were identified in Figure C.1, Appendix C.

The machine learning detection of the matched trees was performed using the imagery predictors, which were summarized by zonal statistics (Section 4.3.4.6) by band (e.g., Red, Green, or Blue). In addition, the zonal statistics of the 2018 canopy height model was included as a predictor for post-drought tree height.

We examined the efficacy of applying machine learning models (i.e. Random Forest and XGBoost) to detect or classify the mortality status of the matched trees. The accuracy and precision of the mortality detection was evaluated for error in two ways. First, the user's accuracy was determined by comparing the correctly classified matched trees against the matched tree labeled (i.e., remotely sensed trees whose status has been manually identified using orthoimagery) dataset. Second, the machine learning models predicted classifications were compared to the field-based mortality status as of 2018. Therefore, we were able to produce both a traditional confusion matrix and field validate our results.

In addition to completing the modeling, we examined whether tree height and the mean number of neighbors influenced whether mortality classification is correctly predicted compared to the field-validated, matched trees. We examined the relationship of local forest structure because we viewed many large tree clumps in the imagery. We surmised that these tree clumps affected mortality detection. We expected the machine learning detection of mortality to be influenced by several factors: a) post-drought tree height, b) number of pre-drought lidar neighbors (i.e., as a measure of tree clumping), c) the accuracy of applying a collapsed mortality class, and d) shadows. We hypothesized that tree mortality detection increased with height and decreased as the number of neighbors increases. We applied the pre-drought number of lidar neighbors for the analysis. To evaluate the influence of matched tree post-drought height and neighbors, an analysis of variance (ANOVA) was performed.

4.3.4 Datasets for Question 1

4.3.4.1 Airborne Lidar and Orthoimagery Collection

The 2018 National Ecological Observatory Network (NEON) high resolution RGB imagery (Gallery, 2022; Krause and Goulden, 2015) were accessed to identify the mortality status of all matched trees. In addition, the NEON 2018 lidar data were analyzed to produce a canopy height model (CHM) during the lidar segmentation processing, which is described in Section 3.3.3.2. The CHM dataset was used to acquire mean lidar tree height information for the

matched trees, post-drought. In addition, zonal statistics were calculated per matched tree for the 2018 CHM data and included in the detection analyses. Acquisition details are provided in Table 3.1.

4.3.4.2 Field Tree Measurements

The pre-drought (2011 and 2012) and post-drought (2018) field-based tree measurements were described in Section 2.4.2. All the research described herein involved analysis of the matched trees, and the matched tree methods were described in Section 3.3.3.4. The matched trees inherited the field-based metrics, per tree. In addition, the number of neighbors and mean distance to neighbors were quantified per field and remotely sensed tree and were described in Section 2.6.1.

4.3.4.3 Post-drought Survivorship, Mortality, and Decay Status

The NEON 2018 orthoimagery was used to classify the survivorship, mortality, and decay status according to the rubric in Table B.1, Appendix B. The image classification was ascertained by the primary author for all time periods. The 2018 mortality status of the matched trees was concurrent with the field measurements. All image classification steps were conducted in ArcMap Pro, Version 2.8 ("ESRI ArcGIS Pro Version 2.8," 2021).

4.3.4.4 Data Processing

Except where noted, all statistical analysis and machine learning were performed using the R Studio environment (version 2023.03.0) using R statistical software (version 4.2.3).

4.3.4.5 Mortality and Decay Class Consolidation

The survivorship, mortality, and decay classes applied to the matched trees were consolidated into live, dead, and shadow to promote comparison with the mortality status of the field trees in 2018. Figure C.1, Appendix C displays the consolidated Basic Tree Mortality Classes applied for Questions 1 and 2.

4.3.4.6 Zonal Statistics

Zonal Statistics were calculated for all pixels that occupied the canopy area within each matched tree segment, respectively. These values were inputs into the machine learning analyses for Questions One and Two. Zonal Statistics were quantified per matched tree for the CHM as well as the red, green, and blue visible bands, respectively. For each matched tree, zonal statistics were calculated in ArcGIS Pro Version 2.8 ("ESRI ArcGIS Pro Version 2.8," 2021). For each band or CHM, respectively, the following zonal statistics were calculated: count, area, minimum, maximum, range, mean, standard deviation, sum, variety, majority, minority, median, and 90th percentile. Although many of these metrics are related, machine learning pre-processing recipes can reduce highly correlated predictor variables (Figure C.2, Appendix C).

4.3.4.7 Machine Learning

The "Tidymodels" package (version 1.0.0) in the R Studio environment (version 2023.03.0) using R statistical software (version 4.2.3) was applied to conduct all machine learning steps. This package provides a consistent interface and vernacular of functions, which facilitates multiple machine learning models to be performed and compared. The Tidymodels interface provided a set of data pre-processing functions to prepare data prior to all modeling, which is described in Figure C.2, Appendix C. The pre-processing steps were applied consistently to each of the datasets analyzed.

After data pre-processing was completed, Random Forest (Breiman, 2001) and XGBoost (i.e., a gradient boosted decision tree) (Chen and Guestrin, 2015) machine learning models were both applied (Figure C.3, Appendix C). Random Forest and XGBoost provided the capacity to model multiple classes. The two modeling approaches were applied to ensure consistency in the detection of variables of importance, model coefficients, accuracy, precision, and detections. Figure C.3, Appendix C described the machine learning model steps

4.3.5 Question 2: Are there differences in the detection of mortality by conifer species?

After the machine learning mortality detection was conducted for Question 1, the results were examined to determine if taxonomic status influenced detection. To do so, the frequency of correct mortality detections was compared to the field-detected mortality rates, by species. In addition, the number of trees predicted as shadows were also evaluated by species.

4.3.6 Question 3: Can mortality and decay status be detected over time with machine learning*?*

The goal of this question was to determine if changes in survivorship, mortality, and decay of matched trees could be detected with machine learning using repeat measures (i.e., annual remote sensing datasets (i.e., 2017, 2018, and 2019). Here, a dead tree is defined as a snag with needles or most branching intact. In contrast, a decaying tree is defined as a snag with no apparent needles and few branches, a log, or coarse woody debris). As described in Section 4,3.3, Question One, only matched trees alive pre-drought will be selected for analysis.

The image classification process (Table B.1, Appendix B) was consistently applied to the 2017 to 2019 remotely sensed trees with several notable exceptions. First, the matched trees were image classified for their survivorship, mortality, and decay status, by year, using the respective year's orthoimagery datasets (i.e., NEON 2017-2019). In addition, the lidar-derived canopy height models (CHM) from 2017-2018 were included as predictors for those years, respectively. The purpose of including the canopy height model in 2017 and 2018 and excluding it in 2019 was to test whether canopy height aids in the detection of decaying trees. Decaying trees are typically shorter in stature compared to live and newly dead trees. Since sample sizes need to be sufficient for machine learning, the mortality and decay classes were consolidated or collapsed into "detailed" classes, Figure C.1, Appendix C for accuracy assessments.

4.3.7 Datasets for Question 3

4.3.7.1 Airborne Lidar and Orthoimagery Collection

The 2017 to 2019 National Ecological Observatory Network (NEON) high resolution RGB imagery (Gallery, 2022; Krause and Goulden, 2015) were accessed to identify the

mortality status of all matched trees, respectively, following the drought, by year. In addition, the NEON 2017 and 2018 lidar data were analyzed to produce a canopy height model (CHM), respectively. The CHM datasets were used to acquire mean lidar tree height information for the matched trees, post-drought. In addition, zonal statistics were calculated per matched tree for the 2017 and 2018 CHM data and included in the detection analyses. Further details regarding the zonal statistics are described in Section 4.3.7.6. Acquisition details are provided in Table 4.1.

Table 4.1.
Remote Sensing Acquisition Parameters. These parameters including data type and vendor at the time of collection, time of acquisition, active or remote sensing sensor used to acquire data, acquisition parameters detailing how data was collected, and the geographic coordinate information of the acquisition.

Data Type & Vendor	Data acquisition	Sensor	Acquisition Parameters	Coordinate Information
Airborne lidar, National Ecological Observatory Network (NEON)	Post-drought Summer 2017 & 2018	Optech, Inc Gemini lidar sensor 12SEN311	≥4-6 pulses/m2 100khz	ITRF00, NAVD88, UTM
Orthoimagery Red, Green, and Blue (RGB) NEON	Post-drought Summer 2017-2019	Phase One D8900 and IXU-RS-1000	0.1m resolution 30 to 50% lateral overlap, 60% image overlap	ITRF00, UTM

4.3.7.2 Field Tree Measurements

The field tree measurements data are consistent with Section 4.3.4.2. However, this analysis did not involve examining mortality detection and neighbor density.

4.3.7.3 Post-drought Survivorship, Mortality, and Decay Status

All matched trees were identified for their survivorship, mortality, and decay status by manually identifying their status using imagery from the respective period. The mortality and decay status classification of the 2018 period was concurrent with the steps for Question 1, Section 4.3.4.3. For Question 3, the image classification of survivorship, mortality, and decay status of the matched trees was extended to include the 2017 and 2019 NEON orthoimagery data, which represented one to three years post-drought. The steps for the image classification

were consistent with the 2018 process to identify the survivorship, mortality, and decay class of each matched, remotely sensed tree, Table B.1, Appendix B. The image classification was ascertained by the primary author for all time periods. Although the 2018 mortality status of the matched trees was concurrent with the field measurements, the 2017 and 2019 remotely sensed data are not supported with field validation. All image classification steps were conducted in ArcMap Pro, Version 2.8 ("ESRI ArcGIS Pro Version 2.8," 2021).

4.3.7.4 Data Processing

Except where noted, all statistical analysis and machine learning were performed using the R Studio environment (version 2023.03.0) using R statistical software (version 4.2.3).

4.3.7.5 Mortality and Decay Class Consolidation

The survivorship, mortality, and decay classes applied to the matched trees were consolidated into the Detailed Tree Mortality Classes, which were provided in Figure C.1, Appendix C.

4.3.7.6 Zonal Statistics

The steps to produce the zonal statistics, per period, were consistent to Section 4.3.4.6.

4.3.7.7 Machine Learning

We evaluated the ability of machine learning to detect tree survivorship, mortality, and decay classes with repeat measures for up to three years post-drought using the matched trees, Table 4.4. We did so by examining the performance of two machine learning models, Random Forests and XGBoost. Imagery and lidar-based predictors were collected annually from 2017 to 2019. The machine learning steps to conduct the analyses for all time periods were consistent to Section 4.3.4.7.

4.3.8 Question 4: What are the annual changes in survivorship, mortality, and decay trends of the most common fir and pine species (A. concolor and P. lambertiana, respectively) up to three years post-drought?

We compared differences in post-drought tree counts and changes in frequency by year per survivorship, mortality, and decay between the two most common species, White fir (*A. concolor*) and Sugar pine (*P. lambertiana*). We selected these two species as the tree counts and frequencies in the other species were too low for adequate comparison. The manually classified matched tree survivorship, mortality, and decay classes of the most common fir, White fir, and pine, Sugar pine, were visually compared and contrasted with the pre-drought survivorship status. The comparison allowed the exploration of trends and potential differences in mortality and decay, over time. The combined coarse woody debris class was split to also include snags (i.e., standing dead trees). By doing so, the decay patterns over time could be examined in greater detail.

The tree counts and change in class frequencies were examined from pre-drought to 2019. During the drought, tall Ponderosa pine (*P. ponderosa*) mortality in lower, adjacent elevations to the study area was widespread early in the drought. Since Ponderosa and Sugar pine are both attacked by the Western bark beetle, *D. ponderosae*, we expected that Sugar pine will demonstrate earlier mortality and decay rates that than White fir, which had no such lower elevation analog with shared bark beetle (i.e., fir engraver) induced mortality. If differences in survivorship, mortality, and decay can be tracked over time, new approaches to evaluating overstory tree fate and concomitant changes in aboveground carbon storage can be developed.

4.3.9 Datasets for Question 4

The matched trees with their manually identified survivorship/mortality and decay status in Section 4.3.7.3 were the inputs for the analysis.

4.4 RESULTS

4.4.1 Question 1: How is post-drought mortality of matched trees detected by machine learning and validated with field-based mortality?

The results of both the Random Forest and XGBoost modeling detected 85% and 80% of the drought-induced, field-based morality, respectively, Table 4.2.

Table 4.2.
Machine learning detected mortality status of matched trees compared to imagery classified and field-based mortality status in 2018. Machine learning models used include the Random Forest (RF) and XGBoost (XGBoost) machine learning models

A. Machine learning confusion matrix, the labeled imagery classified results are presented horizontally, and the predicted results are presented vertically, for RF and XGB

	RF Labeled			XGBoost Labeled		
Predicted	**Dead**	**Live**	**Shadow**	**Dead**	**Live**	**Shadow**
Dead	107	33	1	101	20	1
Live	12	295	1	15	313	1
Shadow	7	23	38	10	18	38

Variables of Importance RF: Green Median, Blue Mean, Green 90Th Percentile, Red Majority, Blue Max, Red Variety, Green Standard Deviation, Green Max
Variables of Importance XGB: Green Median, Blue Mean, Green 90th Percentile, Red Majority, Green Majority, Blue Majority, CHM Min., Blue Max

RF AUC=0.970, F1=0.8
XGB AUC=0.973, F1=0.82
The metrics used to assess detection included the Tidymodels-based computation of multiclass Area Under the Receiving Operating Curve (i.e., AUC), which is computed according to the methods of (Hand, T, 2001), and the F1 score. The F1 score is a multiclass metric of precision whereby a true class assignment is made by the user, such as dead, and the "truth regarding relevance" is assessed.

B. Machine learning by field validated confusion matrix, predicted values are presented horizontally, and the field-based (observed) mortality of matched trees using remotely sensed predictors is presented vertically, confusion matrix for RF and XGB

Field Tree Mortality Status 2018	**Machine Learning Detection of Mortality Status**	**Detected Count**		**Field Count**
Live	Live	RF=270	XGB=285	Live
Live	Dead	RF=32	XGB=23	n=346
Live	Shadow	RF=44	XGB=38	
Dead	Dead	RF=103	XGB=93	
Dead	Live	RF=13	XGB=19	Dead
Dead	Shadow	RF=21	XGB=25	n=137

We found a non-linear relationship of tree height and mortality classification error in both the field-validated and image classified data (Figure 4.4). The tallest trees had the greatest frequency of incorrect detections followed by the shortest tree. The trees in the 10-30m height

strata had the fewest incorrect mortality detections. The number of neighbors yielded a slight increase in incorrect mortality detections; however, the trend was not statistically significant.

4.4.2 Question 2: Are there differences in the detection of mortality of matched trees by conifer species?

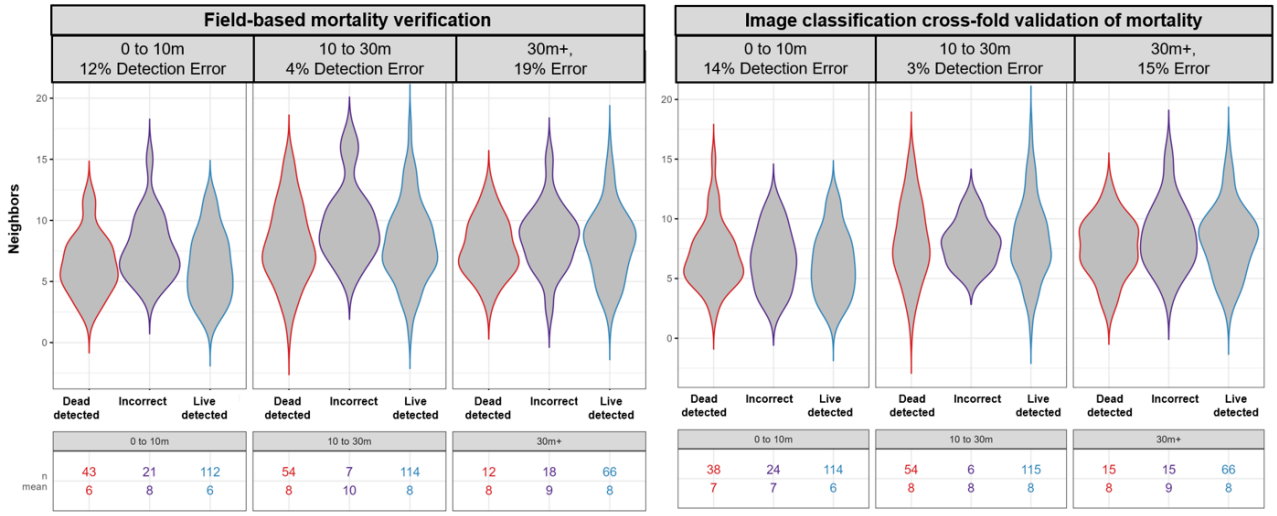

Figure 4.4. Mortality detection and error by number of neighbors per height strata as verified by field-based and image classification assessed mortality status in 2018 with Random Forest.

We found that the frequency of mortality of California Incense Cedar, *C. decurrens*, was too rare in the in-situ population and test population to assess detection power. Despite smaller sample sizes from the test dataset (Table 4.3), both pine species were the best detected with the fewest shadows despite not being the tallest trees. The most poorly predicted species by both models was Red fir (*A. magnifica*). Unlike the other species, Red fir had a higher incidence of shadow detections of dead trees, which may be due to the significant height of conspecifics shading shorter Red fir trees that died. Table 4.3 indicates that shadows are an important source of bias in the detection of mortality by species except for Jeffrey pine, *P. jeffreyi*.

Table 4.3.
Mortality by species in 2018 as measured by field observation and detected by two machine learning models, Random Forest and XGBoost, a gradient boosted machine.

Species	Example	Matched counts	Matched Field tree mortality & Total Frequency of	Machine Learning Counts of Field Validated	Count & Frequency of field verified	Frequency of field verified mortality detected as shadow

			Field Mortality	Dead (both models)	detected mortality	
A. concolor, White fir		1,491	Matched 22% Field 35%	RF & XGB= 102	RF=83 81% XGB=70 69%	RF=13 13% XGB=16 16%%
A. magnifica, Red fir		206	Matched 23% Field 38%	RF=16 XGB=13	RF=8 50% XGB=5 38%	RF=7 44% XGB=7 54%
C. decurrens, CA incense cedar		264	Matched 19% Field <1%	RF=1 XGB=0	RF=1 100% XGB=0 0%	RF=0 0% XGB=0 0%
P. jeffreyi, Jeffrey pine	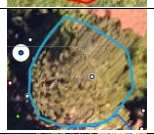	203	Matched 33% Field 7%	RF=5 XGB=4	RF=5 100% XGB=4 100%	RF=0 0% XGB= 0%
P. lambertiana, Sugar pine		373	Matched 60% Field 20%	RF=18 XGB=17	RF=15 83% XGB=14 82%	RF=2 11% XGB=2 12%

4.4.3 Question *3: Can mortality and decay status be detected over time with machine learning with repeat measures*?

Overall, the live and shadow classes (Table 4.4) were the best detected classes across all years by both models. The mixed-top class was better detected than expected in 2017 and 2018, but it was poorly detected in 2019 without the CHM. The coarse woody debris class detection was fair in 2017 and 2018, but in 2019 a larger number of coarse woody debris samples resulting from the mortality likely improved performance. The dead red phase class was poorly predicted and had low sample sizes. The dead gray phase had successful classification in 2017 and 2018. Although the 2019 modeling did not include the CHM, it seemed likely that low sample sizes contributed to poor detection compared to the exclusion of the CSM for the gray phase dead class. The mixed-top and gray phase classes had small sample sizes and poor prediction compared to the live and shadow classes whose sample sizes were adequate and the accuracy was greater.

Table 4.4.
Image Classification based Detection of Mortality and Decay Classes of Lidar Trees in 2017, 2018, and 2019. Detection completed with Random Forest (RF) and XGBoost (XBG).

Mortality and Decay Class	Image Classification Example	2017 Label	2018 Label	2019 Label	2017 Detect of Test Data	2018 Detect* of Test Data	2019 Detect** of Test Data
Live	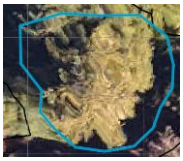	1,626	1,650 ↑1.5%	1,594 ↓3%	RF & XGB 396 96% n=412	RF 305 92% XGB 204 62% n=331	RF 374 97% XGB 370 96% n=384
Mixed Top		121	136 ↑12%	135 No change	RF 21 72% XGB 18 62% n=29	RF & XGB 19 86% n=22	RF 22 51% XGB 20 47% n=43
Red Phase Dead		148	74 ↓50%	4 ↓95%	RF 21 57% XGB 25 68% n=37	Not tested due to class size	Not tested due to class size
Gray Phase Dead		291	370 ↑27%	138 ↓63%	RF 62 85% XGB 64 88% n=73	RF 69 86% XGB 63 79% n=80	RF 23 64% XGB 16 44% n=36
Coarse Woody Debris	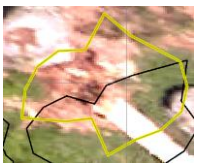	188	267 ↑42%	537 ↑101%	RF: 32 70% XGBoost 31 67% n=46	RF 36 60% XGB 42 70% n=60	RF 111 83% XGB 109 82% n=133
Shadow		271	187 ↓31%	249 ↑33%	RF & XGB 60 91% XGB n=66	RF 25 89% XGB 26 93% n=28	RF 53 78% XGB 60 88% n=68

*A total of 2,814 Matched and Visually matched trees were part of the analysis dataset for all years. However, the canopy height model from the 2018 data produced 647 lidar trees with NA values reducing the machine learning dataset to 2,167
**2019 classes were examined without the CHM

4.4.4 Question 4: What are the annual changes in survivorship, mortality, and decay trends of the most common fir and pine species (A. concolor and P. lambertiana, respectively) up to three years post-drought?

White fir and sugar pine appeared to display consistent trends in both mortality and decay timing, which was unexpected. We surmised that Sugar pine would experience earlier mortality and decay due to the presence of *D. ponderosae* in Ponderosa pines at adjacent, lower elevations. Differences in 2018 and 2019 in terms of snag and coarse woody debris classes were due to a shift in the imagery and alignment with the lidar segments.

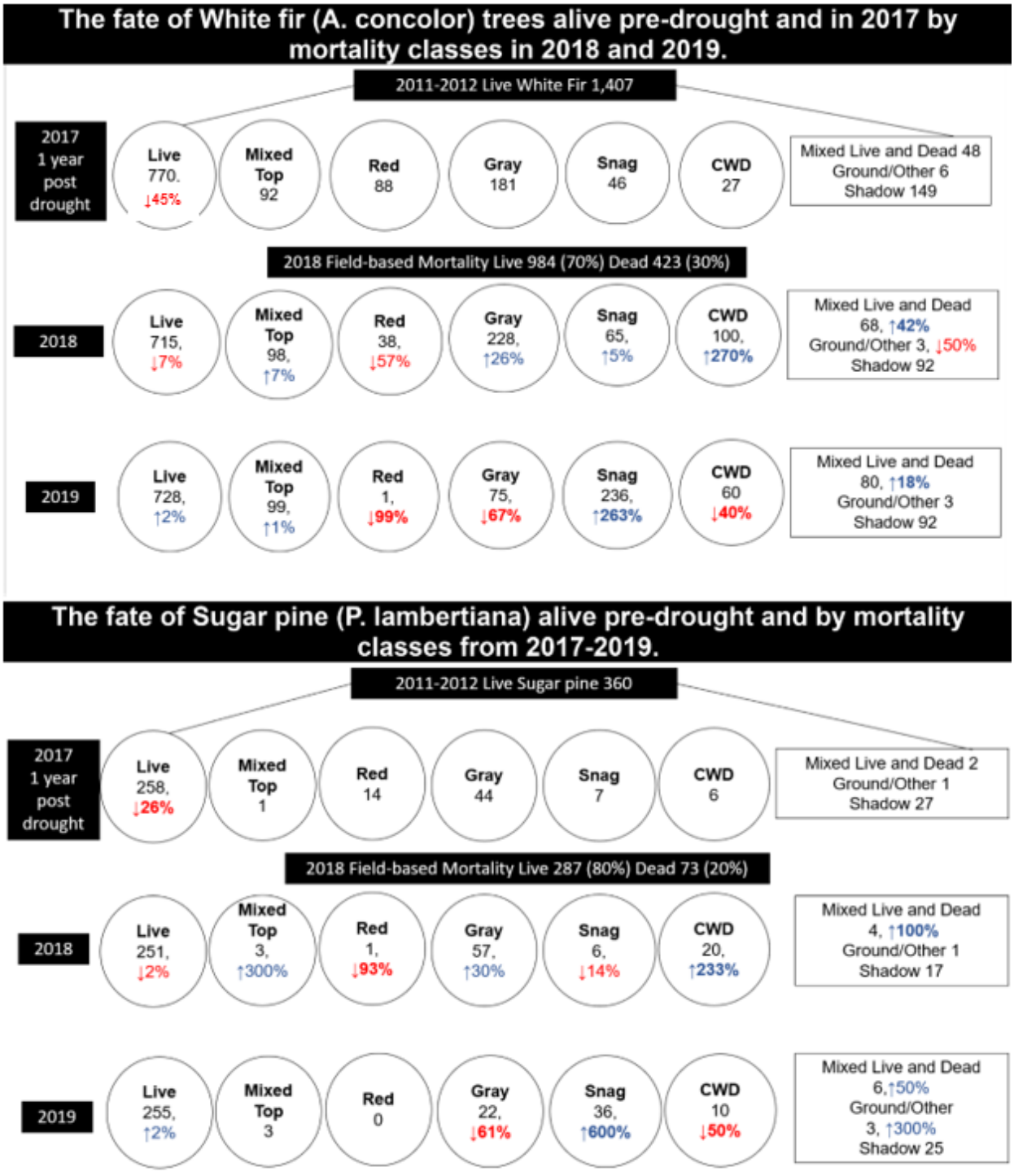

Figure 4.5. The fate of A. concolor and P. lambertiana overstory trees one to three years post-drought in the study area. This figure shows the counts and frequencies of annual survivorship, mortality, and decay status per class as well as changes by class in labeled matched trees.

4.5 DISCUSSION

We endeavored to provide foundational knowledge of how remotely sensed trees can be applied with repeated measures to evaluate population trends. In this study, we demonstrated that matched trees (i.e., remotely sensed trees matched to in-situ or field trees) are an effective means of repeat measures for detecting individual overstory tree survivorship, mortality, and decay trends with two machine learning methods, Random Forests and XGBoost. Since matched trees represent in-situ conditions, they improve the ability to validate results as well as account for uncertainty and bias. We found that when applying a basic three classification system to predict live, dead, and shadows, the accuracy (0.97) and F1 (0.8) scores were consistent and high for both models, respectively. However, when the predicted status was compared to field mortality, the overall accuracy of both models declined. For example, shadows were predicted as dead trees (<=18%) and more frequently than shadows for live trees (<=13%) for Random Forests and XGBoost, respectively. Yet, the frequencies of detecting live as dead or dead as live averaged 10% for both models. Importantly, we found that applying matched trees in our examination revealed that our remotely sensed tree methods were biased towards the detection of pine mortality (i.e., *P. jeffreyi* and *P. lambertiana*) compared to fir (*A. concolor* and *A. magnifica*). If our results of live and dead tree frequencies were applied across species in the Sierra, bias would likely inflate the occurrence of mortality in pine species by a factor of three. Finally, we found success with repeat measures in the machine learning prediction of survivorship, mortality, and decay of matched trees on an annual basis for up to 3 years post-drought with consistent patterns detected in White fir and Sugar pine.

The repeated measures study of survivorship, mortality, and decay was conducted to determine if population trends of overstory trees could be monitored. This finding is important as it demonstrates that it is possible to capture mortality stage transition at the scale of overstory

trees, but field validation is important for the successful evaluation of patterns. We found that detecting states was robust across variations in methods such as using remotely sensed orthoimagery with and without a lidar-derived canopy surface model for 2017 to 2019. We tested the efficacy of using machine learning models with and without lidar-based predictors since airborne lidar is infrequently and repeatedly collected at the fidelity required for individual tree detection.

The approach described herein of applying matched trees to model the detection of individual overstory tree survivorship has important utility to future ecological research and management. We demonstrated that our remotely sensed methods were useful in capturing important changes in tree survivorship and decay over time, but our results provided important insight into how bias can affect the capture of population trends on a taxonomic basis. By using matched trees for the successful deployment of machine learning models, we provided an example for improving future population trend studies with remotely sensed trees.

Question 1: How is post-drought mortality of matched trees detected by machine learning and validated with field-based mortality?

Our comparison of the predictions with field-based conditions revealed both the strong influence of shadows on missed detections (e.g., 10-20%) and the occurrence of incorrect (e.g., dead as live or live as dead), but consistent, detections at ~10% (Table 4.2). The Random Forest model predicted dead trees better while XGBoost best predicted live trees. The results of the Random Forest and XGBoost modeling detected 85% and 80%, respectively, of the morality. Comparing the machine learning detections and the in-situ conditions was useful for considering potential sources of error in our models that could diminish detection.

First, we found error in how the tree mortality predictions were validated by the field data. We did so by comparing the labeled, predicted, and in-situ status of the matched trees for the most parsimonious model, Random Forest. Our study was opportunistic in nature; therefore, the field data was collected prior to this study's initiation. The field conditions did not include or

describe the ground and vegetation conditions adjacent to the tree of interest, which was captured in the imagery within the canopy segment. In other words, field data collect just the status of the tree itself. A lidar derived tree segment coupled with imagery can display not only the tree crown, it can also include pixels composed of shadows, ground material, and other vegetation.

Error was most frequently associated with mixed mortality classes, which means that the segment likely included a live tree crown and other pixels representing the ground or dead vegetation. For example, 12 of 16 matched trees were predicted as live according to the machine learning models. However, these trees were field assessed as dead and labeled in the imagery as belonging to the Live and Coarse Woody Debris class. Live and Coarse Woody Debris is a mixed class that either represents a live tree and coarse woody debris or a decomposed tree and subordinate live vegetation (i.e., tree regeneration, shrubs, etc.). For future research, it will be necessary to improve how field and remotely sensed data are collected to ensure the capability to validate the remotely sensed data. Mixed classes serve an important purpose in capturing the variability inherent in the in-situ population, but they may yield reduced accuracy in modeling if the field validation procedures do not account for the variability.

A second source of error was bias related to the remotely sensed detection and image classification methods. The image collection or processing (e.g., orthorectification) yielded bias that reduced the sample sizes that were detected, which can reduce the application of remotely sensed datasets for ecological assessment (Campbell, James B., Wynne, 2011). For example, the mortality status of a significant number of matched trees were unknown either because the imagery was occluded by shadows or the mortality status was mixed (e.g., mixed live and dead). The NEON program conducts a balanced orthorectification process to reduce relief displacement and improve the resolution of tree crowns (Gallery, 2019). However, very tall trees may appear to have a swirled or mixed crown that reduces accurate identification and labeling,

which thereby diminishes correct classification. We discovered six percent of the matched trees were excluded from the machine learning analysis due to being of an unknown status. In addition, shadows produced the greatest bias and reduced the number of matched trees that could be predicted with the machine learning models (Table 4.2). Eight percent of the matched trees were in full shadow. Error associated with imagery processing can contribute a substantial source of error, which can greatly diminish tree mortality detection or other forms of detection such as species identification.

A third source of bias on successful tree mortality detection may be local tree structure. Specifically, high tree density in multiple strata forest stands may complicate detecting tree mortality. We attempted to explore the influence of local forest structure on machine learning based mortality detection by investigating whether the number of neighbors influenced tree mortality detection by height strata. A slight, but not statistically significant, increase in the mean number of neighbors was associated with incorrect predictions. Since remotely sensed trees on average contain two additional subordinate trees within the canopy prior to and following the drought (Table 2.2) in the study area, it is likely the detection error could be influenced by tree density. We believe that nadir position of the imagery relative to the tree of interest within the lidar segment plays an important role in influencing overstory tree detection whether it is for species or survivorship status.

We suspect that if the sample size were larger, it may have been possible to discriminate a statistically significant relationship. However, we did not expect the number of incorrect detections to be greatest in the tallest trees (Figure 4.4), which was true in both the field-validated and image classified trees. Additional examination of these incorrect detections will be necessary to determine the sources of error. For example, it is unknown if trees in the red phase were misclassified because they appeared dead in imagery, but the field assessment reported the tree as alive.

Question 2: Are there differences in the detection of mortality of matched trees by conifer species?

Pinus species tree mortality was overrepresented while *Abies* mortality was significantly underrepresented by remotely sensed trees (Table 4.3). Sugar pine, *P. lambertiana*, experienced 20% mortality of the in-situ conifer population. However, 60% of the matched Sugar pine were correctly identified as dead. Similarly, 33% of matched Jeffrey pine trees, *P. jeffreyi*, were correctly identified as dead. Yet only 7% of the Jeffrey pine were part of the conifer-based mortality. It is possible that the lidar segmentation algorithm employed, watershed segmentation, was more effective at detecting pine than fir species. In addition, we suspect that the canopy shape of pines also yields a fuller view of the crown than fir trees. Consequently, the pine trees may be more frequently segmented and better detected with machine learning. Overall, the pine trees were not as tall as the fir trees, yet they were better represented.

The fir trees accounted for 92% of the in-situ mortality. However, the matched fir tree mortality represented 20% of the in-situ mortality. This disparity indicates two important problems. First, much of the fir mortality was missed because it was most common in the subordinate trees <12m in height, which were hidden from the remote sensing sensors. Second, the fir trees overall were less likely to be captured by remotely sensed trees compared to the less represented pines. Understanding the bias inherent in the remotely sensed methods is important to addressing how population trends are represented. If taxonomic information were also collected exclusively by remotely sensed methods, the *Pinus* species would appear to be sustaining greater intra-species mortality compared to *Abies*.

In addition to the differences in taxonomic capture of mortality, the Random Forest and XGBoost models also showed significant differences in mortality detection by species. Overall, the XGBoost model performed very poorly in detecting mortality Red fir. It also performed more poorly in detecting mortality in White fir than Random Forest. However, both Random Forest and XGBoost performed consistently well in modeling mortality detection in both pine species.

In much of the labeled imagery, the pine canopies in this study occupied the entire lidar tree segment. In contrast, the fir tree canopies appeared to occupy a portion of the segmented canopy. This means that some portion of the fir tree canopy was occupied by other imagery such as shadow or the ground. Pixels composed of shadow or ground can skew the zonal statistics values of these matched trees and reduce the likelihood that they will be correctly predicted. It is possible that deep learning models may improve detection of all species as these models can account for spatial orientation of pixels, which can discriminate texture (Chang et al., 2019; Fricker et al., 2019).

Question 3: Can mortality and decay status be detected over time with machine learning?

We expected the live and shadow classes (Table 4.4) to be the best detected classes, which was correct. The correct predictions are likely attributable to two factors. First, these classes were composed of larger and statistically significant sample sizes compared to the other classes. Second, the tree crowns of these matched trees were likely composed of pixels that were consistent in color in the training and test datasets. However, the 2019 shadow class was not as well predicted, which was expected since this model did not include the canopy height model. Trees in the 0-10m height strata (Figure 2.6) are most frequently impacted by shadows, which dampens the mortality detection of an already underrepresented height strata.

It was expected that the mixed-top and dead-red classes would be difficult to detect with machine learning (Table 4.4). We thought that the small samples sizes and greater variability in color values in both classes would complicate model detection. However, the mixed-top class performed better than the red-phase. Our explanation for the improved model prediction of mixed-top was that the inclusion of the canopy height model in 2017 and 2018 aided the mixed-top prediction. The mixed-top class was uniformly taller in tree height while the dead-red phase had high variability in tree heights. Since the 2019 modeling did not include the canopy height model, the mixed class was poorly predicted with just imagery alone.

Ecologically, the mixed-top class represents two classes of trees that should be separated if sufficient samples are available in the future. The first class should include a browning crown (i.e., crown fade) class, which is a hallmark of bark beetle attack on pine trees. If crown fade is detected, it may aid researchers and managers in the early detection of a bark beetle outbreak as well as hazard tree identification. It was not possible to split the mixed-top class in study. Unfortunately, the number of browning crowns (i.e., crown fade) (Fettig et al., 2019) were too small in tree counts to allow for machine learning (Näsi et al., 2015). Unfortunately, the only high resolution (0.1m) drought related imagery was collected after the close of the tree mortality event, which precluded more closely examining a greater number of crown fade trees that would have been present earlier in the drought. The second class proposed for the mixed-top class should include decadent tree crowns. Decadent tree crowns appear as a broken or decaying top surrounded by a live canopy (Franklin et al., 2002). Decadent tree crowns may be important markers of mature trees; thus, remotely sensed trees coupled with field validation could aid in tracking mature forests spatially and temporally.

The Coarse Woody Debris class (Figure C.2, Appendix C) was poorly predicted (Table 4.4) in 2017 and 2018 and differed most significantly from the field validated data. The lack of precision in detection of this class was consistent across both models (i.e., Random Forest and XGBoost). We surmise that the poor prediction in the 2017 and 2018 modeling may be due to the class containing too much variability. The coarse woody debris class was created from combining three classes: snag, coarse woody debris, and live-coarse woody debris. The collapsed coarse woody debris class likely contained too great a range of height and color values, which resulted in poor detection. The class performance greatly improved in 2019 when the sample sizes increased and the canopy height model was not included as a predictor.

Question 4: What are the annual changes in survivorship, mortality, and decay trends of the most common fir and pine species (A. concolor and P. lambertiana, respectively) up to three years post-drought?

We thought Sugar pine would have a greater frequency of trees in decay in 2017 than White fir. Tall Sugar pines are the preferred host for the Western pine bark beetle, *D. brevicomis*. In 2015 and 2016 during the drought, tall Ponderosa pine in adjacent lower elevations to the study area experienced extensive mortality due to the drought and *D. brevicomis* attack (Axelson et al., 2019; Fettig et al., 2019). The expectation was that the *D. brevicomis* spread from lower elevations and infected the taller Sugar pine earlier than fir engraver induced mortality. However, the Sugar pine and White fir survivorship, mortality, and decay classes of the matched trees displayed similar trends up to three years post-drought (Figure 4.5).

We detected bias in our remotely sensed methods due to finding increases in the coarse woody debris to snag classes from 2018 to 2019. Due to this unexpected frequency change, we manually inspected each of the matched trees again in the 2018 and 2019 imagery. We found that minor shifts in imagery alignment with the lidar canopies were observed between 2018 and 2019. This shift resulted in snags being outside of the lidar tree boundary in 2018 and inside in 2019, which resulted in 2019 trees being labeled as coarse woody debris and 2019 as snags. It is important to note that the 2019 machine learning models did not include the CHM, yet the coarse woody debris class was well detected. This result suggests that in the absence of airborne lidar high resolution, imagery may be sufficient to detect coarse woody debris.

If future studies of overstory tree fate include the identification of taxonomic status, mortality, and decay, then the ecological fate of overstory trees could be evaluated with repeat measures with remotely sensed trees. We surmise that such studies will be most effective using deep learning approaches. Fettig et al., 2019 was able to demonstrate successful detection of taxonomic and survivorship status with RGB data. However, these studies will require significant sample sizes with ground validation to evaluate method efficacy, uncertainty, and bias.

Future Research

The remote sensing of individual trees from lidar coupled with high resolution imagery is a relatively new technology and research application (Fricker et al., 2019; Jeronimo et al., 2018; Ma, 2018; Paz-Kagan et al., 2017). As such, the opportunity to assess individual tree mortality with repeat measures over large areas is only now becoming possible (Hemming-Schroeder et al., 2023). Researchers have investigated machine and deep learning based mortality detection (Axelson et al., 2019; Hemming-Schroeder et al., 2023; Stovall et al., 2019; Young et al., 2017). However, researchers as well as managers are also interested in using such approaches to identify forest decay (Wong et al., 2023); the accumulation of surface fuels and coarse woody debris or "heavy fuels" (Rowell et al., 2020); and regeneration (Diez et al., 2021; Wagner et al., 2020). The approaches presented in this study could be adapted to deep learning approaches to detect changes in aboveground live and dead carbon storage changes (Xu et al., 2018). For example, the fate of remotely sensed trees could be tracked over time using a single collection of airborne lidar and repeat collections of imagery (i.e., repeat measures). Such studies could be invaluable in detecting changes wrought by a range of disturbances whose impacts are increasingly amplified by climate change. For example, individual overstory tree crown scorch and burn severity (Arkin et al., 2023; Hamilton et al., 2021) can be evaluated across the broad extents of large wildfire footprints.

The successful detection of decay classes such as snags and coarse woody debris by machine learning was unexpected. We expected this class to require deep learning for detection. The detection of advanced decay with only orthoimagery using machine learning is a positive outcome. Future research could determine if it is possible to detect both the stages of decay as well as regeneration. Developing such a classification schema should be supported with field validation. In addition to traditional field sampling, field validation could include sampling with improved geolocation and unmanned aerial vehicles (Arroyo-Mora et al., 2019; Hastings et al., 2020; Mohammadpour, Pegah, and Viegas, 2022; Paczkowski et al., 2021) or

possibly terrestrial lidar measurements (Hancock et al., 2017; Hauglin et al., 2014; Huang et al., 2019; Rocha et al., 2023). These datasets could provide very high spatial resolution products to further test these concepts.

In conclusion, there are a significant array of field-based mobile, UAV, fixed-wing, and satellite based sensors available that can greatly expand our capacity to study forests in three dimensions (Donager et al., 2021; Marchi et al., 2018; Mohammadpour, Pegah, and Viegas, 2022; Näsi et al., 2015; Paczkowski et al., 2021; Zhu, 2018). There are n-dimensional possibilities for applying these sensors and field studies to improve the sampling and census of tree populations. Creativity will not be the limiting factor for developing novel means to capture tree population trends. Yet, field testing and validation will remain a necessity to apply such tools and innovation to the assessment of ecological trends and forest resistance (Falk et al., 2019).

Our next steps are to apply the methods described herein to the detection of survivorship of remotely sensed trees produced as inputs into a landscape-wide analysis toolset. LICOSim is a comprehensive lidar-based assessment toolset that is designed to assess forest resistance and resilience in fire-adapted forests of the Sierra Nevada, LICOSim (Bartl-Geller, Bryce N., Kane, 2022; Bartl-Geller, Bryce N., Smith, 2023). LICOSim tools are applied across entire lidar acquisitions to assess overstory tree patterns and their departure from an identified range of reference conditions to plan relevant treatments (Bartl-Geller, Bryce N., Kane, 2022; Bartl-Geller, Bryce N., Smith, 2023). Importantly, the tool is effective because each reference condition is relevant to a specific vegetation type, topographic position, and climate. Our goal is to update the LICOSim assessment tools to include the assessment forest structure patterns in the context of background and elevated forest mortality. Ultimately, we aim to provide forest managers with improved knowledge of the status of forest resistance in high resolution across broad extents to empower more efficient, effective, and ecologically based management.

APPENDIX C, Chapter 4

C.1: Mortality Classes for Machine Learning Prediction

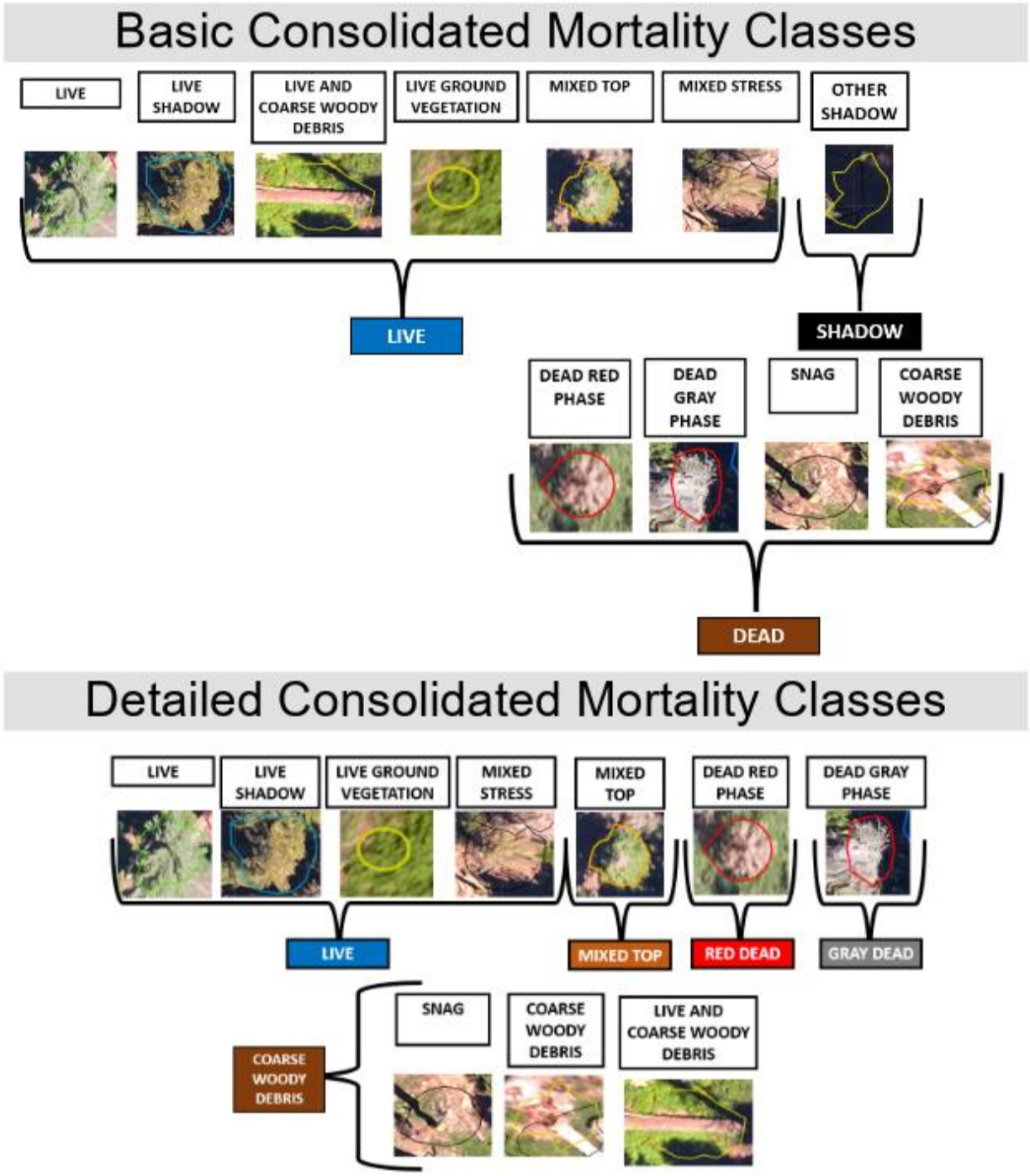

Figure C.1. Basic and detailed mortality classes for machine learning. The mortality and decay classes described in Table 1 were collapsed to a basic class to allow comparison with the binary field-based mortality status. For machine learning purposed, the mortality and decay classes were collapsed into a detailed classification system to provide more balanced samples for machine learning. The machine learning was conducted to detect mortality and decay across the matched trees.

C.2: Machine Learning Processing for Mortality Detection

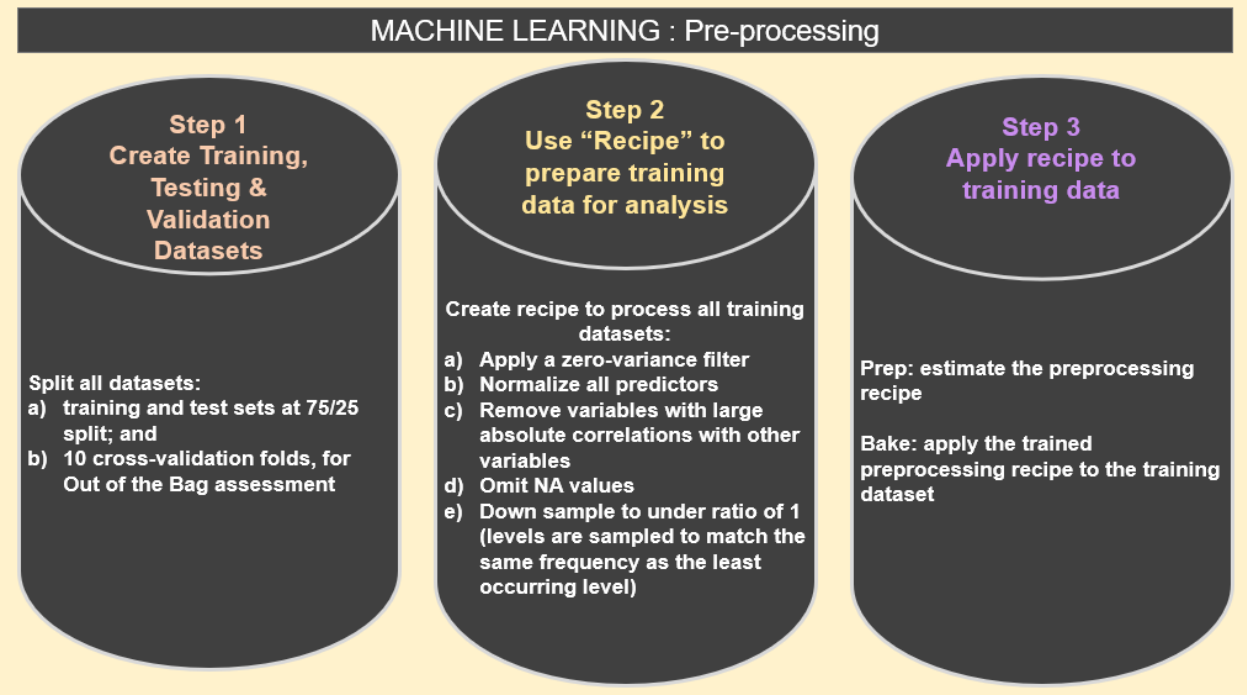

Figure C.2. The pre-processing steps to prepare the Questions One-Three datasets for machine learning modeling.

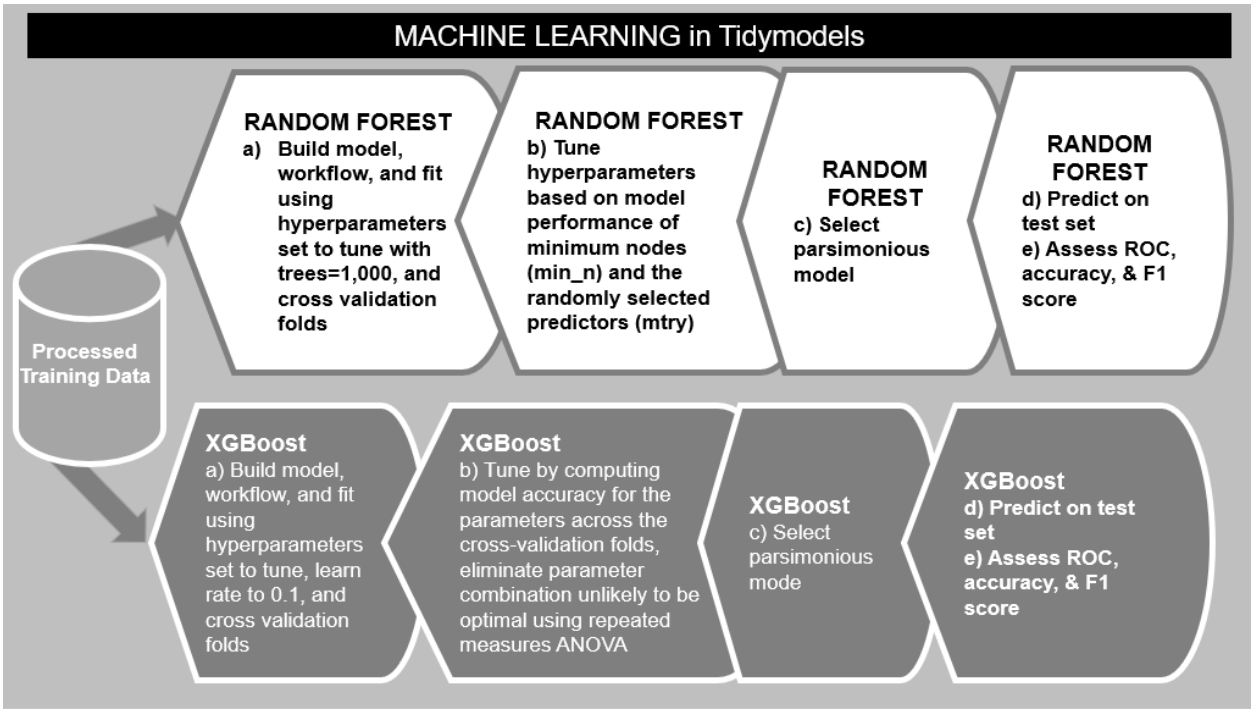

Figure C.3. The machine learning steps to build model workflows, hyperparameter tuning, model selection and predictions using Random Forest and XGBoost classification models.

C.3: Crosswalk of matched tree metrics

Table C.1.
Lidar-based and field-based metrics used to predict overstory tree mortality (matched trees) in the Study Area. Metrics denotes with * are described in the methods section of Chapter One, and ** denotes metrics calculated in Chapter Two.

Lidar-based metrics	**Field-based metrics**
NA	Taxonomic status
NA	Presence/absence of bark beetle
For the matched trees, the pre- and post-drought mortality status was inherited from the field-based metrics for validation purposes.	Pre (2011 and 2012) and post-drought (2018) mortality status as live or dead as measured in the field
Pre-drought height, direct from lidar*	Pre-drought height estimated from allometric equations*
Post-drought mean height derived from the NEON 2017 canopy height model*	Post-drought height estimated from allometric equations
Pre-drought tree stature, classified from 1-6, which represents DBH size classes up to >100cm	Pre-drought tree stature, classified from 1-6, which represents DBH size classes up to >100cm
Post-drought DBH	Post-drought DBH
Pre-drought canopy area*	Pre-drought canopy area estimated from allometric equation
Pre- and post-drought basal area as estimated from height derived DBH and species specific allometric equations, per time period	Pre- and post-drought basal area as estimate from species specific allometric equations using DBH as the input
Latitude and longitude, from lidar*	Latitude and longitude, from stem mapping
Number of lidar tree neighbors alive pre-drought within 10m of the matched tree, up to 30	Number of field tree neighbors alive pre-drought within 10m of the matched tree, up to 30
Mean distance of all lidar neighbors, per matched tree	Mean distance of all field tree neighbors, per matched tree
Number of field trees intersecting the canopy of the lidar tree, pre-drought. This metric is a surrogate for canopy depth, which can be measured by height strata by canopy cover with lidar	NA
Number of field trees intersecting the canopy of the lidar tree, post-drought. The neighbors measured were alive, pre-drought. This metric is a surrogate for canopy depth, which can be measured by height strata by canopy cover with lidar	NA

4.6 CITATIONS

Allen, B., Dalponte, M., Ørka, H.O., Næsset, E., Puliti, S., Astrup, R., Gobakken, T., 2022. UAV-Based Hyperspectral Imagery for Detection of Root, Butt, and Stem Rot in Norway Spruce. Remote Sens. 14, 1–16. https://doi.org/10.3390/rs14153830

Allen, B.H., 2005. Sierran Mixed Conifer, California Wildlife Habitat Relationships System. Sacramento.

Allen, C.D., Breshears, D.D., McDowell, N.G., 2015. On underestimation of global vulnerability to tree mortality and forest die-off from hotter drought in the Anthropocene. Ecosphere 6, 1–55. https://doi.org/10.1890/ES15-00203.1

Antonarakis, A.S., Siqueira, P., Munger, J.W., 2017. Using multi-source data from lidar, radar, imaging spectroscopy, and national forest inventories to simulate forest carbon fluxes. Int. J. Remote Sens. 38, 5464–5486. https://doi.org/10.1080/01431161.2017.1341666

Arkin, J., Coops, N.C., Daniels, L.D., Plowright, A., 2023. A novel post-fire method to estimate individual tree crown scorch height and volume using simple RPAS-derived data. Fire Ecol. 19. https://doi.org/10.1186/s42408-023-00174-7

Arroyo-Mora, J., Kalacska, M., Inamdar, D., Soffer, R., Lucanus, O., Gorman, J., Naprstek, T., Schaaf, E., Ifimov, G., Elmer, K., Leblanc, G., 2019. Implementation of a UAV–Hyperspectral Pushbroom Imager for Ecological Monitoring. Drones 3, 12. https://doi.org/10.3390/drones3010012

Asner, G.P., Brodrick, P.G., Anderson, C.B., Vaughn, N., Knapp, D.E., Martin, R.E., 2016. Progressive forest canopy water loss during the 2012–2015 California drought. Proc. Natl. Acad. Sci. 113, E249–E255. https://doi.org/10.1073/pnas.1523397113

Asner, G.P., Martin, R.E., Knapp, D.E., Tupayachi, R., Anderson, C.B., Sinca, F., Vaughn, N.R., Llactayo, W., 2017. Airborne laser-guided imaging spectroscopy to map forest trait diversity and guide conservation. Science 355, 385–389. https://doi.org/10.1126/science.aaj1987

Atkinson, P.M. and Foody, G.M., 2002. Uncertainty in remote sensing and GIS: fundamentals., in: Uncertainty in Remote Sensing and GIS. John Wiley & Sons, Ltd, pp. 1–18.

Axelson, J., Battles, J., Bulaon, B., Cluck, D., Cousins, S., Cox, L., Estes, B., Fettig, C., Hefty, A., Hishinuma, S., Hood, S., Kocher, S., McMahon, D., Mortenson, L., Koltunov, A., Kuskulis, E., Poloni, A., Ramirez, C., Restaino, C., Safford, H., Slaton, M., Smith, S., Tubbesing, C., Wayman, R., Young, D., 2019. The California Tree Mortality Data Collection Network — Enhanced communication and collaboration among scientists and stakeholders, California Agriculture. https://doi.org/10.3733/ca.2019a0001

Babcock, C., Finley, A.O., Andersen, H.E., Pattison, R., Cook, B.D., Morton, D.C., Alonzo, M., Nelson, R., Gregoire, T., Ene, L., Gobakken, T., Næsset, E., 2018. Geostatistical estimation of forest biomass in interior Alaska combining Landsat-derived tree cover, sampled airborne lidar and field observations. Remote Sens. Environ. 212, 212–230. https://doi.org/10.1016/j.rse.2018.04.044

Babcock, C., Finley, A.O., Bradford, J.B., Kolka, R., Birdsey, R., Ryan, M.G., 2015. LiDAR based prediction of forest biomass using hierarchical models with spatially varying coefficients. Remote Sens. Environ. 169, 113–127. https://doi.org/10.1016/j.rse.2015.07.028

Barbour, M., Kelley, E., Maloney, P., Rizzo, D., Royce, E., Fites-Kaufmann, J., 2002. Present and past old-growth forests of the Lake Tahoe Basin, Sierra Nevada, US. J. Veg. Sci. 13, 461–472. https://doi.org/10.1111/j.1654-1103.2002.tb02073.x

Bartl-Geller, Bryce N., Kane, V.R., 2022. LICOsim workshop: Forest and Shrubland LiDAR Derived Products Outreach Session.

Bartl-Geller, Bryce N., Smith, E., 2023. LICOsim case study: Restoration planning tools for ICO based treatments - Bryce.

Batchelor, J.L., Wilson, T.M., Olsen, M.J., Ripple, W.J., 2023. New Structural Complexity Metrics for Forests from Single Terrestrial Lidar Scans. Remote Sens. 15, 1–19. https://doi.org/10.3390/rs15010145

Begon, M. and C.R.T., 2021. Ecology: From Individuals to Ecosystems, 5th Edition, 5th Editio. ed. Wiley.

Bird, J.P., Woodworth, B.K., Fuller, R.A., Shaw, J.D., 2021. Uncertainty in population estimates: A meta-analysis for petrels. Ecol. Solut. Evid. 2, 1–13. https://doi.org/10.1002/2688-8319.12077

Breiman, L.E.O., 2001. Random forests. Mach. Learn. 45, 5–32. https://doi.org/10.1023/A:1010933404324

Brodrick, P.G., Asner, G.P., 2017. Remotely sensed predictors of conifer tree mortality during severe drought. Environ. Res. Lett. 12, 115013. https://doi.org/10.1088/1748-9326/aa8f55

Calamita, F., Imran, H.A., Vescovo, L., Mekhalfi, M.L., La Porta, N., 2021. Early identification of root rot disease by using hyperspectral reflectance: the case of pathosystem grapevine/armillaria. Remote Sens. 13, 1–22. https://doi.org/10.3390/rs13132436

Campbell, James B., Wynne, R.H., 2011. Introduction to Remote Sensing, Fifth. ed. The Guilford Press, New York.

Campbell, M.J., Dennison, P.E., Hudak, A.T., Parham, L.M., Butler, B.W., 2018. Quantifying understory vegetation density using small-footprint airborne lidar. Remote Sens. Environ. 215, 330–342. https://doi.org/10.1016/j.rse.2018.06.023

Canelles, Q., Aquilué, N., James, P.M.A., Lawler, J., Brotons, L., 2021. Global review on interactions between insect pests and other forest disturbances. Landsc. Ecol. 36, 945–972. https://doi.org/10.1007/s10980-021-01209-7

Cansler, C.A., Hood, S.M., Varner, J.M., van Mantgem, P.J., Agne, M.C., Andrus, R.A., Ayres, M.P., Ayres, B.D., Bakker, J.D., Battaglia, M.A., Bentz, B.J., Breece, C.R., Brown, J.K., Cluck, D.R., Coleman, T.W., Corace, R.G., Covington, W.W., Cram, D.S., Cronan, J.B., Crouse, J.E., Das, A.J., Davis, R.S., Dickinson, D.M., Fitzgerald, S.A., Fulé, P.Z., Ganio, L.M., Grayson, L.M., Halpern, C.B., Hanula, J.L., Harvey, B.J., Kevin Hiers, J., Huffman, D.W., Keifer, M.B., Keyser, T.L., Kobziar, L.N., Kolb, T.E., Kolden, C.A., Kopper, K.E., Kreitler, J.R., Kreye, J.K., Latimer, A.M., Lerch, A.P., Lombardero, M.J., McDaniel, V.L., McHugh, C.W., McMillin, J.D., Moghaddas, J.J., O'Brien, J.J., Perrakis, D.D.B., Peterson, D.W., Prichard, S.J., Progar, R.A., Raffa, K.F., Reinhardt, E.D., Restaino, J.C., Roccaforte, J.P., Rogers, B.M., Ryan, K.C., Safford, H.D., Santoro, A.E., Shearman, T.M., Shumate, A.M., Sieg, C.H., Smith, S.L., Smith, R.J., Stephenson, N.L., Stuever, M., Stevens, J.T., Stoddard, M.T., Thies, W.G., Vaillant, N.M., Weiss, S.A., Westlind, D.J., Woolley, T.J., Wright, M.C., 2020. The Fire and Tree Mortality Database, for empirical modeling of

individual tree mortality after fire. Sci. Data 7, 1–14. https://doi.org/10.1038/s41597-020-0522-7

Casas, Á., García, M., Siegel, R.B., Koltunov, A., Ramírez, C., Ustin, S., 2016. Burned forest characterization at single-tree level with airborne laser scanning for assessing wildlife habitat. Remote Sens. Environ. 175, 231–241. https://doi.org/10.1016/j.rse.2015.12.044

Chang, T., Rasmussen, B.P., Dickson, B.G., Zachmann, L.J., 2019. Chimera: A multi-task recurrent convolutional neural network for forest classification and structural estimation. Remote Sens. 11, 1–29. https://doi.org/10.3390/rs11070768

Chen, T., Guestrin, C., 2015. XGBoost: Reliable Large-scale Tree Boosting System, in: Proceedings of the 22nd SIGKDD Conference on Knowledge Discovery and Data Mining, San Francisco, CA, USA. pp. 1–6.

Chen, Wei, Hu, X., Chen, Wen, Hong, Y., Yang, M., 2018. Airborne LiDAR remote sensing for individual tree forest inventory using trunk detection-aided mean shift clustering techniques. Remote Sens. 10, 1–25. https://doi.org/10.3390/rs10071078

Clark, J.S., 2003. Uncertainty and variability in demography and population growth: A hierarchical approach. Ecology 84, 1370–1381. https://doi.org/10.1890/0012-9658(2003)084[1370:UAVIDA]2.0.CO;2

Cohen, W.B., Yang, Z., Stehman, S. V., Schroeder, T.A., Bell, D.M., Masek, J.G., Huang, C., Meigs, G.W., 2016. Forest disturbance across the conterminous United States from 1985-2012: The emerging dominance of forest decline. For. Ecol. Manage. 360, 242–252. https://doi.org/10.1016/j.foreco.2015.10.042

Congalton, R.G., 2001. Accuracy assessment and validation of remotely sensed and other spatial information. Int. J. Wildl. Fire 10, 321–328. https://doi.org/10.1071/wf01031

Das, A.J., Slaton, M.R., Mallory, J., Asner, G.P., Martin, R.E., Hardwick, P., 2022. Empirically validated drought vulnerability mapping in the mixed conifer forests of the Sierra Nevada. Ecol. Appl. 32, 1–19. https://doi.org/10.1002/eap.2514

Diez, Y., Kentsch, S., Fukuda, M., Caceres, M.L.L., Moritake, K., Cabezas, M., 2021. Deep learning in forestry using uav-acquired rgb data: A practical review. Remote Sens. 13, 1–43. https://doi.org/10.3390/rs13142837

Diffenbaugh, N.S., Swain, D.L., Touma, D., Lubchenco, J., 2015. Anthropogenic warming has increased drought risk in California. Proc. Natl. Acad. Sci. U. S. A. 112, 3931–3936. https://doi.org/10.1073/pnas.1422385112

Donager, J.J., Sánchez Meador, A.J., Blackburn, R.C., 2021. Adjudicating perspectives on forest structure: How do airborne, terrestrial, and mobile lidar-derived estimates compare? Remote Sens. 13, 1–18. https://doi.org/10.3390/rs13122297

Donato, D.C., Harvey, B.J., Turner, M.G., 2016. Regeneration of montane forests 24 years afer the 1988 Yellowstone fires: A fire-catalyzed shif in lower treelines? Ecosphere 7, 1–16. https://doi.org/10.1002/ecs2.1410/supinfo

Duncanson, L., Dubayah, R., 2018. Monitoring individual tree-based change with airborne lidar. Ecol. Evol. 8, 5079–5089. https://doi.org/10.1002/ece3.4075

Duncanson, L., Neuenschwander, A., Hancock, S., Thomas, N., Fatoyinbo, T., Simard, M., Silva, C.A., Armston, J., Luthcke, S.B., Hofton, M., Kellner, J.R., Dubayah, R., 2020.

Biomass estimation from simulated GEDI, ICESat-2 and NISAR across environmental gradients in Sonoma County, California. Remote Sens. Environ. 242. https://doi.org/10.1016/j.rse.2020.111779

Earles, J.M., North, M.P., Hurteau, M.D., 2014. Wildfire and drought dynamics destabilize carbon stores of fire-suppressed forests. Ecol. Appl. 24, 732–740. https://doi.org/10.1890/13-1860.1

Edson, C., Wing, M.G., 2011. Airborne light detection and ranging (LiDAR) for individual tree stem location, height, and biomass measurements, Remote Sensing. https://doi.org/10.3390/rs3112494

ESRI ArcGIS Pro Version 2.8, 2021.

Fadili, M., Renaud, J.P., Bock, J., Vega, C., 2019. RegisTree: a registration algorithm to enhance forest inventory plot georeferencing. Ann. For. Sci. 76. https://doi.org/10.1007/s13595-019-0814-2

Falk, D.A., Watts, A.C., Thode, A.E., 2019. Scaling Ecological Resilience. Front. Ecol. Evol. 7, 1–16. https://doi.org/10.3389/fevo.2019.00275

Fassnacht, F.E., Latifi, H., Stereńczak, K., Modzelewska, A., Lefsky, M., Waser, L.T., Straub, C., Ghosh, A., 2016. Review of studies on tree species classification from remotely sensed data. Remote Sens. Environ. 186, 64–87. https://doi.org/10.1016/j.rse.2016.08.013

Ferraz, A., Saatchi, S., Bormann, K.J., Painter, T., 2018. Fusion of NASA Airborne Snow Observatory (ASO) Lidar Time Series over Mountain Forest Landscapes. Remote Sens. https://doi.org/10.3390/rs10020164

Ferrell, G.T., Otrosina, W.J., Demaris Jr., C.J., 1994. Predicting susceptibility of white fir during a drought-associated outbreak of the fir engraver, Scolytusventralis, in California. Can. J. For. Res. 24, 302–305.

Fettig, C.J., Mortenson, L.A., Bulaon, B.M., Foulk, P.B., 2019. Tree mortality following drought in the central and southern Sierra Nevada, California, U.S. For. Ecol. Manage. 432, 164–178. https://doi.org/10.1016/j.foreco.2018.09.006

Finley, A.O., Banerjee, S., Zhou, Y., Cook, B.D., Babcock, C., 2017. Joint hierarchical models for sparsely sampled high-dimensional LiDAR and forest variables. Remote Sens. Environ. 190, 149–161. https://doi.org/10.1016/j.rse.2016.12.004

Franklin, J.F., Spies, T.A., Pelt, R. Van, Carey, A.B., Thornburgh, D.A., Berg, D.R., Lindenmayer, D.B., Harmon, M.E., Keeton, W.S., Shaw, D.C., Bible, K., Chen, J., 2002. Disturbances and structural development of natural forest ecosystems with silvicultural implications, using Douglas-fir forests as an example. For. Ecol. Manage. 155, 399–423. https://doi.org/10.1016/S0378-1127(01)00575-8

Frazer, G.W., Magnussen, S., Wulder, M.A., Niemann, K.O., 2011. Simulated impact of sample plot size and co-registration error on the accuracy and uncertainty of LiDAR-derived estimates of forest stand biomass. Remote Sens. Environ. 115, 636–649. https://doi.org/10.1016/j.rse.2010.10.008

Freiderichs, K., 1958. A Definition of Ecology and Some Thoughts About Basic Concepts. Ecology 39, 154–159.

Fricker, G.A., Ventura, J.D., Wolf, J., North, M.P., Frank, W., 2019. A Convolutional Neural

Network classifier identifies tree species in mixed-conifer forest from hyperspectral imagery 1–24.

Friedlingstein, P., Jones, M.W., O'Sullivan, M., Andrew, R.M., Bakker, D.C.E., 2022. Global Carbon Budget 2021, raport Earth System Science Data. Earth Syst. Sci. Data 14, 1917–2005.

Fry, D.L., Stephens, S.L., Collins, B.M., North, M.P., Franco-Vizcaíno, E., Gill, S.J., 2014. Contrasting spatial patterns in active-fire and fire-suppressed mediterranean climate old-growth mixed conifer forests. PLoS One 9. https://doi.org/10.1371/journal.pone.0088985

Furniss, T.J., Larson, A.J., Kane, V.R., Lutz, J.A., 2020. Wildfire and drought moderate the spatial elements of tree mortality. Ecosphere 11. https://doi.org/10.1002/ecs2.3214

Gallery, W., 2022. Neon Algorithm Theorectical Basis Document (Atbd) Aop Digital Camera Image Orthorectification Prepared By.

Gallery, W. (NEON), 2019. NEON Algorithm Theoretical Basis Document (ATBD): Camera Mosaic, NEON Airborne Observation Platform.

Gibson, P.B., Waliser, D.E., Guan, B., Deflorio, M.J., Ralph, F.M., Swain, D.L., 2020. Ridging associated with Drought across the Western and Southwestern United States: Characteristics, trends, and predictability sources. J. Clim. 33, 2485–2508. https://doi.org/10.1175/JCLI-D-19-0439.1

Goodwin, M.J., North, M.P., Zald, H.S.J., Hurteau, M.D., 2020. Changing climate reallocates the carbon debt of frequent-fire forests. Glob. Chang. Biol. 26, 6180–6189. https://doi.org/10.1111/gcb.15318

Grafström, A., Schelin, L., 2014. How to Select Representative Samples. Scand. J. Stat. 41, 277–290. https://doi.org/10.1111/sjos.12016

Grulke, N., Maxfield, J., Riggan, P., Schrader-Patton, C., 2020. Pre-emptive detection of mature pine drought stress using multispectral aerial imagery. Remote Sens. 12, 1–23. https://doi.org/10.3390/rs12142338

Guan, H., Zhang, J., Ma, Q., Liu, M., Wu, F., Guo, Q., Su, Y., Hu, T., Wang, R., Ma, Q., Yang, Q., Sun, X., Li, Y., Jin, S., 2020. A Novel Framework to Automatically Fuse Multiplatform LiDAR Data in Forest Environments Based on Tree Locations. IEEE Trans. Geosci. Remote Sens. 58, 2165–2177. https://doi.org/10.1109/TGRS.2019.2953654

Hajek, P., Link, R.M., Nock, C.A., Bauhus, J., Gebauer, T., Gessler, A., Kovach, K., Messier, C., Paquette, A., Saurer, M., Scherer-Lorenzen, M., Rose, L., Schuldt, B., 2022. Mutually inclusive mechanisms of drought-induced tree mortality. Glob. Chang. Biol. 28, 3365–3378. https://doi.org/10.1111/gcb.16146

Hamilton, D.A., Brothers, K.L., Jones, S.D., Colwell, J., Winters, J., 2021. Wildland fire tree mortality mapping from hyperspatial imagery using machine learning. Remote Sens. 13, 1–18. https://doi.org/10.3390/rs13020290

Hamraz, H., Contreras, M.A., Zhang, J., 2017. Forest understory trees can be segmented accurately within sufficiently dense airborne laser scanning point clouds. Sci. Rep. 7, 1–9. https://doi.org/10.1038/s41598-017-07200-0

Hancock, S., Anderson, K., Disney, M., Gaston, K.J., 2017. Measurement of fine-spatial-resolution 3D vegetation structure with airborne waveform lidar: Calibration and validation

with voxelised terrestrial lidar. Remote Sens. Environ. 188, 37–50. https://doi.org/10.1016/j.rse.2016.10.041

Hartmann, H., Bastos, A., Das, A.J., Esquivel-Muelbert, A., Hammond, W.M., Martínez-Vilalta, J., Mcdowell, N.G., Powers, J.S., Pugh, T.A.M., Ruthrof, K.X., Allen, C.D., 2022. Climate Change Risks to Global Forest Health: Emergence of Unexpected Events of Elevated Tree Mortality Worldwide. Annu. Rev. Plant Biol. 73, 673–702. https://doi.org/10.1146/annurev-arplant-102820-012804

Harvey, B.J., Donato, D.C., Turner, M.G., 2016. High and dry: Post-fire tree seedling establishment in subalpine forests decreases with post-fire drought and large stand-replacing burn patches. Glob. Ecol. Biogeogr. 25, 655–669. https://doi.org/10.1111/geb.12443

Hastings, J.H., Ollinger, S. V., Ouimette, A.P., Sanders-DeMott, R., Palace, M.W., Ducey, M.J., Sullivan, F.B., Basler, D., Orwig, D.A., 2020. Tree species traits determine the success of LiDAR-based crown mapping in a mixed temperate forest. Remote Sens. 12. https://doi.org/10.3390/rs12020309

Hauglin, M., Lien, V., Næsset, E., Gobakken, T., 2014. Geo-referencing forest field plots by co-registration of terrestrial and airborne laser scanning data. Int. J. Remote Sens. 35, 3135–3149. https://doi.org/10.1080/01431161.2014.903440

Hemming-Schroeder, N.M., Gutierrez, A.A., Allison, S.D., Randerson, J.T., 2023. Estimating Individual Tree Mortality in the Sierra Nevada Using Lidar and Multispectral Reflectance Data Journal of Geophysical Research : Biogeosciences. J. Geophys. Res. Biogeosciences, 128, 128, 1–18. https://doi.org/10.1029/2022JG007234

Holling, C.S., 1973. Resilience and Stability of Ecological Systems. Annu. Rev. Ecol. Syst. 4, 1–23.

Holmgren, J., Lindberg, E., 2019. Tree crown segmentation based on a tree crown density model derived from Airborne Laser Scanning. Remote Sens. Lett. 10, 1143–1152. https://doi.org/10.1080/2150704X.2019.1658237

Hu, T., Ma, Q., Su, Y., Battles, J.J., Collins, B.M., Stephens, S.L., Kelly, M., Guo, Q., 2019. A simple and integrated approach for fire severity assessment using bi-temporal airborne LiDAR data. Int. J. Appl. Earth Obs. Geoinf. 78, 25–38. https://doi.org/10.1016/J.JAG.2019.01.007

Huang, C. ying, Anderegg, W.R.L., Asner, G.P., 2019. Remote sensing of forest die-off in the Anthropocene: From plant ecophysiology to canopy structure. Remote Sens. Environ. 231, 111233. https://doi.org/10.1016/j.rse.2019.111233

Huang, K., Yi, C., Wu, D., Zhou, T., Zhao, X., Blanford, W.J., Wei, S., Wu, H., Ling, D., Li, Z., 2015. Tipping point of a conifer forest ecosystem under severe drought. Environ. Res. Lett. 10. https://doi.org/10.1088/1748-9326/10/2/024011

Huang, S., Ramirez, C., Kennedy, K., Mallory, J., 2017. A new approach to extrapolate forest attributes from field inventory with satellite and auxiliary data sets. For. Sci. 63, 232–240. https://doi.org/10.5849/forsci.16-028

Hudak, A.T., Strand, E.K., Vierling, L.A., Byrne, J.C., Eitel, J.U.H., Martinuzzi, S., Falkowski, M.J., 2012. Quantifying aboveground forest carbon pools and fluxes from repeat LiDAR surveys. Remote Sens. Environ. 123, 25–40. https://doi.org/10.1016/j.rse.2012.02.023

Huemmrich, K.F., 1996. Effects of shadows on vegetation indices. Int. Geosci. Remote Sens. Symp. 4, 2372–2374. https://doi.org/10.1109/igarss.1996.516990

Huesca, M., Ustin, S.L., Shapiro, K.D., Boynton, R., Thorne, J.H., 2021. Detection of drought-induced blue oak mortality in the Sierra Nevada Mountains, California. Ecosphere 12. https://doi.org/10.1002/ecs2.3558

Jakubowski, M.K., Li, W., Guo, Q., Kelly, M., 2013. Delineating individual trees from lidar data: A comparison of vector- and raster-based segmentation approaches. Remote Sens. 5, 4163–4186. https://doi.org/10.3390/rs5094163

Jeronimo, S.A.M., 2018. Restoring forest resilience in the Sierra Nevada mixed-conifer zone, with a focus on measuring spatial patterns of trees using airborne lidar. University of Washington.

Jeronimo, S.M., 2015. LiDAR individual tree detection for assessing structurally diverse forest landscapes. Univ. Washingt. University of Washington, Seattle, WA.

Jeronimo, S.M.A., Bartl-Geller, B.N., Griffey, V., van Wagtendonk, L., Shaw, M., Kane, V.R., 2019. Using lidar data to develop silvicultural restoration options and identify potential American marten habitat. Final report to the USDA Forest Service: Malheur National Forest and Wallowa-Whitman National Forest. Agreement 18-CO-11060400-16.

Jeronimo, S.M.A., Kane, V.R., Churchill, D.J., McGaughey, R.J., Franklin, J.F., 2018. Applying LiDAR individual tree detection to management of structurally diverse forest landscapes. J. For. 116, 336–346. https://doi.org/10.1093/jofore/fvy023

Jiao, W., Wang, L., McCabe, M.F., 2021. Multi-sensor remote sensing for drought characterization: current status, opportunities and a roadmap for the future. Remote Sens. Environ. 256, 112313. https://doi.org/10.1016/j.rse.2021.112313

Kane, V.R., Bakker, J.D., McGaughey, R.J., Lutz, J.A., Gersonde, R.F., Franklin, J.F., 2010a. Examining conifer canopy structural complexity across forest ages and elevations with LiDAR data. Can. J. For. Res. 40, 774–787. https://doi.org/10.1139/X10-064

Kane, V.R., Bartl-Geller, B.N., North, M.P., Kane, J.T., Lydersen, J.M., Jeronimo, S.M.A., Collins, B.M., Monika Moskal, L., 2019. First-entry wildfires can create opening and tree clump patterns characteristic of resilient forests. For. Ecol. Manage. 454, 117659. https://doi.org/10.1016/j.foreco.2019.117659

Kane, V.R., Lutz, J.A., Roberts, S.L., Smith, D.F., McGaughey, R.J., Povak, N.A., Brooks, M.L., 2013. Landscape-scale effects of fire severity on mixed-conifer and red fir forest structure in Yosemite National Park. For. Ecol. Manage. 287, 17–31. https://doi.org/10.1016/j.foreco.2012.08.044

Kane, V.R., McGaughey, R.J., Bakker, J.D., Gersonde, R.F., Lutz, J.A., Franklin, J.F., 2010b. Comparisons between field- and LiDAR-based measures of stand structural complexity. Can. J. For. Res. 40, 761–773. https://doi.org/10.1139/X10-024

Kattenborn, T., Leitloff, J., Schiefer, F., Hinz, S., 2021. Review on Convolutional Neural Networks (CNN) in vegetation remote sensing. ISPRS J. Photogramm. Remote Sens. 173, 24–49. https://doi.org/10.1016/j.isprsjprs.2020.12.010

Kennedy, R.E., Ohmann, J., Gregory, M., Roberts, H., Yang, Z., Bell, D.M., Kane, V., Hughes, M.J., Cohen, W.B., Powell, S., Neeti, N., Larrue, T., Hooper, S., Kane, J., Miller, D.L., Perkins, J., Braaten, J., Seidl, R., Braaten, J., Hooper, S., Neeti, N., Gregory, M., Kane, J.,

Ohmann, J., Bell, D.M., Cohen, W.B., Powell, S., Roberts, H., Larrue, T., Kennedy, R.E., Yang, Z., Perkins, J., Hughes, M.J., 2017. An empirical, integrated forest biomass monitoring system. Environ. Res. Lett. 13, 025004. https://doi.org/10.1088/1748-9326/aa9d9e

Khatri-chhetri, P., van Wagtendonk, L., Hendryx, S.M., Kane, V.R., 2023. Remote Sensing of Environment Enhancing individual tree mortality mapping : The impact of models , data modalities , and classification taxonomy. Remote Sens. Environ. 300, 113914. https://doi.org/10.1016/j.rse.2023.113914

Knapp, E.E., Bernal, A.A., Kane, J.M., Fettig, C.J., North, M.P., 2021. Variable thinning and prescribed fire influence tree mortality and growth during and after a severe drought. For. Ecol. Manage. 479, 118595. https://doi.org/10.1016/j.foreco.2020.118595

Krause, K., Goulden, T., 2015. NEON L0-to-L1 Discrete Return LiDAR Algorithm Theoretical Basis Document. https://doi.org/NEON.DOC.001292

Krofcheck, D.J., Hurteau, M.D., Scheller, R.M., Loudermilk, E.L., 2017. Restoring surface fire stabilizes forest carbon under extreme fire weather in the Sierra Nevada. Ecosphere 8. https://doi.org/10.1002/ecs2.1663

Lamping, J.E., Zald, H.S.J., Madurapperuma, B.D., Graham, J., 2021. Comparison of low-cost commercial unpiloted digital aerial photogrammetry to airborne laser scanning across multiple forest types in california, usa. Remote Sens. 13. https://doi.org/10.3390/rs13214292

Leisso, N., 2016. Neon Normaliszed Difference Vegetation Index (Ndvi), Enhanced Vegetation Index (Evi), Atomospherically Resistant Vegetation Index (Arvi), Canopy Xanthophyll Cycle (Pri), and Canopy Lignin (Ndli) Algorithm Theoretical Basis Document Prepared By.

Li, W., Guo, Q., Jakubowski, M.K., Kelly, M., 2012. A new method for segmenting individual trees from the lidar point cloud. Photogramm. Eng. Remote Sensing 78, 75–84. https://doi.org/10.14358/PERS.78.1.75

Lindberg, E., Holmgren, J., Olofsson, K., Wallerman, J., Olsson, H., 2013. Estimation of tree lists from airborne laser scanning using tree model clustering and k-MSN imputation. Remote Sens. 5, 1932–1955. https://doi.org/10.3390/rs5041932

Lines, E.R., Fischer, F.J., Owen, H.J.F., Jucker, T., 2022. The shape of trees: Reimagining forest ecology in three dimensions with remote sensing. J. Ecol. 110, 1730–1745. https://doi.org/10.1111/1365-2745.13944

Lisiewicz, M., Kamińska, A., Kraszewski, B., Stereńczak, K., 2022. Correcting the Results of CHM-Based Individual Tree Detection Algorithms to Improve Their Accuracy and Reliability. Remote Sens. 14. https://doi.org/10.3390/rs14081822

Lund, J., Medellin-Azuara, J., Durand, J., Stone, K., 2018. Lessons from California's 2012–2016 Drought. J. Water Resour. Plan. Manag. 144, 04018067. https://doi.org/10.1061/(asce)wr.1943-5452.0000984

Ma, K., Chen, Z., Fu, L., Tian, W., Jiang, F., Yi, J., Du, Z., Sun, H., 2022. Performance and Sensitivity of Individual Tree Segmentation Methods for UAV-LiDAR in Multiple Forest Types. Remote Sens. 14. https://doi.org/10.3390/rs14020298

Ma, Q., 2018. Quantifying Forest Structure Parameters and Their Changes from LiDAR Data

and Satellite Imagery in the Sierra Nevada. University of California, Merced. https://doi.org/10.21425/F59335464

Marchi, N., Pirotti, F., Lingua, E., 2018. Airborne and Terrestrial Laser Scanning Data for the Assessment of Standing and Lying Deadwood: Current Situation and New Perspectives. Remote Sens. 10, 1356. https://doi.org/10.3390/rs10091356

McCune, B., Grace, J.B.., Urban, D.L., 2002. Analysis of Ecological Communities. Gleneden Beach.

McGaughey, R.J., 2018a. FUSION/LDV: Software for LIDAR Data Analysis and Visualization: Version 3.70. USDA Forest Service Pacific Northwest Research Station, Seattle, WA.

McGaughey, R.J., 2018b. FUSION / LDV : Software for LIDAR Data Analysis and Visualization. U.S. Department of Agriculture, Forest Service, Pacific Northwest Research Station, University of Washington, Seattle, WA, USA.

Meddens, A.J.H., Hicke, J.A., Vierling, L.A., 2011. Evaluating the potential of multispectral imagery to map multiple stages of tree mortality. Remote Sens. Environ. 115, 1632–1642. https://doi.org/10.1016/j.rse.2011.02.018

Melo, J., Baker, T., Nemitz, D., Quegan, S., Ziv, G., 2023. Satellite-based global maps are rarely used in forest reference levels submitted to the UNFCCC. Environ. Res. Lett. 18. https://doi.org/10.1088/1748-9326/acba31

Millar, C.I., Stephenson, N.L., 2015. Temperate forest health in an era of emerging megadisturbance. Science (80-.). 349, 823–826. https://doi.org/10.1126/science.aaa9933

Miller, J.D., Thode, A.E., 2007. Quantifying burn severity in a heterogeneous landscape with a relative version of the delta Normalized Burn Ratio (dNBR). Remote Sens. Environ. 109, 66–80. https://doi.org/10.1016/j.rse.2006.12.006

Mohammadpour, Pegah, and Viegas, C., 2022. Applications of Multi-Source and Multi-Sensor Data Fusion of Remote Sensing for Forest Species Mapping., in: Advances in Remote Sensing for Forest Monitoring. John Wiley & Sons, Ltd, pp. 255–297. https://doi.org/https://doi.org/10.1002/9781119788157.ch12

Mokroš, M., Mikita, T., Singh, A., Tomaštík, J., Chudá, J., Wężyk, P., Kuželka, K., Surový, P., Klimánek, M., Zięba-Kulawik, K., Bobrowski, R., Liang, X., 2021. Novel low-cost mobile mapping systems for forest inventories as terrestrial laser scanning alternatives. Int. J. Appl. Earth Obs. Geoinf. 104. https://doi.org/10.1016/j.jag.2021.102512

Moskal, L.M., Zheng, G., 2012. Retrieving forest inventory variables with terrestrial laser scanning (TLS) in urban heterogeneous forest. Remote Sens. 4, 1–20. https://doi.org/10.3390/rs4010001

Murray, J., Gullick, D., Blackburn, G.A., Whyatt, J.D., Edwards, C., 2019. ARBOR: A new framework for assessing the accuracy of individual tree crown delineation from remotely-sensed data. Remote Sens. Environ. 231, 111256. https://doi.org/10.1016/j.rse.2019.111256

Näsi, R., Honkavaara, E., Lyytikäinen-Saarenmaa, P., Blomqvist, M., Litkey, P., Hakala, T., Viljanen, N., Kantola, T., Tanhuanpää, T., Holopainen, M., 2015. Using UAV-based photogrammetry and hyperspectral imaging for mapping bark beetle damage at tree-level. Remote Sens. 7, 15467–15493. https://doi.org/10.3390/rs71115467

Nitoslawski, S.A., Wong-Stevens, K., Steenberg, J.W.N., Witherspoon, K., Nesbitt, L., Konijnendijk van den Bosch, C.C., 2021. The Digital Forest: Mapping a Decade of Knowledge on Technological Applications for Forest Ecosystems. Earth's Futur. 9, 1–28. https://doi.org/10.1029/2021EF002123

North, M., Chen, J., Oakley, B., Song, B., Rudnicki, M., Gray, A., Innes, J., 2004. Forest stand structure and pattern of old-growth western hemlock/Douglas-fir and mixed-conifer forests. For. Sci. 50, 299–311.

North, M., Innes, J., Zald, H., 2007. Comparison of thinning and prescribed fire restoration treatments to Sierran mixed-conifer historic conditions. Can. J. For. Res. 37, 331–342. https://doi.org/10.1139/X06-236

North, M., Oakley, B., Chen, J., Erickson, H., Gray, A., Izzo, A., Schowalter, T., 2002. Vegetation and ecological characteristics of mixed conifer and red fir forests at the teakettle experimental forest.

North, M.P., 2002. Vegetation and ecological characteristics of mixed-conifer and red fir forests at the Teakettle Experimental Forest.

North, M.P., Stevens, J.T., Greene, D.F., Coppoletta, M., Knapp, E.E., Latimer, A.M., Restaino, C.M., Tompkins, R.E., Welch, K.R., York, R.A., Young, D.J.N., Axelson, J.N., Buckley, T.N., Estes, B.L., Hager, R.N., Long, J.W., Meyer, M.D., Ostoja, S.M., Sa, H.D., Shive, K.L., Tubbesing, C.L., Vice, H., Walsh, D., Werner, C.M., Wyrsch, P., 2019. Tamm Review : Reforestation for resilience in dry western U . S . forests 432, 209–224. https://doi.org/10.1016/j.foreco.2018.09.007

Odum, E. and G.W.B., 1971. Fundamentals of ecology. W B Saunders Co; 3rd edition (January 1, 1971).

Olofsson, P., Foody, G.M., Herold, M., Stehman, S. V., Woodcock, C.E., Wulder, M.A., 2014. Good practices for estimating area and assessing accuracy of land change. Remote Sens. Environ. 148, 42–57. https://doi.org/10.1016/j.rse.2014.02.015

Paczkowski, S., Datta, P., Irion, H., Paczkowska, M., Habert, T., Pelz, S., Jaeger, D., 2021. Evaluation of early bark beetle infestation localization by drone-based monoterpene detection. Forests 12, 1–17. https://doi.org/10.3390/f12020228

Painter, T.H., Berisford, D.F., Boardman, J.W., Bormann, K.J., Deems, J.S., Gehrke, F., Hedrick, A., Joyce, M., Laidlaw, R., Marks, D., Mattmann, C., McGurk, B., Ramirez, P., Richardson, M., Skiles, S.M.K., Seidel, F.C., Winstral, A., 2016. The Airborne Snow Observatory: Fusion of scanning lidar, imaging spectrometer, and physically-based modeling for mapping snow water equivalent and snow albedo. Remote Sens. Environ. 184, 139–152. https://doi.org/10.1016/j.rse.2016.06.018

Pascual, C., Martín-Fernández, S., García-Montero, L.G., García-Abril, A., 2013. Algorithm for improving the co-registration of LiDAR-derived digital canopy height models and field data. Agrofor. Syst. 87, 967–975. https://doi.org/10.1007/s10457-013-9612-2

Paz-Kagan, T., Brodrick, P.G., Vaughn, N.R., Das, A.J., Stephenson, N.L., Nydick, K.R., Asner, G.P., 2017. What mediates tree mortality during drought in the southern Sierra Nevada? Ecol. Appl. 27, 2443–2457. https://doi.org/10.1002/eap.1620

Persson, H.J., Olofsson, K., Holmgren, J., 2022. Two-phase forest inventory using very-high-resolution laser scanning. Remote Sens. Environ. 271, 112909.

https://doi.org/10.1016/j.rse.2022.112909

Piermattei, L., Karel, W., Wang, D., Wieser, M., Mokroš, M., Surový, P., Koreň, M., Tomaštík, J., Pfeifer, N., Hollaus, M., 2019. Terrestrial Structure from Motion Photogrammetry for Deriving Forest Inventory Data. Remote Sens. 11, 950. https://doi.org/10.3390/rs11080950

Polewski, P., Yao, W., Heurich, M., Krzystek, P., Stilla, U., 2015. Detection of single standing dead trees from aerial color infrared imagery by segmentation with shape and intensity priors. ISPRS Ann. Photogramm. Remote Sens. Spat. Inf. Sci. 2, 181–188. https://doi.org/10.5194/isprsannals-II-3-W4-181-2015

Potapov, P., Li, X., Hernandez-Serna, A., Tyukavina, A., Hansen, M.C., Kommareddy, A., Pickens, A., Turubanova, S., Tang, H., Silva, C.E., Armston, J., Dubayah, R., Blair, J.B., Hofton, M., 2021. Mapping global forest canopy height through integration of GEDI and Landsat data. Remote Sens. Environ. 253, 112165. https://doi.org/10.1016/j.rse.2020.112165

Pötzschner, F., Baumann, M., Gasparri, N.I., Conti, G., Loto, D., Piquer-Rodríguez, M., Kuemmerle, T., 2022. Ecoregion-wide, multi-sensor biomass mapping highlights a major underestimation of dry forests carbon stocks. Remote Sens. Environ. 269. https://doi.org/10.1016/j.rse.2021.112849

Povak, N., Kane, V.R., Collins, B., Lydersen, J., Kane, J.T., n.d. Decomposing multi-scaled drivers of severity patterns across land ownerships for an extreme wildfire event. Landsc. Ecol.

Qin, H., Zhou, W., Yao, Y., Wang, W., 2022. Individual tree segmentation and tree species classification in subtropical broadleaf forests using UAV-based LiDAR, hyperspectral, and ultrahigh-resolution RGB data. Remote Sens. Environ. 280, 113143. https://doi.org/10.1016/j.rse.2022.113143

R: A language and environment for statistical computing., 2022.

R Studio: Integrated Development for R., 2022.

Rocchini, D., Boyd, D.S., Féret, J.B., Foody, G.M., He, K.S., Lausch, A., Nagendra, H., Wegmann, M., Pettorelli, N., 2016. Satellite remote sensing to monitor species diversity: potential and pitfalls. Remote Sens. Ecol. Conserv. 2, 25–36. https://doi.org/10.1002/rse2.9

Rocchini, D., Foody, G.M., Nagendra, H., Ricotta, C., Anand, M., He, K.S., Amici, V., Kleinschmit, B., Förster, M., Schmidtlein, S., Feilhauer, H., Ghisla, A., Metz, M., Neteler, M., 2013. Uncertainty in ecosystem mapping by remote sensing. Comput. Geosci. 50, 128–135. https://doi.org/10.1016/j.cageo.2012.05.022

Rocha, K.D., Silva, C.A., Cosenza, D.N., Mohan, M., Klauberg, C., Schlickmann, M.B., Xia, J., Leite, R. V., de Almeida, D.R.A., Atkins, J.W., Cardil, A., Rowell, E., Parsons, R., Sánchez-López, N., Prichard, S.J., Hudak, A.T., 2023. Crown-Level Structure and Fuel Load Characterization from Airborne and Terrestrial Laser Scanning in a Longleaf Pine (Pinus palustris Mill.) Forest Ecosystem. Remote Sens. 15. https://doi.org/10.3390/rs15041002

Roche, J.W., Goulden, M.L., Bales, R.C., 2018. Estimating evapotranspiration change due to forest treatment and fire at the basin scale in the Sierra Nevada, California. Ecohydrology 11, 1–10. https://doi.org/10.1002/eco.1978

Rowell, E., Loudermilk, E.L., Hawley, C., Pokswinski, S., Seielstad, C., Queen, Ll.L., O'Brien, J.J., Hudak, A.T., Goodrick, S., Hiers, J.K., 2020. Coupling terrestrial laser scanning with

3D fuel biomass sampling for advancing wildland fuels characterization. For. Ecol. Manage. 462, 117945. https://doi.org/10.1016/j.foreco.2020.117945

Sciences, W., 2011. Dinkey Creek / Tea Kettle 2010.

Shivaprakash, K.N., Swami, N., Mysorekar, S., Arora, R., Gangadharan, A., Vohra, K., Jadeyegowda, M., Kiesecker, J.M., 2022. Potential for Artificial Intelligence (AI) and Machine Learning (ML) Applications in Biodiversity Conservation, Managing Forests, and Related Services in India. Sustain. 14, 1–20. https://doi.org/10.3390/su14127154

Shive, K.L., Preisler, H.K., Welch, K.R., Safford, H.D., Butz, R.J., O'Hara, K.L., Stephens, S.L., 2018. From the stand scale to the landscape scale: predicting the spatial patterns of forest regeneration after disturbance. Ecol. Appl. 28, 1626–1639. https://doi.org/10.1002/eap.1756

Smith, T.F., Rizzo, D.M., North, M., 2005. Patterns of mortality in an old-growth mixed-conifer forest of the southern Sierra Nevada, California. For. Sci. 51, 266–275. https://doi.org/10.1093/forestscience/51.3.266

Song, X.-P., 2018. Global Estimates of Ecosystem Service Value and Change: Taking Into Account Uncertainties in Satellite-based Land Cover Data. Ecol. Econ. 143, 227–235. https://doi.org/10.1016/j.ecolecon.2017.07.019

Sousa, D., Davis, F.W., 2020. Scalable mapping and monitoring of Mediterranean-climate oak landscapes with temporal mixture models. Remote Sens. Environ. 247, 111937. https://doi.org/10.1016/j.rse.2020.111937

Stears, A.E., Adler, P.B., Albeke, S.E., Atkins, D.H., Studyvin, J., Laughlin, D.C., 2022. plantTracker: An R package to translate maps of plant occurrence into demographic data. Methods Ecol. Evol. 13, 2129–2137. https://doi.org/10.1111/2041-210X.13950

Stephens, S.L., Bernal, A.A., Collins, B.M., Finney, M.A., Lautenberger, C., Saah, D., 2022. Mass fire behavior created by extensive tree mortality and high tree density not predicted by operational fire behavior models in the southern Sierra Nevada. For. Ecol. Manage. 518, 120258. https://doi.org/10.1016/j.foreco.2022.120258

Stephens, S.L., Collins, B.M., Fettig, C.J., Finney, M.A., Hoffman, C.M., Knapp, E.E., North, M.P., Safford, H., Wayman, R.B., 2018. Drought, Tree Mortality, and Wildfire in Forests Adapted to Frequent Fire. Bioscience XX, 1–12. https://doi.org/10.1093/biosci/bix146

Stephenson, N.L., Das, A.J., 2020. Height-related changes in forest composition explain increasing tree mortality with height during an extreme drought. Nat. Commun. 11, 1–14. https://doi.org/10.1038/s41467-020-17213-5

Stephenson, N.L., Das, A.J., Ampersee, N.J., Bulaon, B.M., Yee, J.L., 2019. Which trees die during drought? The key role of insect host-tree selection. J. Ecol. 107, 2383–2401. https://doi.org/10.1111/1365-2745.13176

Stephenson, N.L., Van Mantgem, P.J., 2005. Forest turnover rates follow global and regional patterns of productivity. Ecol. Lett. 8, 524–531. https://doi.org/10.1111/j.1461-0248.2005.00746.x

Stovall, A.E.L., 2020. Height Related Drought Mortality Supplement. Nat. Commun.

Stovall, A.E.L., Shugart, H., Yang, X., 2019. Tree height explains mortality risk during an intense drought. Nat. Commun. 10, 1–6. https://doi.org/10.1038/s41467-019-12380-6

Su, Y., Guo, Q., Jin, S., Guan, H., Sun, X., Ma, Q., Hu, T., Wang, R., Li, Y., 2020. The Development and Evaluation of a Backpack LiDAR System for Accurate and Efficient Forest Inventory. IEEE Geosci. Remote Sens. Lett. 18, 1660–1664. https://doi.org/10.1109/lgrs.2020.3005166

Swain, D.L., 2015. A tale of two California droughts: Lessons amidst record warmth and dryness in a region of complex physical and human geography. Geophys. Res. Lett. 42, 9999–10003. https://doi.org/10.1002/2015GL066628

Swann, A.L.S., Laguë, M.M., Garcia, E.S., Field, J.P., Breshears, D.D., Moore, D.J.P., Saleska, S.R., Stark, S.C., Villegas, J.C., Law, D.J., Minor, D.M., 2018. Continental-scale consequences of tree die-offs in North America: Identifying where forest loss matters most. Environ. Res. Lett. 13. https://doi.org/10.1088/1748-9326/aaba0f

Swatantran, A., Dubayah, R., Roberts, D., Hofton, M., Blair, J.B., 2011. Mapping biomass and stress in the Sierra Nevada using lidar and hyperspectral data fusion. Remote Sens. Environ. 115, 2917–2930. https://doi.org/10.1016/j.rse.2010.08.027

Taylor-Rodriguez, D., Finley, A.O., Datta, A., Babcock, C., Andersen, H.-E., Cook, B.D., Morton, D.C., Baneerjee, S., 2018. Spatial Factor Models for High-Dimensional and Large Spatial Data: An Application in Forest Variable Mapping.

Taylor, A.H., 2004. Identifying forest reference conditions on early cut-over lands, Lake Tahoe Basin, USA. Ecol. Appl. 14, 1903–1920. https://doi.org/10.1890/02-5257

United States Forest Service, Region 5, P.S.R., 2019. California 2018 Aerial Detection Survey.

US Department of Agriculture, 2010. National Agriculutural Imagery Program County Mosaic.

USDA, 2023. National Agricultural Imagery Program GeoHub [WWW Document]. URL https://naip-usdaonline.hub.arcgis.com/ (accessed 4.6.23).

Vauhkonen, J., Ene, L., Gupta, S., Heinzel, J., Holmgren, J., Pitkänen, J., Solberg, S., Wang, Y., Weinacker, H., Hauglin, K.M., Lien, V., Packalén, P., Gobakken, T., Koch, B., Næsset, E., Tokola, T., Maltamo, M., 2012. Comparative testing of single-tree detection algorithms under different types of forest. Forestry 85, 27–40. https://doi.org/10.1093/forestry/cpr051

Versace, S., Gianelle, D., Frizzera, L., Tognetti, R., Garfì, V., Dalponte, M., 2019. Prediction of competition indices in a Norway spruce and silver fir-dominated forest using lidar data. Remote Sens. 11. https://doi.org/10.3390/rs11232734

Vincent, L., Vincent, L., Soille, P., 1991. Watersheds in Digital Spaces: An Efficient Algorithm Based on Immersion Simulations. IEEE Trans. Pattern Anal. Mach. Intell. 13, 583–598. https://doi.org/10.1109/34.87344

Voelker, S.L., Merschel, A.G., Meinzer, F.C., Ulrich, D.E.M., Spies, T.A., Still, C.J., 2019. Fire deficits have increased drought sensitivity in dry conifer forests: Fire frequency and tree-ring carbon isotope evidence from Central Oregon. Glob. Chang. Biol. 25, 1247–1262. https://doi.org/10.1111/gcb.14543

Wagner, F.H., Sanchez, A., Aidar, M.P.M., Rochelle, A.L.C., Tarabalka, Y., Fonseca, M.G., Phillips, O.L., Gloor, E., Aragão, L.E.O.C., 2020. Mapping Atlantic rainforest degradation and regeneration history with indicator species using convolutional network. PLoS One 15, e0229448. https://doi.org/10.1371/journal.pone.0229448

Wayman, R.B., Safford, H.D., 2021. Recent bark beetle outbreaks influence wildfire severity in

mixed-conifer forests of the Sierra Nevada, California, USA. Ecol. Appl. 31, 1–19. https://doi.org/10.1002/eap.2287

Wiggins, H.L., Nelson, C.R., Larson, A.J., Safford, H.D., 2019. Using LiDAR to develop high-resolution reference models of forest structure and spatial pattern. For. Ecol. Manage. 434, 318–330. https://doi.org/10.1016/j.foreco.2018.12.012

Wing, B.M., Ritchie, M.W., Boston, K., Cohen, W.B., Olsen, M.J., 2015. Individual snag detection using neighborhood attribute filtered airborne lidar data. Remote Sens. Environ. 163, 165–179. https://doi.org/10.1016/j.rse.2015.03.013

Wong, T., Sani-mohammed, A., Yao, W., Heurich, M., 2023. Automatic Classification of Single Tree Decay Stages from Combined ALS Data and Aerial CIR Imagery using Machine Learning. arXiv, Cornell Univ. 48.

Xu, Q., Man, A., Fredrickson, M., Hou, Z., Pitkänen, J., Wing, B., Ramirez, C., Li, B., Greenberg, J.A., 2018. Quantification of uncertainty in aboveground biomass estimates derived from small-footprint airborne LiDAR. Remote Sens. Environ. 216, 514–528. https://doi.org/10.1016/j.rse.2018.07.022

Yan, W., Guan, H., Cao, L., Yu, Y., Li, C., Lu, J.Y., 2020. A self-adaptive mean shift tree-segmentation method using UAV LiDAR data. Remote Sens. 12, 1–14. https://doi.org/10.3390/rs12030515

Yang, Q., Su, Y., Jin, S., Kelly, M., Hu, T., Ma, Q., Li, Y., Song, S., Zhang, J., Xu, G., Wei, J., Guo, Q., 2019. The influence of vegetation characteristics on individual tree segmentation methods with airborne LiDAR data. Remote Sens. 11, 1–18. https://doi.org/10.3390/rs11232880

Young, D.J.N., Stevens, J.T., Earles, J.M., Moore, J., Ellis, A., Jirka, A.L., Latimer, A.M., 2017. Long-term climate and competition explain forest mortality patterns under extreme drought. Ecol. Lett. 20, 78–86. https://doi.org/10.1111/ele.12711

Young, D.J.N., Werner, C.M., Welch, K.R., Young, T.P., Safford, H.D., Latimer, A.M., 2019. Post-fire forest regeneration shows limited climate tracking and potential for drought-induced type conversion. Ecology 100, 1–13. https://doi.org/10.1002/ecy.2571

Yun, Z., Zheng, G., Geng, Q., Monika Moskal, L., Wu, B., Gong, P., 2022. Dynamic stratification for vertical forest structure using aerial laser scanning over multiple spatial scales. Int. J. Appl. Earth Obs. Geoinf. 114, 103040. https://doi.org/10.1016/j.jag.2022.103040

Zhao, K., Popescu, S., Nelson, R., 2009. Lidar remote sensing of forest biomass: A scale-invariant estimation approach using airborne lasers. Remote Sens. Environ. 113, 182–196. https://doi.org/10.1016/j.rse.2008.09.009

Zhen, Z., Quackenbush, L.J., Zhang, L., 2016. Trends in automatic individual tree crown detection and delineation-evolution of LiDAR data. Remote Sens. 8, 1–26. https://doi.org/10.3390/rs8040333

Zhou, T., Popescu, S., 2019. waveformlidar: An R package for waveform LiDAR processing and analysis. Remote Sens. 11, 1–19. https://doi.org/10.3390/rs11212552

Zhou, T., Popescu, S., Malambo, L., Zhao, K., Krause, K., 2018. From LiDARWaveforms to hyper point clouds: A novel data product to characterize vegetation structure. Remote Sens. 10, 1–23. https://doi.org/10.3390/rs10121949

Zhu, X., 2018. FOREST LEAF WATER CONTENT ESTIMATION USING LiDAR AND HYPERSPECTRAL DATA. University of Twente. https://doi.org/10.3990.1.9789036545334

Chapter 5: CONCLUSION

Remotely sensed trees have become more ubiquitous in forest ecology and management, yet their application requires a greater understanding of how they represent ecological trends. In chapter two, I endeavored to compare remotely sensed tree to field tree or in-situ trends in response to a drought-induced tree mortality event. I sought to explore how varying resolutions of data and error influenced the detection and reporting of mortality trends by remotely sensed trees. It became clear that remotely sensed trees represented the largest trees in any area, the top of the canopy that is visible to remote sensing. In chapter three, I matched remotely sensed trees to field trees and evaluated the seen and unseen mortality trends of matched and unmatched field trees. This chapter yielded important differences in mortality trends by height and species that can influence how remotely sensed trees depict population trends. Finally, in chapter four, I tested how well machine learning models could detect the survivorship, mortality, and decay of matched trees with repeat measures for up to 3 years following the drought. Together, these studies provided the foundation for applying remotely sensed trees to ecologically based studies and revealed the importance of assessing uncertainty and bias.

At the outset of this dissertation study, the goals were to use remotely sensed trees to detect and predict conifer tree mortality trends following a drought in the southern Sierra Nevada, California. Specifically, the intention was to detect and predict drought-induced mortality trends at the scale of individual trees using remotely sensed trees as proxies for the study. As the study developed, it became increasingly clear that methods themselves were more foundational as a scientific contribution than the quesitons themselves, which will be discussed later.

At the outset of the study, it became clear that a fundamental knowledge gap existed in the study approach from an ecological perspective. If remotely sensed trees are to be applied

as proxies in this dissertation study, then the trees they represent must first be identified. In other words, one cannot proceed in measuring population trends if there is great uncertainty (Frazer et al., 2011) regarding which individuals are being sampled.

For any ecologist employing methods to directly census or sample representative individuals of a population, the concept of applying methods without addressing uncertainty can lead to fallacious assumptions. Although it is nearly impossible to perfectly census a population with repeat measures, it is important to understand how well a population is measured (bias) and represented (uncertainty). Yet, uncertainty is a serious and pervasive factor in the remote sensing of forest conditions, which has global implications. A recently study by (Melo et al., 2023) identified that 54% of the world's nations are not using freely available, satellite based maps and products of global forest change for their national reporting requirements to the United Nations Framework Convention on Climate (UNFCC). Melo et al., 2023 reported that the primary concern raised by researchers and government agency staff about using the satellite-based forest measurement data was the uncertainties in the data.

Aboveground forest carbon measurements are an important input into the assessment of the global carbon budget. However, these measurements are derived from moderate to coarse resolution remote sensing products, and the uncertainty of these forest measurements is not trivial (Friedlingstein et al., 2022). The role of uncertainty in estimating aboveground forest biomass was assessed for Sierran Mixed Conifer, the forest type analyzed in this dissertation. The researchers reported that uncertainty was greatest in low stature forests where the generalized allometric equation greatly overestimated aboveground forest carbon (Xu et al., 2018). Uncertainty is not a problem unique to remotely sensed forest carbon assessments (Babcock et al., 2015;), it is a core challenge in the application of all remote sensing (Campbell, James B., Wynne, 2011).

In the last decade or so, the ability to assess individual trees with remote sensing has become broadly available (Donager et al., 2021; Duncanson and Dubayah, 2018; Jeronimo et

al., 2018; Versace et al., 2019; Wiggins et al., 2019; Wing et al., 2015; Xu et al., 2018; Zhao et al., 2009). More recently, repeated measures of remotely sensed individual trees have also emerged (Gutierrez et al, 2023). These advancement are significant as they provide the means to measure forests and forest change at the scale of individual overstory trees, across broad extents. Further, they are the lynchpin to address uncertainty across research and management quesitons related to forests. However, these measurements require uncertainty and bias to be addressed to apply remotely sensed trees to empirical analysis.

Whether individual tree measurements are required for meeting the UNFCC climate conventions or the assessment of forest population changes, field validation and error assessment are necessary to determine what trends are being measured and how well they are represented. Although studies have employed empirically based assessment to quantify forest carbon (Babcock et al., 2015) and evaluate the ecological trends of remotely sensed data at the scale of individual trees (Das et al., 2022), a framework for addressing uncertainty and bias in repeated measures of remotely sensed trees was required for this dissertation study to proceed.

Collectively, these dissertation chapters serve as a roadmap to demonstrate how uncertainty and bias are addressed prior to employing remotely sensed trees (hereafter “lidar trees) with repeated measures to assess population trends. In Chapter Two, pre and post-event lidar and in-situ tree data were compared. This examination defined what individual trees were sampled and best represented by lidar trees. The results revealed that the lidar trees collected pre- and post-drought represented overstory trees and on average contained one dominant tree and two additional subordinate trees. The methods in Chapter Two are easily reproducible for any ecological analysis as the datasets are publicly available and the methods are documented.

In Chapter Three, the in-situ or field trees were pairwise matched or coregistered to the remotely sensed trees at a rate of 71% by the matching algorithm and 85% when manual matching was included. While past studies have demonstrated the efficacy of matching in-situ data to modeled trees (Fadili et al., 2019; Hauglin et al., 2014; Pascual et al., 2013), this study

included the measurement error both in the modeling method to segment the remotely sensed trees and the method employed to match the trees. The 12% error rate in the segmentation algorithm to produce the remotely sensed trees was an important limiting factor in reducing the available lidar trees for matching. High resolution imagery (0.1 m resolution) was invaluable for assessing segmentation and matching error. Identifying the matched and unmatched trees was the essential step to identify the population subset lidar trees represented, overstory trees. Equally important, it identified the remaining trees and population trends that lidar trees missed.

While it is necessary to identify the subset of the population being measured with lidar trees, matching lidar trees confers the information necessary to conduct and validate empirically based ecological studies. If lidar trees are to be employed as proxies for in-situ studies, inheriting the predictor variables of the in-situ tree enables the validation of detection and promotes predictive analyses. In this study, each matched lidar tree acquired the ecological metrics collected in the field: taxonomic status, stature, location, pre- and post-drought mortality, decay, and presence of bark beetles.

In Chapter Four, the matched trees were analyzed for their ability to detect survivorship, mortality, and decay trends of trees following the drought. In this study, repeat high resolution orthoimagery at 0.1m resolution and conterminously collected, lidar-based canopy height models (CHM) acquired from 2017 to 2019 were analyzed. These multi-year imagery and CHM data were important predictors of mortality and decay detection of the matched trees. Since the matched trees now represented in-situ overstory trees, it was possible to test whether lidar-only, fine scale forest structure metrics could predict mortality. The results of Chapter Four revealed that matched trees are effective proxies for evaluating the decay process of overstory trees, post-drought. Importantly, the matched trees could follow the fate of individual overstory trees through time creating the possibility to examine changes in forests. However, we also discovered that our methods were biased towards pine versus fir trees, which can impact the

interpretation of mortality trends of remotely sensed trees if both taxonomic and mortality trends were monitored.

This framework as well as the individual tree measurements and bias assessed have applicability to a range of other studies. For example, this study involved measuring the surviving and dead basal area and bias of individual trees by taxonomic status. These measurements are relevant to the quantification of forest carbon fluxes and could support more precise flux measurements. Further, we were able to assess the decay transitions of overstory trees, which is ecologically important and of interest to those measuring carbon fluxes.

This framework or similar approaches could also be applied to the assessment of fuels, physics-based fire modeling, and post-fire tree mortality. For example, this framework could support the research questions of studies such as (Rocha et al., 2023) who used remotely sensed trees to evaluate crown-level structure and fuel loading in Longleaf Pine forests in Florida. The information they collected with lidar could be supplemented with taxonomic information and imagery to also support an ecological assessment. There are many other such studies where tree matching and multi-temporal imagery can support expanded research questions and ecological analysis.

This research study was performed out of opportunity. The field and remotely sensed data were collected prior to the inception of this study and for different research questions. Although the data were relevant for addressing how lidar trees reflect overstory tree, post-drought mortality and decay trends, the data were not appropriate to adequately address all the research questions proposed. For example, the pre-drought imagery was too poor of spatial resolution to detect the mortality status of the lidar trees. In addition, imagery and field data were not collected during the drought. Had these data been collected, questions such as whether shorter stature trees died after overstory trees or whether mortality varied by taxonomic status could be addressed. A proactive, pre, during, and post event dataset along with relevant biophysical drivers should improve the prediction of overstory tree trends.

Despite the challenges inherent in the datasets applied, mortality and decay trends of overstory trees were successfully modeled. Future work related to the outcomes of this study involve applying the mortality and decay modeling developed in this study to a suite of lidar-derived tools to assess forest resilience in the Sierra Nevada. As described in the introduction and discussion in Chapter Three, the University of Washington's Forest Resilience Lab LICOSim tools (Bartl-Geller, Bryce N., Kane, 2022; Bartl-Geller, Bryce N., Smith, 2023) are applied to high resolution airborne lidar to assess fine scale forest structure patterns based on lidar trees. Our goal is to improve the capture of mortality and decay condition to the overstory tree patterns to analyze forest resistance.

Remotely sensed trees have enormous potential to address a range of important forest ecology and management needs. Hopefully, the roadmap laid out in this study will serve future analyses to adequately detect and predict population trends in response to an increasingly stochastic future.

5.1 CITATIONS

Babcock, C., Finley, A.O., Bradford, J.B., Kolka, R., Birdsey, R., Ryan, M.G., 2015. LiDAR based prediction of forest biomass using hierarchical models with spatially varying coefficients. Remote Sens. Environ. 169, 113–127. https://doi.org/10.1016/j.rse.2015.07.028

Bartl-Geller, Bryce N., Kane, V.R., 2022. LICOsim workshop: Forest and Shrubland LiDAR Derived Products Outreach Session.

Bartl-Geller, Bryce N., Smith, E., 2023. LICOsim case study: Restoration planning tools for ICO based treatments - Bryce.

Campbell, James B., Wynne, R.H., 2011. Introduction to Remote Sensing, Fifth. ed. The Guilford Press, New York.

Donager, J.J., Sánchez Meador, A.J., Blackburn, R.C., 2021. Adjudicating perspectives on forest structure: How do airborne, terrestrial, and mobile lidar-derived estimates compare? Remote Sens. 13, 1–18. https://doi.org/10.3390/rs13122297

Duncanson, L., Dubayah, R., 2018. Monitoring individual tree-based change with airborne lidar. Ecol. Evol. 8, 5079–5089. https://doi.org/10.1002/ece3.4075

Fadili, M., Renaud, J.P., Bock, J., Vega, C., 2019. RegisTree: a registration algorithm to enhance forest inventory plot georeferencing. Ann. For. Sci. 76. https://doi.org/10.1007/s13595-019-0814-2

Frazer, G.W., Magnussen, S., Wulder, M.A., Niemann, K.O., 2011. Simulated impact of sample plot size and co-registration error on the accuracy and uncertainty of LiDAR-derived estimates of forest stand biomass. Remote Sens. Environ. 115, 636–649. https://doi.org/10.1016/j.rse.2010.10.008

Friedlingstein, P., Jones, M.W., O'Sullivan, M., Andrew, R.M., Bakker, D.C.E., 2022. Global Carbon Budget 2021, raport Earth System Science Data. Earth Syst. Sci. Data 14, 1917–2005.

Gutierrez, A.A., Allison, S.D., Randerson, J.T., 2023. Estimating Individual Tree Mortality in the Sierra Nevada Using Lidar and Multispectral Reflectance Data Journal of Geophysical Research : Biogeosciences 1–18. https://doi.org/10.1029/2022JG007234

Hauglin, M., Lien, V., Næsset, E., Gobakken, T., 2014. Geo-referencing forest field plots by co-registration of terrestrial and airborne laser scanning data. Int. J. Remote Sens. 35, 3135–3149. https://doi.org/10.1080/01431161.2014.903440

Jeronimo, S.M.A., Kane, V.R., Churchill, D.J., McGaughey, R.J., Franklin, J.F., 2018. Applying LiDAR individual tree detection to management of structurally diverse forest landscapes. J. For. 116, 336–346. https://doi.org/10.1093/jofore/fvy023

Melo, J., Baker, T., Nemitz, D., Quegan, S., Ziv, G., 2023. Satellite-based global maps are rarely used in forest reference levels submitted to the UNFCCC. Environ. Res. Lett. 18. https://doi.org/10.1088/1748-9326/acba31

Pascual, C., Martín-Fernández, S., García-Montero, L.G., García-Abril, A., 2013. Algorithm for improving the co-registration of LiDAR-derived digital canopy height models and field data. Agrofor. Syst. 87, 967–975. https://doi.org/10.1007/s10457-013-9612-2

Rocha, K.D., Silva, C.A., Cosenza, D.N., Mohan, M., Klauberg, C., Schlickmann, M.B., Xia, J., Leite, R. V., de Almeida, D.R.A., Atkins, J.W., Cardil, A., Rowell, E., Parsons, R., Sánchez-López, N., Prichard, S.J., Hudak, A.T., 2023. Crown-Level Structure and Fuel Load Characterization from Airborne and Terrestrial Laser Scanning in a Longleaf Pine (Pinus palustris Mill.) Forest Ecosystem. Remote Sens. 15. https://doi.org/10.3390/rs15041002

Versace, S., Gianelle, D., Frizzera, L., Tognetti, R., Garfì, V., Dalponte, M., 2019. Prediction of competition indices in a Norway spruce and silver fir-dominated forest using lidar data. Remote Sens. 11. https://doi.org/10.3390/rs11232734

Wiggins, H.L., Nelson, C.R., Larson, A.J., Safford, H.D., 2019. Using LiDAR to develop high-resolution reference models of forest structure and spatial pattern. For. Ecol. Manage. 434, 318–330. https://doi.org/10.1016/j.foreco.2018.12.012

Wing, B.M., Ritchie, M.W., Boston, K., Cohen, W.B., Olsen, M.J., 2015. Individual snag detection using neighborhood attribute filtered airborne lidar data. Remote Sens. Environ. 163, 165–179. https://doi.org/10.1016/j.rse.2015.03.013

Xu, Q., Man, A., Fredrickson, M., Hou, Z., Pitkänen, J., Wing, B., Ramirez, C., Li, B., Greenberg, J.A., 2018. Quantification of uncertainty in aboveground biomass estimates derived from small-footprint airborne LiDAR. Remote Sens. Environ. 216, 514–528. https://doi.org/10.1016/j.rse.2018.07.022

Zhou, T., Popescu, S., Malambo, L., Zhao, K., Krause, K., 2018. From LiDARWaveforms to hyper point clouds: A novel data product to characterize vegetation structure. Remote Sens. 10, 1–23. https://doi.org/10.3390/rs10121949